1-1-2019

Probing atypical noncovalent interactions using electronic structure theory

Katelyn Mae Dreux

PROBING ATYPICAL NONCOVALENT INTERACTIONS USING ELECTRONIC STRUCTURE THEORY

A Dissertation
presented in partial fulfillment of requirements
for the degree of Doctor of Philosophy
in the Department of Chemistry and Biochemistry
The University of Mississippi

by

Katelyn M. Dreux

December 2018

ABSTRACT

Some of the most important topics in modern chemistry involve noncovalent interactions in a variety of ways, from pharmacological processes to materials design. Due to the comparatively weak nature of these interactions, they can be difficult to investigate experimentally. Beyond what might be considered the 'typical' noncovalent interactions such as hydrogen bonding or London dispersion, there are less well known noncovalent interactions such as coordinate covalent, dihydrogen, and nonconventional hydrogen bonding, which have been the focus of much of this research. Through the use of electronic structure theory, fundamental information about the structure, energetics, and molecular properties of noncovalently bound complexes can be determined with surprising accuracy with the thoughtful application of a number of computational techniques. For the smaller complexes, *ab initio* methods such as second-order Møller-Plesset perturbation theory (MP2) or coupled cluster with singles, doubles, and a perturbative treatment of connected triples [CCSD(T)] were used to investigate the intrinsic energetics and vibrational signatures. Complexes with a large number of atoms were studied using density functional theory (DFT) to gain insight into how their surrounding environment can affect the vibrations and binding energies.

DEDICATION

To my mother

Thank you for everything

ACKNOWLEDGEMENTS

A common aphorism often repeated in our research group is 'Graduate school is a collaboration', which I feel is particularly relevant. Professionally, all of the research in this work would not have been possible without the help of fellow graduate students, like Dr. Eric Van Dornshuld, Dr. J. Coleman Howard, Dr. Thomas More Sexton, Dr. Louis E. MacNamara, Dr. John T. Kelly, Thomas L. Ellington and Sarah N. Johnson. I also have to thank some of the dedicated undergraduates that have worked in our lab: Carly Rock and Caroline Rader. Dr. Gregory S. Tschumper has been a great research advisor and has helped tremendously in my academic development. I also want to thank my committee members for their time, feedback, and encouragement: Dr. Walter Cleland, Dr. Steven Davis, Dr. Robert Doerksen, and Dr. Nathan Hammer. The Department of Chemistry and Biochemistry at the University of Mississippi was kind enough to allow my attendance, to provide an excellent graduate education, and to supply financial assistance in the form of tuition wavers and teaching assistantships. The National Science Foundation is also generously thanked for their funding under grant numbers EPS-0903787, CHE-1338056, OIA-1430364, CHE-1664998.

On a more personal note, none of this would have been possible without the support of my family, my mother, and my best friend. Collaboration doesn't stop when you leave the office. It also happens at home when your family and friends

continue to reach out and make you a part of their lives, regardless of where you live and what you are doing. I can say with utter certainty my life would be far more bleak without you. My mother, Tina Jones, has encouraged and supported any random goal or dream I have ever had. I could not have been more lucky than to have her as a parent. Erica Bastian has long been a bastion of sanity in the turbulent waters of my life and I could not imagine my life without her (or her snarky comments). Although I cannot fully express how much the following people have helped, loved, and guided me as a person, I want them to know that they were never far from my thoughts: Mackenzie and Annie, Nanny Deanne and Uncle Eddie, Aunt Roberta and Uncle Mike, Aunt Stephanie and Uncle Ryan, Aunt Stephanie and Uncle Arnold, Aunt Joyce and Uncle Martin, Jensen and Jordan, Jesse and Carlee, Allie and Big Seth and Little Seth and Caleb, Hannah and the sprog, the father figures Mike Jones and Roy Blankenship and many, many more cousins (you may not be listed but I know who you are, I promise). I also want to thank two special people who were lost during my years in graduate school, Uncle Bobby and Tyler, both of them amazing people and sorely missed.

TABLE OF CONTENTS

LIST OF FIGURES

LIST OF TABLES

CHAPTER 1

INTRODUCTION

1.1 Background

Noncovalent interactions have an undeniable impact on the world around us. These interactions affect everything from cloud formation to biochemical reactions and have been widely studied using both experimental and computational approaches.[3–18] With strengths ranging from more than ten to less than one kcal mol^{-1}, noncovalent interactions are incredibly versatile and allow for the formation of different types of molecular systems in a variety of mediums.[16–21] Beyond what might be considered 'typical' noncovalent interactions such as hydrogen bonding and London dispersion forces, there are a multitude of unusual intermolecular bonding phenomena that are also prevalent in many different areas of chemistry. Some of these interactions take the form of coordinate covalent (or dative) bonding, dihydrogen bonds, or nonconventional (or weak) hydrogen bonds.

One of the issues in studying noncovalent interactions, both experimentally and computationally, comes from the ephemeral nature of these bonds and their sometimes very weak nature.[19,20] Computationally, these interactions are not easily described by the most common electronic structure theory techniques as they arise outside of familiar atomic orbital/molecular orbital schema. As the name sug-

gests, the core of electronic structure theory is the description of how electrons behave.[16,22,23] The majority of noncovalent interactions do not involve anything as straightforward as a typical covalent bond, it becomes readily apparent that intermolecular interactions are an exciting challenge for many scientists.

1.2 Electronic Structure Theory

As previously discussed, electronic structure theory is the study of the electronic nature of atoms and molecules, which implies some way to describe the quantum-mechanical behavior of electrons and nuclei. These methods try to consider every electron (and some degree of electron excitations) in an atom or molecule which often comes with a steep computational demand.[24,25] This steep scaling ($\mathcal{O}(N^i)$, where i changes based on the particular method) associated with different electronic structure methods, for example CCSD(T) scales as N^7, where i is 7 and N depends on the number of occupied or virtual numbers. This limits computational investigations to smaller complexes (typically less than *ca.* 150 atoms overall) although the application of different approximations (such as density fitting) or mixed technique (like quantum-mechanics/molecular modeling) has increased the upper reaches of both system size and accuracy.[26]

There are several different approaches to computational chemistry and some of the most basic are the orbital wavefunction based *ab initio* methods and density functional theory. *Ab initio* methods are derived purely from quantum-mechanical principles and include such methods as Hartree-Fock[27–29] (HF), second-order Møller-Plesset perturbation theory[30] (MP2), or coupled-cluster with singles, doubles and

connected perturbative triples substitutions[31,32] (CCSD(T)). Density functional theory (DFT) tries to describe a system of atoms or molecules based on the electron density which has led to the creation of many different functionals such as B3LYP[33,34] or M06-2X[35]. Each of these approaches has their own strengths and weaknesses, which will be discussed in greater depth later.

$$\hat{\mathcal{H}}\Psi = E\Psi \tag{1.1}$$

Electronic structure theory is based on finding a solution to the nonrelativistic, time-independent Schrödinger equation (Equation 1.1), which contains the wavefunction (Ψ), the Hamiltonian operator ($\hat{\mathcal{H}}$), and the solution to the electronic Schrödinger equation (E).[36] Ψ is an eigenfunction that theoretically contains all possible information about an atom or molecule and can take the form of either atomic/molecular orbitals or electron density orbitals depending on the type of electronic structure computation. $\hat{\mathcal{H}}$ is a mathematical operator (Equation 1.2) which describes the interactions between electrons and nuclei based on their relative positions.[24,37] These interactions are separated into potential and kinetic energy, $\hat{V}$ and $\hat{T}$, respectively. The potential energy is further separated into three parts, the repulsive force between nuclei or $\hat{V}_{NN}$, the repulsive force between electrons or $\hat{V}_{ee}$, and the attractive Coulombic force between nuclei and electrons denoted as $\hat{V}_{eN}$. Then there is the kinetic energy of the nuclei, $\hat{T}_N$, and that of the electrons, $\hat{T}_e$. All of the above terms are expressed in their general mathematical form in Equation 1.3.

$$\hat{\mathcal{H}} = \hat{V}_{ee} + \hat{V}_{NN} + \hat{V}_{eN} + \hat{T}_e + \hat{T}_N \tag{1.2}$$

Solutions to the Schrödinger equation are the electronic energy of a system (atoms or molecules). However, the energy is dependent on the geometry and electronic state of the system in question and therefore Equation 1.1 also contains information about the geometrical and electronic structure of the system, which is useful in the prediction of physical properties such as the vibrational spectra or ionization potential.[36,37] Several issues immediately emerge when trying to solve the Schrödinger equation for any system with more than one electron: the many-body terms of the Hamiltonian and the construction of an appropriate and useful wavefunction. The former is addressed in the next section.

$$\hat{\mathcal{H}} = \sum_{i=1}^{N}\sum_{l>1}^{N}\frac{1}{r_{il}} + \sum_{j=1}^{M}\sum_{p>1}^{M}\frac{Z_j Z_p}{R_{jp}} - \sum_{i=1}^{N}\sum_{j=1}^{M}\frac{Z_j}{r_{ij}} - \sum_{i=1}^{N}\frac{1}{2}\nabla_i^2 - \sum_{j=1}^{M}\frac{1}{2M_j}\nabla_j^2 \qquad (1.3)$$

1.2.1 Born-Oppenheimer Approximation

Despite the evolution computational chemistry has undergone since its introduction in the early 20th century, all electronic structure methods begin with applying the Hamiltonian operator to solve the Schrödinger equation. $\hat{\mathcal{H}}$ can only be straightforwardly applied to complexes with a single electron as it avoids the problem of a multi-reference system, i.e. the position of the nuclei affect the position of other nuclei as well as as that of the electrons and same thing occurs for electrons.[24,37,38] In order to use $\hat{\mathcal{H}}$ on a many-electron system, the Born-Oppenheimer approximation is invoked.[39]

Born and Oppenheimer noted that the majority of the energy of a molecular

system originates from the motion of electrons orbiting the nucleus and were able to mathematically derive a simplified version of the Hamiltonian operator.[39] The basis for this approximation relies on the fact that the mass of a proton is roughly 2000 times that of an electron. Due to this large difference in mass, electrons are unsurprisingly moving much faster than the nuclei that they orbit. The Born-Oppenheimer approximation takes advantage of these facts to reduce two terms in the Hamiltonian operator, $\hat{T}_N$ and $\hat{V}_{NN}$. The kinetic energy of the nuclei is essentially zero when compared that of the electrons, so $\hat{T}_N$ is set to 0. Moreover, the nuclei are now considered 'fixed' in space so the potential energy between them is constant. The modified Born-Oppenheimer Hamiltonian is shown in Equation 1.4.[37,38]

$$\hat{\mathcal{H}} = \hat{V}_{ee} + constant + \hat{V}_{eN} + \hat{T}_e + 0 \tag{1.4}$$

At this point, the only remaining terms in $\hat{\mathcal{H}}$ are the kinetic energy of the electrons, the repulsive potential energy between electrons, the attractive potential energy between electrons and nuclei, and the constant potential energy between nuclei. This allows for the explicit treatment of electrons and the nuclei are only treated based on their fixed coordinates. Now, this much simplified version of the Hamiltonian operator is used to obtain information about the electronic, vibrational, rotational, and translational properties of a many-electron system.[37,39]

1.2.2 Hartree-Fock Theory

Although our understanding of the nature of subatomic particles as both particles and waves is an essential part of modern physical chemistry, the basis of

many computational chemistry method involves the Hartree-Fock (HF) approximation which is built on the same foundation as linear combinations of atomic orbitals to create molecular orbitals[40] (LCAO-MO) theory. In LCAO-MO theory, molecular orbitals are constructed based on the overlap of atomic (s, p, d, f, etc.) orbitals. In the same way quantum-mechanical wavefunction theory uses one-electron orbitals that resemble atomic orbitals to build a molecular wavefunction.[24,37] One-electron orbital functions (shown in Equation 1.5) are comprised of a spatial and spin part, ψ and α/β, respectively, and are referred to as 'spin orbitals'. ψ is a function of the coordinates of the electron and resembles an s atomic orbital. The spin function is added to create an antisymmetric wavefunction that obeys the Pauli exclusion principle.[37,41]

$$\chi_i = \begin{cases} \psi_i(\mathbf{r})\alpha(\omega) \\ \\ \psi_i(\mathbf{r})\beta(\omega) \end{cases} \tag{1.5}$$

The product of many one-electron spin orbitals is a molecular orbital like that seen in Equation 1.6. This is a wavefunction which is antisymmetric to the exchange of any two electrons with the same spatial or spin coordinate.[37] These wavefunctions are considered uncorrelated due to the fact the motion of two electrons with opposite spins are not related. Now the wavefunction has a shape that resembles a molecular orbital, obeys all of the basic principles of quantum mechanics, and is comprised of a specific set of functions that HF equations can be solved for.[24,37]

$$\Psi_0 = \chi_i\chi_j \cdots \chi_n \tag{1.6}$$

The Hartree-Fock approximation often is referred to as the self-consistent field (or SCF) method based on its iterative nature towards self-consistency. This approximation uses the so-called Fock operator in place of the Hamiltonian to reduce the idea of explicit electrons in orbitals to a mean field of electron density.[27,28] The Fock operator shown in Equation 1.7 is composed of the kinetic energy of the electrons and attractive force between the nuclei and electrons ($\hat{h}$), the Coulomb operator ($\hat{J}$), and the exchange operator ($\hat{K}$).[24,37] For any electron in the system of n electrons, one electron is affected by a field created by the $n-1$ surrounding electrons through the application of $\hat{J}$. This procedure is repeated for every electron in the system until the orbitals stop changing and self-consistency is reached. From this procedure, a set of optimized orbitals describing the atomic or molecular system is obtained. It is important to note however, that like in LCAO-MO theory, electrons are placed in the lowest energy orbitals first and these orbitals are considered 'occupied' while some orbitals are empty and considered 'unoccupied' or 'virtual'. With HF theory, only the occupied orbitals are optimized.[37,38] HF theory, then, must result in a HF *energy* and a set of HF *orbitals*, and the HF orbitals are used as a starting point for other, more rigorous *ab initio* methods.

$$\hat{f}(\mathbf{x}) = \hat{h}(\mathbf{x}) + \sum_j \hat{J}_j(\mathbf{x}) - \sum_j \hat{K}_j(\mathbf{x}) \tag{1.7}$$

The spin orbitals discussed above in Equation 1.5 describe one general case of a closed-shell system where all orbitals are occupied by two electrons, i.e. all electrons are paired and the multiplicity is one, and the HF orbitals are referred to as closed-shell orbitals. However not all molecular systems are closed-shell, such as

the ground electronic state of O_2 or the methylium cation. In such instances when not all electrons are paired, the wavefunction must be modified or unrestricted (UHF). In the RHF wavefunction, electrons that occupy the same orbital have the same spatial function and opposite spin functions. To create an unrestricted wavefunction, the electrons in the same orbitals have different *spatial* and spin functions, shown in Equation 1.8.[24,37,38] The UHF wavefunction incorporates the repulsion effects of these unpaired electrons on orbitals of the same spin at the cost of increased computational demand. In a more technical sense, the wavefunction is not an eigenfunction of the total spin operator anymore. The UHF solutions to the Schrödinger equation are generally lower in energy than their RHF counterparts due to the relaxation of spin symmetry in the spatial orbitals.[24] A subsequent attempt to reduce the demands of UHF and return the spin attributes of RHF yielded the restricted open-shell reference (ROHF) which only treats open-shell orbitals in a UHF-like manner by separating the spatial functions of the unpaired electrons.[42]

$$\chi_i = \begin{cases} \psi_i'(\mathbf{r})\alpha(\omega) \\ \psi_i''(\mathbf{r})\beta(\omega) \end{cases} \tag{1.8}$$

HF scales formally as $\mathcal{O}(N^4)$ but practically as $\mathcal{O}(N^2)$ and is the backbone of all other *ab initio* methods.[43] The energy computed using the HF method is variational and size-extensive.[24,37] For the energy to be variational guarantees that the HF energy will always be an upper bound the exact, 'true' ground state energy of a system and therefore will never overestimate the energetic stability of an atom or molecule. The size-extensive property implies that the cost of a computation

of $n\times$[atom] is the same as [atom$_n$]. Although the energy computed using the HF method constitutes the majority of the energy of a system, there is no correlation between the motion of electrons of opposite spin due to the approximation which reduces the surrounding electrons to an average field.

1.2.3 Post-Hartee-Fock Theory

Despite the relative success of HF theory, the glaring problem of accounting for electron correlation between electrons of opposite spin remains. Increasing the amount of electron correlation in a system is vital as noncovalent interactions are not well-described by HF. Post-HF methods use different approaches to incorporate more electron correlation. Electron correlation is recovered by including electron excitations (sometimes called 'substitutions'). In the 'real' world, electrons can be excited to higher orbitals via the introduction of energy into a system.[44] In computational chemistry, electrons can be 'excited' to valence orbitals using different mathematical techniques like the fluctuation potential as in Møller-Plesset perturbation theory or creation/annihilation operators as in coupled-cluster theory.[24,30–32]

In HF theory, the ground state determinant, $|\psi_0\rangle$, is created from the occupation of the lowest energy spin orbitals.[37] To achieve some measure of electronic excitations, HF introduces single excitations with the application of $\hat{f}$ normally indicated by $|\psi_a^b\rangle$, that is the excitations of an electron a into an unoccupied orbital b. The resulting singly excited determinant has the unique property of not interacting with the ground state determinant and thus greatly reduces the off-diagonal elements of the density matrix created by the application of the Fock operator to a matrix of spin orbitals, χ_i.[24,37] This property is known as Brillouin's theorem and is

mathematically expressed as $\langle\psi_0|\hat{H}|\psi_a^b\rangle$.[37]

$$\hat{H} = \hat{H}_0 + \lambda\hat{\Phi} \tag{1.9}$$

In perturbation theory, complex problems are divided into a large term that has a known solution (and is hopefully easy to compute) and a small term that an exact solution is not known for (and is subsequently more difficult to handle) as shown in Equation 1.9.[45] The latter is referred to as the 'perturbation' and the former on its own is usually considered the zeroth-order solution the perturbative method. Møller-Plesset perturbation theory (MPn, where n is the order of the perturbation) uses the Fock operator as its zeroth-order solution and the perturbation is a fluctuation potential (Equation 1.10). $\hat{\Phi}$ distorts the mean field generated using $\hat{f}$ to improve the initial guess provided by HF.[24,30]

$$\hat{\Phi} = \hat{H} - \hat{f} - \hat{h}_{nuc} \tag{1.10}$$

The most common form of Møller-Plesset perturbation theory is MP2. This second order perturbation includes single excitations from the zeroth-order perturbation ($\hat{f}$), double excitations from the first-order perturbation (MP1), triple excitations from the combination of the singly and doubly excited determinants, and some disconnected quadruple excitations from the combined MP1 double excitations.[24] From Brillouin's theorem, excitations that are more than than two orders of magnitude apart cannot couple so excitations beyond 4th-order are not possible with MP2. MP2 scales as $\mathcal{O}(N^5)$ and unlike HF, it is a non-iterative procedure.[43]

In coupled-cluster theory, excitations occur through the use of the excitation operator shown in Equation 1.11, which is a Taylor series that can be expanded until the full configuration interaction (FCI) limit is reached. The FCI limit occurs when all possible excitations of all electrons (N) have been incorporated into the wavefunction.[24,31,32] A closer look at the terms of $\hat{T}$ reveals individual terms $\hat{T}_n$ such that n is the order of the excitation, e.g. $\hat{T}_1$ contains only single excitations. Increasing n recovers more electron correlation as more excitations are considered.

$$\hat{T} = 1 + \hat{T} + \frac{\hat{T}_2^2}{2!} + \frac{\hat{T}_3^3}{3!} + ...\frac{\hat{T}_N^N}{N!} \tag{1.11}$$

$$\hat{T_1} = \sum_{a,b} t_a^b \Psi_a^b = \sum_{a,b} t_a^b a_b^\dagger a_a \tag{1.12}$$

$$\hat{T_2} = \sum_{\substack{a>i \\ b>j}} t_{ai}^{bj} \Psi_{ai}^{bj} \tag{1.13}$$

The MPn excitations were incorporated into the Hamiltonian through the fluctuation operator in a non-iterative procedure which distorted the original HF orbitals. Another way to picture the excitation of an electron is through annihilation and creation operators, a_a and $\mathrm{a}_b^\dagger$, respectively. Equation 1.12 denotes the 'annihilation' of an electron in orbital a which is then 'created' in orbital b and results in a single excitation. Equation 1.13 shows the $\hat{T}_2$ operator that allows for the excitation of two electrons at the same time. The order of coupled-cluster method depends on the terms in the excitation operator, $\hat{T}$. If $\hat{T} \approx \hat{T}_1$, then the coupled-cluster sin-

gles (CCS) model is invoked and only single excitations are considered. For strictly double excitations, coupled-cluster doubles (CCD) has an excitation operator that is $\hat{T} \approx \hat{T}_2$. As with MP2, the order of the excitation is not limited to the order of the coupled-cluster expansion, i.e. coupled-cluster singles and doubles (CCSD) can include up to triple excitations and $\hat{T} \approx \hat{T}_1 + \hat{T}_2$.[24,31] The excitation operator is applied to wavefunction as an exponential ansatz, $e^{\hat{T}}|\psi\rangle$.

CCSD(T) is considered the 'gold standard' of computational chemistry, containing all single and double excitations as well as the corrected triples excitations from the connected CCSD amplitudes.[24] The CCSD(T) method has been shown to give energies, structures, and vibrational frequencies that are within spectroscopic accuracy (10 cm^{-1}) and 1% of CCSDT(Q) results.[1,46] Generally, coupled-cluster methods scale anywhere from $\mathcal{O}(N^5 - N^8)$ with CCSD and CCSDT scaling as $\mathcal{O}(N^6)$ and $\mathcal{O}(N^8)$, respectively.[43] The perturbative nature of the triples correction allows CCSD(T) to scale as $\mathcal{O}(N^7)$ instead of the $\mathcal{O}(N^8)$ with nearly identical results.[47] Due the more feasible scaling, high accuracy, and well understood convergence CCSD(T) is often used as the standard against which all other methods are compared.

1.2.4 Density Functional Theory

Unlike typical wavefunction based methods like MP2 or CCSD(T) which are based on combinations of atomic orbitals to create molecular orbitals, DFT is based on a physical observable, the electron density or ρ.[48] The use of a physical observable has several advantages, like the obvious ability to include and compare with experimental data to ensure the basic description of an atom or molecule is correct or the reduced computational demand of having a functional that depends only on the

coordinates of the electrons, $\rho(\mathbf{x,y,z})$.[48,49] However despite these two facts, the meteoric rise of DFT as one of the most common computational chemistry techniques did not truly begin until the Kohn-Sham orbitals were developed.[48,49] Since then DFT has been widely used, adapted and parameterized for systems from a formaldehyde monomer to supramolecular complexes like carbon nanotubes, leading to the creation of dozens of different density functionals.[14,23,26,35,48–54]

The electron density lends itself very well to the consideration of potential energy using a classical approach for the attractive interaction between the electron density and the nuclei and the repulsion between electrons. Unfortunately, the kinetic energy is not so straightforward, requiring the use of fermion statistical mechanics which does not include an initial guess for the wavefunction and is not variational.[49] This early approximation was not considered very useful or accurate for chemists trying to study molecular and atomic interactions. It wasn't until almost four decades later that DFT was revitalized through the introduction of the Hohenberg-Kohn theorem and Kohn-Sham orbitals.[48]

The first part of the Hohenberg-Kohn theorem proved the existence of a solution to the potential energy of a system using the electron density but gave no exact quantitative way to obtain the solution. Secondly and arguably of more importance, the energy from electron density is variational in nature.[48,49] This provides a foundation for the improvement of the electron density orbitals (not unlike that of the HF orbitals) with the guarantee that the computed energy of the molecular system will not be lower than the 'true' energy.[24,49]

At this point, it is apparent that the electron density is used to create a

three dimensional picture of the molecular system that can be turned into molecular orbitals which form a wavefunction in a very similar manner to HF theory but the formation of these orbitals has not been discussed. The Kohn-Sham approach to electron density orbitals greatly reduced the cost of the computation of the initial wavefunction and subsequent optimization of the orbitals and increasing the accuracy of the initial guess by demonstrating that the electron density of a system can be represented by a combination of non-interacting electrons.[14,23,48] The Hamiltonian operator is subsequently reduced in complexity to a one electron operator.[49] The energy of the system shown in Equation 1.14 can then be divided into two parts, the classic terms ($\hat{T}_{non}$, $\hat{V}_{Ne}$, and $\hat{V}_{ee}$) and the corrections to these terms that account for the quantum-mechanical nature of electrons (ΔT and ΔV_{ee}).[48,49] These corrections are referred to as the exchange-correlation energy, which has no known exact solution, and many different approximate functionals have been used to create different density functional methods.

$$E(\rho(\mathbf{x},\mathbf{y},\mathbf{z})) = \hat{T}_{non} + \hat{V}_{Ne} + \hat{V}_{ee} + \Delta T + \Delta V_{ee} \tag{1.14}$$

Although the basis of every DFT method is the same (i.e. using the localized electron density of a molecular complex to construct an initial wavefunction built as a system of non-interacting electrons to solve the Schrödinger equation), a variety of approximations for the exchange-correlation energy have arisen by using experimental or more accurate computational data for a set of molecules to create an exchange-correlation functional.[48,49,55,56] For this reason, DFT relies heavily on the parameterization built into each different functional and is therefore not sys-

tematically improvable.[52,56–58] Another difficulty with DFT is that without *a priori* knowledge that a particular density functional method was designed for the system of interest and has been shown to have good agreement with more sophisticated *ab initio* methods or experimental results, there is no certainty a particular functional will provide an accurate description.[14,23,26,35,49,52–54] The majority of DFT methods scale as $\mathcal{O}(N^3)$, far less computationally demanding than the MP2 and CCSD(T) methods, and have been shown to provide answers that are qualitatively (and sometimes quantitatively) as accurate as these *ab initio* methods when properly applied.[26,55,56]

1.2.5 Potential Energy Surface

In previous sections, the main focus has been detailing how to obtain accurate energies using computational chemistry methods with little mention of how the information provided by these methods is useful. Computational chemists often refer to the potential energy surface of a molecule or complex, a many dimensional space that relates the internal coordinates and energy of a system for a particular method (like HF, MP2, etc.) and basis set. The energy of a molecule or complex depends on the degrees of freedom within the system, $3N-6$ (or $3N-5$ for linear systems) where N is the number of atoms. These degrees of freedom correspond to the number of internal coordinates needed to completely describe a system in space.[24,37,49] For a simple diatomic molecule there is only one degree of freedom, the distance between atoms A and B shown in Fig. 1.1. For a polyatomic molecule like water (H_1OH_2), there are three internal coordinates which determine the total energy: the OH_1 bond length, the OH_2 bond length, and the H_1OH_2 bond angle. Taking symmetry into

account, the OH_1 and OH_2 bond lengths are the same but the degrees of freedom do not change.

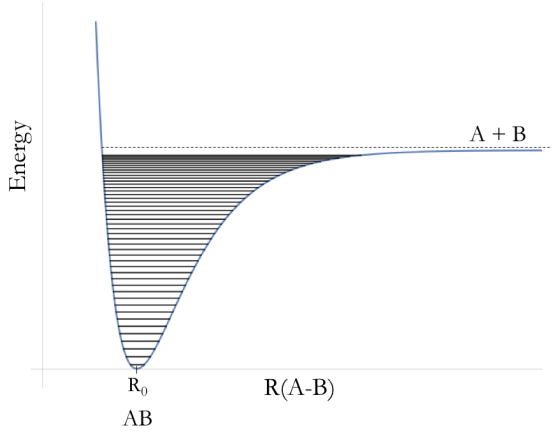

Figure 1.1. Potential energy surface of a diatomic molecule.

The lowest point of the potential energy surface is the global minimum and corresponds to the equilibrium or minimized geometry (R_0 in Fig. 1.1) of a system at a particular level of theory. For larger systems with more than two atoms, there can be more than one minimum on the potential energy surface.[49] Dissociation (A + B in Fig. 1.1) occurs when the fragments of system, either atoms or molecules, are separated by an infinite distance and are no longer interacting. The electronic dissociation energy of a system refers to the energy difference between the system at its equilibrium geometry and the completely dissociated fragments. As the geometry of a system changes, so do the molecular orbitals and the total energy.[24,37,49]

Fig. 1.2 shows the difference between harmonic (shown in blue) and anharmonic (shown in gold) potential energy surfaces.[59] It is immediately apparent that the anharmonic curve more closely describes what is known to happen in nature,

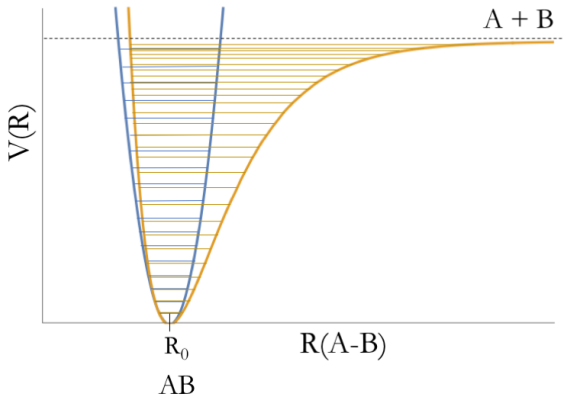

Figure 1.2. Harmonic and anharmonic potential energy surfaces.

that atoms and molecules can dissociate and that the vibrational energy levels of an atom or molecule become closer together as the total energy increases. In the harmonic approximation, there is no dissociation of atoms or molecules and the vibrational energy levels are quantitized. However, all potential energy surfaces are harmonic in nature unless anharmonic corrections are included at great computational demand.[59–62] Despite the differences the harmonic approximation is a very accurate for many systems near at the equilibrium geometry and at the first vibrational state, as shown in Fig. 1.2 where the harmonic and anharmonic curves are nearly identical at the bottom of the potential energy surface.

1.3 Noncovalent Interactions

Noncovalent interactions have a crucial role in many important chemical processes, from the stacking of DNA nucleobases to the self-assembly of polymers. The strength of noncovalent interactions can span from 1 to 10 kcal mol^{-1} in most cases.

These interactions have been seen in many different environments, from gases to solids and extreme temperatures and pressures. There are several different types of noncovalent interactions: electrostatic, dispersion, induction, and exchange, which can be further narrowed down into dipole-dipole, ionic, π-π, and so on interactions.[22,26] Hydrogen bonding and dispersion forces might be some of the most well known and studied examples.[22] From these very general categories, more specialized and unexpected noncovalent interactions have been discovered, such as sulfur-containing hydrogen bonds, dative bonds, and dihydrogen bonding.[26]

Hydrogen bonds (X-H$\cdots$Y, where X and Y are typically O or N) can be found nearly everywhere in nature and have a huge impact on molecular assembly and two of the most common examples of this are the stacking of DNA base pairs and the phases of water.[14,17,22,63] Through careful study both computationally and experimentally, 'typical' hydrogen bonds have been observed to be pseudo-linear (the intermolecular X-H$\cdots$Y bond), have a elongated donor bond length (X-H), and a corresponding appreciable shift in the X-H vibrational frequency upon complexation.[22] Hydrogen bonds involving a hydroxyl group have been widely studied from the smallest H_2O dimer to tertiary conformations of proteins.[1,17,22,64–69]

In past few decades, the idea of a hydrogen bond has been expanded beyond the typical O-H$\cdots$O, O-H$\cdots$N, N-H$\cdots$O, and N-H$\cdots$N schema to include elements like P and S, despite their weaker electronegativities. Unlike N and O which have electronegativities of 3.04 and 3.44, the electronegativities of these third row elements do not exceed 2.6. Evidence of X-H$\cdots$Y interactions (where X,Y = P,S) has been observed, particularly in biochemical and materials processes, leading a new

flavor of hydrogen bonding called 'non-conventional' or sulfur-containing hydrogen bonds.[70–86] A step beyond the prototypical H_2O dimer, the analogous H_2S dimer (shown in Fig. 1.3) has been studied far less extensively and is one of the most basic examples of a sulfur-containing hydrogen bond along with the H_2O/H_2S dimers. A thorough investigation of these complexes can give some insight into the similarities of differences between these isovalent complexes.

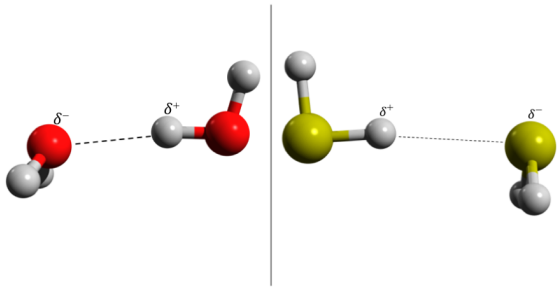

Figure 1.3. 'Typical' hydrogen bond in $(H_2O)_2$ and a 'weak' hydrogen bond in $(H_2S)_2$.

London dispersion forces (more commonly: dispersion forces) arise from the momentary dipoles created by the interactions of two or more fragments. Dispersion interactions are some of the weakest noncovalent interactions individually and one of the most difficult to describe despite their ubiquitous presence in many different types of chemistry.[22,24,26] On an individual level, the dispersion attraction between two fragments is typically very small (< 2 kcal mol^{-1}).[22] One of the characteristics of complexes that are solely dispersion-bound, like $H_2O \cdots O_2$, is an extremely shallow potential energy surface that requires a significant amount of electron correlation to properly characterize because changes in geometry have a minute effect on the total energy.[22,87]

Weakly-bound van der Waals systems such as $H_2O \cdots O_2$ and $H_2O \cdots N_2$ have garnered interest in atmospheric chemistry due to their potential impact on the global radiation budget.[88–96] While ultraviolet light is absorbed by O_2 and O_3 in the stratosphere and infrared (IR) light is absorbed by gases in the troposphere, the majority of visible light from the Sun reaches the Earth. This radiation is primarily absorbed by bodies of water on the surface, and the rest is reflected back into the atmosphere in the far infrared region. The far IR radiation emitted by the Earth is then absorbed by gases in the atmosphere. These gases are referred to as greenhouse gases (GHG) and have a net warming affect on the atmosphere.[97] How and how much the presence of abundant gases like N_2 and O_2 and their interaction with water effects the atmosphere is widely unknown.[89–91]

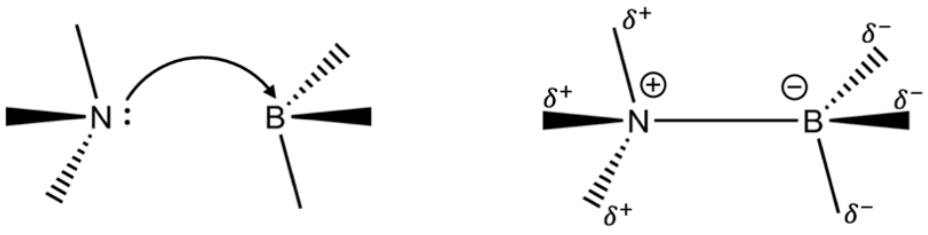

Figure 1.4. Coordinate covalent bond between BH_3 and NH_3

Another kind of unusual hydrogen bond interaction is the dihydrogen bond that arises between the hydridic hydrogen attached to B ($BH^{\delta-}$, shown in Fig. 1.4) and the protonic hydrogen attached to the N ($NH^{\delta+}$, shown in Fig. 1.4) of an adjacent molecule in BH_3NH_3 clusters.[98,99] These hydridic H atoms are a result of the coordinate covalent, often called dative, bond between B and N. The dative

bond is an strong intramolecular bond that arises from N donating electrons into the empty p-orbital on B. As a result of the transfer of electrons to B, N draws more electron density from its H atoms. B now has an excess amount of electron density which is pushed towards the attached H atoms, forming hydridic hydrogens ($H^{\delta-}$). Umeyama and Morokuma estimated the strength of the BN coordinate covalent bond to be nearly 45 kcal mol^{-1} with SCF/4-31G, due largely to electrostatic interactions[100]. Other studies using MP2 with a larger basis set have suggested the dissociation energy is closer to 35 kcal mol^{-1} and that BH_3NH_3 is stabilized by charge transfer[101,102].

Ammonia borane has been widely studied as a potential hydrogen storage device due to its high H content in addition to its unusual intra- and inter-molecular interactions.[103] Ammonia borane has been shown to exhibit different physical properties (particularly the BN bond length and stretching frequency) at different pressures, temperatures, and phases. The effects of different sizes and orientations of ammonia clusters and crystal models has not been explicitly characterized and a rigorous investigation of such could provide valuable insight into these properties.

The underlying focus of these projects are the unusual intermolecular interactions that govern how these systems behave. All of the noncovalently bound complexes discussed above will be investigated computationally. Applying electronic structure theory methods to some of the most fundamental interactions in chemistry will allow for a greater depth of understanding and hopefully contribute meaningful information that can help guide future computational and experimental studies.

CHAPTER 2

Anchoring the $H_2O \cdots O_2$ potential energy surface

All of the computations on $H_2O \cdots O_2$ *were performed by Katelyn M. Dreux. Thomas L. Ellington performed all computations on* $H_2O \cdots N_2$.

2.1 Introduction

Earth's atmosphere is comprised of 78% N_2, 21% O_2, and less than 1% of other gases, under completely dry conditions.[104] The amount of water vapor in the atmosphere is variable at any given time, but typical values range from 1-4% depending on temperature and altitude. Given the high abundances of N_2, O_2 and H_2O, along with water's propensity to form non-covalent complexes, the chemistry of van der Waals complexes plays an important role in the troposphere. The $(H_2O)_2$ dimer is a strong absorber of near infrared (IR) radiation, particularly in the OH stretching region.[105,106] $H_2O \cdots O_2$ and $H_2O \cdots N_2$ have been evaluated as enhanced absorbers of IR radiation in the far-IR region, which includes the low-energy intermolecular modes of both complexes and is distinctly separate from the near-IR region where H_2O is known to absorb.[89,91,107,108] Upon complexation, new intermolecular vibrational modes are formed between the fragments that could have appreciable IR activity. In addition, the monomer vibrations can be perturbed in the complex, leading to enhanced IR activity. Although absorption and emission of electromagnetic

radiation can be characterized in various ways this study focuses on IR intensities as a measure of radiative transfer. An indication of greenhouse effects from these van der Waals complexes could be evidenced by an increase in the IR intensity of the vibrational mode of the fragments and/or large IR intensity for any newly-formed intermolecular modes of the complex.[89] Large frequency shifts or IR intensity changes after dimerization could also be helpful for directly detecting a particular complex in the atmosphere or laboratory.[91]

A number of prior studies of the $H_2O \cdots O_2$ dimer have utilized Møller-Plesset perturbation theory to characterize stationary points on the potential energy surface.[89,92–95,109,110] The most extensive *ab initio* investigation of the potential energy surface examined twelve different structures of the $H_2O \cdots O_2$ dimer at the MP2/aug-cc-pVTZ level of theory.[109] In some cases, quadratic configuration interaction or coupled-cluster single point energy computations (e.g. QCISD and CCSD) were also performed to recover more dynamical electron correlation which slightly reduced the dissociation energy of global minimum.[88,90,91,96,107,111–116] Several studies also considered the multireference nature of O_2, which has a $^3\Sigma_g^-$ ground state. However, the results from multi-reference computations were consistent with those from single-reference MP2 calculations.[93,109,116]

The global minimum identified by these studies (structure I, shown in Fig. 2.1) is a C_s structure with a $^3A''$ electronic state and an electronic dissociation energy well below 1 kcal mol^{-1}. Most correlated wavefunction based methods with basis sets of at least triple-zeta quality yield dissociation energies for the global minimum of just over 0.7 kcal mol^{-1}.[91,109] There is, however, significant variation in some

intermolecular geometrical parameters of the optimized structures. The OH$\cdots$O and OO$\cdots$H angles (denoted α and β, respectively, in Fig. 2.1) exhibit variations of more than 20 degrees because the potential energy surface of $H_2O\cdots O_2$ is very shallow.[93,107,116] Eleven other stationary points with C_s or C_{2v} symmetry (structures II-XII, Fig. 2.1) have also been identified that are within 0.5 kcal mol^{-1} of the global minimum.

In this work, coupled-cluster theory (specifically the CCSD(T) method) is used to characterize these twelve stationary points on the potential energy surface of the $H_2O\cdots O_2$ dimer (Fig. 2.1), six C_{2v} structures and six C_s structures (including the global minimum). Dissociation energies, geometrical parameters and harmonic vibrational frequencies of both the fragments and complex are compared to those from second-order Møller-Plesset perturbation theory. Frequency shifts and IR intensity changes are used to monitor changes in the spectroscopic fingerprints of each monomer species upon complexation. The IR intensities of the low-energy intermolecular vibrational frequencies (< 150 cm^{-1}) are also examined to discern the potential of the $H_2O\cdots O_2$ complex to play a role as an enhanced absorber in the atmosphere. Our group performed a similar analysis of six key stationary points on the potential energy surface of $H_2O\cdots N_2$.[108] As such, this paper also provides a direct comparison of these two important complexes, $H_2O\cdots O_2$ and $H_2O\cdots N_2$.

2.2 Computational Methods

Full geometry optimizations and harmonic vibrational frequency computations were performed for each dimer structure and the isolated fragments with second

order Møller-Plesset perturbation theory[30] and coupled-cluster method with single, double, and perturbative triple substitutions[32] using a spin unrestricted Hartree-Fock (UHF) reference wavefunction for all open-shell species (O_2 and $H_2O\cdots O_2$) and a spin restricted Hartee-Fock (RHF) reference for the closed-shell systems (H_2O). These computations were performed with the analytic gradients and Hessians available in `CFOUR`[117], and the corresponding results are labeled as UMP2 and UCCSD(T). All energies, optimized structures and harmonic vibrational frequencies were computed with the correlation consistent family of basis sets in which diffuse functions were added to the "heavy" (non-hydrogen) atoms (i.e. cc-pVXZ for H and aug-cc-pVXZ for O where X = T, Q, and 5). These basis sets are denoted haXZ throughout the remainder of this manuscript. In addition, a series of single point MP2 and CCSD(T) energies were computed that employed a spin restricted Hartree-Fock (ROHF) reference for the open shell systems, (i.e. ROMP2 and ROCCSD(T)). Explicitly correlated F12 single point energies were also computed with the ha5Z basis set and associated default density fitting basis sets in the `Molpro2010`[118] program to estimate the complete basis set (CBS) limit. Partially spin-restricted explicitly correlated coupled-cluster computations (denoted ROCCSD(T)-F12) employ an ROHF reference, and a cluster operator that neglects some spin coupling in order to reduce spin contamination.[119,120] Unrestricted explicitly correlated coupled-cluster computations (denoted UCCSD(T)-F12) also used an ROHF reference, but the method is more susceptible to spin contamination because the unmodified cluster and spin-squared operators do not commute.[119,120] The `Gaussian09`[121] software package was used for all UMP2 and ROMP2 calculations. All UCCSD(T) and ROCCSD(T) cal-

culations were done using `CFOUR`, whereas `Molpro2010` was used for the explictly correlated computations. Pure angular momentum functions ($5d$, $7f$, $9g$) were used rather than Cartesian functions ($6d$, $10f$, $15g$). All Cartesian forces associated with the optimized structures have been converged to less than 1×10^{-4} E_h/a_0.

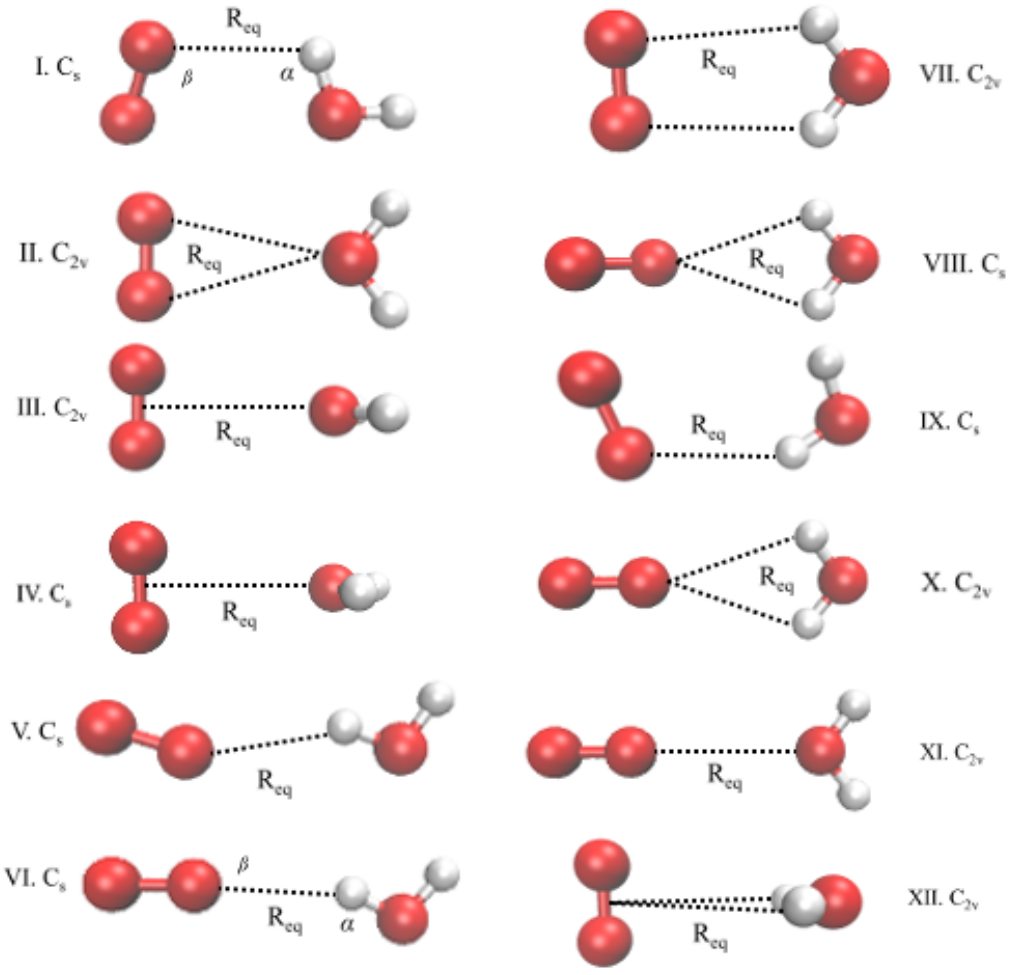

Figure 2.1. Twelve structures and point group symmetries of the $H_2O \cdots O_2$ system along with select intermolecular parameters (R_{eq}, α, β) described in the text.

2.3 Results and Discussion

2.3.1 O_2 and H_2O Fragments

Table 2.1 lists the intramolecular bond lengths and bond angle along with harmonic vibrational frequencies and IR intensities of O_2 and H_2O. The differences between the optimized haTZ and haQZ bond lengths and bond angle are minimal, less than 0.006 Å and 0.2°, and deviations between corresponding harmonic vibrational frequencies do not exceed 25 cm^{-1}. Higher-order correlation effects have a more substantial impact on the fragments, particularly for O_2. Relative to the UCCSD(T) results, UMP2 overestimates the OO bond length by 0.01 Å and underestimates the frequency by 120 cm^{-1} with both haTZ and haQZ basis sets. The deviations between MP2 and CCSD(T) for the H_2O fragment are smaller, with maximum unsigned deviations of 0.001 Å for the OH bond length, 0.1° for the HOH angle, and 30 cm^{-1} for any frequency. At the CCSD(T)/haQZ level, the largest IR intensity of 73 km mol^{-1} corresponds to the HOH bend at 1651 cm^{-1}. For the twelve $H_2O \cdots O_2$ structures discussed in the following sections, the OO and OH bond lengths change by no more than 0.004 Å and the HOH bond angle by less than 0.2°.

Table 2.1. Geometrical parameters (R in Å, θ in °) of O_2 and H_2O along with harmonic vibrational frequencies (ν in cm^{-1}) and non-zero IR intensities (in parentheses in km mol^{-1})

	R(OO)	ν	R(OH)	θ(HOH)	ν_1	ν_2	ν_3
UMP2/haTZ	1.224	1454.7	0.961	104.1	3824.5 (7.6)	1630.1 (73.8)	3951.9 (75.8)
UMP2/haQZ	1.219	1479.7	0.959	104.3	3840.5 (6.8)	1632.8 (73.5)	3966.4 (78.5)
UCCSD(T)/haTZ	1.213	1574.4	0.962	104.2	3813.6 (4.6)	1647.9 (72.4)	3924.3 (54.9)
UCCSD(T)/haQZ	1.208	1595.7	0.959	104.4	3831.8 (4.2)	1650.5 (72.5)	3941.4 (57.8)

The experimentally determined fundamental frequency of O_2 is 1580.2 cm^{-1},

which has reasonably good agreement with the UCCSD(T)/haQZ harmonic vibrational frequency (within 16 cm^{-1}).[122] For the OH stretches and HOH bend of H_2O, the CCSD(T)/haQZ harmonic frequencies differ from experimental results by nearly 200 cm^{-1}.[123] The CCSD(T)/haQZ IR intensities for the HOH bend and HOH stretches are within 10 km mol^{-1} of experimental results.[123] Although the deviations between harmonic frequency computations and experimental results are large in the fragment HOH bending and stretching modes, any observed frequency shifts or IR intensity changes should give qualitative insight into the effects of complexation on the H_2O and O_2 fragments.

2.3.2 Nature and Structures of the Dimer

The structures in Figure 2.1 are shown in the order of increasing electronic energy at the UMP2/haQZ level of theory, with I as the global minimum and XII as the highest energy stationary point. Six C_{2v} structures (II, III, VII, X-XII) have been considered, one of which is a local minimum (structure VII) on the UMP2 surface. The other six stationary points have C_s symmetry (I, IV-VI, VIII, IX), including the global minimum (structure I). Although structure I is consistently identified as the global minimum here and elsewhere[93,107,109], some variation in the exact orientation of the O_2 fragment relative to H_2O is observed for this stationary point. As such, the following discussion primarily focuses on the geometrical parameters of structure I. The UCCSD(T)/haQZ optimized global minimum has intermolecular angles of α=110° and β=106° and an intermolecular separation of R_{eq}= 2.64 Å (Fig. 2.1). Using either UMP2 or UCCSD(T) with a haTZ or haQZ basis, α and β change by less than ± 10° for structure I. Similar parameters were reported at the QCISD/6-

311++G(2*d*,2*p*) level of theory (α=126°, β=109°, R_{eq}=2.57 Å)[91] and from MP2/aug-cc-pVTZ optimizations (α=102°, β=112°, R_{eq}=2.57 Å).[93,109]

Table 2.2. Number of imaginary frequencies n_i

	I	II	III	IV	V	VI	VII	VIII	IX	X	XI	XII
UMP2/haTZ	0	1	1	0	1	2	0	1	2	2	1	1
UMP2/haQZ	0	1	1	1	1	2	0	1	2	2	1	2
UCCSD(T)/haTZ	0	1	1	1	1	2	1	1	2	2	1	2
UCCSD(T)/haQZ	0	1	1	1	1	2	1	1	2	2	1	2

Table 2.2 lists the number of imaginary frequencies associated with structures I – XII of the $H_2O\cdots O_2$ dimer. One of the most significant features of the data is that the number of minima changes with computational protocol. At the UMP2/haTZ level of theory, three of the stationary points (structures I, IV, and VII) examined in this study are minima. With the larger haQZ basis set, however, structure IV becomes a transition state with an a″ imaginary frequency of $37i$ cm^{-1}, whereas structure XII changes from a transition state to a second order saddle point (n_i = 2). Structure VII is also a transition state with both the haTZ and haQZ basis sets at the UCCSD(T) level, having a single imaginary frequency with b_2 symmetry. The global minimum is structure I, regardless of method or basis set. As can be seen in Table 2.2, structures II, III, IV, V, VII, VIII and XI are transition states and structures VI, IX, X and XII are second-order saddle points on the UCCSD(T)/haTZ and UCCSD(T)/haQZ surfaces.

Structure VI provides a more extreme example of this sensitivity. Reference 4 reported a minimum $H_2O\cdots O_2$ structure from MP2 computations with the 6-311++G($2df, 2pd$) basis set that had geometrical parameters (α = 178°, β = 179°,

R_{eq} = 2.43 Å) very similar to those for structure VI at the UMP2/haTZ ($\alpha = 180°$, $\beta = 169°$, R_{eq} = 2.47 Å). However, structure VI is a second-order saddle point (n_i = 2) at all levels of theory employed in this study while it is a minimum at the MP2/6-311++G($2df, 2pd$) level of theory regardless of whether the core electrons are correlated or not. Although structure I was not considered in Reference 4, it remains a lower-energy minimum on the MP2/6-311++G($2df, 2pd$) potential energy surface.

Table 2.3. Intermolecular separations (R_{eq} in Å)

	I[a]	II[b]	III[b]	IV[b]	V[a]	VI[a]	VII[a]	VIII[a]	IX[a]	X[a]	XI[a]	XII[a]
UMP2/haTZ	2.81	3.12	3.16	3.13	2.46	2.47	2.86	2.90	2.60	2.92	3.82	3.15
UMP2/haQZ	2.75	3.14	3.20	3.16	2.47	2.48	2.87	2.91	2.62	2.92	3.83	3.18
UCCSD(T)/haTZ	2.66	3.13	3.18	3.15	2.42	2.48	2.85	2.88	2.56	2.87	3.81	3.13
UCCSD(T)/haQZ	2.64	3.17	3.22	3.18	2.43	2.49	2.87	2.89	2.54	2.88	3.83	3.15

[a] R(H$\cdots$O)

[b] R(O$\cdots$MP) where MP denotes the midpoint of the OO bond

Table 2.3 lists key UMP2/haXZ and UCCSD(T)/haXZ (X=T,Q) intermolecular separations, R_{eq}, for each optimized structure. Cartesian coordinates, harmonic vibrational frequencies, and IR intensities for every optimized structure are available in the **??**. The intermolecular separation of structures II-IV is measured from the midpoint of the O_2 bond to the oxygen of H_2O while R_{eq} for structures I and V-XII is the shortest intermolecular O$\cdots$H distance (Fig. 2.1). For structures II-XII, these intermolecular parameters are quite similar regardless of method or basis set used for the optimization, never differing by more than 0.05 Å. The global minimum (structure I) has slightly larger deviations (> 0.1 Å), indicating a large basis and substantial amounts of electron correlation are needed to adequately describe

the non-covalent interaction. However, R_{eq} changes by less than 0.02 Å between UCCSD(T)/haTZ and UCCSD(T)/haQZ for structure I.

2.3.3 Harmonic Vibrational Frequencies and IR Intensities

As shown in Table 2.2, structure I is the only minimum at the UCCSD(T) level of theory, and the nature of each stationary point remains consistent with both haTZ and haQZ basis sets. For this reason, after a brief discussion of prior computational and experimental results, the remainder of this section will focus on the harmonic vibrational frequencies of the global minimum (structure I). Previous vibrational frequency computations of the global minimum were done at the QCISD/6-311++G$(2d, 2p)$ level of theory using the harmonic oscillator linear dipole moment approximation (HOLD), which agree to within 50 cm^{-1} of UCCSD(T)/haQZ results and IR intensities of the OH stretching modes have deviations less than 10 km mol^{-1}.[91] However, this previous study focused primarily on the OH stretching modes of the $H_2O \cdots O_2$ dimer, whereas the current investigation considers the IR intensities and frequencies of the intermolecular modes as well as the intramolecular frequency shifts and IR activity changes.

Experimentally, the ground state of the $H_2O \cdots O_2$ dimer determined via microwave spectroscopy has C_{2v} symmetry like that seen in structure II.[96] Computationally, however, structure II is a transition state with an imaginary frequency of b_2 symmetry at $40i$ cm^{-1} at the UCCSD(T)/haQZ level of theory. A previous study investigated rotations of the O_2 and H_2O fragments in structure I and found the conrotatory motion to be degenerate while the disrotatory motion experiences a slight splitting.[109] That study noted that the transitions between these low-lying

states due to the small barrier of the disrotatory intermolecular vibration would be interpreted by microwave spectroscopy as a structure with C_{2v} symmetry.[109]

Table 2.4. Harmonic vibrational frequencies (ν in cm^{-1}) and IR intensities (in parentheses in km mol^{-1}) of structure I

Mode	UMP2/haTZ		UMP2/haQZ		UCCSD(T)/haTZ		UCCSD(T)/haQZ	
a′	3947.5	(73.4)	3962.4	(76.4)	3921.8	(54.4)	3939.3	(58.6)
a′	3819.8	(6.3)	3836.2	(5.7)	3810.6	(3.2)	3829.1	(2.9)
a′	1642.4	(70.7)	1639.9	(78.2)	1645.2	(95.0)	1647.7	(93.6)
a′	1574.3	(19.0)	1577.4	(11.9)	1582.9	(0.3)	1601.3	(0.4)
a′	127.8	(42.5)	108.4	(49.6)	85.7	(71.5)	83.5	(73.7)
a′	72.7	(16.2)	74.4	(17.6)	80.5	(9.5)	78.7	(4.9)
a′	48.6	(28.7)	45.8	(22.6)	47.3	(13.9)	41.3	(17.2)
a″	117.4	(0.7)	111.3	(3.4)	103.7	(4.4)	103.2	(0.0)
a″	86.4	(225.5)	79.7	(217.5)	71.7	(214.8)	67.5	(215.5)

Frequency shifts and IR intensities can often provide the means to spectroscopically identify non-covalent complexes. For the global minimum at the UMP2/haQZ level of theory, there is a substantial shift (+98 cm^{-1}) and slight increase in the IR intensity (from 0 to 12 km mol^{-1}) for the OO stretch in the dimer at 1577 cm^{-1}, which can be seen in Table 2.4. The OO stretch is strongly coupled to the HOH bend on the UMP2 surface. However, the frequency shift decreases to only +6 cm^{-1} and the mode remains IR inactive on the UCCSD(T)/haQZ surface (1601.3 cm^{-1} and <1 km mol^{-1}). At the UCCSD(T)/haQZ level of theory, the mode associated with HOH bend shifts by close to -3 cm^{-1} and has an increase in IR intensity of +21 km mol^{-1}. The changes are even smaller for the symmetric and asymmetric OH stretches of H_2O, not exceeding ± 3 cm^{-1} and ± 1 km mol^{-1}. As such, the HOH bend is the only intramonomer mode with any appreciable increase in IR intensity (from 73 to 94 km mol^{-1}, almost 29%).

By inspecting the far IR (less than 150 cm^{-1}) intermolecular modes of the $H_2O \cdots O_2$ dimer, another potential mechanism leading to green house effects can be evaluated. Structure I has five modes in this region (Table 2.4). However, only two modes have substantial IR intensities at the UCCSD(T)/haQZ level of theory. One a′ mode is moderately IR active and has an intensity of 74 km mol^{-1} at 84 cm^{-1}. The largest IR intensity corresponds to the lowest energy mode of a″ symmetry at 68 cm^{-1} and with an intensity of 216 km mol^{-1}, more than double the IR intensity of any other inter- or intramolecular mode of the $H_2O \cdots O_2$ global minimum.

2.3.4 Energetics

Relative electronic energies of structures I-XII with respect to the global minimum (structure I) are listed in Table 2.5. In addition to UMP2/haXZ and UCCSD(T)/haXZ energies, ROMP2 and ROCCSD(T) single point computations were performed based on the corresponding UMP2/haXZ or UCCSD(T)/ haXZ optimized geometry. Explicitly correlated UCCSD(T)-F12 and ROCCSD (T)-F12 energies at UCCSD(T)/haQZ optimized geometries were included to probe convergence to the CBS limit. It is readily apparent from Table 2.5 that the potential energy surface is extremely flat with all relative electronic energies within 0.5 kcal mol^{-1} of the global minimum for structures II-XII. Energetically, increasing the basis set from haTZ to haQZ has little effect, less than 0.05 kcal mol^{-1} for UMP2 or UCCSD(T). Given the open shell nature of O_2 and $H_2O \cdots O_2$, the energetics are more sensitive to electron correlation than basis set effects with maximum deviations of 0.08 kcal mol^{-1} when comparing UMP2 to UCCSD(T).

The spin formalism has a noticeable affect on the MP2 results. ROMP2 un-

derestimates the relative electronic energies by more than 0.1 kcal mol^{-1} in some cases. In contrast, the spin restricted and unrestricted coupled-cluster results are virtually indistinguishable. ROCCSD(T)/haXZ and UCCSD(T)/haXZ have deviations less than 0.01 kcal mol^{-1}. UCCSD(T)-F12/ha5Z and ROCCSD(T)-F12/ha5Z differ by no more than 0.02 kcal mol^{-1}. The T1 and D1 diagnostics from explicitly correlated single computations never exceed 0.01 and 0.02, respectively, with an ha5Z basis set.[124]

Table 2.5. Relative Electronic Energies in kcal mol^{-1}

	I	II	III	IV	V	VI	VII	VIII	IX	X	XI	XII	D_e^a
UMP2/haTZ	0.00	0.06	0.13	0.15	0.25	0.27	0.27	0.29	0.32	0.31	0.33	0.45	0.72
UMP2/haQZ	0.00	0.07	0.16	0.17	0.23	0.26	0.28	0.30	0.30	0.31	0.38	0.47	0.70
ROMP2/haTZ[b]	0.00	0.01	0.05	0.05	0.23	0.21	0.12	0.19	0.29	0.25	0.13	0.25	0.56
ROMP2/haQZ[b]	0.00	0.01	0.07	0.06	0.18	0.18	0.12	0.19	0.24	0.24	0.17	0.27	0.53
UCCSD(T)/haTZ	0.00	0.10	0.16	0.18	0.17	0.28	0.28	0.28	0.25	0.28	0.33	0.44	0.74
UCCSD(T)/haQZ	0.00	0.11	0.18	0.19	0.18	0.27	0.26	0.27	0.24	0.28	0.37	0.44	0.70
ROCCSD(T)/haTZ[b]	0.00	0.10	0.16	0.18	0.17	0.28	0.28	0.28	0.25	0.28	0.33	0.44	0.74
ROCCSD(T)/haQZ[b]	0.00	0.11	0.17	0.19	0.18	0.27	0.26	0.27	0.24	0.28	0.37	0.44	0.69
UCCSD(T)-F12a/ha5Z[c]	0.00	0.11	0.18	0.19	0.18	0.27	0.25	0.26	0.23	0.28	0.38	0.43	0.66
UCCSD(T)-F12b/ha5Z[c]	0.00	0.11	0.18	0.19	0.18	0.27	0.25	0.26	0.23	0.28	0.39	0.43	0.66
ROCCSD(T)-F12a/ha5Z[c]	0.00	0.09	0.17	0.18	0.18	0.26	0.23	0.24	0.22	0.26	0.37	0.42	0.64
ROCCSD(T)-F12b/ha5Z[c]	0.00	0.09	0.17	0.18	0.18	0.26	0.23	0.24	0.22	0.26	0.37	0.42	0.64

[a] $D_e = E(O_2) + E(H_2O) - E(I)$

[b] Single point energies with UMP2/haXZ or UCCSD(T)/haXZ optimized structures

[c] Single point energies with UCCSD(T)/haQZ optimized structures

The deviations between UCCSD(T)/haQZ and UCCSD(T)-F12/ha5Z relative electronic energies are less than 0.02 kcal mol^{-1}, indicating that this property is well converged to the CBS limit. The electronic dissociation energies (D_e, the energy of the fully optimized isolated monomers relative to structure I) obtained with the explicitly correlated methods, tend to be about 0.04 kcal mol^{-1} smaller than

the corresponding UCCSD(T)/haQZ and ROCCSD(T)/haQZ results. D_e is 0.70 kcal mol^{-1} on both UMP2/haQZ and UCCSD(T)/haQZ surfaces, which decreases to ≈0.65 kcal mol^{-1} according to the explicitly correlated coupled-cluster computations. Previous estimates from MP2/aug-cc-pVTZ and QCISD/6-311++G(2*d*,2*p*) computations are nearly identical, predicting slightly larger energies of 0.76 and 0.72 kcal mol^{-1}, respectively.[91,93,109] Correcting the UCCSD(T)/haQZ electronic dissociation energy with the harmonic zero-point vibrational energy, yields a D_0 value of 0.17 kcal mol^{-1}. Interestingly, the dimer is slightly unbound on the UMP2/haQZ surface ($D_0 = -0.04$ kcal mol^{-1}), but both values would certainly change if anharmonic effects were evaluated.

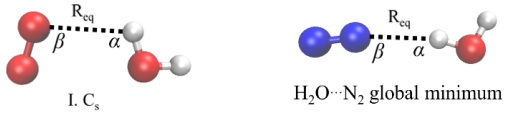

Figure 2.2. Global minima of the $H_2O\cdots O_2$ (left) and $H_2O\cdots N_2$ (right) dimers along with select intermolecular geometrical parameters (R_{eq}, α, β) described in the text.

2.3.5 Comparison to $H_2O\cdots N_2$

The results obtained in this study for the $H_2O\cdots O_2$ global minimum brings up several interesting points of divergence with the related $H_2O\cdots N_2$ van der Waals system (Fig. 2.2). The following section compares and contrasts geometrical parameters, harmonic vibrational frequencies, IR intensities, and energetics of the $H_2O\cdots O_2$ global minimum to those of the $H_2O\cdots N_2$ global minimum.

Geometrically, the global minimum of the $H_2O\cdots N_2$ dimer has the greatest similarity to structure VI of the $H_2O\cdots O_2$ dimer, a second-order saddle point on

the UCCSD(T)/haQZ surface. The CCSD(T)/haQZ intermolecular arrangement of the $H_2O\cdots N_2$ minimum is more linear, with both α and β (Fig. 2.2) near 170° compared to roughly 110° in the $H_2O\cdots O_2$ global minimum. R_{eq} of the $H_2O\cdots N_2$ global minimum is 2.35 Å, nearly 0.3 Å shorter than the corresponding intermolecular separation in structure I of the $H_2O\cdots O_2$ system.[108]

Although the potential energy surface of $H_2O\cdots N_2$ is also quite flat, no discrepancies in the number of imaginary frequencies were observed for any structure when using the same basis sets and comparable electronic structure methods. As with $H_2O\cdots O_2$, frequency shifts upon complexation are small according to coupled-cluster computations, although the associated IR intensity changes are generally larger for $H_2O\cdots N_2$ (e.g., roughly +60 km mol^{-1} and +20 km mol^{-1} for the asymmetric and symmetric OH stretches, respectively).[108] The global minimum of $H_2O\cdots N_2$ has only a single intermolecular mode in the far IR with moderate IR intensity on the CCSD(T)/haQZ surface: an a′ mode at 165 cm^{-1} with an intensity of 81 km mol^{-1}, which is smaller than that of the intramolecular OH asymmetric stretch (117 km mol^{-1}).[108] In contrast, the $H_2O\cdots O_2$ dimer, has an a″ intermolecular mode at 68 cm^{-1} with an IR intensity of 216 km mol^{-1} which is more than two times larger than that of any other mode.

The global minimum of the $H_2O\cdots N_2$ system has a dissociation energy of 1.22 kcal mol^{-1} at the CCSD(T) CBS limit estimated from CCSD(T)-F12/ha5Z computations. Comparatively, structure I of the $H_2O\cdots O_2$ dimer has a CCSD(T) CBS D_e of 0.65 kcal mol^{-1} estimated from ROCCSD(T)-F12/ha5Z and UCCSD(T)-F12/ha5Z explicitly correlated coupled-cluster computations.

2.4 Conclusions

To summarize the results of this research, structure I is the only minimum on the UCCSD(T)/haQZ surface out of the twelve $H_2O \cdots O_2$ dimer stationary points examined. The global minimum has an electronic dissociation energy of approximately 0.65 kcal mol^{-1} near the CCSD(T) CBS limit. According to coupled-cluster theory, there were no significant frequency shifts, IR intensity changes, or geometrical changes of the fragments upon complexation. Although the UMP2 energetics are similar to those from coupled-cluster computations, the method incorrectly identifies two structures as minima. In addition, the UMP2 results suggest the OO harmonic frequency shift upon complexation is substantially larger (ca. +100 cm^{-1}) than the UCCSD(T) value (ca. +5 cm^{-1}). Both methods indicate there are two intermolecular modes (one a$'$ and one a$''$) with appreciable IR intensity in the far IR region. The IR intensity of the lowest a$''$ mode exceeds 200 km mol^{-1}, which is more than double the largest IR intensity of any other mode. Even though the related $H_2O \cdots N_2$ dimer is more strongly bound it does not possess any intermolecular vibrational modes with IR intensities as large as those seen here for the $H_2O \cdots O_2$ dimer.

CHAPTER 3

Unusual intra- and inter-molecular interactions in ammonia borane

All experimental results were obtained by Louis E. McNamara, John T. Kelly, Ashley M. Wright, and Nathan I. Hammer. Katelyn M. Dreux, Ashley M. Wright, and Gregory S. Tschumper performed all computations.

3.1 Introduction

Since it was first synthesized in 1955[125] ammonia borane has generated a large amount of interest both experimentally[126–144] and computationally[98,100–102,145–167]. The coordinate covalent, often called dative, bond between boron and nitrogen is an intramolecular bond with an interaction energy of -43.91 kcal mol^{-1} at the estimated CCSD(T) complete basis set (CBS) limit that arises from nitrogen donating a pair of electrons into the empty p-orbital on boron.[166] The presence of both hydridic and protonic hydrogens in BH_3NH_3 allows for the formation of dihydrogen bonds ($BH^{\delta-}\cdots H^{\delta+}N$) between adjacent molecules. These interactions give rise to short intermolecular H-H distances in the crystal structure (< 2.2 Å) and an interaction energy of approximately -4 to -6 kcal mol^{-1} between BH_3NH_3 subunits (on the same order of a typical H-bond).[98]

Ammonia borane has been the focus of several experimental investigations in an attempt to understand the behavior of BH_3NH_3 as a gas, solid, or in solu-

tion. Gas-phase microwave spectroscopy determined the monomer BN bond length to be 1.658 Å (r_s = 1.6576 Å) with a dipole moment of 5.22 Debye.[132,133] The rotational barrier of BH_3NH_3 around the BN bond was estimated to be 2.07 kcal mol^{-1} experimentally which agrees well with extrapolated CCSD(T) CBS results of 1.95 kcal mol^{-1}.[132,133,155] An infrared (IR) matrix isolation study of BH_3NH_3 assigned the monomer ^{11}BN stretch at 968 cm^{-1}, an assignment that was later challenged and reassigned to 610 cm^{-1}.[131,152] A vapor-phase IR study of BH_3NH_3 was unable to observe the BN stretch experimentally. However, the resolved spectra showed good agreement with the previous matrix isolation study in several regions.[158] The first Raman spectra of BH_3NH_3 were obtained in solutions of ammonia or dimethyl ether with the BN stretch assigned to 787 and 755 cm^{-1}, respectively.[128,129] When the X-ray crystal structure of ammonia borane was determined in 1956, the BN bond length was estimated between 1.5 and 1.6 Å with a tetragonal space group $I4mm$.[126,127] Four decades later, a neutron diffraction structure of ammonia borane obtained at 200 K revealed different results, including an orthorhombic space group ($Pmn2_1$) and a BN bond length of 1.58 Å.[135] It has since been shown that ammonia borane at standard pressure undergoes a crystal phase change from orthorhombic ($Pmn2_1$) at lower temperature to tetragonal ($I4mm$) as the temperature rises above 225 K.[137,139,140] Raman spectra of the orthorhombic solid crystal reveals a BN stretch near 790 cm^{-1} (789 cm^{-1} at 224 K and 794 cm^{-1} at 88 K).[137,139] Temperature dependent IR and NMR measurements from 10-200 K suggest that the local symmetry of the BH_3NH_3 molecules is lower than that obtained from diffraction data at 10 K, and the numbers of modes observed in the far-IR exceeds predictions from group

theory.[137,142] Furthermore, this region of the spectrum exhibits complex temperature dependence well below the phase transition near 220 K that could be attributed to subtle changes in the dihydrogen bonding network.[137,142] The predicted number of vibrational modes in the tetragonal phase of ammonia borane is 21, 12 of which are Raman active based on the $I4mm$ crystal symmetry.[137] The $Pmn2_1$ symmetry of orthorhombic ammonia borane lifts the E degeneracy to A' and A'' as well as activating a number of acoustic and librational low-energy modes which results in 45 vibrational degrees of freedom (all Raman active).[137,138]

Computational investigations have focused primarily on anti-parallel orientations of nearest neighbor in isolated clusters of $(BH_3NH_3)_{n\leq 8}$[146–149,151,152,157,160,167] with little consideration of clusters that mimic either the tetragonal or orthorhombic crystal structures[98,152,153,156] in which the dipole moments of the BH_3NH_3 molecules are more closely aligned. Dipole-dipole interactions as well as dihydrogen bonding both have a stabilizing effect on $(BH_3NH_3)_n$ clusters. A symmetry adapted perturbation theory (SAPT) analysis of the C_{2h} dimer found the electrostatic component was the largest attractive contribution to the interaction energy, more than twice the magnitude of the contribution from either dispersion or induction.[148] Using Hartree-Fock (HF) and second-order Møller-Plesset perturbation theory (MP2) with a 6-31G(d) basis set, Dillen and Verhoeven noted that the BN bonds contract and BN stretching frequencies shift to higher energy in $(BH_3NH_3)_n$ isolated gas-phase clusters and models of the crystal as n increases, thereby leading to improved agreement with experimental observations.[152] One theoretical analysis of a crystal structure model containing nine BH_3NH_3 subunits reported that the contraction of the BN bond

length arises primarily from dipole-dipole interactions whereas dihydrogen bonding contributes nearly as much as dipole/dipole interaction to the interaction energy.[156] A separate computational study of smaller BH_3NH_3 clusters (n=3,4,5) found that dihydrogen bonding was the primary stabilizing interaction.[160]. A recently published paper using density functional theory has also indicated that ammonia borane clusters have strong zwitterionic character that gives rise to strong cooperative effects when arrangement in an anti-parallel fashion for clusters up to $(BH_3NH_3)_{54}$.[167]

This paper presents a coordinated theoretical and experimental investigation of ammonia borane. For the first time, the experimental spectrum of solid ammonia borane is determined using Raman under liquid nitrogen spectroscopy (RUNS).[168] The effects of size and orientation on the BN bond length and stretching frequencies are examined computationally both in isolated clusters of BH_3NH_3 (such as those shown in Figure 3.1) and in models of the orthorhombic crystalline solid (such as those shown in Figure 3.2). Finally, the computational results for the various crystal models are compared to experimental spectroscopic (RUNS, Raman, IR, INS) and structural data.

3.2 Methodology

3.2.1 Computational Details

Full geometry optimizations and harmonic vibrational frequency computations were performed on the BH_3NH_3 monomer (1-C_{3v}, Figure 3.1) using a variety of methods and basis sets. The density functionals M06L[169], M06-2X[35], and B3LYP[33,34] were compared to second-order Møller-Plesset perturbation the-

ory (MP2[30]), coupled cluster singles and doubles (CCSD[32]), and coupled cluster singles, doubles and perturbative triples (CCSD(T)[32]). Three different correlation-consistent families of basis sets[170] were considered, polarized valence (i.e. cc-pVXZ, denoted VXZ where X=D,T,Q), augmented polarized valence basis sets (i.e. aug-cc-pVXZ, denoted aVXZ where X=D,T,Q), and polarized core valence (i.e. cc-pCVXZ, denoted CVXZ where X=D,T,Q). Two Pople-style split valence basis sets, 6-31++G(d,p) and 6-311++G($2df,2pd$)[171], were also used in conjunction with B3LYP, M06L, M06-2X and MP2. The frozen core approximation was invoked for all MP2, CCSD, and CCSD(T) computations, excluding the one 1s-like orbitals for B and N from the electron correlation calculations. All MP2 and density functional computations were performed using the `Gaussian09`[172] software package. CCSD and CCSD(T) computations were done using `CFOUR`[117]. Spherical functions ($5d, 7f, 9g$) were used instead of Cartesian functions ($6d, 10f, 15g$). Cartesian forces did not exceed 1.0×10^{-5} E_h/a_0.

MP2, M06L, M06-2X, and B3LYP computations with the 6-31++G(d,p), 6-311++G($2df,2pd$) and aVXZ (where X=D,T,Q) basis sets were performed to characterize the optimized geometry and harmonic vibrational frequencies of the C_{2h} dimer (2-C_{2h}, Figure 3.1). CCSD and CCSD(T) optimized geometries and harmonic vibrational frequencies were also obtained for the C_{2h} dimer with aVXZ (where X=D,T) basis sets.

Based on the calibration performed for the monomer and C_{2h} dimer (*vida infra*), the M06-2X functional and 6-311++G($2df,2pd$) basis set were selected to perform full geometry optimizations and compute the harmonic vibrational frequen-

cies for the clusters depicted in Figure 3.1 that were taken from Ref. 152. In the crystal structure models, only the central BH_3NH_3 molecule (circled in Figure 3.2) was optimized. The corresponding M06-2X/6-311++G($2df, 2pd$) harmonic vibrational frequencies were then computed. In all harmonic vibrational frequency computations the ^{11}B isotope was used unless explicitly stated otherwise.

3.2.2 Experimental Details

Solid phase Raman spectra and RUNS spectra were obtained using a LabRAM HR Evolution Raman spectrometer with an 1800 gr/mm grating. The excitation source of 532 nm was obtained by using the second harmonic of a continuous Nd:YAG laser. RUNS spectra were taken by holding the sample in an insulating ceramic bowl and then immersing the sample in liquid nitrogen.

3.3 Results and Discussion

3.3.1 Experiment

Figure 3.3 contains the full (500-4000 cm^{-1}) Raman spectrum of tetragonal ammonia borane at 298 K. Table 3.1 lists the intramolecular vibrational frequencies of ammonia borane at near ambient temperatures using Raman and IR spectroscopy. The room temperature Raman spectrum of tetragonal ammonia borane performed in this study shows good agreement (within $\pm$ 5 cm^{-1}) with previous results obtained using Raman spectroscopy at 298 K for the NH, BH, and BN stretching regions.[137]

The intermolecular (100-500 cm^{-1}), BN stretching (600-950 cm^{-1}), BH deformation (1100-1400 cm^{-1}), NH deformation (1500-1800 cm^{-1}), BH stretching (2200-2600 cm^{-1}) and NH stretching (3100-3400 cm^{-1}) regions of ammonia borane at 77

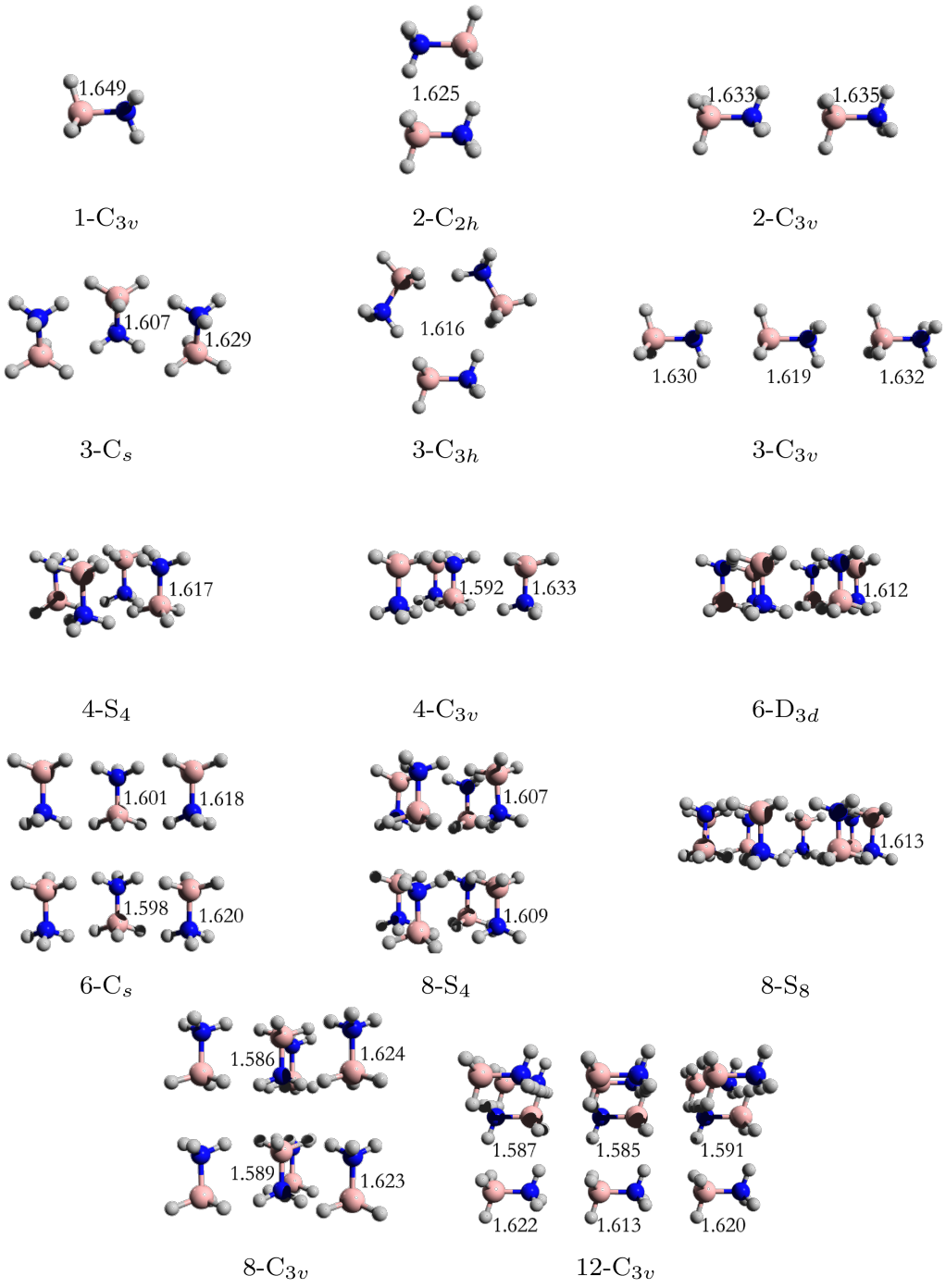

Figure 3.1. Isolated clusters and symmetry unique BN bond lengths (in Å) of the M06-2X/6-311++G($2df, 2pd$) optimized clusters where the labels denote the point group symmetry and the number of fragments.

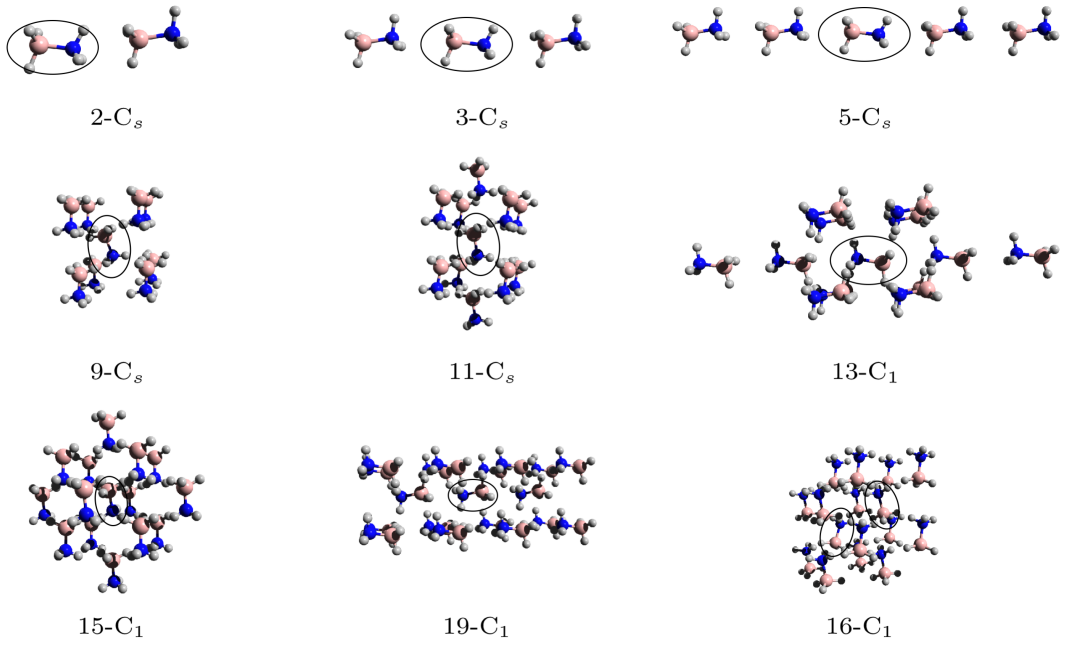

Figure 3.2. Models constructed from orthorhombic crystal structure of BH_3NH_3 where the circle denotes the fragment being optimized in the field of the surrounding $n-1$ fragments ($n-2$ in 16-C_1).

K are shown in Figure 3.3. Table 3.2 contains the RUNS data for orthorhombic ammonia borane as well as Raman, IR, and inelastic neutron scattering (INS) peaks at cryogenic temperatures. The N_2 stretching mode appears as a sharp peak at 2330 cm^{-1} in Figure 3.3.[168] Below 100 K, there are more observed Raman peaks than predicted based on the $Pmn2_1$ space group due to overtone bands as well some peaks that were unable to be assigned, denoted as 'overtone' and 'unassigned' in Table 3.2 taken from Ref. 137. In ammonia borane at cryogenic temperatures, another intermolecular mode is observed at 156 cm^{-1} and the dominant low energy mode shifts to higher energy, the ^{10}BN and ^{11}BN stretches shift to slightly higher energy, seven separate peaks are observed in the BH stretching region, and in the NH stretching region the three peaks at 298 K decompose into five peaks. The spectrum predicted using RUNS seem to be in good agreement with previous Raman data at 88 K, although some new peaks were observed at 3332, 2313, and 2272 cm^{-1}.[137]

3.3.2 Calibration of BH_3NH_3 and $(BH_3NH_3)_2$

Although a wide range of post-HF and DFT methods can provide a reliable description of the structure and vibrational frequencies of BH_3NH_3, the frequency shifts induced by the interactions in BH_3NH_3 clusters is more challenging (Supporting Information). The anti-parallel C_{2h} dimer (cluster 2-C_{2h} in Figure 3.1) is the global minimum at all levels of theory considered here, with an electronic binding energy of -15.81 kcal mol^{-1} at the CCSD(T)/aTZ level of theory, in good agreement with the CCSD(T)/CBS binding energy of -15.4 kcal mol^{-1} computed using MP2/aTZ optimized geometries.[165] The two BN stretching modes in the C_{2h} dimer experience substantial shifts to higher energy relative to the monomer (+60 cm^{-1} for the a_g

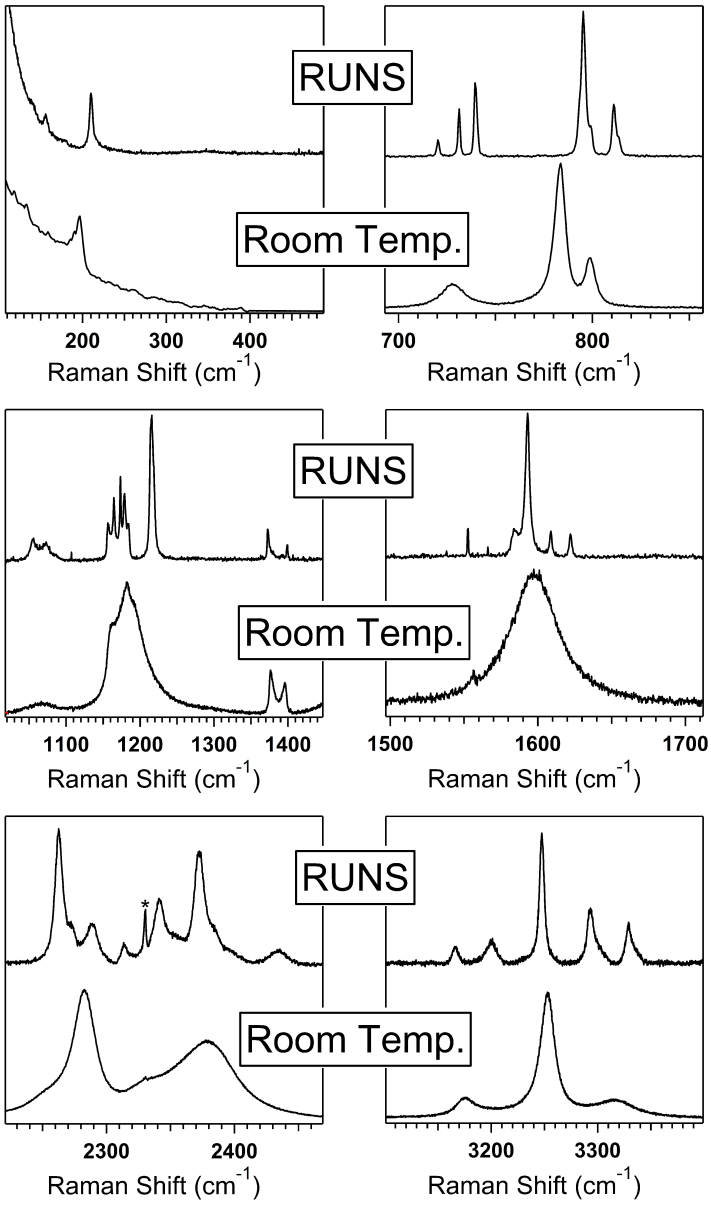

Figure 3.3. Comparison of ammonia borane at room temperature and at 77 K under liquid nitrogen spectroscopy. N_2 stretch denoted by (*).

Table 3.1. The intramolecular vibrations of ammonia borane at or near ambient temperatures.

	Ref 137 Raman 298 K	This work Raman 298 K	Ref 142 IR 270 K
NH stretch	3316	3315	3323
	3250	3252	3253
	3176	3175	3180
BH stretch	2375	2376	2360
	2328	2330	
	2279	2280	2281
		2221	
			2217
NH_3 deformation	1600	1599	1602
			1546
	1450		1452
		1393	1393
		1378	1375
	1357		
BH_3 deformation	1189	1187	1225
	1155	1165	1182
NBH rock	1065		1072
	727	728	726
BN stretch	800	799	799
	784	783	784

Table 3.2. The intramolecular vibrations of ammonia borane at cryogenic temperatures.

	Raman 88 K Ref 137	RUNS 77 K This work	INS 30 K Ref 136	IR 10 K Ref 142
NH stretch	3338			3341
		3332		3332
	3331	3329		
	3300	3299		3309
	3290	3293		3296
	3247	3248		3252
	3240			3230
unassigned	3202	3201		3200
unassigned	3165	3167		3164
				3060
				2546
BH stretch	2434	2435		2433
	2400	2396		
		2384		2380
unassigned	2373	2373		
	2356			
	2343	2341		2344
		2313		2313
	2289	2289		2291
		2272		
	2263	2263		2261
				2231
				2169
				2120
				2103
NH_3 deformation	1622	1622		1622
	1609	1609		1609
	1593	1593		
	1585	1584	1580	1584
		1566		1572
		1552		
		1538		
overtone	1470		1474	1467
overtone	1454	1453	1452	1445
	1400	1399	1423	
	1374	1372	1367	
BH_3 deformation	1220	1216	1231	
	1214	1184	1213	1214
	1180	1179	1189	1182
	1173	1174	1177	1173
	1166	1165		1160
	1157	1157	1154	
NBH rock	1086	1073	1098	1087
	1073	1055	1076	1055
	1056	811	1049	1014
^{10}BN stretch	813	811		814
	810			811
^{11}BN stretch	798	799	798	799
	794	795		795
NBH rock	740	740		740
	731	731	737	731
	721	720	726	720
				712

symmetric stretch and +68 cm^{-1} for the b_u asymmetric stretch at the CCSD(T)/aTZ level of theory). Although these shifts are reproduced with several model chemistries, the combination of the M06-2X functional and 6-311++G($2df, 2pd$) basis set is among the least demanding. The frequency shifts computed at this level of theory are within 2 cm^{-1} and the electronic binding energy is within 0.3 kcal mol^{-1} of the corresponding CCSD(T)/aTZ values. Based on these results, our subsequent investigations into crystal models and isolated gas-phase clusters have been carried out using the M06-2X functional and the 6-311++G($2df, 2pd$) basis set.

3.3.3 Isolated Clusters of $(BH_3NH_3)_n$

A second dimer configuration with C_{3v} symmetry is also shown in Figure 3.1. In fact, at least two minima have been characterized at the M06-2X/6-311++G($2df, 2pd$) level of theory for all $(BH_3NH_3)_n$ clusters where $n = 2, 3, 4, 6, 8$. Only one configuration for the largest cluster, $(BH_3NH_3)_{12}$, has been examined. All these isolated gas-phase clusters are shown in Figure 3.1 along with the symmetry unique BN bond lengths in Å. In addition, Table 3.3 lists the electronic binding energies (E_{bind}), normalized binding energies per monomer (E_{bind}/n, denoted E_n), and the largest ^{11}BN stretching frequencies (ω_{BN}^{max}) for each of the fully optimized $(BH_3NH_3)_n$ clusters. For this discussion, the isolated clusters are divided into three categories: linear (2-C_{3v}, 3-C_{3v}), symmetry equivalent (2-C_{2h}, 3-C_{3h}, 4-S_4, 6-D_{3d}, 8-S_4, 8-S_8), and centrally coordinated (3-C_s, 4-C_{3v}, 6-C_s, 8-C_{3v}, 12-C_{3v}).

It can be seen in Table 3.3 that the symmetry equivalent clusters tend to be the lowest energy isomers (2-C_{2h}, 3-C_s, 4-S_4, 6-D_{3d}, and 8-S_4), except cluster 3-C_s which is 0.20 kcal mol^{-1} lower in energy than the symmetry equivalent trimer

(cluster 3-C_{3h}). Additionally, the cooperative effects between BH_3NH_3 molecules are most evident in the electronic binding energies of clusters 2-C_{2h}, 3-C_s, 4-S_4, 6-D_{3d}, and 8-S_8 (Table 3.3). Cluster 2-C_{2h} has an electronic binding energy of -6.94 kcal mol^{-1} whereas cluster 3-C_s has an electronic binding energy of -29.20 kcal mol^{-1}. Although the number of intermolecular contacts increases by a factor of two, E_{bind} increases by more than 420%. In a similar fashion, cluster 4-S_4 has four monomers with four nearest neighbor contacts comparable to the one in the 2-C_{2h} dimer, yet the electronic binding energy increases by more than 700% to -49.08 kcal mol^{-1}. Clusters 6-D_{3d} and 8-S_8 have electronic binding energies of -82.76 kcal mol^{-1} for the 6-D_{3d} cluster and -108.52 kcal mol^{-1} for the 8-S_8 cluster, represent increases of more than 1100% and 1500%, respectively.

The shortest BN bond lengths shown in Figure 3.1 occur in the centrally coordinated clusters, ranging from 1.607 to 1.585 Å. Of the centrally coordinated clusters 4-C_{3v}, 8-C_{3v}, and 12-C_{3v} have the largest contractions of BN bond lengths (from -0.057 to -0.064 Å) relative to the 1-C_{3v} monomer. The largest BN stretching frequencies are also observed in the centrally coordinated clusters, as seen in Table 3.3. Figure 3.4 shows the shift in BN stretching frequencies with respect to the monomer BN stretch at 685 cm^{-1} upon complexation. The highest energy BN stretching frequencies are observed in the central molecule of clusters 4-C_{3v}, 8-C_{3v}, 12-C_{3v}. The largest frequency shifts are +167 and +175 cm^{-1} observed in the 8-C_{3v} and 12-C_{3v} clusters.

Table 3.3. Electronic binding energies (E_{bind} in kcal mol^{-1}), the normalized electronic binding energy (E_n in kcal mol^{-1}), and highest energy BN stretching modes (ω_{BN}^{max} in cm^{-1}) of isolated BH_3NH_3 clusters (n=2-4,6,8,12) at the M06-2X/6-311++G($2df, 2pd$) level of theory.

Linear	E_{bind}	E_n	ω_{BN}^{max}
2-C_{3v}	−6.94	−3.47	730
3-C_{3v}	−15.71	−5.24	770
Symmetry Equivalent	E_{bind}	E_n	ω_{BN}^{max}
2-C_{2h}	−16.10	−8.05	750
3-C_{3h}	−27.00	−9.00	777
4-S_4	−49.08	−12.27	771
6-D_{3d}	−82.76	−13.79	785
8-S_8	−108.52	−13.57	781
8-S_4	−13.57	−14.72	802
Centrally Coordinated	E_{bind}	E_n	ω_{BN}^{max}
3-C_s	−29.20	−9.73	794
4-C_{3v}	−39.44	−9.86	830
6-C_s	−73.74	−12.29	823
8-C_{3v}	−97.55	−12.19	852
12-C_{3v}	−158.08	−13.17	861

3.3.4 Intramolecular Modes of Crystal Models

Crystal models 2-C_s to 19-C_1 (Figure 3.2) were used to model the $Pmn2_1$ crystal structure of ammonia borane, with coordinates taken from the neutron diffraction study at 200 K by Klooster *et. al.*[135]. The central BH_3NH_3 molecule around which the model crystal environment is built is denoted by a circle in Figure 3.2 to clearly indicate which BH_3NH_3 was optimized in the field of the surrounding $n-1$ molecules constrained to their crystal structure geometries. In model 16-C_1, two BH_3NH_3 subunits were allowed to fully optimize in the field of the surrounding $n-2=14$ subunits, creating a conjoined model of two staggered 9-C_s crystal structures. The intramolecular BN bond length of the optimized central BH_3NH_3 molecule (R_{BN}) as well as the deviations from the optimized monomer 1-C_{3v} (ΔR_{mon}) and the crystal structure geometry (ΔR_x) are reported in Table 3.4 along with the shortest intermolecular H-H distance (R_{HH}). Several different stretching modes are listed in Table 3.4 including the ^{11}BN, ^{10}BN, symmetric BH and NH stretching frequencies (ω_{11}, ω_{10}, ω_{BH}, and ω_{NH}) and the corresponding frequency shifts compared to the 1-C_{3v} monomer. For all the BN stretching modes, the frequency shifts were the same for the ^{11}BN and ^{10}BN stretches when compared to the ^{11}BN and ^{10}BN stretching frequencies of the monomer (685 and 701 cm^{-1}, respectively). In this case, the symmetric BH and NH stretches are defined as the XH stretching modes in which all hydrogens are elongating or contracting at the same time (even though the environments of each XH bond are slightly different). The harmonic frequencies, IR intensities and Raman activities for each structure can be found in the SI.

By allowing the geometry of the central BH_3NH_3 molecule to relax, the BN

bond lengthens by no more than 0.05 Å for all the models considered in this investigation. As the size of the model grows, the BN bond contracts once again, approaching the crystal bond length of 1.58 Å while the BN stretching frequency moves to higher energy and the BH and NH stretching frequencies shift to lower energy.[135]. The HF/6-31G(d) computations reported in Ref. 152 for many of the same crystal models agree reasonably well with the BN stretching frequencies computed here.[152] However HF/6-31G(d) consistently overestimates the BH and NH stretches by more than 100 and 300 cm^{-1}, respectively, compared to experimental values.[152]

The head-to-tail crystal models (2-C_s, 3-C_s, 5-C_s) have the longest BN bond lengths, largest intermolecular H-H distances, and smallest frequency shifts. Including the nearest neighbor BH_3NH_3 molecules (9-C_s) does not perturb the BN bond length or BN and BH stretches significantly but the NH stretch decreases in energy by nearly 50 cm^{-1}. 11-C_s and 13-C_1 have both head-to-tail BH_3NH_3 interactions and nearest neighbor hydrogens which have a larger impact on the BN bond length and stretching frequency. Models 11-C_s and 13-C_1 have nearly identical BN bond lengths (within 0.002 Å), BN stretching frequencies (within 7 cm^{-1}), and BH and NH stretching frequencies (within 1 cm^{-1}) indicating that increasing the length of the head-to-tail interaction beyond the two closest BH_3NH_3 molecules has little effect. The 15-C_1 crystal model has a slightly longer (by 0.01 Å) BN bond length, the BN and BH stretching frequencies decrease by nearly 30 and 15 cm^{-1}, respectively, and the NH frequencies increase by 10 cm^{-1} compared to 13-C_1. 19-C_1 has the smallest BN bond length of 1.606 Å and largest frequency shifts of +109 cm^{-1} and −65 for the BN and NH stretches. Allowing two BH_3NH_3 molecules in a crystal

model to relax (16-C_1) gives bond lengths and frequencies consistent with 9-C_s for the results listed in Table 3.4. The harmonic ^{11}BN and ^{10}BN stretching frequencies computed for model 19-C_1, 795 and 811 cm^{-1}, are within two cm^{-1} of the experimentally observed RUNS frequencies for ammonia borane at 77 K. That type of fortuitous agreement is not expected in general due to anharmonic effects. Indeed, the experiment BH stretching frequencies are overestimated by more than 20 cm^{-1} by the harmonic M06-2X/6-311++G($2df, 2pd$) frequencies. The differences are larger for the NH stretching frequencies (on the order of 100 cm^{-1}).

3.3.5 Intermolecular Modes of Crystal Models

The far-IR energy (below 500 cm^{-1}) lattice and intermolecular modes are listed in Table 3.5 for crystal models 9-C_s, 16-C_1, 19-C_1 along with the experimental infrared (IR), inelastic neutron scattering (INS), and Raman frequencies at various temperatures.[136,138,142] 16-C_1 has more vibrational degrees of freedom by virtue of allowing two BH_3NH_3 molecules to relax which has a larger impact on the intermolecular modes, giving results that are more consistent with experiment. There is very little coupling of vibrational modes between the two optimized subunits of model 16-C_1. However, the BH_3 and NH_3 twists and rocks are slightly coupled causing these modes to shift by up to $\pm$20 cm^{-1} compared to 9-C_s. Although some modes (NH_3 twist, BH_3 rock, NH_3 rock, and translation) agree fairly well with the IR spectrum at 10 K, without including anharmonic effects it is a tentative correlation at best.[142]

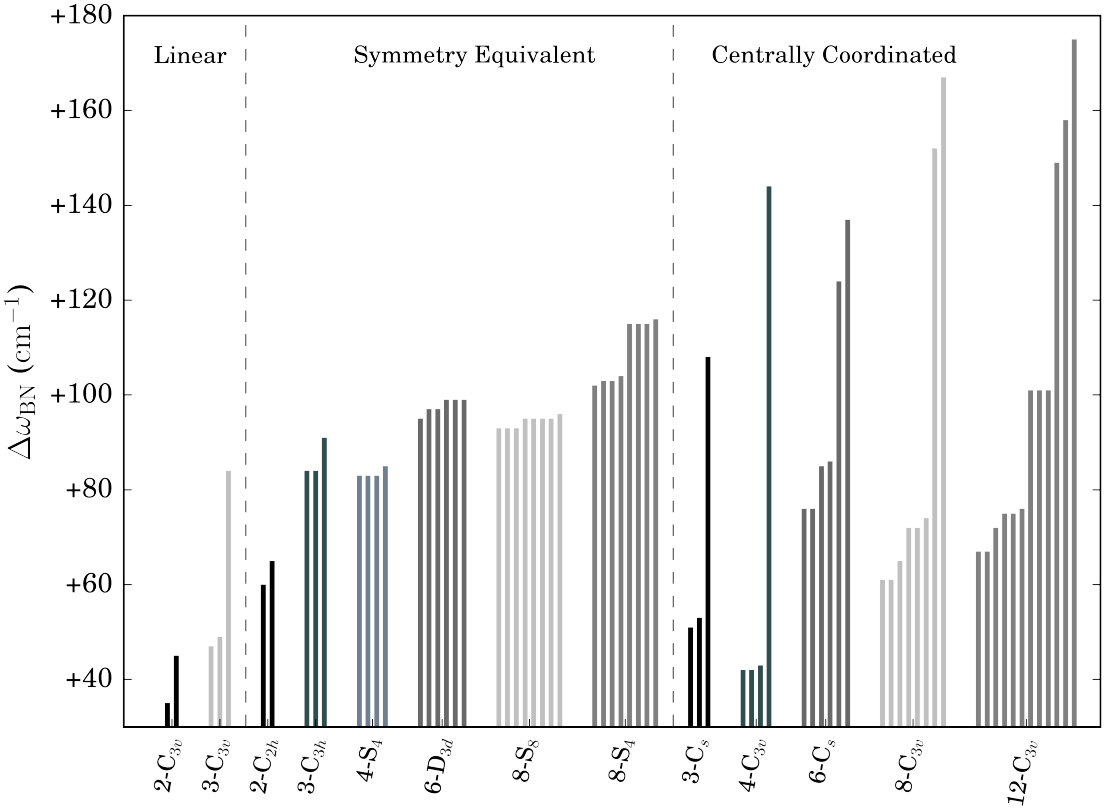

Figure 3.4. The frequency shifts (in cm^{-1}) of the BN stretching modes from the monomer BN stretch (685 cm^{-1}) upon complexation for the isolated clusters.

Table 3.4. BN bond length (R_{BN} in Å), change in BN bond length from optimized isolated monomer 1-C_{3v} and the crystal structure geometry (ΔR_{mon} and ΔR_x in Å), shortest intermolecular H-H distance (R_{HH} in Å), the BN, symmetric BH and symmetric NH stretching frequencies (ω_{11}, ω_{10}, ω_{BH}, and ω_{NH} in cm^{-1}), and the BN, BH, and NH frequency shifts ($\Delta\omega_{BN}$, $\Delta\omega_{BH}$, and $\Delta\omega_{NH}$ in cm^{-1}) for all the crystal models in Figure 2 at the M06-2X/6-311++G($2df, 2pd$) level of theory.

	R_{BN}	ΔR_{mon}	ΔR_x	R_{HH}	ω_{11}^a	ω_{10}^b	ω_{BH}	ω_{NH}	$\Delta\omega_{BN}$	$\Delta\omega_{BH}$	$\Delta\omega_{NH}$
2-C_s	1.633	−0.016	0.048	2.34	729	745	2478	3498	+44	−16	0
3-C_s	1.633	−0.016	0.048	2.60	729	745	2472	3491	+44	−23	−7
5-C_s	1.630	−0.019	0.046	2.60	735	752	2468	3492	+50	−27	−6
9-C_s	1.629	−0.020	0.045	1.96	737	752	2471	3443	+52	−23	−55
11-C_s	1.616	−0.033	0.032	1.95	769	786	2467	3441	+85	−28	−57
13-C_1	1.614	−0.036	0.029	1.95	776	793	2465	3440	+91	−29	−58
15-C_1	1.624	−0.025	0.039	2.04	747	764	2449	3451	+62	−46	−47
19-C_1	1.606	−0.043	0.022	1.95	794	811	2455	3432	+109	−40	−65
16-C_1 R	1.629	−0.020	0.044	1.96	735	752	2473	3439	+50	−22	−59
L	1.626	−0.023	0.041	1.94	743	760	2452	3446	+58	−43	−51
9-C_1 [152]	1.653	−0.036		2.03	684		2560	3706	+80	+0	+15
11-C_1 [152]	1.625	−0.064		2.01	760		2561	3711	+156	+1	+20
19-C_1 [152]	1.612	−0.077		2.00	798		2544	3704	+194	−16	+13
Exp't	1.58[c]			2.02[c]	795[d]	811[d]	2435[d]	3332[d]			

[a] ^{11}BN stretching frequency

[b] ^{10}BN stretching frequency

[c] Reference 135

[d] RUNS 77 K. This work.

Table 3.5. The low energy intermolecular lattice modes (in cm^{-1}) of solid ammonia borane.

				IR 10 K	Raman 15 K	INS 30 K	Raman 77 K
	9-C_s	16-C_1	19-C_1	Ref 142	Ref 138	Ref 136	This work
BH_3 twist	371	397	352	359	337	399	
		390		337	337	334	
				319			
NH_3 twist	198	236	193	256	221	202	210
		219		235	212		
				209			
BH_3 rock	162	170	170	175	185	171	156
		156					
NH_3 rock	152	147	158	141	159	150	
		138		128	150		
Rotation	127	136	117		116		
		131					
Translation	111	115	116				
		113					
Translation	78	90	104	87	100	94	
		75					

3.3.6 Correlation of Spectrochemical Physical Properties

Figure 3.5a shows the correlation between changes in BN bond lengths (ΔR_{BN}) and BN stretching frequency shifts ($\Delta\omega_{BN}$) upon complexation for all the isolated clusters as well as the optimized BH_3NH_3 unit of the crystal structures in Figure 3.2. This correlation continues in the BN bond lengths and BN stretching frequencies (shown in Figure 3.5b). There is no clear correlation between the BN frequency shifts and the number of monomers or the electronic binding energies or the normalized binding energy (Figures 3.5c, 3.5e, and 3.5f). Figure 3.5d shows the increase in electronic binding energy as the number of monomers increases in the isolated clusters, as well as the correlation for both the symmetry equivalent (Equiv) and centrally oriented (Center) clusters.

3.4 Conclusions

Raman under liquid nitrogen spectroscopy (RUNS) shows good agreement with previous low temperature spectroscopic studies performed on the orthorhombic polymorph of ammonia borane and provides a more resolved spectrum, particularly in the BH and NH stretching regions. A rigorous comparison of methods and basis sets on the monomer and the C_{2h} dimer was carried out (Supporting Information) which determined that the M06-2X/6-311++G($2df, 2pd$) level of theory provides good agreement between computational demand and an accurate description of the unusual inter- and intramolecular interactions of $(BH_3NH_3)_n$. Minimum energy isolated clusters show higher energy BN stretching modes for clusters arranged around a central BH_3NH_3 molecule, with frequency shifts as large as +175 cm^{-1} for the 12-C_{3v}

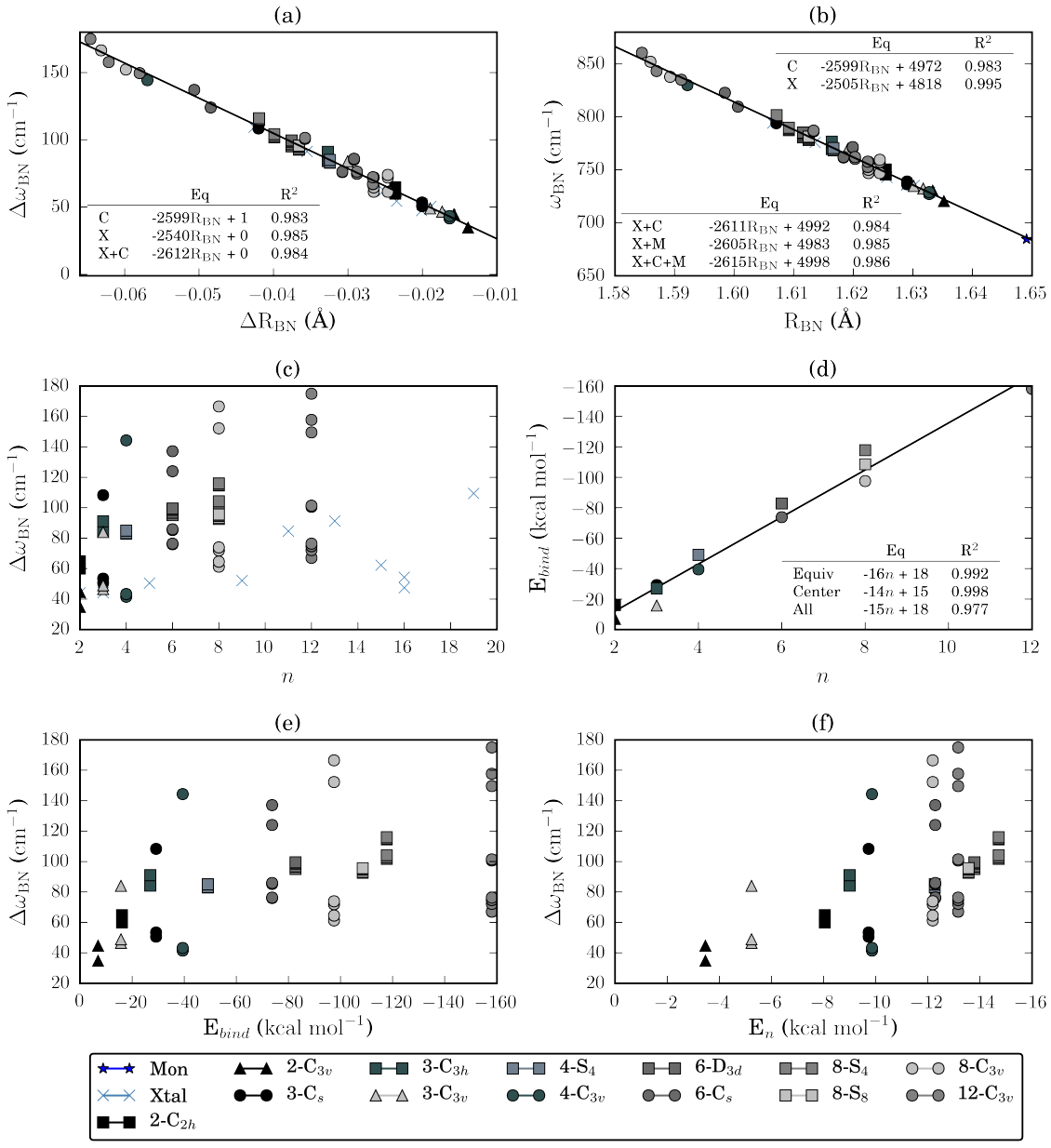

Figure 3.5. Plots of the correlation between various properties of ammonia borane clusters and crystal models. The table inserts contain the linear regression lines and R^2 values for sets of data, including the isolated clusters (Cluster, C), the crystal models (Xtal, X) and the BH_3NH_3 monomer (Mon, M). See Section 3.6 for additional details.

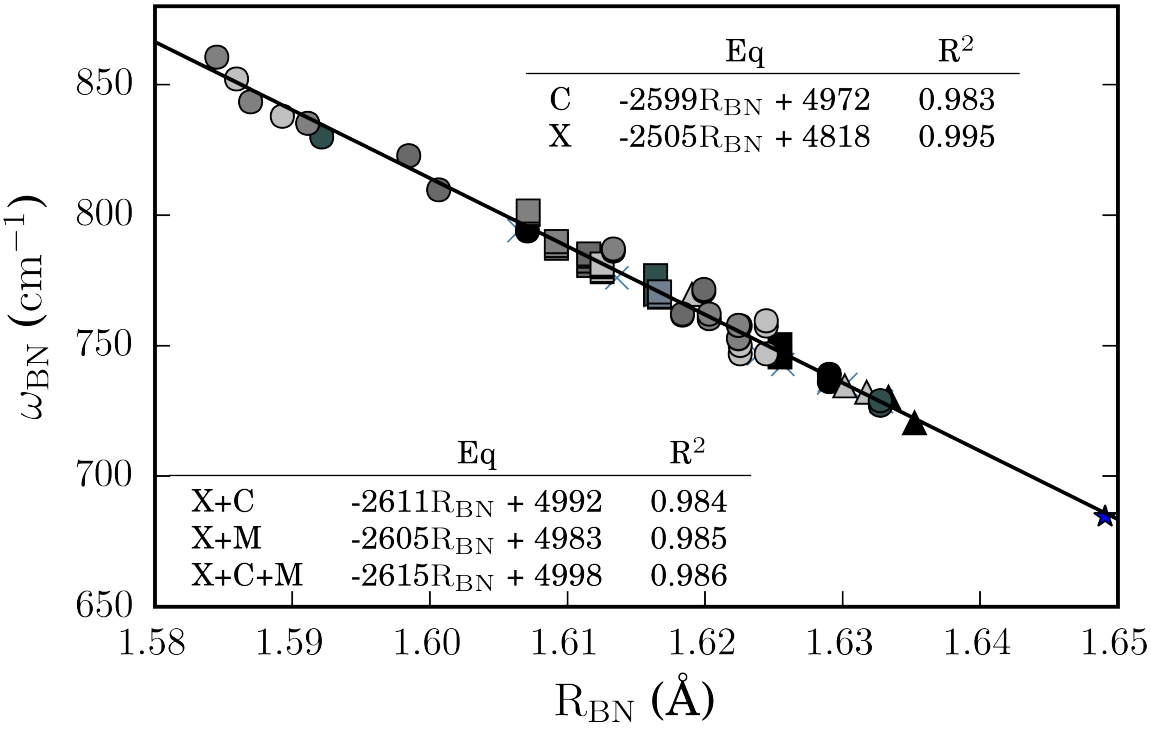

Figure 3.6. Table of Content Image

cluster. The 19-C_1 crystal model has a BN stretching frequency in embarrassingly good agreement (within 2 cm^{-1}) of the experimental RUNS data. This corresponds to a frequency shift +109 cm^{-1} relative to the BN stretching frequency of the isolated monomer. For the intermolecular and lattice modes of solid ammonia borane, 16-C_1 presents the best agreement with experiment likely due to the optimization of two central fragments rather than just one.

CHAPTER 4

Investigating non-coventional hydrogen bonded $HXH\cdots YH_2$ complexes

J. Coleman Howard performed all computations on the H_2O dimer. Computations on the H_2O/H_2S and $(H_2S)_2$ dimers were carried out by Katelyn M. Dreux.

4.1 Introduction

The importance of hydrogen bonding involving the hydroxyl (OH) group is widely appreciated, and the water dimer has long served as a theoretical and experimental paradigm for probing this important interaction.[64–69] The isovalent thiol or sulfhydryl (SH) group is also capable of participating in analogous non-covalent interactions that are sometimes referred to as weak hydrogen bonds or sulfur-containing hydrogen bonds. The properties of molecules and reactions involving H_2S and other sulfur-containing molecules have solicited few investigations since the 1970's.[70–73] Despite the prevalence and importance of these attractive SH interactions, particularly in biochemical systems containing cysteine residues[81,173–177] or other thiol-containing biomolecules,[74–86,178,179] the homo- and heterogeneous S analogues of $(H_2O)_2$ depicted in Figure 4.1 have received comparatively little attention. Investigations into the homogeneous $(H_2S)_2$ and heterogeneous H_2O/H_2S dimers provide insight into interactions with sulfur-containing molecules as well as accurate energetics and vibrational signatures to compare with the H_2O dimer.

In the case of the heterogeneous H_2O/H_2S complex, two different but energetically competitive hydrogen bonding motifs can be adopted[70] in which the atom accepting the hydrogen bond, denoted Y in Figure 4.1, can be either O or S, and $HXH\cdots YH_2$ is used in the text to indicate the directionality of the hydrogen bond in the heterodimer. Both structures have been observed experimentally in cryogenic matrices.[180,181] MP2 and CCSD(T) computations[182–184] indicate that the $HOH\cdots SH_2$ arrangement (i.e., X=O and Y=S) is favored over $HSH\cdots OH_2$ (i.e., X=S and Y=O), although the opposite conclusion can be reached if dynamical electron correlation is not included.[185–187] The $HOH\cdots SH_2$ configuration has a CCSD(T) electronic dissociation energy (D_e) of 2.90 kcal mol^{-1} near the complete basis set (CBS) limit whereas the binding is slightly weaker (2.66 kcal mol^{-1}) for the $HSH\cdots OH_2$ structure.[184,188] For comparison, the magnitude of the dissociation energy is *ca.* 2 kcal mol^{-1} larger, or approximately 5 kcal mol^{-1}, for $(H_2O)_2$ at the CCSD(T) CBS limit.[1,189–191]

The homogeneous $(H_2S)_2$ system adopts a hydrogen bonding arrangement that is similar to its isovalent counterpart $(H_2O)_2$, but there are a couple of key structural differences. The distance between the heavy atoms in Figure 4.1, $R(X\cdots Y)$, is appreciably larger for X,Y=S than for X,Y=O.[66,192–195] Additionally, the angle between the $X\cdots Y$ axis and the vector of the bisector of the H−Y−H angle of the acceptor fragment decreases noticeably when O is replaced by S (from *ca.* 125° to *ca.* 90°) which is a trend that can also be observed in other complexes that form hydrogen bonds with divalent S.[196] The H_2S dimer has been detected both in cryogenic matrices and the gas phase.[2,181,193,197,198] MP2 and CCSD(T) computations

indicate the hydrogen bond in $(H_2S)_2$ is appreciably weaker than the heterogeneous system.[2,75,76,183,184,187,188,199–212] It has an electronic dissociation energy of only 1.69 kcal mol^{-1} near the CCSD(T) CBS limit.[184,212]

The four SH stretching frequencies of $(H_2S)_2$ and OH stretching frequencies of $(H_2O)_2$ have been measured in the gas phase[2,69,193] but not in the mixed dimer. Matrix isolation experiments[197–199,213] suggest that definitive assignment of the stretching vibrations in the heterogeneous H_2O/H_2S system could be challenging in the gas phase due to overlap with corresponding vibrational bands from the homogeneous H_2S and H_2O dimers that would also likely be present in the experiments. Fortunately, sophisticated quantum chemistry computations can be quite helpful in such situations. The SH stretching frequencies of the H_2S dimer, for example, are reliably reproduced when CCSD(T) harmonic vibrational frequencies are combined with MP2 anharmonic corrections from second-order vibrational perturbation theory (VPT2). With a high-quality quadruple-ζ correlation consistent basis set for both methods, this procedure of combining CCSD(T) harmonic frequencies with MP2 VPT2 corrections systematically underestimates the stretching frequencies with an average absolute deviation of 14 cm^{-1}.[212] For the H_2O dimer, a similar VPT2 analysis was also performed with the CCSD(T) method, and the average absolute deviation from the experimental stretching frequencies was only 2 cm^{-1}.[1,214]

This investigation extends these prior computational vibrational analyses to all four dimer systems corresponding to the unique X,Y=O,S permutations in Figure 4.1. For the three sulfur-containing dimers, canonical CCSD(T) anharmonic frequencies from VPT2 computations are presented for the first time. By examining

the anharmonic fundamental frequencies, overtones, combination bands and their corresponding infrared (IR) intensities at the same high level of theory, this study provides insight into the gas-phase IR spectra of these species that will help distinguish spectral features of the two mixed dimer conformations from those of the two homogeneous dimers. The effects of the harmonic and anharmonic zero-point vibrational energy (ZPVE) on the energetics of mixed dimer configurations ($HOH\cdots SH_2$ and $HSH\cdots OH_2$) is also examined.

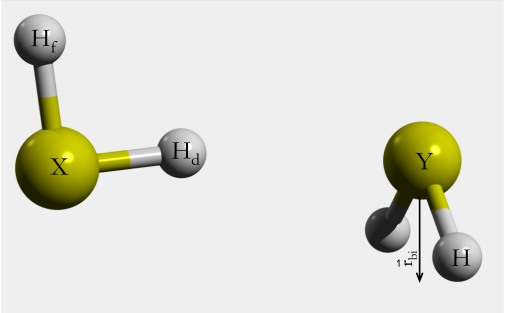

Figure 4.1. General C_s structure of the $HXH\cdots YH_2$ complexes, where X,Y=O,S and H_f, H_d and H indicate the free, donor, and acceptor hydrogens, respectively. $\vec{r}_{bi}$ is the vector bisecting Θ(HYH).

4.2 Computational Details

Full geometry optimizations and harmonic vibrational frequency computations of all dimer structures and their respective monomers were performed using analytic gradients and Hessians for second-order Møller-Plesset perturbation theory[30] (MP2) and coupled-cluster singles, doubles, and connected triples[32] (CCSD(T)) methods while employing a family of correlation consistent family of basis sets[170,171] augmented with diffuse functions on heavy (non-hydrogen) atoms as well an addi-

tional set of tight-d functions on S (i.e. cc-pV$\mathcal{X}$Z for H, aug-cc-pV$\mathcal{X}$Z for O, and aug-cc-pVD($\mathcal{X}+d$)Z for S) denoted ha($\mathcal{X}+d$)Z, where $\mathcal{X}$=D,T,Q,5 for MP2 and $\mathcal{X}$=D,T,Q for CCSD(T). All MP2 and CCSD(T) computations were performed with `Gaussian09`[172] and `CFOUR`,[117] respectively. MP2 optimized geometries and harmonic vibrational frequencies were also computed employing the Boys-Bernardi counterpoise (CP) procedure[215,216] as implemented in `Gaussian09` to correct for the inconsistency commonly referred to as basis set superposition error (BSSE).[217,218] Single point energy computations have been performed on the CCSD(T)/ha(Q+d)Z optimized geometries at the CCSD(T)/ha($\mathcal{X}+d$)Z level of theory, where $\mathcal{X}$=5,6. Anharmonic corrections to the harmonic MP2 and CCSD(T) vibrational frequencies were computed for the H_2S monomer as well as the $(H_2S)_2$, $HOH\cdots SH_2$, and $HSH\cdots OH_2$ dimers using the VPT2 algorithms available in `Gaussian09` and `CFOUR`, respectively.[219] The analogous data for H_2O and $(H_2O)_2$ were taken from Ref. 1. The frozen-core approximation was adopted for all MP2 and CCSD(T) computations, omitting the two core electrons of O and ten core electrons of S from the correlation procedure. Additionally, spherical functions ($5d, 7f, 9g, 13h$) were used instead of the default Cartesian functions ($6d, 10f, 15g, 21h$). For the optimized geometries, the Cartesian forces did not exceed 3.5×10^{-6} E_h/a_0.

4.3 Results and Discussion

4.3.1 H_2S Monomer

Table 4.1 shows the experimental bond lengths, bond angles, and fundamental vibrational frequencies of H_2S as well as the corresponding deviations of a variety of

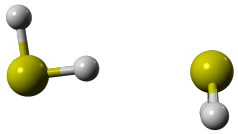

$(H_2S)_2$

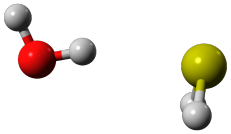

$HOH\cdots SH_2$

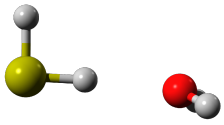

$HSH\cdots OH_2$

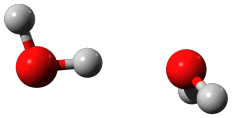

$(H_2O)_2$

Figure 4.2. Hydrogen-bonded dimers fully optimized within the C_s point group at the MP2/ha(Q+d)Z level of theory.

computed values. All theoretical values reported in Table 4.1 were computed with the ha(Q+d)Z basis set (unless specifically noted otherwise), but it is worth noting that increasing the size of the basis set to ha(5+d)Z changes the SH bond lengths and HSH bond angle by less than 0.0004 Å and 0.01°, respectively, at the MP2 level of theory. Compared to the CCSD(T) values in Table 4.1, the MP2 SH bond lengths are only slightly shorter (by 0.005 Å) and the HSH bond angle somewhat smaller (by 0.1°).

The MP2 and CCSD(T) bond lengths and angles computed with the ha(Q+d)Z basis set deviate by less than 0.003 Å and 0.3° from the experimental gas-phase results reported in Ref. 192. For the corresponding VPT2 vibrational frequencies, MP2 overestimates the SH stretching modes by more than 70 cm^{-1}. This result for H_2S is in stark contrast to the situation for H_2O where the MP2/haQZ VPT2 frequencies are within 15 cm^{-1} of experiment.[1] Increasing the basis set from MP2/ha(Q+d)Z to MP2/ha(5+d)Z does not improve the description of the SH stretching modes, as the two sets of VPT2 anharmonic vibrational frequencies differ by less than 0.4 cm^{-1}. Fortunately, the CCSD(T)/ha(Q+d)Z anharmonic vibrational frequencies for H_2S show much better agreement with experiment ($\pm$ 5 cm^{-1}).

The last two columns in Table 4.1 combine CCSD(T) harmonic frequencies with VPT2 anharmonic corrections (δVPT2) obtained from MP2 computations with the same basis set. These composite values show much better agreement with experiment (within 12 cm^{-1}) than the MP2/ha(Q+d)Z VPT2 frequencies with deviations as large as +73 cm^{-1}. These results indicate that combining the CCSD(T) harmonic

vibrational frequencies and the VPT2 corrections computed with the MP2 method can reliably describe the molecular vibrations of H_2S despite MP2 significantly overestimating the fundamental SH stretching frequencies.

The VPT2 infrared (IR) intensities of the H_2S monomer are very weak and do not exceed 2 km mol^{-1} at any level of theory used in this investigation. There are several overtones (2 ν_i) and combination bands ($\nu_i + \nu_j$ where $i \neq j$) of H_2S with IR intensities nearly equal to those of the fundamental modes. The first overtone of ν_2 (2 ν_2) appears in the SH stretching region with an IR intensity similar to that of ν_1. It is also worth noting that the ν_1+ν_2 and ν_1+ν_3 peaks combination bands *ca.* 3800 cm^{-1} have the largest VPT2 IR intensities at the CCSD(T)/ha(Q+*d*)Z level of theory, but the magnitude still does not exceed 1 km mol^{-1}. The geometrical parameters and Cartesian coordinates of the optimized structures as well as the full set of frequencies and IR intensities can be found in the Supporting Information for both the harmonic and VPT2 computations discussed in this section.

Table 4.1. Experimental geometrical parameters (R in Å and Θ in degrees) and fundamental vibrational frequencies (ν in cm^{-1}) of H_2S along with deviations associated with select optimized structures and VPT2 frequencies.

	Expt. Refs. 192, 193	MP2 ha(Q+*d*)Z	CCSD(T) ha(Q+*d*)Z	CCSD(T)[a,b] aug-cc-pVQZ	Composite[b] ha(Q+*d*)Z
R(SH)	+1.3356	−0.0028	+0.0027	+0.0043	+0.0027
Θ(HSH)	+92.11	+0.14	+0.26	+0.25	+0.26
ν_3 asym	2628	+73	−2	+6	+11
ν_1 sym	2614	+71	+4	+6	+12
ν_2 bend	1183	+4	−1	−3	0

[a] Ref. 212
[b] CCSD(T) harmonic frequencies with MP2 VPT2 corrections

4.3.2 Dimer Geometries

Fig. 4.2 shows the four hydrogen bonded dimers being compared in this study, $(H_2S)_2$, $HOH\cdots SH_2$, $HSH\cdots OH_2$, and $(H_2O)_2$. The intramolecular bond lengths and angles ($R(XH_d)$, $R(XH_f)$, and $\Theta(H_dXH_f)$ of the donor fragment and R(YH) and Θ(HYH) of the acceptor fragment) in the sulfur-containing dimers change by less than 0.001 Å and 0.1°, respectively, when increasing the basis set from ha(Q+d)Z to ha(5+d)Z at the MP2 level of theory. The CP procedure changes the MP2/ha(Q+d)Z intramolecular bond lengths by approximately 0.0002 Å and the intramolecular bond angles by less than 0.03°. MP2/ha(Q+d)Z and CCSD(T)/ha(Q+d)Z XH and YH bond lengths differ by 0.006 Å or less while the HXH and HYH bond angles are identical.

Similar to the trends just described for the intramolecular bond lengths and angles, the four intermolecular parameters of interest are quite insensitive to the use of basis sets larger than ha(Q+d)Z and the use of the CP procedure, neither of which changes $R(X\cdots Y)$ and $R(H_d\cdots Y)$ by more than 0.02 Å or $\Theta(XH_d\cdots Y)$ and $\Theta(X\cdots Y\vec{r_{bi}})$ by more than 1°. More significant deviations are observed, however, between the MP2/ha(Q+d)Z and CCSD(T)/ha(Q+d)Z optimized intermolecular bond lengths and angles, but the differences still do not exceed 0.06 Å and 5°, respectively.

Based on the performance of the ha(Q+d)Z basis set described above, Table 4.2 lists only the CCSD(T)/ha(Q+d)Z intramolecular bond lengths and angles for these different $HXH\cdots YH_2$ complexes. Interestingly, the intramolecular bond lengths and angles of the hydrogen bonded acceptor do not depend appreciably on the identity of the donor. If H_2O accepts a hydrogen bond from H_2O vs. H_2S, the

acceptor bond lengths differ by approximately 0.001 Å and the HYH bond angle by less than 0.1° (bottom left of Table 4.2). The changes are even smaller when H_2S is the acceptor (bottom right of Table 4.2). Similarly, the geometrical parameters of the donors do not depend on whether the acceptor is H_2O or H_2S. Comparing $(H_2O)_2$ to $HOH\cdots SH_2$ (top left of Table 4.2), the donor and free bond lengths ($R(XH_d)$ and $R(XH_f)$, respectively) differ by approximately 0.002 Å and the bond angles by 0.1°. The same trend occurs when H_2S is the donor in $(H_2S)_2$ and $HSH\cdots OH_2$ (top right of Table 4.2) where the donor and free bond lengths differ by 0.001 Å or less and the bond angle does not change by more than 0.1°.

Table 5.1 lists some CCSD(T)/ha(Q+d)Z optimized intermolecular bond lengths and angles that are defined by the labels in Fig. 4.1. As expected based on their relative atomic van der Waals and density radii (0.66 and 1.55 Å for O and 1.04 and 1.80 Å for S),[220–222] the intermolecular heavy atom distance ($R(X\cdots Y)$) increases by approximately 0.6 Å whenever X or Y changes from O to S. The intermolecular hydrogen bond length ($R(H_d\cdots Y)$) also increases for the same reason ($(H_2O)_2 < HSH\cdots OH_2 < HOH\cdots SH_2 < (H_2S)_2$). For the mixed H_2O/H_2S configurations, $HOH\cdots SH_2$ has an intermolecular hydrogen bond length that is 0.3 Å longer than its $HSH\cdots OH_2$ counterpart. There are two intermolecular bond angles that are of particular interest in this study, the hydrogen bond angle denoted $\Theta(XH_d\cdots Y)$ and the acceptor tilt angle between the $X\cdots Y$ axis and the vector bisecting the HYH angle of the acceptor, labeled $\vec{r_{bi}}$ in Fig. 4.1. The latter angle is denoted $\Theta(X\cdots Y\vec{r_{bi}})$ in Table 5.1. The hydrogen bond angles, $\Theta(XH_d\cdots Y)$, are all quasi-linear, ranging from 164° for $HOH\cdots SH_2$ to 176° for $HSH\cdots OH_2$. The accep-

tor tilt angle, $\Theta(\mathrm{X}\cdots\mathrm{Y}\vec{r}_{bi})$, is much larger when H_2O accepts the hydrogen bond in $(H_2O)_2$ and $HSH\cdots OH_2$ than when H_2S accepts the hydrogen bond in $(H_2S)_2$ and $HOH\cdots SH_2$ (125° and 151° vs. 90° and 81°, respectively) due to the differences in the orbital hybridization of O and S in the monomer.[223] This significant change is readily apparent in the heterodimer where interchanging the identity of the donor and acceptor from $HOH\cdots SH_2$ to $HSH\cdots OH_2$ increases $\Theta(\mathrm{X}\cdots\mathrm{Y}\vec{r}_{bi})$ by approximately 70°. The Cartesian coordinates and tables of geometrical parameters of all sulfur-containing dimers can be found in the Supporting Information.

The vibrationally averaged intermolecular bond lengths, $R_\alpha(\mathrm{X}\cdots\mathrm{Y})$ and $R_\alpha(\mathrm{XH}_d\cdots\mathrm{Y})$, of each $\mathrm{HXH}\cdots\mathrm{YH}_2$ dimer are listed in Table 5.1. For the $\mathrm{X}\cdots\mathrm{Y}$ heavy atom distance the $R_\alpha(\mathrm{X}\cdots\mathrm{Y})$ values differ from their equilibrium counterparts by 0.07 Å or less with the dimers where H_2O accepts the hydrogen bond ($(H_2O)_2$ and $HSH\cdots OH_2$) having slightly larger deviations. The equilibrium and vibrationally averaged intermolecular hydrogen bond lengths ($R(\mathrm{XH}_d\cdots\mathrm{Y})$ and $R_\alpha(\mathrm{XH}_d\cdots\mathrm{Y})$, respectively) have a deviation of at least 0.10 Å for all dimers, which is not unexpected given the relatively small molar mass of H. Overall, the same trends of the $\mathrm{X}\cdots\mathrm{Y}$ distance elongating by approximately 0.6 Å as H_2O fragments are replaced with H_2S and the intermolecular hydrogen bond lengths increasing from $(H_2O)_2 < HOH\cdots SH_2 < HSH\cdots OH_2 < (H_2S)_2$ remains the same for both equilibrium and vibrationally averaged intermolecular bond lengths. Experimentally, the $\mathrm{O}\cdots\mathrm{O}$ intermolecular distance of the H_2O dimer is 2.98 Å, which is within 0.01 Å of the $R_\alpha(\mathrm{X}\cdots\mathrm{Y})$ value of 2.97 Å.[1,224] Based on this agreement, the CCSD(T) method with an ha(Q+d)Z basis seems to be accurately describing these small hydrogen bonded complexes.

Table 4.2. Select CCSD(T)/ha(Q+d)Z optimized bond lengths (R in Å) and angles (Θ in degrees) of the hydrogen bonded dimers. All $(H_2O)_2$ values taken from Ref 1.

	H_2O Donor (X=O)		H_2S Donor (X=S)	
	Y=O	Y=S	Y=O	Y=S
R(XH_d)	0.965	0.963	1.342	1.341
R(XH_f)	0.958	0.959	1.338	1.338
Θ(HXH)	104.7	104.6	92.7	92.6
	H_2O Acceptor (Y=O)		H_2S Acceptor (Y=O)	
	X=O	X=S	X=O	X=S
R(YH)	0.960	0.959	1.339	1.339
Θ(HYH)	104.8	104.7	92.4	92.5

Table 4.3. Select CCSD(T)/ha(Q+d)Z optimized intermolecular equilibrium bond lengths (R in Å), vibrationally averaged intermolecular bond lengths (R_α in Å), and angles (Θ in degrees) of the hydrogen bonded dimers (shown in Fig. 4.1). All $(H_2O)_2$ values taken from Ref. 1.

	Intermolecular Parameters			
	$(H_2O)_2$	$HSH\cdots OH_2$	$HOH\cdots SH_2$	$(H_2S)_2$
R(X$\cdots$Y)	2.91	3.56	3.49	4.16
R($H_d\cdots$Y)	1.95	2.22	2.55	2.83
R_α(X$\cdots$Y)	2.97	3.61	3.52	4.20
R_α($H_d\cdots$Y)	2.03	2.31	2.65	2.94
Θ($XH_d\cdots$Y)	173	176	164	171
Θ(X$\cdots$Y$\vec{r}_{bi}$)	125	151	81	90

4.3.3 Dimer Energetics

Table 5.2 lists the electronic dissociation energies without (D_e) and with zero-point vibrational energy (ZPVE) corrections from the harmonic approximation and from VPT2 anharmonic computations (D_0^{harm} and D_0^{VPT2}, respectively) as well as the CP-corrected electronic dissociation energies (D_e^{CP}) for the hydrogen bonded dimers. Additional thermodynamic quantities, such as the enthalpy, entropy and free energy are also listed (ΔH, ΔS, and ΔG). MP2/ha(Q+*d*)Z and CCSD(T)/ha(Q+*d*)Z energetics indicate that $(H_2S)_2$ is the most weakly bound of the dimers examined, that $(H_2O)_2$ is the most strongly bound and that the two configurations of the heterodimer fall somewhere in between: $(H_2S)_2 < HSH\cdots OH_2 \approx HOH\cdots SH_2 < (H_2O)_2$. At the CCSD(T)/ha(Q+*d*)Z level of theory, the electronic dissociation energies (D_e) are 2.68 and 2.91 kcal mol^{-1} for $HSH\cdots OH_2$ and $HOH\cdots SH_2$, respectively, but only 1.67 kcal mol^{-1} for $(H_2S)_2$. These values agree to within 0.02 kcal mol^{-1} of previous estimates of the CBS limit CCSD(T) electronic dissociation energies for these dimers.[184] As can be seen in Table 5.2, the inclusion of CCSD(T)/ha(Q+*d*)Z VPT2 ZPVE corrections causes an appreciable (roughly 40%) decrease in the dissociation energy, which is particularly noticeable in the H_2S dimer where D_0^{VPT2} drops below 1 kcal mol^{-1}. The CCSD(T)/ha(Q+*d*)Z D_0^{VPT2} values of $(H_2O)_2$, $HSH\cdots OH_2$, $HOH\cdots SH_2$, and $(H_2S)_2$ are 3.11, 1.71, 1.66, and 0.95 kcal mol^{-1}, respectively, which is consistent with previous estimates of the dissociation energies of $HSH\cdots OH_2$, $HOH\cdots SH_2$, and $(H_2S)_2$ compared to that of $(H_2O)_2$.[184,188,212] For $(H_2O)_2$, D_0 has been experimentally measured as 3.16 kcal mol^{-1}, which shows very good agreement with CCSD(T)/ha(Q+*d*)Z D_0^{VPT2} of 3.11 kcal mol^{-1}.[1,225] Similar agreement

could be expected for $(H_2S)_2$, HSH$\cdots$OH$_2$, and HOH$\cdots$SH$_2$, should low temperature gas-phase D_0 become available.

The enthalpy of dimerization (ΔH) of the H_2O dimer at 373 K is estimated to be -3.59 ± 0.5 kcal mol^{-1} in the gas-phase while the entropy (ΔS) is approximately -18.59 ± 1.3 cal mol^{-1} K^{-1}.[226] At the CCSD(T)/ha(Q+*d*)Z level of theory, ΔH and ΔS of $(H_2O)_2$ at 298.15 K are -3.55 kcal mol^{-1} and -20.05 cal mol^{-1} K^{-1}, respectively, indicating that these thermodynamic quantities are adequately described despite the differences in temperature.[1] The enthalpies of dimerization of $(H_2O)_2$, HSH$\cdots$OH$_2$, HOH$\cdots$SH$_2$, and $(H_2S)_2$, are -3.55, -1.53, -1.68, and -0.55 kcal mol^{-1}, respectively, and follows a similar trend as the dissociation energies, where ΔH of $(H_2O)_2$ is the most favorable, HSH$\cdots$OH$_2$ and HOH$\cdots$SH$_2$ are close in enthalpy, and ΔH of $(H_2S)_2$ is less than a third that of the H_2O dimer. For all the hydrogen-bonded dimers, the CCSD(T)/ha(Q+*d*)Z free energies of dimerization (ΔG) are unfavorable indicating that the formation of these dimers at 298.15 K is not spontaneous and the largest contribution to the free energy arises from entropy.

The two configurations of the H_2O/H_2S dimer are essentially isoenergetic, and the identity of the lowest energy structure depends on whether the ZPVE is included or not. Examining the electronic energies, the HOH$\cdots$SH$_2$ configuration lies approximately 0.2 kcal mol^{-1} below the HSH$\cdots$OH$_2$ structure, despite having a slightly longer intermolecular hydrogen bond length. At the MP2/ha(Q+*d*)Z level of theory, the inclusion of ZPVE corrections (harmonic and anharmonic) reverses the situation and leads to an HSH$\cdots$OH$_2$ minimum that is slightly lower in energy (by 0.06 and 0.13 kcal mol^{-1}, respectively) than HOH$\cdots$SH$_2$. If harmonic and an-

harmonic ZPVE effects are instead computed at the CCSD(T)/ha(Q+d)Z level of theory, this energetic separation decreases to only 0.01 kcal mol^{-1} with the harmonic ZPVE corrections and 0.06 kcal mol^{-1} with the VPT2 ZPVE corrections. These relative energies change by less than 0.01 kcal mol^{-1} when larger basis sets are used ($\mathcal{X}$=5,6) or the CP procedure is employed. This competition between giving or receiving a hydrogen bond is remarkably similar to the situation for the HF/HCl dimer where the FH$\cdots$ClH configuration lies 0.2 kcal mol^{-1} below the ClH$\cdots$FH minimum near the CCSD(T) CBS limit, but the two minima become isoenergetic (within 0.03 kcal mol^{-1}) after the ZPVE correction is included.[227] In contrast, the HF/H_2O dimer has only one configuration that corresponds to a minimum (where HF donates a hydrogen bond to H_2O).[228]

Not surprisingly the dissociation energies are more sensitive to the methods and basis sets used than the relative energies of the two H_2O/H_2S configurations. For both MP2 and CCSD(T) as the size of the basis set increases for the sulfur containing dimers, D_e changes by 0.17 kcal mol^{-1} or less from ha(D+d)Z to ha(T+d)Z and by 0.04 kcal mol^{-1} or less from ha(T+d)Z to ha(Q+d)Z. D_e of the two H_2O/H_2S dimers converges more quickly than that of $(H_2S)_2$, particularly with the MP2 method where the electronic dissociation energy of the H_2S dimer changes by approximately 0.01 kcal mol^{-1} going from ha(Q+d)Z to ha(5+d)Z and 0.01 kcal mol^{-1} going from ha(5+d)Z to ha(6+d)Z. Single point energy computations on the CCSD(T)/ha(Q+d)Z optimized geometries with an ha(5+d)Z or ha(6+d)Z basis change the CCSD(T) electronic dissociation energies by approximately 0.01 kcal mol^{-1}, indicating that the electronic dissociation energy is reasonably converged with

the ha(Q+d)Z basis set. MP2/ha(Q+d)Z overestimates the CCSD(T)/ha(Q+d)Z D_e values for $(H_2S)_2$, $HSH\cdots OH_2$, and $HOH\cdots SH_2$ by approximately 0.2 kcal mol^{-1} despite agreeing to within 0.02 kcal mol^{-1} for $(H_2O)_2$. The MP2/ha(Q+d)Z dissociation energies of $HSH\cdots OH_2$, $HOH\cdots SH_2$, and $(H_2S)_2$ with harmonic ZPVE corrections change by less than 0.02 kcal mol^{-1} when the basis set is increased from ha(Q+d)Z to ha(5+d)Z. The MP2/ha(Q+d)Z CP and non-CP corrected electronic dissociation energies differ by no more than 0.12 kcal mol^{-1}. At the CCSD(T)/ha(Q+d)Z level of theory, CP corrections change the electronic dissociation energy by approximately 0.10 kcal mol^{-1}. See the Supporting Information for tables of the dissociation energies of all dimers with all basis sets considered here along with the individual ZPVE contributions of the sulfur-containing dimers.

4.3.4 Dimer Vibrational Frequencies

As with the energetic quantities, the harmonic vibrational frequencies (see the Supporting Information) of these dimers are well converged with the ha(Q+d)Z basis set. With the MP2 method, the ha(Q+d)Z and ha(5+d)Z harmonic vibrational frequencies of $(H_2S)_2$, $HOH\cdots SH_2$, $HSH\cdots OH_2$ differ by less than 4 cm^{-1}. The CP procedure also has a small impact on the vibrational frequencies computed with these large correlation consistent basis sets, changing the MP2/ha(Q+d)Z harmonic frequencies by less than 7 cm^{-1}. Far more significant deviations are observed between the CCSD(T)/ha(Q+d)Z and MP2/ha(Q+d)Z harmonic frequencies where the latter overestimates the former by as much as 80 cm^{-1} for the SH stretching modes. This is a stark contrast from $(H_2O)_2$ where MP2/haQZ and CCSD(T)/haQZ harmonic frequencies agree to within approximately 20 cm^{-1}.[1]

Table 4.4. Select MP2/ha(Q+d)Z and CCSD(T)/ha(Q+d)Z dissociation energies with and without counterpoise-corrections (D_e and D_e^{CP} in kcal mol^{-1}), including the harmonic and VPT2 zero-point vibrational corrected dissociation energies (D_0^{harm} and D_0^{VPT2} in kcal mol^{-1}), and thermodynamical quantities at 298.15 K (ΔH^a, $T\Delta S^a$, and ΔG^a in kcal mol^{-1}) of the hydrogen-bonded dimers. All $(H_2O)_2$ values taken from Ref. 1.

	$(H_2O)_2$	$HSH\cdots OH_2$	$HOH\cdots SH_2$	$(H_2S)_2$
MP2				
D_e	+4.99	+2.81	+3.02	+1.88
D_e^{CP}	+4.87	+2.71	+2.91	+1.79
D_0^{harm}	+2.92	+1.66	+1.60	+0.99
D_0^{VPT2}	+3.15	+1.86	+1.73	+1.14
ΔH	−3.37	−1.50	−1.65	−0.64
$T\Delta S$	−7.19	−4.49	−4.98	−3.85
ΔG	+2.62	+2.98	+3.33	+3.21
CCSD(T)				
D_e	+5.01	+2.68	+2.91	+1.66
D_e^{CP}	+4.87	+2.59	+2.81	+1.59
D_0^{harm}	+2.92	+1.51	+1.50	+0.80
D_0^{VPT2}	+3.11	+1.71	+1.66	+0.95
ΔH	−3.55	−1.53	−1.68	−0.55
$T\Delta S$	−5.98	−4.43	−4.90	−3.62
ΔG	+2.43	+2.89	+3.22	+3.06

[a] Computed as $E[HXH\cdots YH2] - E[H_2X] - E[H_2Y]$

The VPT2 anharmonic SH stretching frequencies of $(H_2S)_2$ are listed in Table 4.5 and no overtone or combination bands were included due to their weak IR intensities (less than 2 km mol^{-1}). As in the anharmonic spectrum of $(H_2O)_2$, there are four resonances (two Fermi and two Darling-Dennison) present in $(H_2S)_2$.[1] These resonances fall below 500 cm^{-1} and do not perturb the SH stretching modes of $(H_2S)_2$.[60–62] A previous experimental gas-phase study assigned both the asymmetric SH acceptor (ν_9) and free SH_f (ν_1) stretching frequencies at 2618 cm^{-1}, the symmetric SH (ν_2) acceptor frequency at 2605 cm^{-1}, and the donor SH_d (ν_3) stretching frequency at 2590 cm^{-1}.[2] (Refer to Fig. 4.1 for the definition of XH_f, XH_d and YH bonds.) The CCSD(T)/haQZ VPT2 vibrational frequencies of $(H_2S)_2$ presented in this work show good agreement (within +5 cm^{-1}) for the acceptor stretches and the SH_f stretch. The largest deviation (+16 cm^{-1}) occurs for the SH_d stretching frequency. As with the H_2S monomer, MP2/ha(Q+*d*)Z significantly overestimates the experimental SH stretching frequencies (by up to +79 cm^{-1}) even after including the corresponding VPT2 corrections. The composite method, which combines the CCSD(T)/ha(Q+*d*)Z harmonic frequencies with the MP2/ha(Q+*d*)Z VPT2 corrections, decreases the maximum discrepancy to +31 cm^{-1}. Interestingly, although the MP2/ha(Q+*d*)Z VPT2 procedure significantly overestimates the SH stretching frequencies for both H_2S and $(H_2S)_2$, it provides the most accurate estimate of the experimental donor frequency shift (with respect to the symmetric stretch of the H_2S monomer, $\Delta\nu(XH_d)$), of -22 cm^{-1} due to fortuitous error cancellation.

Table 4.6 lists the CCSD(T)/ha(Q+*d*)Z VPT2 stretching frequencies of the two H_2O/H_2S dimer configurations as well any overtones or combination bands with

an IR intensity greater than 1 km mol^{-1}. The HSH$\cdots$OH$_2$ and HOH$\cdots$SH$_2$ structures have two and three Fermi resonances, respectively, all of which fall well below 500 cm^{-1}. Consequently, the CCSD(T)/ha(Q+d)Z VPT2 IR spectrum of HOH$\cdots$SH$_2$ has eight peaks in the SH to OH region with an intensity $\geq$ 2 km mol^{-1} of which four are fundamental modes, one is an overtone, and three are combination bands. For HSH$\cdots$OH$_2$, there are also eight peaks with IR intensities larger than 1 km mol^{-1} in the XH stretching regions of which four are fundamental modes and four are overtones. The fundamental XH stretching frequencies of HSH$\cdots$OH$_2$ and HOH$\cdots$SH$_2$ are very close in energy (usually within 6 cm^{-1}) except for the OH donor stretch of HOH$\cdots$SH$_2$. At the CCSD(T)/ha(Q+d)Z level of theory, the XH$_d$ donor frequency shifts for HSH$\cdots$OH$_2$ and HOH$\cdots$SH$_2$ are -10 and -34 cm^{-1} with respect to the symmetric stretch of the corresponding monomer. The most intense fundamentals in the mixed dimer correspond to the free and donor OH stretches (ν_1 and ν_2) in the HOH$\cdots$SH$_2$ configuration and the donor SH$_d$ stretch (ν_3) and the a$''$ OH acceptor stretch (ν_9) of HSH$\cdots$OH$_2$. For HOH$\cdots$SH$_2$, there is one combination band with a noticeable IR intensity (ν_7+ν_2) which appears close to the free OH stretch (ν_1). HSH$\cdots$OH$_2$ has two combination bands with noticeable IR intensities (ν_{12}+ν_9 and ν_{11}+ν_9) that appear at higher energy than any of the fundamental modes.

In 1978, an experimental study of H$_2$O/H$_2$S mixtures in an N$_2$ matrix at 20 K reported peaks in the IR spectrum at 3719, 3628, 2624, 2574 and 2570 cm^{-1} that were assigned to the HSH$\cdots$OH$_2$ configuration of the heterodimer, all of which had noticeable intensities.[180] Six years later another spectroscopic investigation of H$_2$O/H$_2$S in an Ar matrix also at 20 K identified features at 3703, 3662, 3590,

3536 and 2587 cm^{-1} that were attributed to the presence of both dimer structures ($HSH\cdots OH_2$ and $HOH\cdots SH_2$).[181] The peaks corresponding to the H_2O/H_2S dimer observed in the OH stretching region have intensities that are less than half that of other peaks in the same region in Ar matrix. This seems to agree with the relatively weak VPT2 IR intensities computed for the H_2O/H_2S dimers and indicates that although the OH stretching frequencies do shift upon complexation there is not a significant corresponding increase in IR intensity like that observed in the H_2O dimer. In contrast the SH stretching modes corresponding to the H_2O/H_2S dimer are some of the larger peaks in the SH stretching region, however no information is given with respect to the relative intensities of the peaks in the OH and SH stretching regions. The experimental Ar matrix study also observed that the IR intensities of the SH stretching modes increases substantially in the H_2O/H_2S spectrum compared to that of the H_2S monomer, a trend that is also seen in the VPT2 IR intensities presented in this work.[181] The assignments, however, are far from conclusive given the significant quantitative and qualitative differences between these experimental spectra. Furthermore, neither the individual nor the combined VPT2 IR spectra for the two isolated minima of the H_2O/H_2S dimer provide a clear match with the experimental spectra. Altogether, these inconsistencies suggest that interactions with the matrix could be perturbing the spectra of the H_2O/H_2S dimer. It is also plausible that other species (e.g., trimers) could be responsible for some of the spectral features. The harmonic vibrational frequencies and IR intensities can be found in the SI along with the corresponding data for the VPT2 fundamentals, overtones and combination bands.

Table 4.5. Select haQ(+d)Z VPT2 vibrational frequencies of $(H_2S)_2$ (ν in cm^{-1}) along with their irreducible representations and and XH_d frequency shifts ($\Delta\nu$ in cm^{-1}) as well as the deviation between VPT2 frequencies from experimental gas phase results taken from Ref. 2.

	Mode	Irrep.	Expt.	MP2	Composite[a]	CCSD(T)
SH_d	ν_3	a′	2590	+73	+31	+16
SH	ν_2	a′	2605	+77	+19	+5
SH_f	ν_1	a′	2618	+78	+17	+3
SH	ν_9	a″	2618	+79	+18	+5
$\Delta\nu(SH_d)$	$\Delta\nu_3$	...	−24	+2	+19	+12

[a] CCSD(T)/ha(Q+d)Z harmonic frequencies with MP2/ha(Q+d)Z VPT2 corrections

Table 4.6. Select CCSD(T)/ha(Q+d)Z VPT2 vibrational frequencies (ν in cm^{-1}) along with their irreducible representations, IR intensities (I in km mol^{-1}), and XH_d frequency shifts ($\Delta\nu$ in cm^{-1}) of the H_2O/H_2S dimers. Overtones (OT) and combination bands (CB) with an IR intensity greater than 1 km mol^{-1} are also listed.

	$HOH\cdots SH_2$					$HSH\cdots OH_2$			
	Mode	Irrep.	ν	I		Mode	Irrep.	ν	I
SH	ν_3	a′	2608	2	SH_d	ν_3	a′	2608	55
SH	ν_9	a″	2621	3	SH_f	ν_2	a′	2615	4
OH_d	ν_2	a′	3621	106	OH	ν_1	a′	3637	8
OH_f	ν_1	a′	3731	112	OH	ν_9	a″	3734	72
$\Delta\nu(OH_d)$	$\Delta\nu_2$	...	−34	...	$\Delta\nu(SH_d)$	$\Delta\nu_3$	...	−10	...
	Mode		ν	I		Mode		ν	I
OT	ν_4	ν_4	3169	3	CB	ν_4	ν_3	2869	4
CB	ν_7	ν_2	3723	9	CB	ν_7	ν_1	3647	2
CB	ν_{12}	ν_1	3779	2	CB	ν_{11}	ν_9	3791	9
CB	ν_{11}	ν_1	3817	2	CB	ν_{12}	ν_9	3792	6

4.4 Conclusions

From this investigation of these sulfur-containing hydrogen bonded dimers, several important results arise. VPT2 anharmonic frequencies computed the CCSD(T) method and ha(Q+*d*)Z basis set are within 5 cm^{-1} of the available experimental data for H_2S and its homogeneous dimer except for the donor SH_d stretch of $(H_2S)_2$ where the deviation grows to 16 cm^{-1}. In contrast MP2/ha(Q+*d*)Z VPT2 anharmonic frequencies overestimate the experimental SH stretches by at least 70 cm^{-1}. The CCSD(T)/ha(Q+*d*)Z energy difference between the two H_2O/H_2S configurations decreases from 0.23 kcal mol^{-1} ($HOH\cdots SH_2$ lower in energy) without ZPVE corrections to 0.01 and 0.06 kcal mol^{-1} ($HSH\cdots OH_2$ is slightly lower in energy) upon the inclusion of harmonic and VPT2 anharmonic ZPVE corrections, respectively. Based on this small energetic difference both $HSH\cdots OH_2$ and $HOH\cdots SH_2$ are likely to be present under most experimental conditions. The CCSD(T)/ha(Q+*d*)Z anharmonic frequencies presented here (including overtones and combination bands with non-negligible IR intensities) will help assign spectral features from and distinguish between the two isoenergetic configurations of the H_2O/H_2S dimer.

CHAPTER 5

Exploring the $(H_2S)_2$ potential energy surface

5.1 Introduction

Recently sulfur-containing compounds have garnered attention for their strong noncovalent interactions, and one of the simplest of these compounds, H_2S, is of particular interest as it is a byproduct of certain pharmacological compounds[139,229–237]. Despite this growing interest and potential applications, relatively little is known about H_2S compared to the isovalent H_2O. The potential energy surface of the H_2O dimer, for instance, has been extensively explored and characterized using a variety of computational methods and techniques[1,64,65,189–191]. As a result, ten $(H_2O)_2$ stationary points were identified and throughly characterized with CCSD(T) computations employing a triple-ζ basis set[190]. Only one configuration corresponded to minimum (i.e. the number of imaginary frequencies, n_i, corresponded to 0) with a dissociation energy around 21 kJ mol^{-1} near the CCSD(T) complete basis set (CBS) limit. The other configurations were found to lie within 15 kJ mol^{-1} of the global minimum at the CCSD(T)/CBS limit. Three configurations were transition states ($n_i = 1$) and the others were higher-order saddle points ($n_i \geq 2$)[190].

Comparatively, the isovalent H_2S dimer has been studied far less rigorously. Most of the previous computational investigations into $(H_2S)_2$ have focused on the hydrogen bonded C_s global minimum labeled Structure I in Fig.

5.1[2,70,183–185,188,202,204,207,209–212]. Only a few studies have considered alternate configurations of $(H_2S)_2$[186,187,199,208,238]. For the $(H_2S)_2$ hydrogen bonded configuration (Structure I), the dissociation energy is 7.11 kJ mol^{-1} at the CCSD(T)/CBS limit[184,212] which is much weaker than that of $(H_2O)_2$ (*ca.* 21 kJ mol^{-1})[1,190]. However, $(H_2S)_2$ is still more strongly bound than other small dimer complexes like H_2O/N_2 and H_2O/O_2 which have dissociation energies of less than 6 kJ mol^{-1} [239,240]. The effects of basis set superposition error are relatively minor for both $(H_2O)_2$ and $(H_2S)_2$ (less than 0.1 kJ mol^{-1}) at the CCSD(T)/CBS limit[190,212]. As with $(H_2O)_2$, it has been demonstrated to obtain accurate energies, geometries, and harmonic vibrational frequencies for the H_2S dimer that CCSD(T) with at least a triple-ζ basis set is required[212]. Unlike the $(H_2O)_2$ global minimum which exhibits substantial changes in OH bond lengths and vibrational stretching frequencies upon dimerization, Structure I of the H_2S dimer shows very little change in either SH bond lengths or vibrational stretching frequencies (see Chapter 5).

Structures I, III, VI, VIII, and X (Fig. 5.1) have been previously identified using either Hartree-Fock (HF), semi-empirical methods or molecular mechanics[186,187,199,238]. Structures I and III have nearly identical configurations, barring the orientation of acceptor hydrogens. In all these investigations, Structure I is the lowest in energy. Only one study computed harmonic vibrational frequencies for some of these configurations which revealed that Structure I is the only minimum on the HF/4-31G(s,p) potential energy surface and Structures VI and VIII are higher-order saddle points[238]. Structures I and III were identified using a molecular mechanics for clusters model potential that also indicated the barrier for interconversion between

the two configurations was approximately 0.8 kJ mol^{-1} [186,187].

The focus of this paper is the systematic investigation of the low-energy stationary points on the $(H_2S)_2$ potential energy surface. For the first time, twelve different configurations of the H_2S dimer are identified and characterized at the same level of theory. Structures II, IV, V, and IX are new stationary points that have not been previously identified to our knowledge. Furthermore, this study presents the first MP2 and CCSD(T) optimized geometries and harmonic vibrational frequencies for Structures I to XII near the CBS limit. The geometries, energetics, and harmonic vibrational frequencies of each configuration are computed to better understand the $(H_2S)_2$ potential energy surface and how it compares to that of $(H_2O)_2$.

5.2 Computational Details

Full geometry optimizations and harmonic vibrational frequencies of all $(H_2S)_2$ configurations shown in Fig. 5.1 and the H_2S monomer were performed using the analytic gradients and Hessians for second-order Møller-Plesset perturbation theory (MP2)[30] and the CCSD(T) coupled-cluster method with singles, doubles, and perturbative triples substitutions[31,32] while employing a family of correlation consistent basis sets[170,171] and including diffuse functions and an additional set of tight-d functions on S (i.e. cc-pVXZ for H and aug-cc-pVD($X+d$)Z for S), denoted ha(X + d)Z where X=D,T,Q,5 for MP2 and X=D,T,Q for CCSD(T). All MP2 and CCSD(T) computations were performed with `Gaussian09` and `CFOUR`, respectively[117,172]. CCSD(T)/ha(X+d)Z single point energy computations (where X=5,6) were performed on both the MP2/ha(5+d)Z and CCSD(T)/ha(Q+d)Z optimized

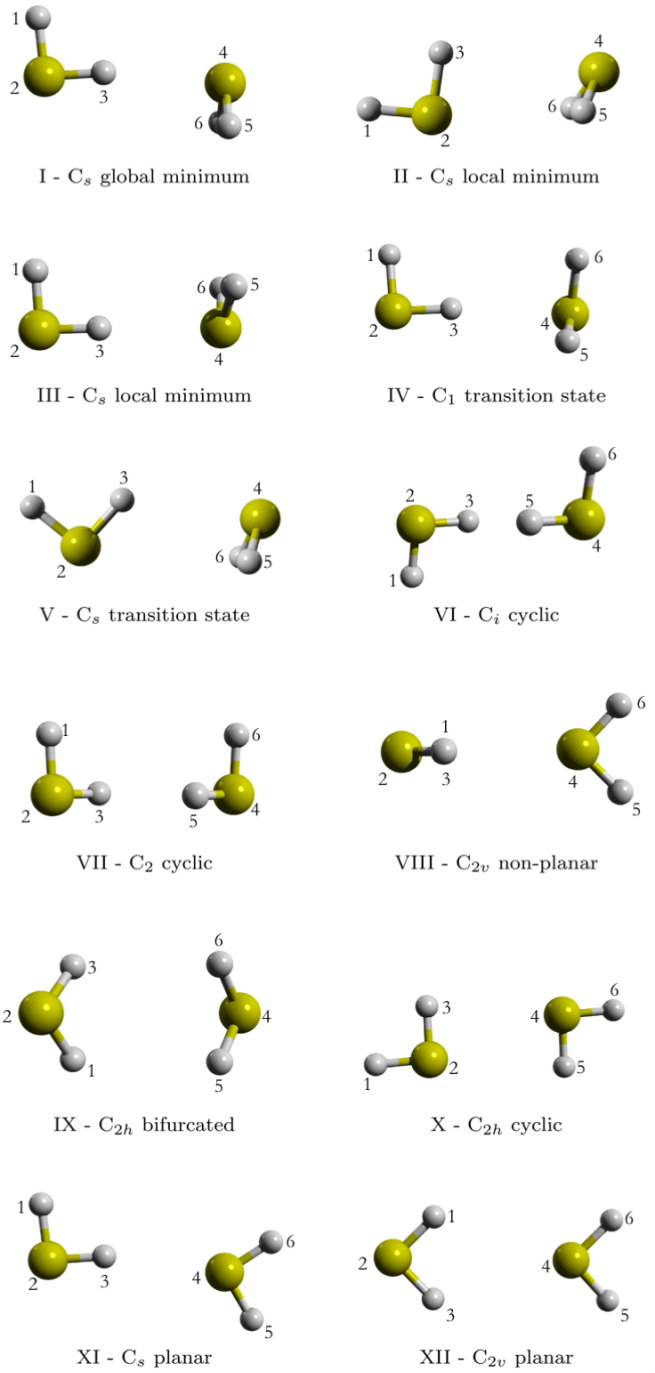

Figure 5.1. $(H_2S)_2$ structures examined in this study along with their corresponding point group symmetries and atom numbering schemes.

geometries using `Molpro2015`[241]. To assess the effect of the inconsistency referred to as basis set superposition error[215,216] (BSSE), additional computations were performed on the MP2/ha($X + d$)Z and CCSD(T)/ha($X + d$)Z optimized geometries using the Boys-Bernardi counterpoise procedure (CP) as detailed elsewhere[242]. The frozen-core approximation was adopted for all MP2 and CCSD(T) computations, excluding the 10 core electrons of S from the correlation procedure. Additionally, spherical functions ($5d, 7f, 9g, 11h, 13i$) were used instead of the Cartesian functions ($6d, 10f, 15g, 21h, 28i$). For the optimized geometries, the final Cartesian forces did not exceed 6.8×10^{-6} E_h/a_0.

5.3 Results and Discussion

5.3.1 Structures

Twelve low-energy configurations (I-XII in Fig. 5.1) of the H_2S dimer have been identified and numbered in ascending relative energy based on CCSD(T)/ha(Q+d)Z computations. This ordering, as well as the number of imaginary frequencies associated with each stationary point, is consistent across all levels of theory except for MP2/ha(D+d)Z and CCSD(T)/ha(D+d)Z. For Structure II, the ha(D+d)Z basis set overestimates the relative energy and gives the impression that Structure II is higher in energy than Structure IV. In the case of Structure IX, MP2/ha(D+d)Z and CCSD(T)/ha(D+d)Z harmonic vibrational frequencies computations have a n_i of three but when the size of the basis set is increased Structure IX has only two imaginary frequencies. MP2/ha(D+d)Z also switches the energetic ordering of Structures IX and X. At all levels of theory, Structures I, II and III are

the only minima ($n_i = 0$). Structures IV-VII are transition states ($n_i = 1$) while Structures VIII-XII are higher-order saddle points ($n_i = 2$ or 3). The Cartesian coordinates of optimized structures and the corresponding harmonic vibrational frequencies for Structures I-XII at the MP2/ha(Q+d)Z and CCSD(T)/ha(Q+d)Z levels of theory are provided in the Supporting Information.

Comparing these H_2S dimer configurations to their H_2O dimer counterparts, the C_s global minimum (I), the C_1 transition state (IV), the C_i cyclic transition state (VI), and the C_s planar second-order saddle point (XI) have not only the same qualitative structures but also the same number of imaginary frequencies[190]. In contrast, Structures II (C_s local minimum), VII (C_2 cyclic), VIII (C_{2v} planar), IX (C_{2h} bifurcated), X (C_{2h} cyclic), and XII (C_{2v} planar) have a different number of imaginary vibrational frequencies (± 1) than the analogous $(H_2O)_2$ stationary points. Finally, Structures III and V do not correspond to any structure on the $(H_2S)_2$ potential energy surface. This indicates that despite similarities between $(H_2O)_2$ and $(H_2S)_2$ configurations, their respective potential energy surfaces are qualitatively different.

Interestingly, the structure of H_2S changes very little upon dimerization and is quite insensitive to the orientation of the fragments in the dimer. The CCSD(T)/ha(Q+d)Z optimized H_2S monomer has an SH bond length of 1.338 Å and an HSH bond angle of 92.4°. These intramolecular geometrical parameters are essentially unchanged in all twelve dimer configurations shown in Fig. 5.1. In the largest deformations, the SH bond elongates by only 0.003 Å to 1.341 Å for the single hydrogen bond donors in Structures I, III, and IV. In all other instances the SH bond

length is either 1.338 or 1.339 Å regardless of whether an H atom is involved in a hydrogen bond or not. Similarly, the changes in the HSH bond angle are minuscule, and this intramolecular bond angle adopts only a small range of values (92.5±0.5°). For the H_2O dimer, several different configurations undergo shifts in intramolecular OH bond lengths and HOH bond angles up to 0.006 Å and 2.6°, respectively, upon dimerization at the CCSD(T)/TZ2P(f,d)+dif level of theory[190].

The CCSD(T)/ha(Q+d)Z intermolecular distances, dipole moments, and number of imaginary frequencies of Structures I-XII are shown in Table 5.1. Structures II and X have the shortest heavy atom distance of 3.73 and 3.65 Å, respectively. Structures VI and VII have the shortest intermolecular $H\cdots H$ distance by more than 0.3 Å. Unsurprisingly, the configurations resembling a single donor/single acceptor hydrogen bonded complex (Structures I, III, IV, and XI) have the shortest distances between the donor H (H_d) and the acceptor S. Structure III, which is a minimum, has one of the longer intermolecular $H_3\cdots S_4$ bond lengths of 3.40 Å. This is consistent with its $(H_2O)_2$ counterpart, which also exhibits a one of the largest $O\cdots H_d$ separations[190].

The dipole moments of the different $(H_2S)_2$ configurations span from 0 to 2.19 Debye with Structures VIII and XII having the largest and Structures I and II having the smallest, non-zero dipole moments. Structures VI, IX, and X have no dipole moment due to symmetry. The H_2O dimer stationary points have a broader range of dipole moments, from 0 to 4.15 Debye. Although the dipole moments of the $(H_2O)_2$ dimers are more substantial, the C_{2v} non-planar (VIII) and C_{2v} planar (XII) configurations of the H_2O dimer also have the largest dipole moments while

the cyclic C_2 (VII) and the hydrogen bonded C_s minimum (I) have the smallest[190].

Table 5.1. Select CCSD(T)/ha(Q+d)Z intermolecular bond lengths (R in Å), dipole moments ($\vec{\mu}$ in Debye), and number of imaginary frequencies (n_i) of the $(H_2S)_2$ stationary points.

	$R(S_2\cdots S_4)$	$R(H_3\cdots H_5)$	$R(H_3\cdots H_6)$	$R(H_3\cdots S_4)$	$\vec{\mu}$	n_i
I	4.16	3.18	3.18	2.83	1.06	0
II	3.73	3.32	3.32	3.40	1.00	0
III	4.18	3.26	3.26	2.84	2.09	0
IV	4.17	3.07	3.24	2.85	1.70	1
V	3.94	3.13	3.13	3.05		1
VI	4.08	2.71	3.73	3.19	0.00	1
VII	4.09	2.70	3.68	3.20	1.40	1
VIII	3.98	4.20	4.20	3.20	2.19	2
IX	4.13	3.61	3.06	3.64	0.00	2
X	3.65	3.88	4.85	3.52	0.00	2
XI	4.31	4.08	3.97	2.98	1.94	2
XII	4.21	4.20	4.63	3.42	2.14	3

5.3.2 Energetics

Table 5.2 lists the relative energies of configurations II-XII of $(H_2S)_2$ with respect to Structure I, which is the global minimum. All configurations are within 4.29 kJ mol^{-1} of Structure I at the CCSD(T)/ha(6+d)Z level of theory. The energetic ordering of Structures I to XII does not change regardless of method with basis set larger than ha(D+d)Z despite the shallow nature of the $(H_2S)_2$ potential energy surface compared to that of the H_2O dimer. The CCSD(T)/ha(6+d)Z relative energies of all transition states (Structures IV-VII) are within 0.81 kJ mol^{-1} of the global minimum. The higher-order saddle points (Structures VIII-XII) are at least 1 kJ mol^{-1} higher in energy than the transition states regardless of method or basis set. The three minima (Structures I, II, III) are very close in energy, separated by no

more than 0.21 and 0.35 kJ mol^{-1} near the CCSD(T)/CBS limit. Structure IV is the transition state between Structures I and III lying less than 0.38 kJ mol^{-1} above the global minimum according to our CCSD(T) computations. Structure V is the transition state between Structures I and II and has a slightly larger relative energy of 0.XX at the CCSD(T)/ha(6+d)Z level of theory. The intrinsic energetics of the $(H_2O)_2$ dimers are very different from that of $(H_2S)_2$. At the CCSD(T)/CBS limit, the $(H_2O)_2$ dimer stationary points increase in energy from I < IV < XI < VI < VII < X < VIII < II < XII < IX (labeled based on their similarity to the $(H_2S)_2$ configuration)[190].

Table 5.2 lists the CP and non-CP corrected dissociation energy, D_e^{CP} and D_e respectively, of Structure I. The electronic dissociation energy of Structure I is 6.99 kJ mol^{-1} at the CCSD(T)/ha(6+d)Z level of theory which agrees well with previous estimates of the dissociation energy at the CCSD(T)/CBS limit (7.09 kJ mol^{-1})[212]. The dissociation energy of the H_2O dimer is three times as large (*ca* 21 kJ mol^{-1}) at the CCSD(T)/CBS limit[190]. For $(H_2S)_2$, MP2 consistently overestimates the dissociation energy by more than 0.8 kJ mol^{-1} for both D_e and D_e^{CP}. Increasing the basis set from ha(Q+d)Z to ha(5+d)Z or ha(6+d)Z changes D_e by no more than 0.07 kJ mol^{-1}, indicating that the electronic dissociation energy has converged. The CP and non-CP corrected dissociation energies agree to within 0.41 and 0.29 kJ mol^{-1} with a ha(Q+d)Z or larger basis set for both MP2 and CCSD(T), respectively. A similar comparison of MP2 and CCSD(T) CP and non-CP corrected dissociation energy of the isovalent H_2O dimer yield a slightly larger (approximately 0.6 kJ mol^{-1}) difference with an aug-cc-pV5Z basis set[190].

Table 5.2. Relative electronic energies of all $(H_2S)_2$ structures in kJ mol^{-1}.

	I	II	III	IV	V	VI	VII	VIII	IX	X	XI	XII	D_e^a	D_e^{CP}
ha(D+d)Z	0.00	0.94	0.43	0.52	1.20	1.35	1.62	2.83	3.73	3.55	4.42	5.28	7.95	6.22
ha(T+d)Z	0.00	0.19	0.34	0.43	0.63	0.83	1.06	2.11	2.81	3.01	3.97	4.69	7.75	6.90
ha(Q+d)Z	0.00	0.18	0.34	0.42	0.61	0.76	0.99	2.09	2.84	3.06	4.05	4.74	7.87	7.46
ha(5+d)Z	0.00	0.12	0.35	0.42	0.56	0.70	0.92	2.08	2.77	3.11	4.11	4.76	7.91	7.68
ha(6+d)Z[b]	0.00	0.14	0.35	0.42	0.56	0.69	0.92	2.09	2.78	3.14	4.12	4.78	7.94	7.79
						CCSD(T)								
ha(D+d)Z	0.00	0.99	0.38	0.46	1.16	1.24	1.49	2.60	3.31	3.52	3.94	4.78	7.01	5.29
ha(T+d)Z	0.00	0.26	0.33	0.39	0.54	0.66	0.88	1.89	2.37	3.07	3.58	4.19	6.81	6.07
ha(Q+d)Z	0.00	0.27	0.34	0.38	0.46	0.60	0.82	1.91	2.41	3.17	3.70	4.28	6.94	6.65
ha(5+d)Z[c]	0.00	0.20	0.35	0.38	0.48	0.53	0.82	1.90	2.33	3.20	3.75	4.29	6.99	6.86
ha(6+d)Z[c]	0.00	0.21	0.35	0.38	0.48	0.52	0.81	1.90	2.32	3.22	3.76	4.29	6.99	6.92

[a] Relative energy of two isolated H_2S monomers (i.e. the electronic dissociation energy).
[b] Single point energies computed using the MP2/ha(5+d)Z optimized geometries.
[c] Single point energies computed using the CCSD(T)/ha(Q+d)Z optimized geometries.

5.3.3 Minima on the $(H_2S)_2$ potential energy surface

This section provides a more detailed examination of the three low-energy minima, Structures I, II and III. In Table 5.1, the CCSD(T)/ha(Q+d)Z intermolecular hydrogen bond length and heavy atom distance, R($H_3\cdots S_4$) and R($S_2\cdots S_4$), of Structure I are 2.83 and 4.16 Å, respectively, and these values for Structure III are only slightly elongated by 0.02 Å or less. Structure II has a R($H_3\cdots S_4$) and R($S_2\cdots S_4$) values of 3.40 and 3.73 Å. Structures I and III have a typical hydrogen bonding motif, where one monomer donates a hydrogen bond to the other and the $S\cdots H_dS$ bond angle is nearly linear. Structure II has a more complex case where one monomer donates two hydrogen bonds and accepts one hydrogen bond (double donor) while the other monomer accepts two hydrogen bonds and donates one hydrogen bond (double acceptor) and therefore the intermolecular bond lengths are

quite different for Structure II.

The CCSD(T)/ha(Q+d)Z rotational constants, $A/B/C$, of Structure I are 96766/1720/1711 MHz while those of Structure III are 96868/1707/1699 MHz, and Structure II has rotational constants of 113556/2114/2108 MHz. The rotational constants of Structures I and III are nearly identical with a maximum absolute deviation of 102 MHz in A and a maximum relative deviation of less than 1%. Given how closely related the orientations Structures I and III are, these minute differences in geometry and rotational constants are not surprising. However, the dipole moment of Structure III is almost twice that of Structure I due to the relative orientations of the H atoms not involved in the hydrogen bond. Like Structure I, Structure III almost has a very small dipole moment of 1.00 Debye.

Table 5.3 provides the CCSD(T)/ha(Q+d)Z harmonic vibrational frequencies for Structures I, II and III. MP2 performs poorly when describing the SH stretches, overestimating the stretching frequencies by up to 62 cm^{-1} for all configurations with an ha(Q+d)Z basis set. See harmonic vibrational frequency tables in the Supporting Information. The harmonic frequencies for Structures I and III are within 5 cm^{-1} of each other for most modes, except for low-energy intermolecular modes ω_8, ω_{11}, and ω_{12}. The SH stretching modes (ω_1, ω_2, ω_3, and ω_9) are even closer together (*ca.* 1 cm^{-1}), which would make it challenging to distinguish the two configurations from each other based on the spectral signatures of these vibrational modes. Compared to Structure I, modes ω_8 and ω_{11} of Structure III are slightly higher in energy and ω_{12} is lower in energy by more than 15 cm^{-1}. For both Structures I and III, the mode with the largest IR intensity is the donor SH stretch (ω_3). The mode with the

next largest IR intensity for Structure I is ω_7 and for Structure III it is ω_6, which leads to the largest differences in the IR spectra. ω_7 in Structure I occurs at 74 cm^{-1} and ω_6 in Structure III occurs at 144 cm^{-1}. A large peak just below the harmonic prediction of 74 cm^{-1} would likely be attributed to configuration I of $(H_2S)_2$ while a large peak near 144 cm^{-1} would likely be attributed to Structure III. Finally, the lowest energy modes (ω_8 and ω_{12}) of Structure I have small IR intensities while the same low energy modes of Structure III are IR inactive.

Interestingly despite the differences in orientation, most of the modes of Structure II that are within 15 cm^{-1} of those of Structures I and III with the exception of modes ω_3, ω_6, ω_7, ω_{10}, and ω_{12}. ω_3 is the symmetric stretch of the double donor monomer (Sym. SH_d) and is the only SH stretch that is substantially (*ca.* 20 cm^{-1}) different from those of Structures I and III. However in Structure II, none of the SH stretching frequencies have IR intensities greater than 1 km mol^{-1}. The modes of Structure II with the largest IR intensities are ω_7 and ω_{11} which correspond low-energy intermolecular modes at 85 and 80 cm^{-1}. These two peaks with large IR intensities appearing close together would likely indicate configuration II of the H_2S dimer.

As previously stated, the energy difference between Structures I, II, and III are minute (0.27 and 0.34 kJ mol^{-1} at the CCSD(T)/ha(Q+*d*)Z level of theory) and the inclusion of zero-point vibrational energy corrections further compresses the relative energies to 0.20 and 0.28 kJ mol^{-1} for Structures II and III, respectively. Additionally, the very small energetic barrier to rotation from Structure III back to Structure I via the Structure IV transition state suggests that the former is unlikely

to be observed experimentally. Although the barrier from Structure I to II through Structure V is slightly higher (0.XX kJ mol^{-1}), Structure II is similarly unlikely to be seen in experiment. A situation like that described above is not unique to the H_2S dimer, having been previously observed for the C_3 bowl structure of $(H_2O)_3$ which is a minimum with a small barrier for interconversion to the cyclic C_1 global minimum.[243]

Table 5.3. CCSD(T)/ha(Q+d)Z harmonic vibrational frequencies (ω in cm^{-1}), irreducible representations, and IR intensties (I in km mol^{-1}) of the $(H_2S)_2$ minima (Structures I-III).

			I		III			II	
	Irrep.	Mode	ω	I	ω	I	Mode	ω	I
ω_1	a′	SH_f str.	2732	3	2731	4	Asym. SH_a str.	2742	1
ω_2	a′	SH_a str.	2720	0	2721	0	Sym. SH_a str.	2722	1
ω_3	a′	SH_d str.	2699	47	2699	47	Sym. SH_d str.	2719	0
ω_4	a′	H_dSH_f bend	1214	4	1216	2	HSH bend	1211	1
ω_5	a′	H_aSH_a bend	1208	1	1208	1	HSH bend	1203	0
ω_6	a′	Int. rock	147	4	144	32	Int. rock	119	16
ω_7	a′	Int. bend	74	26	74	5	Int. bend	85	34
ω_8	a′	Int. str.	56	13	61	0	Int. str.	58	4
ω_9	a″	SH_a str.	2736	0	2736	0	Asym. SH_d str.	2734	0
ω_{10}	a″	Int. wag	256	4	255	4	Int. wag	202	2
ω_{11}	a″	Int. twist	67	11	72	1	Int. twist	80	32
ω_{12}	a″	Int. wag	33	15	15	0	Int. wag	58	5

5.4 Conclusions

Twelve different stationary of $(H_2S)_2$ have been identified and characterized for the first time near the CCSD(T)/CBS limit. All of these configurations are within 4.29 kJ mol^{-1} of the global minimum at the CCSD(T)/ha(6+d)Z level of theory. All MP2 and CCSD(T) computations indicate that Structure I is the global minimum regardless of basis set chosen. The CCSD(T)/ha(6+d)Z electronic dissociation energy of Structure I is 6.99 kJ mol^{-1}. Structures II and III are previously uncharacterized minima on the $(H_2S)_2$ potential energy surface with a relative electronic energy of +0.21 and +0.35 kJ mol^{-1} with respect to Structure I. The geometries of the H_2S fragments undergo almost no distortion in the various dimer configuration, unlike what is observed for the H_2O dimer stationary points. R(SH) falls between 1.338 and 1.341 Å and Θ(HSH) is 92.5±0.5° in the CCSD(T)/ha(Q+d)Z optimized structures for the isolated monomer and all twelve stationary points regardless of their relative orientation.

CHAPTER 6

CONCLUSION

In this work, electronic structure theory methods have been used in a variety of ways, from qualitative trends to quantitative analyses, always with the same goal of uncovering new information to help better the understanding of unusual noncovalent interactions. Using convergent quantum chemistry to study different configurations of the atmospheric dimer, $H_2O \cdots O_2$, one structure (I) is a minimum with a weak binding energy of less than 0.7 kcal mol^{-1} that arises from the dispersion forces between monomers. This structure could potentially absorb far IR radiation based on the relatively large intensities of two low-energy modes. In ammonia borane, the presence dative bonds and dihydrogen bonding between fragments reveals distinct behavior in the isolated clusters and crystal models, with the former containing parallel orientations of BH_3NH_3 fragments and the latter having anti-parallel orientations. This distinction has a larger impact on the physical properties such as BN bond length and stretching frequencies as opposed to cluster size based on cooperative effects. In considering the isovalent sulfur-containing hydrogen bonds in the H_2O/H_2S and $(H_2S)_2$ dimers compared to $(H_2O)_2$, these nonconventional hydrogen bonds are appreciably weaker than their $(H_2O)_2$ counterparts despite having a similar minimum energy structure. Further investigation into the H_2O dimer reveals three different configurations of $(H_2S)_2$ are minimum energy structures.

LIST OF REFERENCES

Bibliography

[1] J. Coleman Howard, Jessica L. Gray, Amanda J. Hardwick, Linh T. Nguyen, and Gregory S. Tschumper. *J. Chem. Theory Comput.*, 10(12):5426–5435, 2014.

[2] Aditi Bhattacherjee, Yoshiyuki Matsuda, Asuka Fujii, and Sanjay. Wategaonkar. *ChemPhysChem*, 14(5):905–914, 2013.

[3] Michel Simard, Dan Su, and James D. Wuest. *J. Am. Chem. Soc.*, 113(12):4696–8, 1991.

[4] Christian G. Claessens and J. Fraser. Stoddart. *J. Phys. Org. Chem.*, 10(5):254–272, 1997.

[5] Dario Braga and Fabrizia Grepioni. *Acc. Chem. Res.*, 33(9):601–608, 2000.

[6] David J. Hill, Matthew J. Mio, Ryan B. Prince, Thomas S. Hughes, and Jeffrey S. Moore. *Chem. Rev. (Washington, D. C.)*, 101(12):3893–4011, 2001.

[7] Shuguang. Zhang. *Biotechnol. Adv.*, 20(5-6):321–339, 2002.

[8] Graeme Cooke and Vincent M. Rotello. *Chem. Soc. Rev.*, 31(5):275–286, 2002.

[9] D. N. Reinhoudt and M. Crego-Calama. *Science (Washington, DC, U. S.)*, 295(5564):2403–2407, 2002.

[10] Johannes A. A. W. Elemans, Alan E. Rowan, and Roeland J. M. Nolte. *J. Mater. Chem.*, 13(11):2661–2670, 2003.

[11] Shuguang. Zhang. *Nat. Biotechnol.*, 21(10):1171–1178, 2003.

[12] I. W. Hamley. *Angew. Chem., Int. Ed.*, 42(15):1692–1712, 2003.

[13] Jean-Marie. Lehn. *Chem. Soc. Rev.*, 36(2):151–160, 2007.

[14] Erin R. Johnson, Shahar Keinan, Paula Mori-Sanchez, Julia Contreras-Garcia, Aron J. Cohen, and Weitao. Yang. *J. Am. Chem. Soc.*, 132(18):6498–6506, 2010.

[15] Chao Wang, Zhiqiang Wang, and Xi. Zhang. *Acc. Chem. Res.*, 45(4):608–618, 2012.

[16] Jan Rezac and Pavel. Hobza. *Chem. Rev. (Washington, DC, U. S.)*, 116(9):5038–5071, 2016.

[17] A. Subha Mahadevi and G. Narahari. Sastry. *Chem. Rev. (Washington, DC, U. S.)*, 116(5):2775–2825, 2016.

[18] Yang Li, Yiguang Wang, Gang Huang, and Jinming. Gao. *Chem. Rev. (Washington, DC, U. S.)*, 118(11):5359–5391, 2018.

[19] C. E. Dykstra and J. M. Lisy. 500(1–3):375–390, 2000.

[20] Klaus Müller-Dethlefs and P. Hobza. 100(1):143–168, 2000.

[21] A. K. Rappe and E. R. Bernstein. 104(26):6117–6128, 2000.

[22] Klaus Müller-Dethlefs and Pavel Hobza. *Chemical Reviews*, 100:143–167, 2000.

[23] Aron J. Cohen, Paula Mori-Sanchez, and Weitao. Yang. *Chem. Rev. (Washington, DC, U. S.)*, 112(1):289–320, 2012.

[24] Trygve Helgaker, Poul Jørgensen, and Jeppe Olsen. John Wiley & Sons Ltd., Chichester, England, 2000.

[25] Andreas Dreuw and Martin Head-Gordon. *Chemical Reviews*, 105(11):4009–4037, 2005.

[26] Jan Řezáč and Pavel Hobza. *Chemical Reviews*, 116:5038–5071, 2016.

[27] D. R. Hartree. *Mathematical Proceedings of the Cambridge Philosophical Society*, 24(1):89110, 1928.

[28] V. Fock. *Zeitschrift für Physik*, 62(11):795–805, Nov 1930.

[29] J. C. Slater. *Phys. Rev.*, 81:385–390, Feb 1951.

[30] C. Møller and M. S. Plesset. *Phys. Rev.*, 46:618, 1934.

[31] R.J. Bartlett. *Ann. Rev. Phys. Chem.*, 32:359, 1981.

[32] G.D. Purvis and R.J. Bartlett. 76(4):1910, 1982.

[33] Axel D. Becke. *J. Chem. Phys.*, 98(7):5648–52, 1993.

[34] C. Lee, W. Yang, and R. G. Parr. *Phys. Rev. B*, 37:785–789, 1988.

[35] Yan Zhao and Donald G. Truhlar. *Acc. Chem. Res.*, 41(2):157–167, 2008.

[36] E. Schrödinger. *Phys. Rev.*, 28:1049–1070, Dec 1926.

[37] A. Szabo and N.S. Ostlund. Dover Books on Chemistry. Dover Publications, 1982.

[38] Ira N. Levine. Prentice Hall, 2000.

[39] M. Born and J. R. Oppenheimer. *Ann. Phys.*, 84:475, 1927.

[40] R. S. Mulliken. *J. Chim. Phys. Phys.-Chim. Biol.*, 46:497–542, 1949.

[41] L. Pauling. Cornell University Press, Ithaca, New York, 3 edition, 1960.

[42] Takashi Tsuchimochi and Gustavo E. Scuseria. *The Journal of Chemical Physics*, 133(14):141102, 2010.

[43] Xiao He and Kenneth M. Merz. *Journal of Chemical Theory and Computation*, 6(2):405–411, 2010.

[44] Nivaldo J. Tro. Pearson, 4th edition, 2016.

[45] *Proceedings of the Royal Society of London A: Mathematical, Physical and Engineering Sciences*, 129(811):598–615, 1930.

[46] Jan Řezáč and Pavel Hobza. *Journal of Chemical Theory and Computation*, 9(5):2151–2155, 2013.

[47] Rodney J. Bartlett. *The Journal of Physical Chemistry*, 93(5):1697–1708, 1989.

[48] W. Kohn, A. D. Becke, and R. G. Parr. *J. Phys. Chem.*, 100(31):12974–12980, 1996.

[49] Christopher J. Cramer. Wiley, 2nd edition, 2004.

[50] Tom. Ziegler. *Chem. Rev.*, 91(5):651–67, 1991.

[51] Qingsheng Zhao, Robert C. Morrison, and Robert G. Parr. *Phys. Rev. A: At., Mol., Opt. Phys.*, 50(3):2138–42, 1994.

[52] E. J. Baerends and O. V.. Gritsenko. *J. Phys. Chem. A.*, 101(30):5383–5403, 1997.

[53] Peter Politzer and Fakher. Abu-Awwad. *Theor. Chem. Acc.*, 99(2):83–87, 1998.

[54] P. Geerlings, F. De Proft, and W. Langenaeker. *Chem. Rev. (Washington, DC, U. S.)*, 103(5):1793–1873, 2003.

[55] Kevin E. Riley, Michal Pitonak, Petr Jurecka, and Pavel. Hobza. *Chem. Rev. (Washington, DC, U. S.)*, 110(9):5023–5063, 2010.

[56] Stefan Grimme, Jens Antony, Stephan Ehrlich, and Helge. Krieg. *J. Chem. Phys.*, 132(15):154104/1–154104/19, 2010.

[57] Petr Jurecka, Jiri Cerny, Pavel Hobza, and Dennis R. Salahub. *J. Comput. Chem.*, 28(2):555–569, 2007.

[58] Narbe Mardirossian and Martin. Head-Gordon. *J. Chem. Theory Comput.*, 12(9):4303–4325, 2016.

[59] Jeanne L. McHale. CRC Press, 2nd edition, 2017.

[60] E. Z. Fermi. *Physik*, 71:250, 1931.

[61] B. T. Darling and D. M. Dennison. *Phys. Rev.*, 57:128, 1940.

[62] D. A. Matthews, J. Vázquez, and J. F. Stanton. *Mol. Phys.*, 105(19–22):2659, 2007.

[63] J. Černý and P. Hobza. *Phys. Chem. Chem. Phys.*, 9(39):5281–5388, 2007.

[64] K. Morokuma and L. Pedersen. 48:3275–3282, 1968.

[65] K. Morokuma and J. R. Winick. 52(3):1301–1306, 1970.

[66] Thomas R. Dyke and J. S. Muenter. *J. Chem. Phys.*, 60(7):2929–2930, 1974.

[67] Leif Fredin, Bengt Nelander, and Göran Ribbegård. *The Journal of Chemical Physics*, 66(9):4065–4072, 1977.

[68] Z. S. Huang and R. E. Miller. *The Journal of Chemical Physics*, 91(11):6613–6631, 1989.

[69] Katharina E. Otto, Zhifeng Xue, Philipp Zielke, and Martin A. Suhm. *Phys. Chem. Chem. Phys.*, 16(21):9849–9858, 2014.

[70] Peter Kollman, John McKelvey, Allan Johnsson, and Steve Rothenburg. *J. Am. Chem. Soc.*, 97:955, 1975.

[71] Alexander M. Mebel, Djamaladdin G. Musaev, and Keiji. Morokuma. *Chem. Phys. Lett.*, 216(3-6):313–18, 1993.

[72] Alexander M. Mebel, Djamaladdin G. Musaev, and Keiji. Morokuma. *J. Phys. Chem.*, 97(29):7543–52, 1993.

[73] Jason M. Gonzales, Djamaladdin G. Musaev, and Keiji. Morokuma. *Organometallics*, 24(21):4908–4914, 2005.

[74] Rajasri Bhattacharyya, Debnath Pal, and Pinak. Chakrabarti. *Protein Eng., Des. Sel.*, 17(11):795–808, 2004.

[75] Himansu S. Biswal and Sanjay. Wategaonkar. *J. Phys. Chem. A*, 113(46):12774–12782, 2009.

[76] Himansu S. Biswal, Pranav R. Shirhatti, and Sanjay. Wategaonkar. *J. Phys. Chem. A*, 113(19):5633–5643, 2009.

[77] Peng Zhou, Feifei Tian, Fenglin Lv, and Zhicai. Shang. *Proteins: Struct., Funct., Bioinf.*, 76(1):151–163, 2009.

[78] Mitsuhiro Takeda, Jun-Goo Jee, Akira M. Ono, Tsutomu Terauchi, and Masatsune. Kainosho. *J. Am. Chem. Soc.*, 133(43):17420–17427, 2011.

[79] Heidar Raissi, Azadeh Khanmohammadi, and Fariba. Mollania. *Bull. Chem. Soc. Jpn.*, 86(11):1261–1271, 2013.

[80] Yuting Yang, Haoming Zhang, Dandamudi Usharani, Weishu Bu, Sangchoul Im, Michael Tarasev, Freeborn Rwere, Naw May Pearl, Jennifer Meagher,

Cuthbert Sun, Jeanne Stuckey, Sason Shaik, and Lucy. Waskell. *Biochemistry*, 53(31):5080–5091, 2014.

[81] Mitsuhiro Takeda, Yohei Miyanoiri, Tsutomu Terauchi, Chun-Jiun Yang, and Masatsune. Kainosho. *J. Magn. Reson.*, 241:148–154, 2014.

[82] Elisabeth K. Nyakatura, Raheleh Rezaei Araghi, Jeremie Mortier, Sebastian Wieczorek, Carsten Baldauf, Gerhard Wolber, and Beate. Koksch. *ACS Chem. Biol.*, 9(3):613–616, 2014.

[83] Cristina Stefaniu, Pierre-Leonard Zaffalon, Alessio Carmine, Quentin Verolet, Samuel Fernandez, Tomasz A. Wesolowski, Gerald Brezesinski, and Andreas. Zumbuehl. *Langmuir*, 31(4):1296–1302, 2015.

[84] Shanshan Tang, Hailiang Zhao, and Lin. Du. *RSC Adv.*, 6(94):91233–91242, 2016.

[85] Alexander Angeloski, James M. Hook, Mohan Bhadbhade, Anthony T. Baker, and Andrew M. McDonagh. *CrystEngComm*, 18(37):7070–7077, 2016.

[86] Laura A. H. van Bergen, Mercedes Alonso, Anna Pallo, Lennart Nilsson, Frank De Proft, and Joris. Messens. *Sci. Rep.*, 6:30369, 2016.

[87] Katelyn M. Dreux and Gregory S. Tschumper. *Comput. Theo. Chem.*, 1072:21–27, 2015.

[88] Mark A. Vincent and Ian H. Hillier. *J. Phys. Chem.*, 99:3109–3113, 1995.

[89] Igor M. Svishchev and Russell J. Boyd. *J. Phys. Chem. A.*, 102:7294–7296, 1998.

[90] Veronica Vaida and Jill E. Headrick. *J. Phys. Chem. A*, 104(23):5401–5412, 2000.

[91] Henrik G. Kjaergaard, Timothy W. Robinson, Daryl L. Howard, John S. Daniel, Jill E. Headrick, and Veronica Vaida. *J. Phys. Chem. A*, 107:10680–10686, 2003.

[92] Zdenek Slanina and Filip Uhlik. *NATO Sci. Ser. IV*, 27:101–110, 2003.

[93] Akiyoshi Sabu, Satomi Kondo, Ryu Saito, Yasuko Kasai, and Kenro Hashimoto. *J. Phys. Chem. A*, 109:1836–1842, 2005.

[94] Jewel A. G. Gomes, John L. Gossage, Harimadhav Balu, Mehmet Kesmez, Ferrel Bowen, Richard S. Lumpkin, and David L. Cocke. *Spectrochim. Acta, Part A*, 61A:3082–3086, 2005.

[95] Zdenek Slanina, Filip Uhlik, Shyi-Long Lee, and Shigeru Nagase. *J. Quant. Spectrosc. Radiat. Transfer*, 97:415–423, 2005.

[96] Yasuko Kasai, Ryu Saito, Kenro Hashimoto, Satomi Kondo, Yoshihiro Sumiyoshi, and Yasuki Endo. *Atmos. Chem. Phys.*, 11:8607–8612, 2011.

[97] Kuo-Nan Liou. Oxford University Press, 1st edition, 1992.

[98] Thomas Richardson, Susan de Gala, Robert H. Crabtree, and Per E. M. Siegbahn. *J. Am. Chem. Soc.*, 117(51):12875–6, 1995.

[99] Robert H. Crabtree. *Chem. Rev.*, 116:8750–8769, 2016.

[100] Hideaki Umeyama and Keiji. Morokuma. *J. Am. Chem. Soc.*, 98(23):7208–20, 1976.

[101] Arne Haaland. *Angew. Chem. Int. Ed.*, 28:992–1007, 1989.

[102] Volker Jonas, Gernot Frenking, and Manfred T. Reetz. *J. Am. Chem. Soc.*, 116(19):8741–53, 1994.

[103] Battelle Memorial Institute, United States. Department of Energy, United States. Department of Energy. Richland Operations Office, United States. Department of Energy. Office of Scientific, and Technical Information. United States. Department of Energy, 2011.

[104] Christopher J. Poulsen, Clay Tabor, and Joseph D. White. *Science (Washington, DC, U. S.)*, 348(6240):1238–1241, 2015.

[105] Robert Kalescky, Wenli Zou, Elfi Kraka, and Dieter Cremer. *Chem. Phys. Lett.*, 554:243–247, 2012.

[106] Veronica Vaida, John S. Daniel, Henrik G. Kjaergaard, Lisa M. Goss, and Adrian F. Tuck. *Quarterly Journal of the Royal Meteorological Society*, 127(575):1627–1643, 2001.

[107] Henrik G. Kjaergaard, Geoffrey R. Low, Timothy W. Robinson, and Daryl L. Howard. *J. Phys. Chem. A*, 106:8955–8962, 2002.

[108] Thomas L. Ellington and Gregory S. Tschumper. *Comput. Theo. Chem.*, 1021:109–113, 2013.

[109] Akiyoshi Sabu, Satomi Kondo, Nobuaki Miura, and Kenro Hashimoto. *Chem. Phys. Lett.*, 391:101–105, 2004.

[110] Larry A. Curtiss and Carlos A. Melendres. *J. Phys. Chem.*, 88:1325–1329, 1984.

[111] Patricia R. B. Barreto, Alessandra F. Albernaz, Amedeo Capobianco, Federico Palazzetti, Andrea Lombardi, Gaia Grossi, and Vincenzo Aquilanti. *Comput. Theor. Chem.*, 990:53–61, 2012.

[112] Richard J. Wheatley and Allan H. Harvey. *J. Chem. Phys.*, 127:1–8, 2007.

[113] Richard J. Wheatley and Timothy C. Lillestolen. *Int. Rev. Phys. Chem.*, 26:449–485, 2007.

[114] Paul D. Cooper, Henrik G. Kjaergaard, Vaughan S. Langford, Allan J. McKinley, Terence I. Quickenden, Timothy W. Robinson, and Daniel P. Schofield. *J. Phys. Chem. A*, 109:4274–4279, 2005.

[115] Andrew J. Bell and Timothy G. Wright. *Phys. Chem. Chem. Phys.*, 6:4385–4390, 2004.

[116] Timothy W. Robinson and Henrik G. Kjaergaard. *J. Chem. Phys.*, 119:3717–3720, 2003.

[117] J.F. Stanton, J. Gauss, M.E. Harding, P.G. Szalay with contributions from A.A. Auer, R.J. Bartlett, U. Benedikt, C. Berger, D.E. Bernholdt, Y.J. Bomble, L. Cheng, O. Christiansen, M. Heckert, O. Heun, C. Huber, T.-C. Jagau, D. Jonsson, J. Jusélius, K. Klein, W.J. Lauderdale, D.A. Matthews, T. Metzroth, L.A. Mück, D.P. O'Neill, D.R. Price, E. Prochnow, K. Ruud, F. Schiffmann, W. Schwalbach, S. Stopkowicz, A. Tajti, J. Vázquez, F. Wang, J.D. Watts, the integral packages MOLECULE (J. Almlöf, P.R. Taylor), PROPS (P.R. Taylor), ABACUS (T. Helgaker, H.J. Aa. Jensen, P. Jørgensen, J. Olsen), ECP routines by A. V. Mitin, and C. van Wüllen. For the current version see http://www.cfour.de.

[118] H.-J. Werner, P. J. Knowles, F. R. Manby, M. Schütz, P. Celani, G. Knizia, T. Korona, R. Lindh, A. Mitrushenkov, G. Rauhut, T. B. Adler, R. D. Amos, A. Bernhardsson, A. Berning, D. L. Cooper, M. J. O. Deegan, A. J. Dobbyn, F. Eckert, E. Goll, C. Hampel, A. Hesselmann, G. Hetzer, T. Hrenar, G. Jansen, C. Köppl, Y. Liu, A. W. Lloyd, R. A. Mata, A. J. May, S. J. McNicholas, W. Meyer, M. E. Mura, A. Nicklass, P. Palmieri, K. Pflüger, R. Pitzer, M. Reiher, T. Shiozaki, H. Stoll, A. J. Stone, R. Tarroni, T. Thorsteinsson, M. Wang, and A. Wolf. MOLPRO, version 2010.1, a package of ab initio programs, 2010.

[119] Peter J. Knowles, Claudia Hampel, and Hans-Joachim Werner. *J. Chem. Phys.*, 99:7294–7296, 1993.

[120] Gerald Knizia, Thomas B. Adler, and Hans-Joachim Werner. *J. Chem. Phys.*,

130:1–20, 2009.

[121] M. J. Frisch, G. W. Trucks, H. B. Schlegel, G. E. Scuseria, M. A. Robb, J. R. Cheeseman, G. Scalmani, V. Barone, B. Mennucci, G. A. Petersson, H. Nakatsuji, M. Caricato, X. Li, H. P. Hratchian, A. F. Izmaylov, J. Bloino, G. Zheng, J. L. Sonnenberg, M. Hada, M. Ehara, K. Toyota, R. Fukuda, J. Hasegawa, M. Ishida, T. Nakajima, Y. Honda, O. Kitao, H. Nakai, T. Vreven, Jr. J. A. Montgomery, J. E. Peralta, F. Ogliaro, M. Bearpark, J. J. Heyd, E. Brothers, K. N. Kudin, V. N. Staroverov, T. Keith, R. Kobayashi, J. Normand, K. Raghavachari, A. Rendell, J. C. Burant, S. S. Iyengar, J. Tomasi, M. Cossi, N. Rega, J. M. Millam, M. Klene, J. E. Knox, J. B. Cross, V. Bakken, C. Adamo, J. Jaramillo, R. Gomperts, R. E. Stratmann, O. Yazyev, A. J. Austin, R. Cammi, C. Pomelli, J. W. Ochterski, R. L. Martin, K. Morokuma, V. G. Zakrzewski, G. A. Voth, P. Salvador, J. J. Dannenberg, S. Dapprich, A. D. Daniels, O. Farkas, J. B. Foresman, J. V. Ortiz, J. Cioslowski, and D. J. Fox. Gaussian 09 Revision C.01. Gaussian Inc. Wallingford CT 2010.

[122] M. F. Crawford, H. L. Welsh, and J. L. Locke. *Physical Review*, 75:1607, 1949.

[123] Henrik G. Kjaergaard, Anna L. Garden, Galina M. Chaban, R. Benny Gerber, Devin A. Matthews, and John F. Stanton. *Journal of Physical Chemistry A*, 112:4324–4335, 2008.

[124] Timothy J. Lee. *Chemical Physics Letters*, 372:362–367, 2003.

[125] Sheldon G. Shore and Robert W. Parry. *J. Am. Chem. Soc.*, 77:6084–5, 1955.

[126] Edward W. Hughes. *J. Am. Chem. Soc.*, 78:502–3, 1956.

[127] Ernest L. Lippert and William N. Lipscomb. *J. Am. Chem. Soc.*, 78:503–4, 1956.

[128] R. C. Taylor and C. L. Cluff. *Nature (London, U. K.)*, 182:390–1, 1958.

[129] Robert C. Taylor. *Adv. Chem. Ser.*, 42:59–70, 1964.

[130] W. Sawodny and J. Goubeau. *Z. Phys. Chem. (Muenchen, Ger.)*, 44(3/4):227–41, 1965.

[131] J. Smith, K. S. Seshadri, and David. White. *J. Mol. Spectrosc.*, 45(3):327–37, 1973.

[132] R. D. Suenram and L. R. Thorne. *Chem. Phys. Lett.*, 78(1):157–60, 1981.

[133] L. R. Thorne, R. D. Suenram, and F. J. Lovas. *J. Chem. Phys.*, 78(1):167–71, 1983.

[134] John D. Carpenter and Bruce S. Ault. *Chem. Phys. Lett.*, 197(1-2):171–4, 1992.

[135] Wim T. Klooster, Thomas F. Koetzle, Per E. M. Siegbahn, Thomas B. Richardson, and Robert H. Crabtree. *J. Am. Chem. Soc.*, 121(27):6337–6343, 1999.

[136] Damian G. Allis, Mark E. Kosmowski, and Bruce S. Hudson. *J. Am. Chem. Soc.*, 126(25):7756–7757, 2004.

[137] Nancy J. Hess, Mark E. Bowden, Vencislav M. Parvanov, Chris Mundy, Shawn M. Kathmann, Gregory K. Schenter, and Tom. Autrey. *J. Chem. Phys.*, 128(3):034508/1–034508/11, 2008.

[138] C. Ziparo, D. Colognesi, A. Giannasi, and M. Zoppi. *J. Phys. Chem. A*, 116(35):8827–8832, 2012.

[139] Ang Liu and Yang. Song. *J. Phys. Chem. C*, 116(3):2123–2131, 2012.

[140] Yu Lin, Hongwei Ma, Charles Wesley Matthews, Brian Kolb, Stanislav Sinogeikin, Timo Thonhauser, and Wendy L. Mao. *J. Phys. Chem. C*, 116(3):2172–2178, 2012.

[141] Shawn M. Kathmann, Christopher J. Mundy, Gregory K Schenter, Tom Autrey, Philippe C. Aeberhard, Bill David, Martin O. Jones, and Timmy Ramirez-Cuesta. *J. Phys. Chem. C.*, 116:5926–59311, 2012.

[142] A. Paolone, F. Teocoli, S. Sanna, O. Palumbo, and T. Autrey. *J. Phys. Chem. C*, 117(2):729–734, 2013.

[143] Johanna Nylén, Lars Eriksson, Daryn Bensen, and Ulrich Häussermann. *J. Chem. Phys.*, 139(054507):1–7, 2013.

[144] Yansum Yao, Xue Yong, John S. Tse, and Michael J. Greschner. *J. Phys. Chem. C.*, 118:29591–29598, 2014.

[145] Amrendra Vijay and D. N. Sathyanarayana. *Chem. Phys.*, 198(3):345–52, 1995.

[146] P. L. A. Popelier. *J. Phys. Chem. A*, 102(10):1873–1878, 1998.

[147] Gabriel Merino, Vladimir I. Bakhmutov, and Alberto. Vela. *J. Phys. Chem. A*, 106(37):8491–8494, 2002.

[148] H. Cybulski and J. Sadlej. *Pol. J. Chem.*, 81(5-6):683–697, 2007.

[149] Christopher J. Cramer and Wayne L. Gladfelter. *Inorg. Chem.*, 36(23):5358–5362, 1997.

[150] Jinshan Li, Feng Zhao, and Fuqian. Jing. *J. Chem. Phys.*, 116(1):25–32, 2002.

[151] Tapas Kar and Steve Scheiner. *J. Chem. Phys.*, 119(3):1473–1482, 2003.

[152] Jan Dillen and Paul Verhoeven. *J. Phys. Chem. A*, 107(14):2570–2577, 2003.

[153] Carole A. Morrison and Muhammad M. Siddick. *Angew. Chem., Int. Ed.*, 43(36):4780–4782, 2004.

[154] Yun Meng, Zhengyu Zhou, Chunsheng Duan, Ben Wang, and Qin. Zhong. *J. Mol. Struct.: THEOCHEM*, 713(1-3):135–144, 2005.

[155] Jean Demaison, Jacques Lievin, Attila G. Csar, and Claudine. Gutle. *J. Phys. Chem. A*, 112(19):4477–4482, 2008.

[156] Mariusz P. Mitoraj. *J. Phys. Chem. A*, 115(51):14708–14716, 2011.

[157] Doris Guerra, Jorge David, and Albeiro. Restrepo. *Phys. Chem. Chem. Phys.*, 14(43):14892–14897, 2012.

[158] Robert L. Sams, Sotiris S. Xantheas, and Thomas A. Blake. *J. Phys. Chem. A*, 116(12):3124–3136, 2012.

[159] Monika Parafiniuk and Mariusz P. Mitoraj. *J. Mol. Model*, 20(2272):2–9, 2014.

[160] Andy D. Zapata-Escobar, Teresa Cárcamo-Camacho, C. Z. Hadad, and Albeiro Restrepo. *Theor. Chem. Acc.*, 135(95):1–12, 2016.

[161] Bing Yuan, Joong-Won Shin, and Elliot R. Bernstein. *J. Chem. Phys.*, 144(144315):1–23, 2016.

[162] Fang Huang, Jinliang Jiang, Mingwei Wen, and Zhi-Xiang Wang. *J. Chem. Theory Comput.*, 13(1):1350074–1350090, 2014.

[163] Vinh S. Nguyen, Myrna H. Matus, Minh T. Nguyen, and David A. Dixon. *J. Phys. Chem. A.*, 112:9946–9954, 2008.

[164] Myrna H. Matus, Daniel J. Grant, Minh T. Nguyen, and David A. Dixon. *J. Phys. Chem. C.*, 113:16553–16560, 2009.

[165] Vinh S. Nguyen, Myrna H. Matus, Daniel J. Grant, Minh T. Nguyen, and David A. Dixon. *J. Phys. Chem. A.*, 111:8844–8856, 2007.

[166] S. Karthikeyan, Robert Sedlak, and Pavel Hobza. *J. Phys. Chem. A.*, 115:9422–9428, 2011.

[167] Kunduchi P. Vijayalakshmi and H. Suresh, Cherumuttathu. *J. Phys. Chem. A.*, 121:2704, 2017.

[168] Robert N. Compton and Nathan I. Hammer. *J. Phys. Conf.*, 548:012017, 2014.

[169] Y. Zhao and D. G. Truhlar. *J. Chem. Phys*, 125(194101):1–18, 2006.

[170] Thom H. Dunning, Jr. *J. Chem. Phys.*, 90(2):1007–1023, 1989.

[171] Michael. J. Frisch, John. A. Pople, and J. Stephen Binkly.

[172] M. J. Frisch, G. W. Trucks, H. B. Schlegel, G. E. Scuseria, M. A. Robb, J. R. Cheeseman, G. Scalmani, V. Barone, B. Mennucci, G. A. Petersson, H. Nakatsuji, M. Caricato, X. Li, H. P. Hratchian, A. F. Izmaylov, J. Bloino, G. Zheng, J. L. Sonnenberg, M. Hada, M. Ehara, K. Toyota, R. Fukuda, J. Hasegawa, M. Ishida, T. Nakajima, Y. Honda, O. Kitao, H. Nakai, T. Vreven, Montgomery Jr., J. A., J. E. Peralta, F. Ogliaro, M. Bearpark, J. J. Heyd, E. Brothers, K. N. Kudin, V. N. Staroverov, R. Kobayashi, J. Normand, K. Raghavachari, A. Rendell, J. C. Burant, S. S. Iyengar, J. Tomasi, M. Cossi, N. Rega, J. M. Millam, M. Klene, J. E. Knox, J. B. Cross, V. Bakken, C. Adamo, J. Jaramillo, R. Gomperts, R. E. Stratmann, O. Yazyev, A. J. Austin, R. Cammi, C. Pomelli, J. W. Ochterski, R. L. Martin, K. Morokuma, V. G. Zakrzewski, G. A. Voth, P. Salvador, J. J. Dannenberg, S. Dapprich, A. D. Daniels, Ö. Farkas, J. B. Foresman, J. V. Ortiz, J. Cioslowski, and D. J. Fox. Gaussian09 Revision D.01. Gaussian Inc. Wallingford CT 2009.

[173] Karine Mazmanian, Karen Sargsyan, Cedric Grauffel, Todor Dudev, and Carmay. Lim. *J. Phys. Chem. B*, 120(39):10288–10296, 2016.

[174] Vasily S. Minkov and Elena V. Boldyreva. *J. Phys. Chem. B*, 117(46):14247–14260, 2013.

[175] Goedele Roos, Nicolas Foloppe, and Joris. Messens. *Antioxid. Redox Signaling*, 18(1):94–127, 2013.

[176] Vasily S. Minkov and Elena V. Boldyreva. *J. Phys. Chem. B*, 118(29):8513–8523, 2014.

[177] Yoichi Yamazaki, Tomoko Nagata, Akihisa Terakita, Hideki Kandori, Yoshinori Shichida, and Yasushi. Imamoto. *Biophysics (Biophys. Soc. Jpn.)*, 10:1–7, 7 pp., 2014.

[178] R. J. Zauhar, C. L. Colbert, R. S. Morgan, and W. J. Welsh. *Biopolymers*, 53(3):233–248, 2000.

[179] Debnath Pal and Pinak. Chakrabarti. *J. Biomol. Struct. Dyn.*, 19(1):115–128, 2001.

[180] Bengt Nelander. *J. Chem. Phys.*, 69:3870–3871, 1978.

[181] A. J. Barnes, R. M. Brentwood, and M. P. Wright. *J. Mol. Struct.*, 118:97, 1984.

[182] Y. B. Wang, Fu-Ming Tao, and Yuh-Kang Pan. *Chem. Phys. Lett.*, 230:481, 1994.

[183] Glenisson de Oliveira and Clifford E. Dykstra. *Chem. Phys. Lett.*, 243(1,2):158–64, 1995.

[184] Benjamin J. Mintz and Jerry M. Parks. *J. Phys. Chem. A.*, 116:1086, 2012.

[185] Roger D. Amos. *Chem. Phys.*, 103:145, 1986.

[186] Glenisson de Oliveira and Clifford E. Dykstra. *Journal of Molecular Structure: THEOCHEM*, 362(3):275 – 282, 1996.

[187] Mark A. Spackman. *J. Phys. Chem.*, 91(12):3179–86, 1987.

[188] Joseph R. Lane and Henrik G. Kjaergaard. *J. Chem. Phys.*, 131(034):307, 2009.

[189] Asger Halkier, Henrik Koch, Poul Jørgensen, Ove Christiansen, Ida M. Beck Nielsen, and Trygve Helgaker. *Theor. Chem. Acc.*, 97(1):150–157, 1997.

[190] G. S. Tschumper, M. L. Leininger, B. C. Hoffman, E. F. Valeev, H. F. Schaefer, and M. Quack. 116(2):690–701, 2002.

[191] Joseph R. Lane. *J. Comput. Theory Chem.*, 9(1):316–323, 2013.

[192] T. H. Edwards, N. K. Moncur, and L. E. Snyder. *The Journal of Chemical Physics*, 46(6):2139–2142, 1967.

[193] L. Fossat-Lechuga, J. M. Flaud, and C. Camy-Peyret. *Can. J. Phys.*, 62:1889, 1984.

[194] Kojiro Koga, Akinori Takami, and Seiichiro. Koda. *Chem. Phys. Lett.*, 293(3,4):180–184, 1998.

[195] Glenisson de Oliveira and Clifford E. Dykstra. *J. Chem. Phys.*, 110(1):289–295, 1999.

[196] F. H. Allen, C. M. Bird, R. S. Rowland, and P. R. Raithby. *Acta Cryst. B*, 53:696–701, 1997.

[197] Anthony J. Tursi and Eugene R. Nixon. *J. Chem. Phys.*, 53:518–521, 1970.

[198] Esa Isoniemi, Mika Pettersson, Leonid Khriachtchev, Jan Lundell, and Markkun Rasane. *J. Phys. Chem. A.*, 103:679–685, 1999.

[199] John R. Sabin. *J. Am. Chem. Soc.*, 93(15):3613, 1971.

[200] Janet E. Del Bene. *J. Phys. Chem.*, 92:2874, 1988.

[201] J. A. Platts, S. T. Howard, and B. R. F. Bracke. *J. Am. Chem. Soc.*, 118:2726, 1996.

[202] Bela Paizs and Sandor Suhai. *J. Comput. Chem.*, 19(6):575–584, 1998.

[203] Robert J. Doerksen, Ajit J. Thakkar, Toshikatsu Koga, and Minako. Hayashi. *J. Mol. Struct.: THEOCHEM*, 488:217–221, 1999.

[204] Jose M. Hermida-Ramon, Enrique M. Cabaleiro-Lago, and Jesus. Rodriguez-Otero. *J. Chem. Phys.*, 122(20):204315/1–204315/5, 2005.

[205] Ravi Joshi, Tapan K. Ghanty, Sergej Naumov, and Tulsi. Mukherjee. *J. Phys. Chem. A*, 111(12):2362–2367, 2007.

[206] Satoshi Maeda and Koichi. Ohno. *J. Phys. Chem. A*, 112(13):2962–2968, 2008.

[207] Katarzyna Walczak, Joachim Friedrich, and Michael Dolg. *Chemical Physics*, 365(1):38 – 43, 2009.

[208] Robert Hellmann, Eckard Bich, Eckhard Vogel, and Velisa. Vesovic. *Phys. Chem. Chem. Phys.*, 13(30):13749–13758, 2011.

[209] Himansu S. Biswal, Surjendu Bhattacharyya, Aditi Bhattacherjee, and Sanjay. Wategaonkar. *Int. Rev. Phys. Chem.*, 34(1):99–160, 2015.

[210] Aditi Bhattacherjee, Yoshiyuki Matsuda, Asuka Fujii, and Sanjay. Wategaonkar. *J. Phys. Chem. A*, 119(7):1117–1126, 2015.

[211] M. Alberti, A. Amat, A. Aguilar, and F. Pirani. *J. Phys. Chem. A*, 120(27):4749–4757, 2016.

[212] Kono H. Lemke. *J. Chem. Phys.*, 146:234301, 2017.

[213] Hideji Tsujii, Kenji Takizawa, and Seiichiro. Koda. *Chem. Phys.*, 285(2-3):319–326, 2002.

[214] Henrik G. Kjaergaard, Anna L. Garden, Galina M. Chaban, R. Benny Gerber, Devin A. Matthews, and John F. Stanton. *The Journal of Physical Chemistry A*, 112(18):4324–4335, 2008.

[215] S.F. Boys and F. Bernardi. *Mol. Phys.*, 19(4):553–566, 1970.

[216] H.B. Jansen and P. Ros. *Chem. Phys. Lett.*, 3:140–143, March 1969.

[217] B. Liu and A. D. McLean. *J. Chem. Phys.*, 59(8):4557–4558, 1973.

[218] Slvia Simon, Miquel Duran, and J. J. Dannenberg. *J. Chem. Phys.*, 105(24):11024–11031, 1996.

[219] Winfried Schneider and Walter Thiel. *Chem. Phys. Lett.*, 157:367–373, 1989.

[220] Linus Pauling. *J. Am. Chem. Society*, 69(3):542–553, 1947.

[221] S. S. Batsanov. *Inorg. Mater.*, 37(9):871–885, Sep 2001.

[222] Martin Rahm, Roald Hoffmann, and N. W. Ashcroft. *Chem. Eur. J.*, 22(41):14625–14632, 2016.

[223] P. G. Sennikov. *J. Phys. Chem.*, 98(19):4973–4981, 1994.

[224] J. A. Odutola and T. R. Dyke. *J. Chem. Phys.*, 72:5062–5070, 1980.

[225] Blithe E. Rocher-Casterline, Lee C. Ch'ng, Andrew K. Mollner, and Hanna Reisler. *J. Chem. Phys.*, 134:21101/1–21101–4, 2011.

[226] L. A. Curtiss, D. J. Frurip, and M. Blander. *J. Chem. Phys.*, 71:2703–2711, 1979.

[227] Johnson Sarah N. and Tschumper Gregory S. *J. Comput. Chem.*, 39(14):839–843, 2018.

[228] Thomas More Sexton, J. Coleman Howard, and Gregory S. Tschumper. *J. Chem. Phys. A*, ASAP, 2018.

[229] John L. Wallace. *Trends Pharmacol. Sci.*, 28(10):501 – 505, 2007.

[230] Ling Li, Matthew Whiteman, Yan Yi Guan, Kay Li Neo, Yvonne Cheng, Shiau Wei Lee, Yujun Zhao, Rajamanian Baskar, Choon-Hong Tan, and Philip K. Moore. *Circulation*, 117(18):2351–2360, 2008.

[231] Martin N. Hughes, Miguel N. Centelles, and Kevin P. Moore. *Free Radical Biol. Med.*, 47(10):1346 – 1353, 2009.

[232] Anna Sparatore, Elena Perrino, Valerio Tazzari, Daniela Giustarini, Ranieri Rossi, Giuseppe Rossoni, Kati Erdman, Henning Schröder, and Piero Del Soldato. *Free Radical Biol. Med.*, 46(5):586 – 592, 2009.

[233] Giuseppe Caliendo, Giuseppe Cirino, Vincenzo Santagada, and John L. Wallace. *J. Med. Chem.*, 53(17):6275–6286, 2010.

[234] Matthew Whiteman and Paul G. Winyard. *Expert Rev. Clin. Pharmacol.*, 4(1):13–32, 2011.

[235] John L. Wallace, Jose G. P. Ferraz, and Marcelo N. Muscara. *Antioxid. Redox Signal.*, 17(1):58–67, 2012.

[236] Ravinder Kodela, Mitali Chattopadhyay, and Khosrow. Kashfi. *ACS Med. Chem. Lett.*, 3(3):257–262, 2012.

[237] Khosrow Kashfi and Kenneth R. Olson. *Biochem. Pharmacol.*, 85(5):689 – 703, 2013.

[238] Ralph C. Kerns and Leland C. Allen. *J. Am. Chem. Soc.*, 100:6584, 1978.

[239] Thomas L. Ellington and Gregory S. Tschumper. *Comput. Theo. Chem.*, 1021:109, 2013.

[240] Katelyn M. Dreux and Gregory S. Tschumper. *Comput. Theo. Chem.*, 1072:21, 2015.

[241] H.J. Werner, P. J. Knowles, F. R. Manby, M. Schütz, P. Celani, G. Knizia, T. Korona, R. Lindh, A. Mitrushenkov, G. Rauhut, T. B. Adler, R. D. Amos,

A. Bernhardsson, A. Berning, D. L. Cooper, M. J. O. Deegan, A. J. Dobbyn, F. Eckert, E. Goll, C. Hampel, A. Hesselmann, G. Hetzer, T. Hrenar, G. Jansen, C. Köppl, Y. Liu, A. W. Lloyd, R. A. Mata, A. J. May, S. J. McNicholas, W. Meyer, M. E. Mura, A. Nicklass, P. Palmieri, K. Pflüger, R. Pitzer, M. Reiher, T. Shiozaki, H. Stoll, A. J. Stone, R. Tarroni, T. Thorsteinsson, M. Wang, and A. Wolf. MOLPRO, version 2015.1, a package of ab initio programs, 2015.

[242] Gregory S. Tschumper. *Reliable Electronic Structure Computations for Weak Noncovalent Interactions in Clusters*, chapter 2, pages 39–90. Wiley-Blackwell, 2009.

[243] Julie A. Anderson, Kelly Crager, Lisa Fedoroff, and Gregory S. Tschumper. *J. Chem. Phys.*, 121(22):11023–11029, 2004.

LIST OF APPENDICES

Appendix A: Chapter 2 Supplementary Information

Supplementary Material for:

Anchoring the potential energy surface of an important atmospheric van der Waals dimer, the $O_2 \cdots H_2O$ complex

Katelyn M. Dreux and Gregory S. Tschumper*

Department of Chemistry and Biochemistry
University of Mississippi, University, Mississippi 38677–1848 USA

Table S1: Cartesian Coordinates (in bohr) of H_2O from CCSD(T)/haQZ optimization

H	0.00000000	-1.43139379	0.98674978
O	0.00000000	0.00000000	-0.12434841
H	0.00000000	1.43139379	0.98674978

Table S2: Cartesian Coordinates (in bohr) of O_2 from CCSD(T)/haQZ optimization

O	0.00000000	0.00000000	-1.14155135
O	0.00000000	0.00000000	1.14155135

Table S3: Cartesian Coordinates (in bohr) of structure I from CCSD(T)/haQZ optimization

H	-5.56322617	0.11025064	0.00000000
O	-3.77425991	-0.17872807	0.00000000
H	-3.04653670	1.48137617	0.00000000
O	1.92519201	1.15606279	0.00000000
O	2.39156123	-1.07762168	0.00000000

Table S4: Cartesian Coordinates (in bohr) of structure II from CCSD(T)/haQZ optimization

O	0.00000000	-1.14073509	-2.19934938
O	0.00000000	0.00000000	3.78204809
O	0.00000000	1.14073509	-2.19934938
H	0.00000000	-1.43159668	4.89334681
H	0.00000000	1.43159668	4.89334681

Table S5: Cartesian Coordinates (in bohr) of structure III from CCSD(T)/haQZ optimization

O	-1.14105104	0.00000000	-2.22952343
O	0.00000000	0.00000000	3.83561508
O	1.14105104	0.00000000	-2.22952343
H	0.00000000	1.43137913	4.94715739
H	0.00000000	-1.43137913	4.94715739

Table S6: Cartesian Coordinates (in bohr) of structure IV from CCSD(T)/haQZ optimization

O	0.06405665	3.80632818	0.00000000
O	0.00464413	-2.19998796	1.14123722
O	0.00464413	-2.19998796	-1.14123722
H	-1.74691248	3.87886706	0.00000000
H	0.58287546	5.54275324	0.00000000

Table S7: Cartesian Coordinates (in bohr) of structure V from CCSD(T)/haQZ optimization

O	-1.66361936	0.76046386	0.00000000
H	2.84810643	-0.07953471	0.00000000
O	-3.50014987	-0.59488854	0.00000000
O	4.66027805	-0.04751910	0.00000000
H	5.14266379	-1.79410306	0.00000000

Table S8: Cartesian Coordinates (in bohr) of structure VI from CCSD(T)/haQZ optimization

O	-4.89145285	0.12778963	0.00000000
O	1.58248006	-0.05089319	0.00000000
O	3.86235909	0.03199979	0.00000000
H	-3.11295131	-0.21966898	0.00000000
H	-5.66969081	-1.50859309	0.00000000

Table S9: Cartesian Coordinates (in bohr) of structure VII from CCSD(T)/haQZ optimization

O	0.00000000	-1.14172692	-2.30626066
O	0.00000000	0.00000000	4.22074022
O	0.00000000	1.14172692	-2.30626066
H	0.00000000	-1.43120130	3.10892526
H	0.00000000	1.43120130	3.10892526

Table S10: Cartesian Coordinates (in bohr) of structure VIII from CCSD(T)/haQZ optimization

O	-4.71928782	0.15556218	0.00000000
O	1.60732895	-0.66345503	0.00000000
O	3.56745088	0.50631255	0.00000000
H	-3.61449437	0.01254026	-1.42930288
H	-3.61449437	0.01254026	1.42930288

Table S11: Cartesian Coordinates (in bohr) of structure IX from CCSD(T)/haQZ optimization

O	1.93147209	1.10414574	0.00000000
H	-2.87127986	0.86789075	0.00000000
O	2.90685299	-0.96010900	0.00000000
O	-4.41336254	-0.08441484	0.00000000
H	-3.87318408	-1.81413366	0.00000000

Table S12: Cartesian Coordinates (in bohr) of structure X from CCSD(T)/haQZ optimization

O	0.00000000	0.00000000	-1.51608245
O	0.00000000	0.00000000	4.84419288
H	0.00000000	-1.42980887	3.73083923
H	0.00000000	1.42980887	3.73083923
O	0.00000000	0.00000000	-3.79826401

Table S13: Cartesian Coordinates (in bohr) of structure XI from CCSD(T)/haQZ optimization

O	0.00000000	0.00000000	-1.46976743
O	0.00000000	0.00000000	4.51541022
H	0.00000000	-1.43129339	5.62702075
H	0.00000000	1.43129339	5.62702075
O	0.00000000	0.00000000	-3.75474972

Table S14: Cartesian Coordinates (in bohr) of structure XII from CCSD(T)/haQZ optimization

O	-1.14220688	0.00000000	-2.39729843
O	0.00000000	0.00000000	4.38241207
O	1.14220688	0.00000000	-2.39729843
H	0.00000000	1.43112673	3.27083581
H	0.00000000	-1.43112673	3.27083581

Table S15: Harmonic vibrational frequencies (in cm^{-1}) and IR intensities (in parentheses in km mol^{-1}) of H_2O. Symmetry labels correspond to orientation given in Table S1.

Symm	UMP2/haTZ		UMP2/haQZ		UCCSD(T)/haTZ		UCCSD(T)/haQZ	
a_1	3824.5	(7.6)	3840.5	(6.8)	3813.6	(4.6)	3831.8	(4.2)
a_1	1630.1	(73.8)	1632.8	(73.5)	1647.9	(72.4)	1650.5	(72.5)
b_2	3951.9	(75.8)	3966.4	(78.5)	3924.3	(54.9)	3941.4	(57.8)

Table S16: Harmonic vibrational frequencies (in cm^{-1}) of O_2.

Symm	UMP2/haTZ	UMP2/haQZ	UCCSD(T)/haTZ	UCCSD(T)/haQZ
Σ_g^+	1454.7	1479.7	1574.4	1595.7

Table S17: Harmonic vibrational frequencies (in cm^{-1}) and IR intensities (in parentheses in km mol^{-1}) of structure II. Symmetry labels correspond to orientation given in Table S4.

Symm	UMP2/haTZ		UMP2/haQZ		UCCSD(T)/haTZ		UCCSD(T)/haQZ	
a_1	3821.1	(6.8)	3837.5	(6.8)	3811.3	(4.2)	3829.8	(4.3)
a_1	1629.8	(75.8)	1633.0	(74.7)	1647.4	(74.1)	1650.5	(73.4)
a_1	1457.9	(< 0.1)	1482.4	(< 0.1)	1579.0	(< 0.1)	1599.9	(< 0.1)
a_1	63.2	(< 0.1)	59.5	(< 0.1)	61.9	(< 0.1)	58.1	(< 0.1)
a_2	56.9	(0.0)	53.0	(0.0)	34.5	(0.0)	39.4	(0.0)
b_1	82.2	(236.9)	81.6	(233.2)	70.5	(233.0)	68.5	(230.1)
b_2	3948.4	(77.4)	3963.2	(79.5)	3921.9	(56.9)	3939.3	(59.2)
b_2	144.9	(21.9)	113.7	(18.0)	64.5	(6.5)	63.6	(5.8)
b_2	29.0i	(52.2)	35.3i	(54.8)	33.4i	(61.9)	39.0i	(62.4)

Table S18: Harmonic vibrational frequencies (in cm^{-1}) and IR intensities (in parentheses in km mol^{-1}) of structure III. Symmetry labels correspond to orientation given in Table S5.

Symm	UMP2/haTZ		UMP2/haQZ		UCCSD(T)/haTZ		UCCSD(T)/haQZ	
a_1	3821.7	(6.8)	3838.0	(6.9)	3811.7	(4.1)	3830.1	(4.3)
a_1	1630.3	(75.0)	1633.5	(73.9)	1647.9	(73.3)	1651.0	(72.7)
a_1	1456.3	(< 0.1)	1480.9	(< 0.1)	1577.3	(< 0.1)	1598.3	(< 0.1)
a_1	59.4	(< 0.1)	55.2	(< 0.1)	58.9	(< 0.1)	54.5	(< 0.1)
a_2	9.6i	(0.0)	33.8i	(0.0)	34.1i	(0.0)	38.5i	(0.0)
b_1	69.5	(234.0)	64.7	(228.2)	61.4	(184.7)	56.0	(165.4)
b_1	103.8	(1.7)	81.9	(4.0)	47.4	(43.3)	46.3	(60.5)
b_2	3948.9	(77.1)	3963.6	(79.2)	3922.2	(56.5)	3939.4	(58.9)
b_2	38.7	(76.2)	20.4	(75.3)	39.9	(74.7)	22.3	(73.9)

Table S19: Harmonic vibrational frequencies (in cm^{-1}) and IR intensities (in parentheses in km mol^{-1}) of structure IV

Symm	UMP2/haTZ		UMP2/haQZ		UCCSD(T)/haTZ		UCCSD(T)/haQZ	
a'	3948.2	(73.9)	3962.8	(76.5)	3921.5	(53.7)	3938.9	(56.4)
a'	3820.9	(7.0)	3837.1	(6.8)	3810.9	(4.3)	3829.5	(4.4)
a'	1630.4	(81.2)	1633.7	(80.1)	1648.0	(79.6)	1651.0	(79.0)
a'	1454.9	(< 0.1)	1479.9	(< 0.1)	1576.2	(< 0.1)	1597.3	(< 0.1)
a'	62.5	(9.7)	59.5	(15.1)	61.3	(8.7)	57.6	(10.4)
a'	22.8	(73.1)	34.8	(66.7)	23.3	(72.8)	30.1	(70.4)
a''	108.9	(7.7)	87.7	(30.7)	69.9	(139.4)	64.0	(123.3)
a''	71.4	(202.6)	66.6	(169.7)	44.7	(53.6)	43.8	(63.0)
a''	18.9	(19.2)	37.2i	(25.8)	55.6i	(28.3)	56.9i	(32.7)

Table S20: Harmonic vibrational frequencies (in cm^{-1}) and IR intensities (in parentheses in km mol^{-1}) of structure V.

Symm	UMP2/haTZ		UMP2/haQZ		UCCSD(T)/haTZ		UCCSD(T)/haQZ	
a′	3951.3	(106.0)	3965.7	(108.7)	3923.4	(83.4)	3940.5	(88.5)
a′	3825.2	(13.3)	3840.7	(10.4)	3813.8	(14.4)	3831.9	(13.1)
a′	1706.8	(0.2)	1638.5	(0.9)	1650.1	(59.2)	1651.4	(57.6)
a′	1630.0	(61.5)	1632.1	(61.5)	1581.5	(0.5)	1599.8	(0.6)
a′	77.5	(60.5)	83.2	(62.9)	104.1	(66.0)	96.2	(62.8)
a′	45.2	(16.8)	39.7	(10.4)	62.7	(9.2)	53.3	(10.9)
a′	17.2	(12.8)	16.1	(23.6)	24.5	(7.0)	21.2	(10.5)
a″	99.1	(81.6)	94.3	(39.3)	131.0	(79.0)	116.7	(66.4)
a″	28.8i	(80.0)	19.5i	(102.2)	33.0i	(125.8)	31.1i	(132.4)

Table S21: Harmonic vibrational frequencies (in cm^{-1}) and IR intensities (in parentheses in km mol^{-1}) of structure VI.

Symm	UMP2/haTZ		UMP2/haQZ		UCCSD(T)/haTZ		UCCSD(T)/haQZ	
a′	3951.7	(105.5)	3966.1	(109.0)	3925.6	(83.0)	3942.4	(87.7)
a′	3825.7	(12.8)	3841.3	(10.1)	3815.9	(10.2)	3833.8	(8.9)
a′	1630.4	(62.9)	1632.0	(63.1)	1648.6	(63.2)	1650.3	(61.5)
a′	1468.2	(0.3)	1485.3	(0.2)	1580.1	(0.2)	1601.3	(0.2)
a′	58.5	(22.0)	63.7	(36.4)	56.9	(14.9)	57.1	(22.8)
a′	33.2	(47.5)	22.8	(36.2)	38.3	(52.6)	25.4	(44.2)
a′	39.8i	(18.1)	-42.5	(21.1)	42.7i	(16.5)	43.6i	(21.1)
a″	66.5	(55.9)	69.4	(13.2)	74.8	(87.6)	67.0	(52.2)
a″	46.7i	(19.1)	-43.8	(51.1)	42.3i	(4.8)	41.9i	(16.5)

Table S22: Harmonic vibrational frequencies (in cm^{-1}) and IR intensities (in parentheses in km mol^{-1}) of structure VII. Symmetry labels correspond to orientation given in Table S9.

Symm	UMP2/haTZ		UMP2/haQZ		UCCSD(T)/haTZ		UCCSD(T)/haQZ	
a_1	3823.5	(8.6)	3839.3	(8.4)	3812.7	(5.2)	3830.6	(5.2)
a_1	1629.3	(97.5)	1632.0	(96.9)	1647.2	(96.8)	1649.9	(96.4)
a_1	1451.0	(0.2)	1475.9	(0.2)	1572.7	(0.5)	1594.0	(0.7)
a_1	52.3	(< 0.1)	51.4	(0.1)	53.6	(< 0.1)	52.4	(< 0.1)
a_2	109.5	(0.0)	92.9	(0.0)	62.7	(0.0)	63.7	(0.0)
b_1	42.8	(215.4)	50.9	(213.1)	36.1	(211.7)	44.5	(210.2)
b_2	3949.8	(62.0)	3963.7	(64.8)	3922.3	(42.6)	3939.0	(44.9)
b_2	119.9	(87.2)	108.9	(82.3)	79.1	(63.6)	87.0	(70.3)
b_2	33.1	(3.0)	29.1	(5.9)	23.2i	(24.8)	8.8i	(18.1)

Table S23: Harmonic vibrational frequencies (in cm^{-1}) and IR intensities (in parentheses in km mol^{-1}) of structure VIII.

Symm	UMP2/haTZ		UMP2/haQZ		UCCSD(T)/haTZ		UCCSD(T)/haQZ	
a′	3825.6	(7.3)	3841.6	(7.2)	3814.6	(4.2)	3832.8	(4.4)
a′	1630.6	(97.5)	1632.2	(99.0)	1646.5	(105.2)	1649.5	(105.9)
a′	1457.0	(1.0)	1483.9	(0.5)	1575.3	(0.1)	1596.7	(0.1)
a′	111.3	(199.3)	108.7	(205.3)	97.7	(201.3)	101.9	(204.9)
a′	51.4	(5.5)	49.2	(2.8)	53.2	(2.6)	51.6	(1.2)
a′	10.2	(12.9)	11.7	(8.2)	8.6	(9.6)	10.5	(6.9)
a″	3950.4	(67.8)	3964.7	(70.3)	3923.2	(49.6)	3940.2	(51.8)
a″	51.9	(8.2)	43.8	(0.2)	44.1	(0.7)	42.4	(1.0)
a″	27.7i	(78.4)	44.8i	(84.9)	54.6i	(83.7)	51.3i	(82.8)

Table S24: Harmonic vibrational frequencies (in cm^{-1}) and IR intensities (in parentheses in km mol^{-1}) of structure IX.

Symm	UMP2/haTZ		UMP2/haQZ		UCCSD(T)/haTZ		UCCSD(T)/haQZ	
a′	3950.0	(71.3)	3964.1	(73.6)	3922.5	(52.6)	3939.8	(57.8)
a′	3823.6	(10.5)	3839.5	(10.3)	3813.0	(8.4)	3831.3	(9.1)
a′	1819.9	(2.5)	1680.2	(3.5)	1648.7	(89.5)	1650.8	(87.3)
a′	1628.1	(90.2)	1629.8	(87.0)	1576.0	(0.5)	1596.9	(0.7)
a′	77.8	(72.3)	84.4	(72.9)	76.4	(48.2)	83.0	(62.4)
a′	57.9	(0.1)	55.4	(0.2)	62.7	(17.5)	62.2	(5.2)
a′	24.3i	(10.4)	20.8i	(8.9)	13.7i	(16.1)	12.2i	(11.1)
a″	111.4	(90.2)	104.4	(76.5)	110.0	(95.4)	107.7	(77.3)
a″	30.0i	(126.5)	27.7i	(137.5)	33.9i	(117.5)	40.6i	(133.8)

Table S25: Harmonic vibrational frequencies (in cm^{-1}) and IR intensities (in parentheses in km mol^{-1}) of structure X. Symmetry labels correspond to orientation given in Table S12.

Symm	UMP2/haTZ		UMP2/haQZ		UCCSD(T)/haTZ		UCCSD(T)/haQZ	
a_1	3825.2	(7.0)	3841.3	(7.1)	3814.3	(4.3)	3832.7	(4.5)
a_1	1630.2	(89.8)	1632.1	(99.1)	1647.4	(106.7)	1650.0	(106.9)
a_1	1615.3	(9.7)	1552.1	(1.1)	1577.7	(0.1)	1598.5	(0.2)
a_1	46.7	(< 0.1)	45.5	(< 0.1)	49.9	(0.1)	48.4	(0.1)
b_1	66.3	(209.4)	77.1	(215.6)	73.2	(215.5)	81.1	(214.9)
b_1	24.3i	(11.8)	20.9i	(3.2)	7.6i	(1.1)	14.2i	(0.4)
b_2	3950.5	(68.9)	3964.8	(70.9)	3923.3	(49.9)	3940.3	(52.1)
b_2	25.5	(7.2)	27.0	(8.7)	41.2	(41.2)	38.2	(32.5)
b_2	27.4i	(78.8)	33.9i	(76.4)	23.6i	(43.4)	28.9i	(51.6)

Table S26: Harmonic vibrational frequencies (in cm^{-1}) and IR intensities (in parentheses in km mol^{-1}) of structure XI. Symmetry labels correspond to orientation given in Table S13.

Symm	UMP2/haTZ		UMP2/haQZ		UCCSD(T)/haTZ		UCCSD(T)/haQZ	
a_1	3821.7	(6.4)	3838.1	(6.5)	3811.5	(4.1)	3830.2	(4.3)
a_1	1629.8	(73.8)	1632.9	(73.0)	1647.6	(73.1)	1650.6	(72.7)
a_1	1481.0	(0.1)	1485.2	(0.1)	1567.9	(0.5)	1589.4	(0.4)
a_1	48.2	(< 0.1)	45.3	(< 0.1)	49.8	(< 0.1)	46.1	(< 0.1)
b_1	60.9	(237.2)	63.2	(234.0)	54.4	(233.6)	56.0	(231.2)
b_1	31.8	(0.4)	27.9	(0.1)	27.1	(0.2)	23.1	(< 0.1)
b_2	3949.0	(76.1)	3963.9	(78.2)	3922.2	(55.7)	3939.7	(58.1)
b_2	29.6	(2.5)	27.6	(0.3)	34.0	(9.3)	28.0	(2.3)
b_2	22.7i	(76.0)	31.6i	(77.0)	15.0i	(67.6)	24.1i	(73.6)

Table S27: Harmonic vibrational frequencies (in cm^{-1}) and IR intensities (in parentheses in km mol^{-1}) of structure XII. Symmetry labels correspond to orientation given in Table S14.

Symm	UMP2/haTZ		UMP2/haQZ		UCCSD(T)/haTZ		UCCSD(T)/haQZ	
a_1	3825.0	(6.6)	3840.8	(6.5)	3814.0	(3.7)	3831.8	(3.8)
a_1	1628.2	(92.3)	1630.9	(92.5)	1646.0	(92.0)	1648.7	(92.6)
a_1	1449.6	(0.1)	1474.7	(0.1)	1570.5	(0.3)	1591.8	(0.5)
a_1	40.7	(< 0.1)	37.3	(< 0.1)	42.7	(< 0.1)	39.9	(< 0.1)
a_2	22.7	(0.0)	42.2i	(0.0)	57.4i	(0.0)	60.7i	(0.0)
b_1	44.9	(86.2)	36.1	(85.2)	29.8	(36.5)	31.5	(42.2)
b_1	33.4i	(31.9)	61.3i	(110.6)	90.2i	(160.3)	91.2i	(155.0)
b_2	3951.5	(67.5)	3965.7	(69.8)	3924.2	(48.6)	3940.9	(51.0)
b_2	61.1	(177.0)	43.8	(98.3)	44.8	(84.8)	40.3	(84.0)

Table S28: Harmonic vibrational frequencies (list from highest to lowest cm^{-1}) and IR intensities (in parentheses in km mol^{-1}) of Structure I from QCISD/6-311++G($2d, 2p$) computations

	Results from this work			Results from Ref. [5]		
Mode	Symm	cm^{-1}	km mol^{-1}	Mode / Symm	cm^{-1}	km mol^{-1}
ω_1	a′	3982.0	(65.5)	not given	3978.9	(65.0)
ω_2	a′	3879.5	(4.4)	not given	3876.7	(4.6)
ω_3	a′	1684.6	(76.9)	not given	1685.6	(76.9)
ω_4	a′	1614.7	(1.3)	not given	1614.8	(1.3)
ω_8	a″	119.8	(21.0)	not given	138.7	(59.6)
ω_5	a′	84.2	(89.8)	not given	97.7	(96.9)
ω_6	a′	72.5	(0.1)	not given	73.5	(177.9)
ω_9	a″	60.3	(216.6)	not given	72.2	(0.3)
ω_7	a′	25.9	(18.2)	not given	30.5	(10.9)

Supplementary Information for 'Probing Dative and Dihydrogen Bonding in Ammonia Borane with Electronic Structure Computations and Raman Under Nitrogen Spectroscopy'

Katelyn M. Dreux,[†] Louis E. McNamara,[†] John T. Kelly,[†] Ashley M. Wright,[†] Nathan I. Hammer,[†] and Gregory S. Tschumper[*,†,‡]

Department of Chemistry and Biochemistry, University of Mississippi, University, Mississippi 38677–1848 USA

E-mail: tschumpr@olemiss.edu

1 Monomer Calibration

Table S1: Monomer bond lengths (R_{BN}, R_{BH}, R_{NH} in Å), dipole moment (μ in Debye), and BN stretching frequency (ω in cm^{-1}).

	R_{BN}	R_{BH}	R_{NH}	μ	ω		R_{BN}	R_{BH}	R_{NH}	μ	ω
B3LYP/6-31++G(d,p)	1.667	1.212	1.019	5.46	636	B3LYP/6-311++G($2df,2pd$)	1.658	1.207	1.015	5.32	645
M06L6-31++G(d,p)	1.660	1.209	1.015	5.54	656	M06L/6-311++G($2df,2pd$)	1.652	1.203	1.013	5.30	658
M06-2X/6-31++G(d,p)	1.658	1.210	1.017	5.48	675	M06-2X/6-311++G($2df,2pd$)	1.649	1.205	1.014	5.28	685
MP2/6-31++G(d,p)	1.661	1.206	1.016	5.54	669	MP2/6-311++G($2df,2pd$)	1.650	1.206	1.013	5.40	684
MP2(AE)/pCVDZ	1.652	1.220	1.022	5.65	682	CCSD(AE)/pCVDZ	1.659	1.223	1.023	5.64	669
CCSD(T)(AE)/pCVDZ	1.660	1.224	1.025	5.64	669						
MP2(AE)/pCVTZ	1.645	1.204	1.012	5.45	692	MP2(AE)/pCVQZ	1.640	1.202	1.011	5.39	694
CCSD(AE)/pCVTZ	1.650	1.207	1.012	5.40	684	CCSD(AE)/pCVQZ	1.645	1.206	1.011	5.32	688
CCSD(T)(AE)/pCVTZ	1.651	1.208	1.014	5.39	685	CCSD(T)(AE)/pCVQZ	1.646	1.207	1.014	5.32	688
B3LYP/DZ	1.654	1.222	1.023	5.59	651	B3LYP/aVDZ	1.659	1.218	1.019	5.28	641
M06L/DZ	1.648	1.218	1.020	5.60	666	M06L/aVDZ	1.650	1.216	1.017	5.28	663
M06-2X/DZ	1.644	1.219	1.021	5.61	694	M06-2X/aVDZ	1.648	1.216	1.018	5.30	687
MP2/DZ	1.657	1.222	1.023	5.66	676	MP2/aVDZ	1.668	1.220	1.021	5.35	652
CCSD/DZ	1.663	1.226	1.024	5.65	662	CCSD/aVDZ	1.675	1.224	1.021	5.30	638
CCSD(T)/DZ	1.663	1.227	1.025	5.65	663	CCSD(T)/aVDZ	1.677	1.225	1.023	5.29	636
B3LYP/TZ	1.659	1.207	1.015	5.38	645	B3LYP/aVTZ	1.659	1.207	1.015	5.27	644
M06L/TZ	1.654	1.202	1.012	5.36	656	M06L/aVTZ	1.654	1.202	1.012	5.25	658
M06-2X/TZ	1.650	1.206	1.015	5.34	682	M06-2X/aVTZ	1.650	1.206	1.014	5.23	682
MP2/TZ	1.650	1.206	1.013	5.44	687	MP2/aVTZ	1.652	1.207	1.014	5.35	682
CCSD/TZ	1.654	1.209	1.013	5.40	677	CCSD/aVTZ	1.656	1.210	1.014	5.28	672
CCSD(T)/TZ	1.655	1.210	1.015	5.39	677	CCSD(T)/aVTZ[a,b]	1.657	1.211	1.016	5.26	671
B3LYP/QZ	1.657	1.206	1.014	5.31	646	B3LYP/aVQZ	1.657	1.206	1.014	5.27	645
M06L/QZ	1.652	1.203	1.011	5.31	658	M06L/aVQZ	1.653	1.203	1.011	5.28	657
M06-2X/QZ	1.647	1.204	1.014	5.28	686	M06-2X/aVQZ	1.648	1.204	1.014	5.24	686
MP2/QZ	1.646	1.205	1.012	5.38	688	MP2/aVQZ	1.647	1.205	1.012	5.35	685
CCSD/QZ	1.649	1.208	1.011	5.32	679	CCSD/aVQZ	1.651	1.209	1.012	5.28	677
CCSD(T)/QZ	1.650	1.209	1.014	5.31	679	CCSD(T)/aVQZ	1.652	1.210	1.014	5.27	675
MP2/DZP[c]	1.656	1.213	1.018		690	QCISD/DZP[c]	1.665	1.217	1.020		673
HF/6-31G(d)[d]	1.689	1.209	1.004	5.57	604	MP2/6-31G(d)[d]	1.664	1.210	1.020	5.65	673
Exp. [e]	1.658	1.216	1.014	5.22							

[a] CCSD(T)/aVTZ with B3LYP/aVTZ anharmonic corrections $\nu = 626$ cm^{-1} taken from Ref 1
[b] CCSD(T)/aVTZ with MP2/aVTZ anharmonic corrections $\nu = 630$ cm^{-1} taken from Ref 1
[c] Taken from Ref 2
[d] Taken from Ref 3
[e] Gas-phase microwave spectroscopy taken from Refs 4, 5
AE - all electron

2 Dimer Calibration

Table S2: Dimer bond lengths (R_{BN}, R_{BH}, R_{NH} in Å), shortest intermolecular H-H distance (R_{HH} in Å), change in bond length upon dimerization (ΔR_{BN} in Å), symmetric a_g and asymmetric b_u BN stretching frequencies (ω_s and ω_a in cm^{-1}), and the frequency shifts of the BN stretching frequencies upon dimerization ($\Delta\omega_s$ and $\Delta\omega_a$ in cm^{-1}).

	R_{BN}	ΔR_{BN}	R_{BH}	R_{NH}	R_{HH}	ω_s	$\Delta\omega_s$	ω_a	$\Delta\omega_a$	E_{bind}
B3LYP/6-31++G(d,p)	1.641	−0.027	1.218	1.028	2.04	702	65	701	65	−13.24
B3LYP/6-311++G(2df, 2pd)	1.634	−0.024	1.213	1.025	2.04	706	61	705	60	−12.69
B3LYP/aVDZ	1.634	−0.025	1.223	1.029	2.01	704	63	702	61	−13.52
B3LYP/aVTZ	1.636	−0.023	1.213	1.024	2.05	703	60	703	59	−12.52
B3LYP/aVQZ	1.634	−0.023	1.212	1.024	2.05	704	59	704	59	−12.49
M06L/6-31++G(d,p)	1.633	−0.027	1.216	1.027	1.99	722	66	717	61	−16.27
M06L/6-311++G(2df, 2pd)	1.628	−0.025	1.210	1.024	1.98	723	65	719	61	−16.04
M06L/aVDZ	1.626	−0.024	1.222	1.029	1.97	728	66	716	53	−16.80
M06L/aVTZ	1.629	−0.024	1.209	1.023	1.99	721	63	718	60	−15.69
M06L/aVQZ	1.629	−0.024	1.209	1.022	2.00	723	65	718	61	−15.24
M06-2X/6-31++G(d,p)	1.632	−0.026	1.217	1.026	2.00	740	65	745	69	−16.43
M06-2X/6-311++G(2df, 2pd)	1.625	−0.024	1.212	1.024	1.99	746	61	750	66	−16.10
M06-2X/aVDZ	1.624	−0.023	1.222	1.027	1.98	748	62	753	66	−16.92
M06-2X/aVTZ	1.626	−0.024	1.213	1.024	1.99	747	64	751	69	−15.94
M06-2X/aVQZ	1.624	−0.023	1.211	1.023	1.99	743	58	748	63	−15.84
MP2/6-31++G(d,p)	1.636	−0.025	1.211	1.023	2.05	733	64	742	73	−14.68
MP2/6-311++G(2df, 2pd)	1.626	−0.024	1.213	1.023	1.98	745	61	752	68	−15.68
MP2/aVDZ	1.642	−0.026	1.226	1.029	1.98	718	66	735	83	−16.45
MP2/aVTZ	1.628	−0.024	1.214	1.023	1.99	746	64	752	71	−15.93
MP2/aVQZ	1.624	−0.023	1.212	1.022	1.98	742	57	749	63	−15.64
CCSD/aVDZ	1.649	−0.026	1.229	1.028	2.02	703	65	700	62	−15.35
CCSD/aVTZ	1.633	−0.023	1.216	1.021	2.02	732	60	725	53	−14.86
CCSD(T)/aVDZ	1.650	−0.026	1.230	1.031	2.00	704	69	724	89	−16.21
CCSD(T)/aVTZ	1.634	−0.023	1.218	1.024	2.00	731	60	740	68	−15.81
HF/6-31G(d)[a]	1.659	−0.030	1.214	1.008	2.21	676	71	678	74	−11.05
MP2/6-31G(d)[a]	1.639	−0.024	1.215	1.020	2.06	735	61	745	72	−15.13

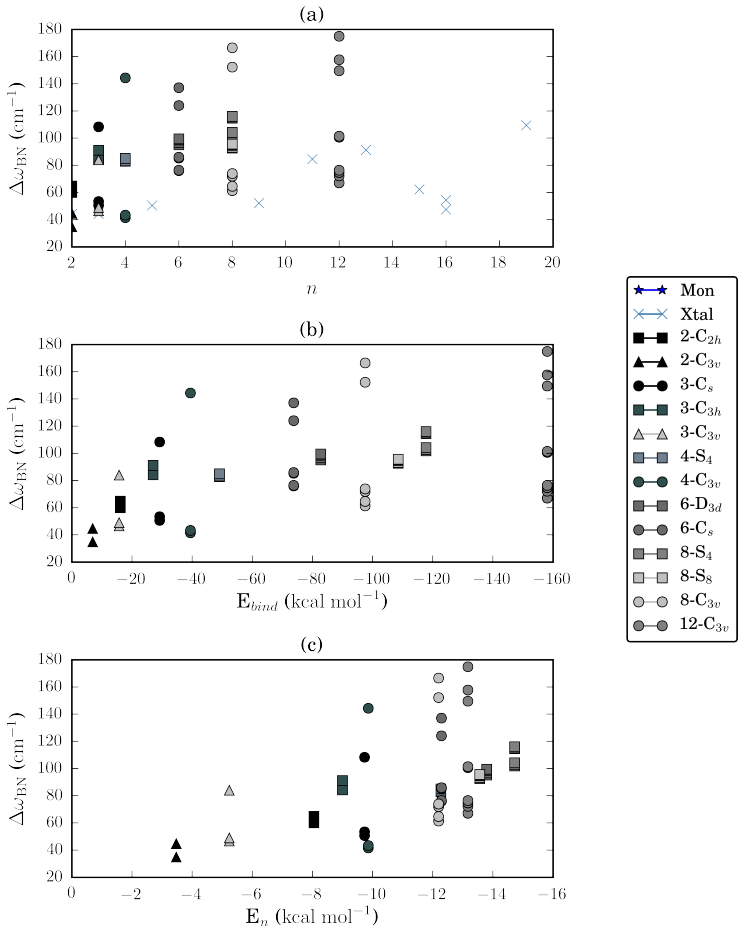

Figure S1: Plots of the correlation between various properties of ammonia borane clusters and crystal models. Figure S1a plots the BN frequency shifts against the number of subunits in the crystal models as well as the isolated clusters. Figure S1b plots the electronic binding energy and BN frequency shifts in the isolated clusters. Figure S1c plots the normalized electronic binding energy and the BN frequency shifts for the isolated clusters. See Section 3.6 of the main text for additional details.

3 Isolated Gas-Phase Clusters

Table S3: Optimized geometry of 1-C_{3v} at the M06-2X/6-311++G($2df, 2pd$) level of theory.

B	0.000000	0.000000	0.000000
N	0.000000	0.000000	1.649098
H	1.164815	0.000000	-0.310126
H	-0.582408	-1.008760	-0.310126
H	-0.582408	1.008760	-0.310126
H	-0.947709	0.000000	2.010611
H	0.473854	-0.820740	2.010611
H	0.473854	0.820740	2.010611

Table S4: Harmonic vibrational frequencies of 1-C_{3v} at the M06-2X/6-311++G($2df, 2pd$) level of theory.

Frequency (cm^{-1})	IR Intensity (km mol^{-1})
3606	45
3498	6
2546	253
2495	58
1665	26
1335	128
1201	87
1201	3
1074	31
685	12
653	2
267	0

Table S5: Optimized geometry of 2-C_{2h} at the M06-2X/6-311++G($2df, 2pd$) level of theory.

N	1.6365175128	0.7736603576	0.
B	1.6206278316	-0.8517226832	0.
H	2.1124954396	1.1339617296	0.8201613741
H	2.1124954396	1.1339617296	-0.8201613741
H	0.6818404592	1.1431352618	0.
H	2.7645514663	-1.2217374581	0.
H	1.032316459	-1.1747957612	1.009746964
H	1.032316459	-1.1747957612	-1.009746964
N	-1.6365175128	-0.7736603576	0.
B	-1.6206278316	0.8517226832	0.

H	-2.1124954396	-1.1339617296	0.8201613741
H	-2.1124954396	-1.1339617296	-0.8201613741
H	-0.6818404592	-1.1431352618	0.
H	-2.7645514663	1.2217374581	0.
H	-1.032316459	1.1747957612	1.009746964
H	-1.032316459	1.1747957612	-1.009746964

Table S6: Harmonic vibrational frequencies of 2-C_{2h} at the M06-2X/6-311++G($2df, 2pd$) level of theory.

Frequency (cm^{-1})	IR Intensity (km mol^{-1})
3604	84
3604	0
3548	0
3548	185
3407	494
3392	0
2555	0
2552	513
2494	413
2484	0
2464	210
2455	0
1662	0
1656	23
1655	29
1654	0
1397	0
1385	221
1246	0
1246	38
1221	8
1216	0
1198	158
1189	0
1102	0
1091	39
1085	101
1080	0
750	20
746	0
728	10
719	0
690	0
687	2

336	0
332	1
246	149
209	0
172	4
165	0
137	0
91	57

Table S7: Optimized geometry of 2-C_{3v} at the M06-2X/6-311++G($2df, 2pd$) level of theory.

N	-0.0000000006	0.	-3.0791848736
B	-0.0000000006	0.	-1.4439451717
H	-0.0000000125	0.9471563569	-3.4439219374
H	0.8202614718	-0.4735781681	-3.4439219374
H	-0.820261461	-0.4735781888	-3.4439219374
H	-1.0068291664	0.581293073	-1.1196506664
H	0.0000000141	-1.1625861714	-1.1196506664
H	1.0068291507	0.5812930984	-1.1196506664
N	-0.0000000006	0.	1.6439963081
B	-0.0000000006	0.	3.2773499749
H	-0.0000000124	0.9386211995	1.2573069281
H	0.8128698086	-0.4693105895	1.2573069281
H	-0.8128697979	-0.46931061	1.2573069281
H	-1.0074647283	0.5816600148	3.6014845226
H	0.0000000141	-1.163320055	3.6014845226
H	1.0074647125	0.5816600402	3.6014845226

Table S8: Harmonic vibrational frequencies of 2-C_{3v} at the M06-2X/6-311++G($2df, 2pd$) level of theory.

Frequency (cm^{-1})	IR Intensity (km mol^{-1})
3598	56
3593	34
3499	8
3494	11
2534	263
2524	210
2487	53
2481	108
1667	21
1665	22
1377	157

1358	176
1218	95
1209	3
1201	3
1200	257
1090	22
1072	39
730	16
720	1
684	2
653	3
266	0
262	0
128	1
104	50
40	1
28	16

Table S9: Optimized geometry of 3-C$_s$ at the M06-2X/6-311++G($2df, 2pd$) level of theory.

N	0.166409545	1.2844905284	0.
B	1.2445221994	0.0926917666	0.
H	-0.427992003	1.2314197607	0.8302966092
H	0.6200301231	2.1919310939	0.
H	-0.427992003	1.2314197607	-0.8302966092
H	0.6084279949	-0.9462644029	0.
H	1.9243398874	0.2078763914	-0.9941732162
H	1.9243398874	0.2078763914	0.9941732162
N	0.1546502232	-0.9163683754	-2.9386398131
B	-0.9222522815	0.3059115376	-2.9500013964
H	0.7791476994	-0.8577317492	-3.7359157513
H	0.7227993648	-0.8843064423	-2.0897142695
H	-0.3141149203	-1.8151050358	-2.9742570311
H	-1.5389006112	0.2211639647	-3.9789770582
H	-1.6213205833	0.13171679	-1.9760829842
H	-0.2636877073	1.3203361644	-2.8839771787
N	0.1546502232	-0.9163683754	2.9386398131
B	-0.9222522815	0.3059115376	2.9500013964
H	0.7227993648	-0.8843064423	2.0897142695
H	0.7791476994	-0.8577317492	3.7359157513
H	-0.3141149203	-1.8151050358	2.9742570311
H	-1.6213205833	0.13171679	1.9760829842
H	-1.5389006112	0.2211639647	3.9789770582
H	-0.2636877073	1.3203361644	2.8839771787

Table S10: Harmonic vibrational frequencies of 3-C_s at the M06-2X/6-311++G(2*df*, 2*pd*) level of theory.

Frequency (cm^{-1})	IR Intensity (km mol^{-1})
3604	67
3603	16
3577	63
3553	42
3551	177
3466	546
3431	122
3422	233
3400	43
2554	112
2552	397
2505	481
2501	401
2495	7
2487	62
2466	129
2465	59
2428	91
1662	4
1662	23
1658	4
1654	8
1652	17
1650	5
1429	54
1379	248
1377	12
1257	21
1252	11
1244	15
1243	22
1216	5
1216	3
1198	215
1194	0
1184	2
1118	15
1101	15
1091	56
1087	131
1083	1

1081	7
794	5
767	16
739	16
736	0
725	2
717	1
716	8
681	0
681	2
399	3
332	2
329	0
264	187
221	1
218	61
193	16
179	2
168	0
167	3
130	14
128	14
69	20
47	11
39	1

Table S11: Optimized geometry of 3-C_{3h} at the M06-2X/6-311++G($2df, 2pd$) level of theory.

B	0.9871742645	-2.2647866491	0.
N	2.2575874012	-1.2653671533	0.
B	1.4677756392	1.9873113161	0.
N	-0.0329536015	2.5878116178	0.
N	-2.2246338013	-1.3224444645	0.
B	-2.4549499054	0.277475333	0.
H	0.365654891	-2.0131565511	1.0108295709
H	0.365654891	-2.0131565511	-1.0108295709
H	1.4122872233	-3.3912887716	0.
H	2.838516333	-1.4118703894	0.8188271253
H	2.838516333	-1.4118703894	-0.8188271253
H	1.9705607329	-0.2820117921	0.
H	1.5606172687	1.3232447007	-1.0108295709
H	2.2307986153	2.9187209991	0.
H	1.5606172687	1.3232447007	1.0108295709
H	-0.7410509912	1.847561551	0.

H	-0.1965425432	3.1641624486	0.8188271253
H	-0.1965425432	3.1641624486	-0.8188271253
H	-2.6419737914	-1.7522920592	-0.8188271253
H	-1.2295097434	-1.5655497589	0.
H	-2.6419737914	-1.7522920592	0.8188271253
H	-3.6430858402	0.4725677725	0.
H	-1.9262721614	0.6899118505	1.0108295709
H	-1.9262721614	0.6899118505	-1.0108295709

Table S12: Harmonic vibrational frequencies of 3-C_{3h} at the M06-2X/6-311++G$(2df, 2pd)$ level of theory.

Frequency (cm^{-1})	IR Intensity (km mol^{-1})
3601	125
3601	0
3544	137
3544	0
3397	546
3382	0
2542	0
2538	393
2489	569
2480	0
2457	210
2448	0
1664	0
1662	44
1660	29
1658	0
1414	0
1410	148
1267	76
1263	0
1209	17
1206	0
1198	115
1188	0
1109	55
1103	0
1092	0
1088	40
777	0
770	6
722	5
714	0

712	2
710	0
315	8
310	0
310	0
194	67
181	0
175	35
173	0
127	0
76	51
53	22
29	0

Table S13: Optimized geometry of 3-C_{3v} at the M06-2X/6-311++G($2df, 2pd$) level of theory.

N	-0.0000000322	-0.0000000185	0.7132154976
B	-0.0000000322	-0.0000000185	-0.9058411219
H	-0.8120207653	0.4688203106	1.1041492039
H	0.0000000194	-0.9376407663	1.1041492039
H	0.8120206492	0.4688204001	1.1041492039
H	1.0052955341	-0.5804076105	-1.2448169502
H	-1.0052955346	-0.5804077213	-1.2448169502
H	-0.0000000962	1.1608152762	-1.2448169502
N	-0.0000000322	-0.0000000185	5.3979202564
B	-0.0000000322	-0.0000000185	3.7661826958
H	0.820145464	0.4735112647	5.7636351107
H	-0.8201455806	0.4735111744	5.7636351107
H	0.00000002	-0.9470224946	5.7636351107
H	1.0061093531	-0.5808774691	3.4378842382
H	-1.0061093535	-0.5808775799	3.4378842382
H	-0.0000000962	1.1617549934	3.4378842382
N	-0.0000000322	-0.0000000185	-3.9736496883
B	-0.0000000322	-0.0000000185	-5.6038137309
H	0.8111819947	0.4683362027	-3.581866042
H	-0.8111821108	0.4683361133	-3.581866042
H	0.0000000194	-0.9366723716	-3.581866042
H	1.0071800233	-0.5814956207	-5.9313879195
H	-1.0071800237	-0.5814957317	-5.9313879195
H	-0.0000000963	1.1629912968	-5.9313879195

Table S14: Harmonic vibrational frequencies of 3-C_{3v} at the M06-2X/6-311++G(2*df*, 2*pd*) level of theory.

Frequency (cm^{-1})	IR Intensity (km mol^{-1})
3595	57
3590	40
3585	38
3499	9
3495	16
3492	12
2531	237
2518	349
2511	104
2486	67
2478	52
2473	171
1668	23
1667	14
1665	19
1400	124
1386	275
1364	178
1225	2
1215	260
1211	4
1210	2
1201	3
1199	343
1092	14
1088	38
1072	39
770	8
735	0
732	11
689	3
686	3
654	3
653	3
265	0
263	0
260	0
169	0
119	85
103	1
95	1

48	0
34	19
30	2
11	1

Table S15: Optimized geometry of 4-S_4 at the M06-2X/6-311++G($2df, 2pd$) level of theory.

N	-0.0652838943	2.4132639719	0.8041323059
B	-0.0642032457	2.3775793948	-0.8121643497
H	0.7649812129	1.9462969361	1.1709368668
H	-0.0909049823	3.3630692906	1.1581615223
H	-0.8692505596	1.9022581049	1.1708143477
H	0.9273335183	2.9615297401	-1.1836040325
H	-0.032652497	1.2065448697	-1.1176799473
H	-1.0856407457	2.907366174	-1.1837612301
N	-2.4132639719	-0.0652838943	-0.8041323059
B	-2.3775793948	-0.0642032457	0.8121643497
H	-1.9022581049	-0.8692505596	-1.1708143477
H	-3.3630692906	-0.0909049823	-1.1581615223
H	-1.9462969361	0.7649812129	-1.1709368668
H	-2.907366174	-1.0856407457	1.1837612301
H	-1.2065448697	-0.032652497	1.1176799473
H	-2.9615297401	0.9273335183	1.1836040325
N	0.0652838943	-2.4132639719	0.8041323059
B	0.0642032457	-2.3775793948	-0.8121643497
H	-0.7649812129	-1.9462969361	1.1709368668
H	0.0909049823	-3.3630692906	1.1581615223
H	0.8692505596	-1.9022581049	1.1708143477
H	-0.9273335183	-2.9615297401	-1.1836040325
H	0.032652497	-1.2065448697	-1.1176799473
H	1.0856407457	-2.907366174	-1.1837612301
N	2.4132639719	0.0652838943	-0.8041323059
B	2.3775793948	0.0642032457	0.8121643497
H	1.9022581049	0.8692505596	-1.1708143477
H	3.3630692906	0.0909049823	-1.1581615223
H	1.9462969361	-0.7649812129	-1.1709368668
H	2.907366174	1.0856407457	1.1837612301
H	1.2065448697	0.032652497	1.1176799473
H	2.9615297401	-0.9273335183	1.1836040325

Table S16: Harmonic vibrational frequencies of 4-S_4 at the M06-2X/6-311++G($2df, 2pd$) level of theory.

Frequency (cm^{-1})	IR Intensity (km mol^{-1})
3589	1
3589	0
3588	157
3503	380
3495	0
3494	0
3438	49
3430	129
3427	0
2530	0
2524	2
2518	692
2518	0
2510	0
2501	299
2480	245
2476	0
2473	0
1667	0
1662	1
1658	67
1644	24
1644	0
1636	0
1416	0
1404	25
1400	361
1295	0
1293	28
1290	0
1214	0
1210	72
1208	18
1193	187
1185	0
1182	0
1113	0
1101	47
1101	0
1088	0
1087	87
1078	21
771	17

769	1
768	0
748	0
742	4
736	0
712	0
711	1
708	14
386	27
377	0
359	0
249	100
232	0
210	1
187	0
182	0
166	0
131	0
130	68
119	1
118	19
94	0
94	0
74	0
47	0

Table S17: Optimized geometry of 3-C_{3v} at the M06-2X/6-311++G($2df, 2pd$) level of theory.

N	0.	-0.0000000011	0.8889324203
B	0.	-0.0000000011	-0.7032155057
H	0.828251951	-0.4781914878	1.2484368765
H	-0.0000000001	0.9563829725	1.2484368765
H	-0.8282519508	-0.478191488	1.2484368765
H	1.0008309565	0.5778300212	-1.0832539847
H	0.0000000001	-1.1556600455	-1.0832539847
H	-1.0008309567	0.577830021	-1.0832539847
N	-0.0000000004	3.3240697765	-0.7807569506
B	-0.0000000004	3.324075531	0.851989996
H	-0.0000000003	2.3670524954	-1.1350579831
H	-0.8206354998	3.7971967736	-1.1432936534
H	0.8206354989	3.7971967738	-1.1432936534
H	-1.0102498145	2.7398452048	1.1727491949
H	1.0102498138	2.7398452051	1.1727491949
H	-0.0000000006	4.4767201267	1.1960311885

N	-2.8787288711	-1.6620348903	-0.7807569506
B	-2.8787338547	-1.6620377675	0.851989996
H	-2.8781511202	-2.6092895786	-1.1432936534
H	-3.6987866197	-1.1879071993	-1.1432936534
H	-2.0499275939	-1.1835262496	-1.1350579831
H	-3.876953356	-2.2383600655	1.1960311885
H	-1.8676506435	-2.2448246076	1.1727491949
H	-2.8779004579	-0.4950206013	1.1727491949
N	2.8787288716	-1.6620348895	-0.7807569506
B	2.8787338551	-1.6620377668	0.851989996
H	2.8781511208	-2.6092895778	-1.1432936534
H	2.0499275942	-1.1835262491	-1.1350579831
H	3.69878662	-1.1879071984	-1.1432936534
H	1.8676506441	-2.2448246071	1.1727491949
H	3.8769533566	-2.2383600645	1.1960311885
H	2.877900458	-0.4950206006	1.1727491949

Table S18: Harmonic vibrational frequencies of 3-C_{3v} at the M06-2X/6-311++G($2df, 2pd$) level of theory.

Frequency (cm^{-1})	IR Intensity (km mol^{-1})
3606	61
3605	0
3563	3
3559	187
3484	427
3453	23
3445	152
3404	19
2556	24
2552	399
2510	325
2503	0
2473	154
2471	106
2451	200
2429	57
1662	3
1661	1
1660	34
1655	0
1649	3
1453	49
1371	340
1367	11

1275	22
1242	15
1242	20
1215	6
1214	0
1199	278
1195	0
1178	3
1124	21
1091	11
1087	125
1083	0
1082	0
830	2
774	10
729	24
727	0
711	0
709	9
679	2
679	0
452	0
329	4
326	0
254	169
232	0
214	3
197	0
173	0
167	0
137	0
125	12
80	0
60	35
38	2
29	0

Table S19: Optimized geometry of 6-D$_{3d}$ at the M06-2X/6-311++G($2df, 2pd$) level of theory.

N	0.0000000041	3.3152815652	0.831526618
B	0.0000000041	3.3058621596	-0.7799796895
H	0.8287047371	2.8384824524	1.1908462561
H	0.0000000053	4.262422058	1.1947088848
H	-0.82870473	2.8384824545	1.1908462561

H	0.9985163888	3.8821281557	-1.1464690519
H	0.0000000027	2.135014153	-1.1098090127
H	-0.9985163792	3.8821281582	-1.1464690519
N	-2.8711180541	1.6576407862	-0.831526618
B	-2.8629606095	1.6529310833	0.7799796895
H	-2.8725502788	0.7015618788	-1.1908462561
H	-3.6913657813	2.1312110336	-1.1947088848
H	-2.0438455434	2.1369205807	-1.1908462561
H	-3.8612797953	1.0763235286	1.1464690519
H	-1.8489764926	1.0675070788	1.1098090127
H	-2.8627634092	2.8058046367	1.1464690519
N	2.8711180582	1.657640779	-0.831526618
B	2.8629606136	1.6529310762	0.7799796895
H	2.8725502805	0.7015618717	-1.1908462561
H	2.0438455487	2.1369205757	-1.1908462561
H	3.6913657866	2.1312110244	-1.1947088848
H	1.8489764953	1.0675070742	1.1098090127
H	3.861279798	1.076323519	1.1464690519
H	2.8627634161	2.8058046295	1.1464690519
N	-0.0000000041	-3.3152815652	-0.831526618
B	-0.0000000041	-3.3058621596	0.7799796895
H	-0.0000000053	-4.262422058	-1.1947088848
H	-0.8287047371	-2.8384824524	-1.1908462561
H	0.82870473	-2.8384824545	-1.1908462561
H	-0.9985163888	-3.8821281557	1.1464690519
H	0.9985163792	-3.8821281582	1.1464690519
H	-0.0000000027	-2.135014153	1.1098090127
N	-2.8711180582	-1.657640779	0.831526618
B	-2.8629606136	-1.6529310762	-0.7799796895
H	-2.0438455487	-2.1369205757	1.1908462561
H	-2.8725502805	-0.7015618717	1.1908462561
H	-3.6913657866	-2.1312110244	1.1947088848
H	-1.8489764953	-1.0675070742	-1.1098090127
H	-2.8627634161	-2.8058046295	-1.1464690519
H	-3.861279798	-1.076323519	-1.1464690519
N	2.8711180541	-1.6576407862	0.831526618
B	2.8629606095	-1.6529310833	-0.7799796895
H	3.6913657813	-2.1312110336	1.1947088848
H	2.8725502788	-0.7015618788	1.1908462561
H	2.0438455434	-2.1369205807	1.1908462561
H	3.8612797953	-1.0763235286	-1.1464690519
H	2.8627634092	-2.8058046367	-1.1464690519
H	1.8489764926	-1.0675070788	-1.1098090127

Table S20: Harmonic vibrational frequencies of 6-D_{3d} at the M06-2X/6-311++G(2*df*, 2*pd*) level of theory.

Frequency (cm^{-1})	IR Intensity (km mol^{-1})
3581	3
3581	0
3580	0
3580	210
3580	209
3494	1110
3494	1108
3490	0
3482	0
3480	0
3429	75
3422	0
3415	175
3415	0
2510	0
2509	970
2509	972
2508	0
2500	0
2499	0
2491	409
2491	411
2488	181
2488	0
2447	183
2441	0
2438	0
2438	152
2438	156
1658	0
1654	2
1654	11
1652	20
1649	0
1426	0
1417	25
1409	0
1409	511
1271	0
1270	0
1268	61

1266	0
1244	0
1242	26
1239	0
1238	25
1197	330
1191	0
1184	0
1182	0
1126	0
1118	0
1108	0
1102	15
1100	209
1090	0
1085	17
785	23
784	0
782	5
781	0
763	0
760	26
750	0
745	0
725	2
722	0
718	5
717	0
403	0
403	1
402	0
268	311
268	312
251	0
234	0
232	0
213	0
202	0
196	0
192	0
171	7
169	1
158	0
140	0
137	0

127	37
108	0
78	0
77	0
48	2
47	2
44	0

Table S21: Optimized geometry of 6-C$_s$ at the M06-2X/6-311++G($2df, 2pd$) level of theory.

B	0.	0.9538512986	1.5865497309
N	0.	0.892212682	3.1860117161
H	0.	-0.1969725192	1.1830146131
H	0.9994062047	1.543055073	1.2325279328
H	-0.9994062047	1.543055073	1.2325279328
H	0.831750676	0.4051254835	3.5311595023
H	-0.831750676	0.4051254835	3.5311595023
H	0.	1.8229730406	3.5900043838
N	2.9554067519	-0.6206563092	1.6494342463
B	2.9657806685	-0.5063376083	3.2637061706
H	3.0229506657	-1.5808058561	1.3267074399
H	3.723820003	-0.1166306097	1.2171192793
H	2.0989836779	-0.2353793866	1.2500544476
H	4.0044524751	-0.9725747111	3.6530821131
H	2.0077352751	-1.1444909325	3.6482167371
H	2.8683752655	0.676072926	3.5151913756
N	-2.9554067519	-0.6206563092	1.6494342463
B	-2.9657806685	-0.5063376083	3.2637061706
H	-3.0229506657	-1.5808058561	1.3267074399
H	-2.0989836779	-0.2353793866	1.2500544476
H	-3.723820003	-0.1166306097	1.2171192793
H	-2.0077352751	-1.1444909325	3.6482167371
H	-4.0044524751	-0.9725747111	3.6530821131
H	-2.8683752655	0.676072926	3.5151913756
B	0.	1.1004895058	-3.0703413712
N	0.	1.1812314432	-1.4739269398
H	0.	-0.0840798779	-3.3587538006
H	0.9935084249	1.6608449286	-3.4768869862
H	-0.9935084249	1.6608449286	-3.4768869862
H	0.8176096103	0.7230289398	-1.0680763639
H	-0.8176096103	0.7230289398	-1.0680763639
H	0.	2.133482959	-1.1202381826
N	2.8835741718	-0.4525558998	-3.061133348
B	2.8939097678	-0.5022036757	-1.4420111084

H	2.8572460156	-1.3865749425	-3.456654123
H	3.7097718856	0.0146128059	-3.4202023621
H	2.0616187665	0.056169131	-3.3973948285
H	3.8863365357	-1.1036466343	-1.1104240697
H	1.8789647228	-1.0769836174	-1.1133550949
H	2.9126344557	0.6512326208	-1.0690863244
N	-2.8835741718	-0.4525558998	-3.061133348
B	-2.8939097678	-0.5022036757	-1.4420111084
H	-2.8572460156	-1.3865749425	-3.456654123
H	-2.0616187665	0.056169131	-3.3973948285
H	-3.7097718856	0.0146128059	-3.4202023621
H	-1.8789647228	-1.0769836174	-1.1133550949
H	-3.8863365357	-1.1036466343	-1.1104240697
H	-2.9126344557	0.6512326208	-1.0690863244

Table S22: Harmonic vibrational frequencies of 6-C_s at the M06-2X/6-311++G($2df, 2pd$) level of theory.

Frequency (cm^{-1})	IR Intensity (km mol^{-1})
3599	67
3599	25
3591	64
3591	10
3574	63
3569	55
3552	40
3550	184
3546	45
3544	139
3491	332
3460	71
3456	329
3437	106
3437	346
3406	70
3400	296
3379	91
2547	130
2545	427
2524	88
2522	318
2499	420
2498	616
2492	7
2483	217

2483	244
2479	124
2477	0
2466	64
2462	163
2461	15
2454	157
2452	77
2423	18
2422	139
1665	4
1664	10
1662	2
1660	2
1659	26
1659	2
1657	15
1654	8
1654	17
1650	3
1647	0
1645	5
1444	1
1438	271
1404	282
1403	1
1395	288
1394	13
1266	23
1255	12
1251	11
1244	15
1244	24
1241	5
1238	7
1238	14
1220	13
1219	2
1217	2
1216	4
1214	78
1211	1
1210	342
1193	214
1193	0

1186	20
1131	23
1112	5
1109	25
1108	3
1099	46
1097	30
1089	13
1087	20
1083	201
1082	35
1078	1
1077	18
823	5
810	1
796	14
772	22
771	1
762	2
762	1
747	3
747	17
744	3
734	0
711	0
709	2
708	13
705	1
704	4
675	1
675	4
411	2
368	0
333	3
330	0
314	1
312	2
273	281
258	64
230	106
218	0
217	13
208	15
185	8
180	0

178	0
177	4
165	4
164	1
163	9
161	0
157	2
145	0
141	23
139	18
132	0
118	11
112	9
110	13
98	8
70	0
51	0
50	16
48	2
42	7
36	1
19	1

Table S23: Optimized geometry of 8-S_4 at the M06-2X/6-311++G($2df, 2pd$) level of theory.

N	1.7430556633	-1.7419927094	-1.5760046957
B	1.6781052075	-1.6782398096	-3.1805793388
H	0.8391058957	-1.9824599212	-1.1692037563
H	2.4165878251	-2.4163807101	-1.226283798
H	1.9853356356	-0.8381335284	-1.1700981452
H	1.3476339702	-2.7718961869	-3.5789132122
H	0.8428931216	-0.8423614448	-3.4489474906
H	2.7718065671	-1.349523194	-3.5801119423
N	1.6948371678	1.6957136877	-3.111754306
B	1.6942049346	1.6945160654	-1.5025591613
H	0.7644617876	1.9210582641	-3.4689834764
H	2.3606743598	2.3608871903	-3.4894072158
H	1.9189098069	0.7651986646	-3.4694178269
H	1.3854594083	2.8088832767	-1.1380961861
H	0.8731252408	0.8735316639	-1.1514115189
H	2.8085877267	1.3851782079	-1.1385591092
N	-1.7430556633	1.7419927094	-1.5760046957
B	-1.6781052075	1.6782398096	-3.1805793388
H	-0.8391058957	1.9824599212	-1.1692037563

H	-2.4165878251	2.4163807101	-1.226283798
H	-1.9853356356	0.8381335284	-1.1700981452
H	-1.3476339702	2.7718961869	-3.5789132122
H	-0.8428931216	0.8423614448	-3.4489474906
H	-2.7718065671	1.349523194	-3.5801119423
N	-1.6948371678	-1.6957136877	-3.111754306
B	-1.6942049346	-1.6945160654	-1.5025591613
H	-0.7644617876	-1.9210582641	-3.4689834764
H	-2.3606743598	-2.3608871903	-3.4894072158
H	-1.9189098069	-0.7651986646	-3.4694178269
H	-1.3854594083	-2.8088832767	-1.1380961861
H	-0.8731252408	-0.8735316639	-1.1514115189
H	-2.8085877267	-1.3851782079	-1.1385591092
N	1.6957136877	-1.6948371678	3.111754306
B	1.6945160654	-1.6942049346	1.5025591613
H	0.7651986646	-1.9189098069	3.4694178269
H	2.3608871903	-2.3606743598	3.4894072158
H	1.9210582641	-0.7644617876	3.4689834764
H	1.3851782079	-2.8085877267	1.1385591092
H	0.8735316639	-0.8731252408	1.1514115189
H	2.8088832767	-1.3854594083	1.1380961861
N	1.7419927094	1.7430556633	1.5760046957
B	1.6782398096	1.6781052075	3.1805793388
H	0.8381335284	1.9853356356	1.1700981452
H	2.4163807101	2.4165878251	1.226283798
H	1.9824599212	0.8391058957	1.1692037563
H	1.349523194	2.7718065671	3.5801119423
H	0.8423614448	0.8428931216	3.4489474906
H	2.7718961869	1.3476339702	3.5789132122
N	-1.6957136877	1.6948371678	3.111754306
B	-1.6945160654	1.6942049346	1.5025591613
H	-0.7651986646	1.9189098069	3.4694178269
H	-2.3608871903	2.3606743598	3.4894072158
H	-1.9210582641	0.7644617876	3.4689834764
H	-1.3851782079	2.8085877267	1.1385591092
H	-0.8735316639	0.8731252408	1.1514115189
H	-2.8088832767	1.3854594083	1.1380961861
N	-1.7419927094	-1.7430556633	1.5760046957
B	-1.6782398096	-1.6781052075	3.1805793388
H	-0.8381335284	-1.9853356356	1.1700981452
H	-2.4163807101	-2.4165878251	1.226283798
H	-1.9824599212	-0.8391058957	1.1692037563
H	-1.349523194	-2.7718065671	3.5801119423
H	-0.8423614448	-0.8428931216	3.4489474906
H	-2.7718961869	-1.3476339702	3.5789132122

Table S24: Harmonic vibrational frequencies of 8-S_4 at the M06-2X/6-311++G($2df, 2pd$) level of theory.

Frequency (cm^{-1})	IR Intensity (km mol^{-1})
3586	0
3586	4
3586	162
3580	0
3579	135
3523	238
3520	0
3515	0
3483	405
3472	0
3460	92
3459	0
3456	29
3418	56
3417	0
3415	152
2526	0
2525	0
2519	0
2511	794
2510	45
2507	0
2506	0
2495	886
2491	0
2489	0
2487	1
2482	0
2474	0
2473	335
2468	2
2458	284
2457	0
2455	17
1669	0
1664	2
1662	0
1657	3
1656	105
1654	0
1649	0

1648	15
1646	0
1644	17
1637	0
1636	0
1443	268
1427	0
1422	5
1417	20
1416	786
1411	0
1302	28
1302	0
1278	0
1277	0
1276	20
1216	0
1215	0
1215	6
1213	9
1211	275
1210	13
1207	299
1207	0
1206	3
1187	199
1185	0
1184	0
1121	0
1119	0
1115	41
1106	0
1105	1
1102	23
1094	83
1092	0
1084	0
1082	106
1079	0
1077	32
802	22
801	1
800	0
790	0
788	0

787	3
767	0
767	4
766	0
739	0
738	10
736	3
735	0
732	4
726	0
705	0
704	17
704	1
398	36
380	0
378	0
368	18
358	0
350	0
256	170
243	37
233	0
232	1
231	0
227	0
185	0
181	0
178	0
177	0
173	0
168	0
160	18
151	4
150	0
144	51
143	0
141	5
135	0
128	15
116	17
107	0
107	2
98	14
97	0
96	0

85	0
60	0
55	0
50	0
30	0

Table S25: Optimized geometry of 8-S_8 at the M06-2X/6-311++G($2df, 2pd$) level of theory.

B	1.6764312861	4.0376536263	0.7672577528
H	2.8243121161	4.2099710741	1.101708243
H	1.2352405035	2.9732721947	1.1619582347
H	0.9866280547	4.9714319773	1.1011627926
B	-4.0376536263	1.6764312861	0.7672577528
H	-2.9732721947	1.2352405035	1.1619582347
H	-4.9714319773	0.9866280547	1.1011627926
H	-4.2099710741	2.8243121161	1.101708243
B	-1.6764312861	-4.0376536263	0.7672577528
H	-1.2352405035	-2.9732721947	1.1619582347
H	-0.9866280547	-4.9714319773	1.1011627926
H	-2.8243121161	-4.2099710741	1.101708243
B	4.0376536263	-1.6764312861	0.7672577528
H	4.9714319773	-0.9866280547	1.1011627926
H	4.2099710741	-2.8243121161	1.101708243
H	2.9732721947	-1.2352405035	1.1619582347
B	1.6696363286	-4.0404681899	-0.7672577528
H	2.8176818754	-4.2129846513	-1.1011627926
H	0.9798088456	-4.9739893446	-1.101708243
H	1.2289739948	-2.9758678677	-1.1619582347
B	-1.6696363286	4.0404681899	-0.7672577528
H	-1.2289739948	2.9758678677	-1.1619582347
H	-2.8176818754	4.2129846513	-1.1011627926
H	-0.9798088456	4.9739893446	-1.101708243
B	-4.0404681899	-1.6696363286	-0.7672577528
H	-2.9758678677	-1.2289739948	-1.1619582347
H	-4.2129846513	-2.8176818754	-1.1011627926
H	-4.9739893446	-0.9798088456	-1.101708243
H	-2.0025090431	-4.8260313609	-1.2484875622
H	-2.2334768894	-3.2030602092	-1.1839113064
H	-0.6928521497	-3.8401570083	-1.183843463
H	3.2030602092	-2.2334768894	-1.1839113064
H	3.8401570083	-0.6928521497	-1.183843463
H	4.8260313609	-2.0025090431	-1.2484875622
H	-3.8401570083	0.6928521497	-1.183843463
H	-4.8260313609	2.0025090431	-1.2484875622

H	-3.2030602092	2.2334768894	-1.1839113064
H	2.2334768894	3.2030602092	-1.1839113064
H	0.6928521497	3.8401570083	-1.183843463
H	2.0025090431	4.8260313609	-1.2484875622
B	4.0404681899	1.6696363286	-0.7672577528
H	4.9739893446	0.9798088456	-1.101708243
H	2.9758678677	1.2289739948	-1.1619582347
H	4.2129846513	2.8176818754	-1.1011627926
H	4.8285072253	1.9965317778	1.2484875622
H	3.8442122486	0.6855989403	1.1839113064
H	3.2053215148	2.225480608	1.183843463
H	2.225480608	-3.2053215148	1.183843463
H	1.9965317778	-4.8285072253	1.2484875622
H	0.6855989403	-3.8442122486	1.1839113064
H	-3.2053215148	-2.225480608	1.183843463
H	-4.8285072253	-1.9965317778	1.2484875622
H	-3.8442122486	-0.6855989403	1.1839113064
H	-1.9965317778	4.8285072253	1.2484875622
H	-0.6855989403	3.8442122486	1.1839113064
H	-2.225480608	3.2053215148	1.183843463
N	1.6398513751	-3.96897975	0.8433930084
N	-3.96897975	-1.6398513751	0.8433930084
N	-1.6398513751	3.96897975	0.8433930084
N	3.96897975	1.6398513751	0.8433930084
N	-3.9660425231	1.6469424681	-0.8433930084
N	-1.6469424681	-3.9660425231	-0.8433930084
N	3.9660425231	-1.6469424681	-0.8433930084
N	1.6469424681	3.9660425231	-0.8433930084

Table S26: Harmonic vibrational frequencies of 8-S_8 at the M06-2X/6-311++G($2df, 2pd$) level of theory.

Frequency (cm^{-1})	IR Intensity (km mol^{-1})
3577	9
3577	0
3576	242
3576	0
3502	0
3499	1672
3495	0
3489	0
3488	0
3432	97
3427	0
3421	0

3419	0
3418	166
2522	0
2521	0
2520	0
2519	1303
2511	0
2508	0
2503	493
2500	0
2500	231
2499	0
2436	247
2433	0
2431	0
2430	0
2429	274
1666	0
1664	0
1659	56
1656	0
1650	0
1646	4
1644	7
1643	0
1641	0
1427	0
1422	9
1414	0
1410	681
1410	0
1252	0
1251	0
1251	71
1251	0
1248	38
1248	0
1247	0
1246	25
1197	450
1192	0
1187	0
1182	1
1181	0
1124	0

1119	0
1108	0
1105	0
1101	54
1095	270
1094	0
1088	0
1087	0
1085	10
781	29
781	0
780	0
779	5
778	0
757	0
757	54
752	0
746	0
743	0
724	2
722	0
719	0
715	3
714	0
393	0
392	0
390	19
389	0
385	0
278	377
264	0
262	0
221	0
207	0
194	0
189	0
181	0
176	0
171	37
158	0
157	0
153	54
143	0
139	0
115	36

102	0
99	0
78	0
67	0
62	3
52	0
28	0
22	0

Table S27: Optimized geometry of 8-C_{3v} at the M06-2X/6-311++G($2df, 2pd$) level of theory.

N	0.	0.0000000005	-3.150939671
B	0.	0.0000000005	-1.5616782979
H	0.8279001452	0.4779883731	-3.5141533924
H	-0.827900146	0.4779883717	-3.5141533924
H	0.0000000008	-0.9559767434	-3.5141533924
H	-0.000000001	1.1556865685	-1.1740087866
H	1.0008539272	-0.5778432827	-1.1740087866
H	-1.0008539262	-0.5778432844	-1.1740087866
N	-2.9100248975	1.680103655	-1.6171584627
B	-2.880803038	1.6632324066	-3.2393669723
H	-2.0932891469	1.2085610505	-1.229308452
H	-3.7271148239	1.211321262	-1.2389444363
H	-2.9125924012	2.6221154849	-1.2389444363
H	-2.8727050441	0.4933738154	-3.5552528991
H	-1.8636267832	2.2411486355	-3.5552528991
H	-3.8708188196	2.2348182835	-3.6179446315
N	0.0000000029	-3.3602073136	-1.6171584627
B	0.0000000029	-3.3264648168	-3.2393669723
H	0.8145224273	-3.8334367506	-1.2389444363
H	-0.8145224206	-3.833436752	-1.2389444363
H	0.0000000021	-2.4171221032	-1.229308452
H	0.0000000039	-4.4696365723	-3.6179446315
H	1.0090782648	-2.7345224527	-3.5552528991
H	-1.00907826	-2.7345224545	-3.5552528991
N	2.9100248945	1.6801036601	-1.6171584627
B	2.8808030351	1.6632324117	-3.2393669723
H	3.7271148218	1.2113212686	-1.2389444363
H	2.0932891448	1.2085610542	-1.229308452
H	2.9125923966	2.62211549	-1.2389444363
H	2.8727050432	0.4933738204	-3.5552528991
H	3.8708188157	2.2348182903	-3.6179446315
H	1.8636267793	2.2411486388	-3.5552528991
N	0.	0.0000000005	1.5144125607

B	0.	0.0000000005	3.1003634834
H	0.8189433002	0.4728171363	1.1293096532
H	-0.818943301	0.4728171348	1.1293096532
H	0.0000000008	-0.9456342696	1.1293096532
H	-0.000000001	1.1552192249	3.4839902887
H	1.0004491958	-0.5776096109	3.4839902887
H	-1.0004491948	-0.5776096126	3.4839902887
N	-2.884042622	1.6651027813	3.1218860207
B	-2.8907372099	1.6689679034	1.4974578973
H	-2.0540727862	1.1859194742	3.4749486086
H	-3.7022432761	1.1903132202	3.4891626731
H	-2.8819631294	2.6110801137	3.4891626731
H	-2.8909606491	0.505004367	1.161488849
H	-1.8828269389	2.2511431774	1.161488849
H	-3.8911152322	2.2465364227	1.1524351083
N	0.0000000029	-3.3302055662	3.1218860207
B	0.0000000029	-3.3379358104	1.4974578973
H	0.8202801513	-3.8013933375	3.4891626731
H	-0.8202801447	-3.8013933389	3.4891626731
H	0.0000000021	-2.3718389504	3.4749486086
H	0.0000000039	-4.4930728508	1.1524351083
H	1.0081337141	-2.7561475462	1.161488849
H	-1.0081337093	-2.7561475479	1.161488849
N	2.8840426191	1.6651027863	3.1218860207
B	2.8907372069	1.6689679084	1.4974578973
H	3.7022432741	1.1903132267	3.4891626731
H	2.0540727842	1.1859194777	3.4749486086
H	2.8819631248	2.6110801188	3.4891626731
H	2.8909606482	0.505004372	1.161488849
H	3.8911152283	2.2465364295	1.1524351083
H	1.8828269349	2.2511431807	1.161488849

Table S28: Harmonic vibrational frequencies of 8-C_{3v} at the M06-2X/6-311++G($2df, 2pd$) level of theory.

Frequency (cm^{-1})	IR Intensity (km mol^{-1})
3600	73
3600	0
3596	47
3596	0
3559	0
3556	180
3555	8
3551	158
3499	339

3468	491
3466	47
3459	3
3445	44
3433	166
3433	165
3427	7
3391	41
2542	59
2538	502
2538	503
2535	4
2532	256
2504	420
2504	421
2497	146
2497	17
2497	152
2489	0
2467	132
2466	48
2466	49
2465	279
2463	107
2445	212
2436	99
2424	55
2415	97
1663	3
1663	1
1662	6
1662	1
1660	1
1660	50
1654	0
1648	2
1643	0
1466	16
1461	208
1394	369
1390	1
1385	472
1382	12
1271	20
1264	12

1241	13
1240	23
1238	4
1238	12
1219	4
1219	0
1214	5
1213	0
1213	207
1208	1
1202	513
1193	0
1190	111
1177	19
1132	20
1115	1
1103	4
1097	88
1092	0
1089	0
1086	13
1082	162
1078	2
1078	0
852	3
838	1
797	7
796	7
760	6
759	35
758	1
757	1
750	4
747	2
733	1
731	7
701	1
700	5
700	6
699	0
699	7
699	8
674	3
674	0
435	0

427	0
324	9
323	9
322	2
322	0
318	0
263	260
263	261
246	42
246	43
233	0
215	0
211	3
205	6
196	1
186	0
171	0
170	0
163	0
154	0
152	3
147	0
141	3
134	1
132	10
129	0
126	0
112	46
111	47
105	11
105	10
98	0
82	0
56	8
47	13
46	13
37	1
32	0
17	0
3	0

Table S29: Optimized geometry of 12-C_{3v} at the M06-2X/6-311++G($2df, 2pd$) level of theory.

N	0.	-0.0000000006	-0.6967407661

B	0.	-0.0000000006	0.887767115
H	-0.8198084973	0.4733166572	-1.0814258207
H	-0.000000001	-0.9466333143	-1.0814258207
H	0.8198084983	0.4733166554	-1.0814258207
H	-1.0005493607	-0.5776674418	1.2772466749
H	0.0000000013	1.1553348842	1.2772466749
H	1.0005493594	-0.577667444	1.2772466749
N	-0.0000000036	-3.358080499	0.8376104735
B	-0.0000000036	-3.3489447674	-0.7757053738
H	-0.0000000026	-2.4093604151	1.2135079098
H	0.8138539384	-3.8253449384	1.2259543554
H	-0.8138539467	-3.8253449367	1.2259543554
H	1.0068360367	-2.7628406008	-1.114021067
H	-1.0068360427	-2.7628405987	-1.114021067
H	-0.0000000049	-4.4988699639	-1.1427563508
N	2.9081830215	1.6790402455	0.8376104735
B	2.9002712458	1.6744723797	-0.7757053738
H	2.9059189252	2.617490654	1.2259543554
H	3.7197728663	1.2078542747	1.2259543554
H	2.0865673272	1.2046802045	1.2135079098
H	3.896135679	2.2494349769	-1.1427563508
H	1.8892721281	2.2533658848	-1.114021067
H	2.8961081659	0.509474708	-1.114021067
N	-2.9081830178	1.6790402518	0.8376104735
B	-2.9002712422	1.674472386	-0.7757053738
H	-2.9059189196	2.6174906603	1.2259543554
H	-2.0865673246	1.204680209	1.2135079098
H	-3.7197728637	1.2078542827	1.2259543554
H	-1.8892721232	2.2533658889	-1.114021067
H	-3.8961356742	2.2494349854	-1.1427563508
H	-2.8961081648	0.5094747143	-1.114021067
N	0.	-0.0000000006	3.9685704752
B	0.	-0.0000000006	5.5555399415
H	-0.8191964519	0.4729632927	3.5847782053
H	-0.000000001	-0.9459265852	3.5847782053
H	0.8191964529	0.4729632909	3.5847782053
H	-1.0006988555	-0.5777537527	5.9370757943
H	0.0000000013	1.1555075059	5.9370757943
H	1.0006988542	-0.5777537549	5.9370757943
N	-0.0000000036	-3.3345695679	5.5542250179
B	-0.0000000036	-3.33259993	3.9317909664
H	-0.0000000026	-2.379105541	5.9153179208
H	0.8200190184	-3.8084312857	5.919161463
H	-0.8200190267	-3.8084312839	5.919161463
H	1.0078621572	-2.7490523379	3.5964840007

H	-1.0078621632	-2.7490523357	3.5964840007
H	-0.0000000049	-4.4851411651	3.5782127095
N	2.8878219579	1.66728478	5.5542250179
B	2.8861162013	1.666299961	3.9317909664
H	2.8881887323	2.6143729435	5.919161463
H	3.7082077533	1.1940583325	5.919161463
H	2.0603658376	1.1895527674	5.9153179208
H	3.8842461905	2.2425705775	3.5782127095
H	1.8768180819	2.2473603998	3.5964840007
H	2.8846802402	0.5016919302	3.5964840007
N	-2.8878219542	1.6672847863	5.5542250179
B	-2.8861161977	1.6662999673	3.9317909664
H	-2.8881887266	2.6143729498	5.919161463
H	-2.060365835	1.1895527719	5.9153179208
H	-3.7082077507	1.1940583405	5.919161463
H	-1.876818077	2.2473604039	3.5964840007
H	-3.8842461856	2.2425705859	3.5782127095
H	-2.8846802391	0.5016919365	3.5964840007
N	0.	-0.0000000006	-5.3860705991
B	0.	-0.0000000006	-3.7949478071
H	-0.8276294314	0.4778320756	-5.7499664718
H	-0.000000001	-0.9556641511	-5.7499664718
H	0.8276294324	0.4778320738	-5.7499664718
H	-1.0007470175	-0.577781559	-3.408585257
H	0.0000000013	1.1555631186	-3.408585257
H	1.0007470162	-0.5777815612	-3.408585257
N	-0.0000000036	-3.3518258458	-3.8690135868
B	-0.0000000036	-3.3288654344	-5.4891575916
H	-0.0000000026	-2.4079921968	-3.4823625638
H	0.81332583	-3.8221276189	-3.4844758539
H	-0.8133258383	-3.8221276171	-3.4844758539
H	1.0087127445	-2.7392945545	-5.8117579825
H	-1.0087127504	-2.7392945523	-5.8117579825
H	-0.0000000049	-4.4746214347	-5.8620936917
N	2.9027663329	1.6759129189	-3.8690135868
B	2.8828820333	1.6644327133	-5.4891575916
H	2.903396699	2.6154246389	-3.4844758539
H	3.7167225316	1.2067029702	-3.4844758539
H	2.0853824153	1.2039960953	-3.4823625638
H	3.8751358367	2.2373107123	-5.8620936917
H	1.8679423	2.2432181382	-5.8117579825
H	2.8766550455	0.4960764084	-5.8117579825
N	-2.9027663293	1.6759129252	-3.8690135868
B	-2.8828820297	1.6644327195	-5.4891575916
H	-2.9033966933	2.6154246452	-3.4844758539

H	-2.0853824127	1.2039960998	-3.4823625638
H	-3.716722529	1.2067029783	-3.4844758539
H	-1.8679422951	2.2432181423	-5.8117579825
H	-3.8751358319	2.2373107207	-5.8620936917
H	-2.8766550444	0.4960764146	-5.8117579825

Table S30: Harmonic vibrational frequencies of 12-C_{3v} at the M06-2X/6-311++G($2df, 2pd$) level of theory.

Frequency (cm^{-1})	IR Intensity (km mol^{-1})
3597	73
3597	0
3593	54
3593	0
3588	50
3588	0
3557	0
3554	180
3554	13
3552	0
3550	225
3548	101
3501	358
3486	321
3469	453
3467	70
3462	54
3459	7
3455	66
3447	46
3436	147
3429	7
3418	32
3392	45
2537	84
2536	1
2533	818
2533	5
2522	20
2519	279
2499	416
2499	418
2494	352
2494	351
2493	0

2487	84
2485	0
2481	0
2464	157
2463	86
2462	209
2460	59
2456	375
2455	107
2449	147
2441	117
2434	70
2427	59
2419	34
2414	150
1664	5
1663	1
1663	0
1663	1
1662	1
1662	3
1661	31
1660	26
1659	14
1655	0
1654	0
1653	0
1648	2
1644	0
1642	0
1466	11
1463	23
1459	369
1409	407
1407	1
1403	524
1399	2
1391	543
1388	13
1270	20
1265	24
1264	24
1264	0
1240	13
1240	3

1240	33
1240	8
1238	1
1238	7
1222	4
1221	0
1220	3
1220	0
1219	17
1215	2
1214	3
1214	0
1212	554
1206	2
1202	710
1199	184
1194	0
1189	34
1178	35
1130	18
1121	7
1116	0
1105	2
1101	8
1100	12
1096	157
1096	156
1094	0
1091	37
1088	0
1087	3
1087	18
1083	151
1078	8
1078	0
861	3
843	0
835	2
794	8
793	8
787	1
786	27
777	5
763	4
762	2

760	1
758	22
753	2
738	2
736	11
731	2
729	9
704	2
703	2
703	0
703	10
695	3
695	0
674	3
674	0
428	0
427	0
421	0
327	6
325	0
321	9
318	2
317	0
315	0
266	400
266	401
255	3
246	30
232	0
219	1
217	0
211	3
207	4
203	6
198	3
191	0
182	0
175	0
172	0
168	0
167	0
164	0
161	0
156	0
153	0

150	0
147	18
135	0
135	8
131	0
129	0
119	1
119	3
115	79
104	0
102	0
95	0
93	1
91	0
84	0
59	14
52	6
51	6
44	3
36	0
31	0
30	1
26	0
16	0
8	0

4 Crystal Models

Table S31: Cartesian coordinates of the 2-C_s crystal model at the M06-2X/6-311++G($2df, 2pd$) level of theory.

N	0.	1.1485421423	6.5515777809
H	0.	2.2138	6.6862
H	0.7553	0.7233	6.9654
B	0.	0.9035594304	4.9863236166
H	0.	-0.2100729293	4.6866992769
H	0.9979315503	1.2903856783	4.4872996628
H	-0.7553	0.7233	6.9654
H	-0.9979315503	1.2903856783	4.4872996628
N	0.	0.4487525812	1.873666763

H	0.	1.3334942635	2.3728980252
H	0.8144881603	-0.0613272511	2.1998202952
B	0.	0.6345734411	0.251436934
H	0.	-0.4845071242	-0.203604842
H	1.0075604622	1.2489260497	-0.0052826411
H	-0.8144881603	-0.0613272511	2.1998202952
H	-1.0075604622	1.2489260497	-0.0052826411

Table S32: Harmonic vibrational frequencies of the 2-C$_s$ crystal model at the M06-2X/6-311++G($2df, 2pd$) level of theory.

Frequency (cm^{-1})	IR Intensity (km mol^{-1})	Raman Activites (Å^4 amu^{-1})
3597	37	24
3587	47	27
3498	12	115
2522	267	69
2520	273	75
2478	86	241
1668	23	4
1667	13	3
1380	220	6
1202	4	7
1201	147	1
1201	4	6
1074	33	2
1072	34	2
729	5	6
657	3	1
655	2	0
270	0	0
96	1	0
58	0	0
48	26	0
44	31	0
17	10	0
14	15	0

Table S33: Cartesian coordinates of the 3-C$_s$ crystal model at the M06-2X/6-311++G($2df, 2pd$) level of theory.

N	0.	0.7653844788	1.594743452
H	0.	1.6390724919	2.1143555007
H	0.8146108702	0.2471556542	1.9100141177
B	0.	0.9851305893	-0.0231852778

H	0.	-0.1231430271	-0.5093952219
H	1.005953986	1.6036331216	-0.2800591976
H	-0.8146108702	0.2471556542	1.9100141177
H	-1.005953986	1.6036331216	-0.2800591976
N	0.	1.1464574465	-3.4190819652
H	0.	2.2138866708	-3.2864855584
H	0.7562100892	0.7242601679	-3.0074933165
B	0.	0.9041856462	-4.9860133552
H	0.	-0.2101	-5.2852
H	0.9981	1.2902	-5.4846
H	-0.7562100892	0.7242601679	-3.0074933165
H	-0.9981	1.2902	-5.4846
N	0.	1.1484158847	6.5515975218
H	0.	2.2138	6.6862
H	0.7553	0.7233	6.9654
B	0.	0.9049516255	4.9853454828
H	0.	-0.210194378	4.6871514454
H	0.9985146558	1.2897383843	4.4881365308
H	-0.7553	0.7233	6.9654
H	-0.9985146558	1.2897383843	4.4881365308

Table S34: Harmonic vibrational frequencies of the 3-C$_s$ crystal model at the M06-2X/6-311++G($2df, 2pd$) level of theory.

Frequency (cm^{-1})	IR Intensity (km mol^{-1})	Raman Activites (Å^4 amu^{-1})
3585	43	25
3579	46	30
3491	17	131
2516	225	48
2508	222	52
2472	115	196
1669	17	3
1665	23	5
1388	219	10
1208	98	3
1207	4	5
1204	82	3
1074	28	2
1072	28	3
729	4	10
665	3	0
658	3	3
255	0	0
81	29	0
78	37	0

54	7	0
37	0	0
33	2	0
22	1	0

Table S35: Cartesian coordinates of the 5-C$_s$ crystal model at the M06-2X/6-311++G($2df, 2pd$) level of theory.

N	0.	0.7837178018	1.5952206905
H	0.	1.6597486731	2.1116689326
H	0.8135048303	0.2686050903	1.9193458375
B	0.	0.988609044	-0.0220909061
H	0.	-0.1228694046	-0.5033333235
H	1.0053703366	1.604970876	-0.2895729885
H	-0.8135048303	0.2686050903	1.9193458375
H	-1.0053703366	1.604970876	-0.2895729885
N	0.	1.1489527861	-3.4208743101
H	0.	2.213763593	-3.2855132392
H	0.7550425525	0.7230329128	-3.0064952975
B	0.	0.9040415957	-4.9859908638
H	0.	-0.2101	-5.2852
H	0.9981	1.2902	-5.4846
H	-0.7550425525	0.7230329128	-3.0064952975
H	-0.9981	1.2902	-5.4846
N	0.	1.1484115619	6.5515981932
H	0.	2.2138	6.6862
H	0.7553	0.7233	6.9654
B	0.	0.9038443183	4.9862276906
H	0.	-0.2100549779	4.6866326157
H	0.9980021421	1.2903376486	4.4873552543
H	-0.7553	0.7233	6.9654
H	-0.9980021421	1.2903376486	4.4873552543
N	0.	1.1484	-8.4064
H	0.	2.2138	-8.2718
H	0.7553	0.7233	-7.9926
B	0.	0.9041	-9.972
H	0.	-0.2101	-10.2712
H	0.9981	1.2902	-10.4706
H	-0.7553	0.7233	-7.9926
H	-0.9981	1.2902	-10.4706
N	0.	1.1484	11.5376
H	0.	2.2138	11.6722
H	0.7553	0.7233	11.9514
B	0.	0.9041	9.972
H	0.	-0.2101	9.6728

H	0.9981	1.2902	9.4734
H	-0.7553	0.7233	11.9514
H	-0.9981	1.2902	9.4734

Table S36: Harmonic vibrational frequencies of the 5-C$_s$ crystal model at the M06-2X/6-311++G($2df, 2pd$) level of theory.

Frequency (cm^{-1})	IR Intensity (km mol^{-1})	Raman Activites (Å^4 amu^{-1})
3585	44	25
3575	47	29
3492	22	138
2510	226	46
2501	220	52
2468	133	198
1669	17	3
1667	22	4
1396	243	12
1208	106	3
1208	4	6
1205	88	3
1074	27	2
1070	27	1
735	2	10
666	3	0
653	4	2
255	0	0
80	37	0
76	33	0
51	3	0
38	0	0
34	2	0
10	0	0

Table S37: Cartesian coordinates of the 9-C$_s$ crystal model at the M06-2X/6-311++G($2df, 2pd$) level of theory.

N	0.	1.1809190662	1.5669717671
H	0.	2.19145722	1.6723901368
H	0.8365055109	0.7993058276	2.0035899705
B	0.	0.7561597597	-0.005728207
H	0.	-0.4559738629	0.0012559651
H	1.0051246635	1.2208705521	-0.4840368045
H	-0.8365055109	0.7993058276	2.0035899705
H	-1.0051246635	1.2208705521	-0.4840368045

N	-2.6974269557	-1.1481292416	-0.9278099767
H	-2.6975361878	-2.2137926013	-0.7927416919
H	-3.4527999996	-0.7232993505	-0.513600665
B	-2.6974787855	-0.9041327583	-2.4930051057
H	-2.6975	0.2101	-2.7922
H	-3.6956	-1.2902	-2.9916
H	-1.9422942291	-0.7235937667	-0.5131657438
H	-1.6994	-1.2902	-2.9916
N	-2.697493093	-1.1484	4.0586
H	-2.6975	-2.2138	4.1932
H	-3.4528	-0.7233	4.4724
B	-2.697494938	-0.9040983808	2.4930060289
H	-2.6974958498	0.2100994298	2.1937734579
H	-3.6956041662	-1.2901981457	1.9944069042
H	-1.9422	-0.7233	4.4724
H	-1.6994048261	-1.2902021479	1.9943920027
N	-2.6975238861	3.7386048491	-0.9273615854
H	-2.6975153709	2.6732403139	-0.7928851378
H	-3.4527906488	4.1637019073	-0.5135848914
B	-2.6975075326	3.9828999999	-2.4930000001
H	-2.6975	5.0971	-2.7922
H	-3.6956	3.5968	-2.9916
H	-1.9421943399	4.1636988455	-0.5136091464
H	-1.6994	3.5968	-2.9916
N	-2.6975031135	3.7385933033	4.0585989548
H	-2.6975	2.6732	4.1932
H	-3.4528	4.1637	4.4724
B	-2.6974661442	3.9829219229	2.4930507734
H	-2.6974965098	5.097101553	2.1938057817
H	-3.6956000001	3.5968084104	1.994393488
H	-1.9422	4.1637	4.4724
H	-1.6994683526	3.5967758578	1.9943365526
N	2.6974269557	-1.1481292416	-0.9278099767
H	2.6975361878	-2.2137926013	-0.7927416919
H	1.9422942291	-0.7235937667	-0.5131657438
B	2.6974787855	-0.9041327583	-2.4930051057
H	2.6975	0.2101	-2.7922
H	1.6994	-1.2902	-2.9916
H	3.4527999996	-0.7232993505	-0.513600665
H	3.6956	-1.2902	-2.9916
N	2.697493093	-1.1484	4.0586
H	2.6975	-2.2138	4.1932
H	1.9422	-0.7233	4.4724
B	2.697494938	-0.9040983808	2.4930060289
H	2.6974958498	0.2100994298	2.1937734579

H	1.6994048261	-1.2902021479	1.9943920027
H	3.4528	-0.7233	4.4724
H	3.6956041662	-1.2901981457	1.9944069042
N	2.6975238861	3.7386048491	-0.9273615854
H	2.6975153709	2.6732403139	-0.7928851378
H	1.9421943399	4.1636988455	-0.5136091464
B	2.6975075326	3.9828999999	-2.4930000001
H	2.6975	5.0971	-2.7922
H	1.6994	3.5968	-2.9916
H	3.4527906488	4.1637019073	-0.5135848914
H	3.6956	3.5968	-2.9916
N	2.6975031135	3.7385933033	4.0585989548
H	2.6975	2.6732	4.1932
H	1.9422	4.1637	4.4724
B	2.6974661442	3.9829219229	2.4930507734
H	2.6974965098	5.097101553	2.1938057817
H	1.6994683526	3.5967758578	1.9943365526
H	3.4528	4.1637	4.4724
H	3.6956000001	3.5968084104	1.994393488

Table S38: Harmonic vibrational frequencies of the 9-C$_s$ crystal model at the M06-2X/6-311++G($2df, 2pd$) level of theory.

Frequency (cm^{-1})	IR Intensity (km mol^{-1})	Raman Activites (Å^4 amu^{-1})
3567	122	49
3545	201	88
3443	39	204
2543	296	80
2521	167	115
2471	82	184
1649	16	2
1630	42	15
1330	77	2
1252	14	5
1203	28	3
1162	66	5
1094	52	1
1091	25	1
737	20	3
726	3	1
712	3	0
371	2	1
198	25	1
162	54	0
152	41	0

127	1	0
111	0	0
78	1	0

Table S39: Cartesian coordinates of the 11-C$_s$ crystal model at the M06-2X/6-311++G$(2df, 2pd)$ level of theory.

amu^{-1}			
N	0.	1.1407739604	1.5656217651
H	0.	2.1423646425	1.7398259278
H	0.8299949684	0.73982984	1.9997825463
B	0.	0.8112500606	-0.0168015765
H	0.	-0.3985845385	-0.1024784873
H	1.0045809347	1.2993819008	-0.4812284923
H	-0.8299949684	0.73982984	1.9997825463
H	-1.0045809347	1.2993819008	-0.4812284923
N	0.	1.1484	-3.4204
H	0.	2.2138	-3.2858
H	0.7553	0.7233	-3.0066
B	0.	0.9041	-4.986
H	0.	-0.2101	-5.2852
H	0.9981	1.2902	-5.4846
H	-0.7553	0.7233	-3.0066
H	-0.9981	1.2902	-5.4846
N	0.	1.1484	6.5516
H	0.	2.2138	6.6862
H	0.7553	0.7233	6.9654
B	0.	0.9041	4.986
H	0.	-0.2101	4.6868
H	0.9981	1.2902	4.4874
H	-0.7553	0.7233	6.9654
H	-0.9981	1.2902	4.4874
N	-2.6974760861	-1.1485923182	-0.9272461245
H	-2.6974708053	-2.2138059586	-0.792847169
H	-3.4528000104	-0.7233899271	-0.5135076672
B	-2.6975159276	-0.9040754224	-2.4929961652
H	-2.6975	0.2101	-2.7922
H	-3.6956	-1.2902	-2.9916
H	-1.9423359555	-0.7231213933	-0.5138244135
H	-1.6994	-1.2902	-2.9916
N	-2.6974762151	-1.1484000011	4.0585999998
H	-2.6975	-2.2138	4.1932
H	-3.4528	-0.7233	4.4724
B	-2.6975129848	-0.9040971454	2.4930106273
H	-2.697517725	0.2101540297	2.1937768305

H	-3.6956133123	-1.2901940757	1.99442206
H	-1.9422	-0.7233	4.4724
H	-1.6994130471	-1.2902058055	1.994378378
N	-2.6975291981	3.7386007039	-0.9273944197
H	-2.6975373618	2.6732362089	-0.7927941955
H	-3.4527908048	4.1637018791	-0.5135851431
B	-2.697520557	3.982899999	-2.4929999996
H	-2.6975	5.0971	-2.7922
H	-3.6956	3.5968	-2.9916
H	-1.9422030875	4.16370063	-0.5135950143
H	-1.6994	3.5968	-2.9916
N	-2.6975018915	3.7385959311	4.0585993651
H	-2.6975	2.6732	4.1932
H	-3.4528	4.1637	4.4724
B	-2.6974916154	3.9829085211	2.4930101863
H	-2.697496527	5.0971015456	2.1938057557
H	-3.6955999999	3.596803578	1.9943972291
H	-1.9422	4.1637	4.4724
H	-1.699381621	3.5967790209	1.99438988
N	2.6974760861	-1.1485923182	-0.9272461245
H	2.6974708053	-2.2138059586	-0.792847169
H	1.9423359555	-0.7231213933	-0.5138244135
B	2.6975159276	-0.9040754224	-2.4929961652
H	2.6975	0.2101	-2.7922
H	1.6994	-1.2902	-2.9916
H	3.4528000104	-0.7233899271	-0.5135076672
H	3.6956	-1.2902	-2.9916
N	2.6974762151	-1.1484000011	4.0585999998
H	2.6975	-2.2138	4.1932
H	1.9422	-0.7233	4.4724
B	2.6975129848	-0.9040971454	2.4930106273
H	2.697517725	0.2101540297	2.1937768305
H	1.6994130471	-1.2902058055	1.994378378
H	3.4528	-0.7233	4.4724
H	3.6956133123	-1.2901940757	1.99442206
N	2.6975291981	3.7386007039	-0.9273944197
H	2.6975373618	2.6732362089	-0.7927941955
H	1.9422030875	4.16370063	-0.5135950143
B	2.697520557	3.982899999	-2.4929999996
H	2.6975	5.0971	-2.7922
H	1.6994	3.5968	-2.9916
H	3.4527908048	4.1637018791	-0.5135851431
H	3.6956	3.5968	-2.9916
N	2.6975018915	3.7385959311	4.0585993651
H	2.6975	2.6732	4.1932

H	1.9422	4.1637	4.4724
B	2.6974916154	3.9829085211	2.4930101863
H	2.697496527	5.0971015456	2.1938057557
H	1.699381621	3.5967790209	1.99438988
H	3.4528	4.1637	4.4724
H	3.6955999999	3.596803578	1.9943972291

Table S40: Harmonic vibrational frequencies of the 11-C_s crystal model at the M06-2X/6-311++G($2df, 2pd$) level of theory.

Frequency (cm^{-1})	IR Intensity (km mol^{-1})	Raman Activites ($Å^4$ amu^{-1})
3559	108	40
3528	195	71
3441	54	169
2520	265	67
2504	181	70
2467	76	189
1651	10	2
1634	33	10
1366	107	1
1254	13	5
1195	25	3
1170	91	3
1093	49	1
1089	25	1
769	15	5
728	4	1
714	2	0
359	4	0
195	51	1
171	19	0
150	39	0
122	0	0
117	0	0
102	0	0

Table S41: Cartesian coordinates of the 13-C_1 crystal model at the M06-2X/6-311++G($2df, 2pd$) level of theory.

amu^{-1}			
B	0.7315532046	-0.3450104413	-9.3629992184
N	-0.1643259892	-1.1608404804	-8.2973910807
H	0.4109284923	-1.6674726357	-7.6294785333
H	-0.7594410461	-0.5167294686	-7.7781060182

H	1.4055695854	0.442472567	-8.73835326
H	-0.0525454321	0.2165034498	-10.0987762911
H	1.4093535326	-1.1534855548	-9.9562841428
H	-0.754085432	-1.83396256	-8.7851600506
H	-0.96769	-0.82801	-4.31759
N	0.0142111419	-1.2356384394	-12.6267828778
H	-0.8276606413	-0.8279640504	-13.1408116485
H	0.0162026669	-2.1959301223	-12.6192698417
H	0.0162165066	-1.0007779612	-11.6955382235
B	1.3033577965	-0.6722676936	-13.3761580389
H	1.38916	-1.07983	-14.48205
H	1.38916	0.49937	-13.26149
N	-3.5466200896	-3.3696673021	-9.8091956438
H	-4.38849	-2.96205	-10.3232
H	-3.54455	-4.32998	-9.80167
H	-3.54455	-3.13491	-8.87801
B	-2.2574869272	-2.8062869636	-10.5585782125
H	-2.17163831	-3.2138666813	-11.664451092
H	-2.1716427887	-1.6346803718	-10.4438941139
H	8.53656	3.12851	-15.62983
H	6.37003	2.5075	-14.39504
H	4.97575	0.99447	-12.81224
N	3.4350473208	-3.3695264295	-9.9199415838
H	2.5931437358	-2.961944848	-10.4337967659
H	3.4371096949	-4.3299805341	-9.9125318172
H	3.4370331125	-3.1349520809	-8.988779332
H	2.80922	0.37346	-11.57744
B	4.7241406291	-2.8062187222	-10.6693203671
H	2.29692	-1.03074	-12.92807
H	4.80997	-3.21387	-11.77523
H	4.80997	-1.63468	-10.55468
N	-0.1258064378	-5.5037008018	-7.1023744749
H	-0.96769	-5.0961	-7.61639
H	-0.12374	-6.46402	-7.09486
H	-0.12374	-5.26896	-6.1712
B	1.1633279014	-4.9403118239	-7.8517497979
H	-1.2639065798	-3.1647754224	-10.1104439876
H	1.2491613866	-5.3479201163	-8.9576398495
H	1.2491112858	-3.768642726	-7.737101906
H	-2.14586	-3.27363	-7.17706
H	-4.3124	-3.89463	-5.94226
H	-5.70667	-5.40767	-4.35947
H	-7.87321	-6.02868	-3.12467
H	5.71773	-3.16479	-10.22126
H	2.1569195538	-5.2988300595	-7.4036690582

H	7.34394	4.4879	-15.73784
H	3.78313	2.35385	-12.92025
N	0.0142172576	3.032480291	-9.3279503452
H	-0.827661	3.4400796886	-9.8420377451
H	0.0162176232	2.0720767877	-9.320542202
H	0.0162040315	3.2672198806	-8.3967998455
B	1.3033584531	3.5958704473	-10.0773207173
H	1.38916	3.18826	-11.18324
H	1.38916	4.76746	-9.96269
N	-3.5466199332	0.8984354472	-6.5103857898
H	-4.38849	1.30604	-7.0244
H	-3.54455	-0.06189	-6.50287
H	-3.54455	1.13318	-5.57921
B	-2.2574882995	1.4618214633	-7.259750426
H	-3.33848	-1.91424	-7.28507
H	-2.1716419737	1.0542161241	-8.3656487246
H	-2.171639765	2.6334100313	-7.145090496
H	-6.89929	-4.04828	-4.46748
H	8.53656	4.7077	-14.40928
N	6.96318	3.0965	-13.93157
H	7.61278	2.57366	-13.26541
H	6.37003	3.70257	-13.47137
B	7.91024	3.87329	-14.95163
H	4.97575	2.57366	-11.59169
N	3.40238	0.96245	-11.11398
N	3.4350457664	0.8983708912	-6.6212918326
H	4.05197	0.43961	-10.44782
H	2.5931391816	1.3058373643	-7.1352354481
H	2.80922	1.56852	-10.65378
H	3.4370331207	-0.0618897111	-6.6136057463
H	3.4371107045	1.1332593562	-5.6900101178
B	4.34943	1.73925	-12.13404
B	4.7241393681	1.461768483	-7.370589818
H	2.29692	3.23735	-9.62927
H	4.80997	1.05422	-8.47643
H	4.80997	2.63341	-7.25587
N	-0.125807262	-1.2356140143	-3.8035783079
H	-0.12374	-2.19593	-3.79606
H	-0.12374	-1.00087	-2.87239
B	1.1633257061	-0.6722381969	-4.5529536262
H	-1.2638974603	1.1032659354	-6.8116840953
H	-2.14586	-1.69443	-5.9565
H	1.2491013581	-1.0798349353	-5.6589170561
H	1.249163142	0.4993697364	-4.438279659
N	-3.71924	-3.30564	-5.4788

H	-3.06965	-3.82848	-4.81264
H	-4.3124	-2.69957	-5.0186
B	-2.77219	-2.52884	-6.49886
H	-5.70667	-3.82848	-3.13891
N	-7.28005	-5.43968	-2.6612
H	-6.63045	-5.96252	-1.99504
H	-7.87321	-4.83361	-2.201
B	-6.33299	-4.66289	-3.68127
H	5.71773	1.1033	-6.92246
H	2.1569190225	-1.0307419195	-4.1048593684

Table S42: Harmonic vibrational frequencies of the 13-C_1 crystal model at the M06-2X/6-311++G($2df, 2pd$) level of theory.

Frequency (cm^{-1})	IR Intensity (km mol^{-1})	Raman Activites ($Å^4$ amu^{-1})
3557	107	171
3524	200	0
3440	61	0
2514	267	189
2500	187	0
2465	82	0
1652	10	2
1634	32	0
1378	113	0
1254	13	3
1195	23	0
1171	98	0
1095	48	6
1090	26	0
776	14	0
732	4	0
717	2	0
358	4	0
194	57	0
170	12	0
154	38	0
123	1	0
117	0	0
101	0	0

Table S43: Cartesian coordinates of the 15-C_1 crystal model at the M06-2X/6-311++G($2df, 2pd$) level of theory.

N	0.0008039838	-0.571911133	0.1780521247

H	0.0008715643	-0.4591137012	1.1891409339
H	0.8324270265	-1.0936126638	-0.0877663219
B	-0.0001125935	0.8868178644	-0.5355103653
H	-0.0001256777	0.6681262946	-1.7313094569
H	1.0036282776	1.4378823359	-0.1537416193
H	-0.8303058485	-1.0945374515	-0.0875424987
H	-1.0043631223	1.4367577339	-0.1534817723
N	-0.001372	4.270263	-0.081851
H	-0.001241	4.134147	0.983356
H	0.754065	3.857375	-0.507593
B	-0.002024	5.836209	-0.323923
H	-0.002225	6.136994	-1.437696
H	0.995901	6.334664	0.062815
H	-0.756535	3.856762	-0.507486
H	-1.000299	6.333854	0.062957
N	0.002671	-5.701726	-0.096041
H	0.002802	-5.837842	0.969166
H	0.758109	-6.114614	-0.521783
B	0.002019	-4.13578	-0.338113
H	0.001818	-3.834995	-1.451886
H	0.999944	-3.637325	0.048625
H	-0.752491	-6.115227	-0.521676
H	-0.996255	-3.638135	0.048767
N	-2.6978428478	1.7802687492	-2.3815124033
H	-2.6980776268	1.6463051837	-3.4475899235
H	-3.4531270162	1.3646065697	-1.9575614532
B	-2.6985999425	3.3447006873	-2.1355429421
H	-2.698684	3.642305	-1.020853
H	-3.696972	3.843435	-2.520797
H	-1.9424820122	1.3642658599	-1.9579381063
H	-1.700772	3.844244	-2.520939
N	-2.696011718	-3.2065549984	-2.3891000013
H	-2.696025	-3.339638	-3.454691
H	-3.451105	-3.621265	-1.964536
B	-2.6966603232	-1.6414569632	-2.1425316271
H	-2.696404468	-1.3431155623	-1.0282898551
H	-3.6949477777	-1.142555658	-2.5278934316
H	-1.940505	-3.620653	-1.964643
H	-1.6987787383	-1.1417038132	-2.5280466558
N	-2.6977584563	1.7724342151	2.5049959645
H	-2.69765651	1.639376716	1.4395014801
H	-3.4527871428	1.3577900736	2.9295523663
B	-2.6982622239	3.3377370018	2.7515170004
H	-2.698335	3.635351	3.866142
H	-3.696623	3.836481	2.366198

H	-1.9421728644	1.3583964555	2.9294455689
H	-1.700423	3.83729	2.366056
N	-2.695654	-3.213508	2.497895
H	-2.695676	-3.346592	1.432304
H	-3.450756	-3.628219	2.922459
B	-2.696272	-1.648258	2.744422
H	-2.696314	-1.350644	3.859047
H	-3.694601	-1.149514	2.359103
H	-1.940156	-3.627607	2.922352
H	-1.698402	-1.148704	2.358961
N	2.6971107629	1.78149773	-2.3822704638
H	2.6969404397	1.6485661026	-3.4479807498
H	1.9415448923	1.3671930847	-1.9577531996
B	2.6963447603	3.346881482	-2.1358788806
H	2.696315	3.644493	-1.021235
H	1.698028	3.845623	-2.521179
H	3.4524729895	1.3673912952	-1.9580655892
H	3.694227	3.846432	-2.521321
N	2.698989	-3.204366	-2.389482
H	2.698975	-3.33745	-3.455073
H	1.943895	-3.619077	-1.964918
B	2.698397	-1.639234	-2.142923
H	2.698116	-1.341082	-1.028431
H	1.700072	-1.140334	-2.528284
H	3.454494	-3.618465	-1.965025
H	3.696256	-1.139574	-2.528412
N	2.697323	1.774674	2.504608
H	2.697302	1.64159	1.439017
H	1.942222	1.359963	2.929172
B	2.696706	3.339925	2.751135
H	2.696664	3.637539	3.86576
H	1.698376	3.838669	2.365816
H	3.452821	1.360576	2.929065
H	3.694576	3.839479	2.365675
N	2.699345	-3.21132	2.497513
H	2.699324	-3.344404	1.431922
H	1.944243	-3.626031	2.922077
B	2.698728	-1.64607	2.74404
H	2.698686	-1.348455	3.858665
H	1.700398	-1.147326	2.358721
H	3.454843	-3.625418	2.92197
H	3.696598	-1.146516	2.35858
N	0.000301	-0.708777	-4.975941
H	0.000432	-0.844893	-3.910734
H	0.755738	-1.121666	-5.401683

B	-0.000351	0.857168	-5.218013
H	-0.000552	1.157954	-6.331786
H	0.997574	1.355623	-4.831275
H	-0.754862	-1.122278	-5.401576
H	-0.998626	1.354814	-4.831133
N	-5.3944240173	-0.717653748	-0.0889540277
H	-5.394219	-0.854035	0.976643
H	-4.6388096419	-1.1313568571	-0.5136921759
B	-5.3948845361	0.8478789147	-0.3307493744
H	-5.395203	1.148811	-1.444409
H	-4.3972309815	1.3467134793	0.05624248
H	-6.149512	-1.131421	-0.514199
H	-6.393277	1.345672	0.056243
N	0.000998	-0.722685	4.798049
H	0.001129	-0.858801	5.863256
H	0.756436	-1.135574	4.372307
B	0.000346	0.843261	4.555977
H	0.000145	1.144046	3.442204
H	0.998271	1.341715	4.942715
H	-0.754164	-1.136186	4.372414
H	-0.997928	1.340906	4.942857
N	5.395682	-0.713424	-0.089502
H	5.39578	-0.849659	0.975879
H	6.151087	-1.126432	-0.51507
B	5.394997	0.852403	-0.3314
H	5.394796	1.153188	-1.445173
H	6.392922	1.350857	0.055338
H	4.640451	-1.127331	-0.514709
H	4.396722	1.350048	0.05548

Table S44: Harmonic vibrational frequencies of the 15-C_1 crystal model at the M06-2X/6-311++G($2df, 2pd$) level of theory.

Frequency (cm^{-1})	IR Intensity (km mol^{-1})	Raman Activites ($Å^4$ amu^{-1})
3563	79	42
3559	109	41
3451	4	165
2541	210	46
2514	137	124
2449	102	138
1643	18	3
1637	32	11
1319	108	17
1244	7	5
1217	41	2

1182	63	10
1091	48	1
1084	34	2
747	14	1
704	3	1
694	2	1
421	1	0
236	9	1
171	34	0
148	26	1
130	16	0
122	4	0
48	14	0

Table S45: Cartesian coordinates of the 19-C_1 crystal model at the M06-2X/6-311++G($2df, 2pd$) level of theory.

N	0.7159766267	-0.0000009638	-0.2181436279
H	0.9100319492	0.000000775	0.7808151953
H	1.1568054162	0.8273056653	-0.6203729577
B	-0.8599442927	0.0000007186	-0.5300348108
H	-0.9736688149	0.000000051	-1.7394381616
H	-1.3334630587	1.0031080602	-0.0406414234
H	1.156803509	-0.827310144	-0.6203699107
H	-1.3334655987	-1.0031045832	-0.0406399036
N	-6.7733410669	2.6975011014	2.3671771446
H	-6.6351700669	2.6975001037	1.3022711446
H	-6.3609170548	1.9422011081	2.7937211446
B	-8.3397450669	2.6975010763	2.6063201446
H	-8.6426080669	2.6975010714	3.7195591446
H	-8.8370590509	1.6994210683	2.2185951446
H	-6.3609170791	3.4528011081	2.7937211446
H	-8.837059083	3.6955810683	2.2185941446
N	-4.2717430236	0.0000001416	-0.2146188554
H	-4.1406560236	0.0000001437	0.8511831446
H	-3.8564920358	0.7553001483	-0.6384108554
B	-5.8365220236	0.0000001165	-0.4641828554
H	-6.1319760236	0.0000001117	-1.5794018554
H	-6.3364030397	0.9980701085	-0.0797628554
H	-3.8564920115	-0.7552998517	-0.6384108554
H	-6.3364030076	-0.9980798915	-0.0797628554
N	-1.7873796199	2.6974902718	2.3837547754
H	-1.6491584672	2.697527327	1.3188112173
H	-1.3749495642	1.9421973954	2.8102985595
B	-3.3537730669	2.6974965281	2.6228991446

H	-3.6566360669	2.6975011515	3.7361381446
H	-3.8510860509	1.6994201484	2.2351731446
H	-1.3749487521	3.4528024629	2.810298668
H	-3.851086083	3.6955801484	2.2351731446
N	3.198607826	2.6974853732	2.400366194
H	3.3367749331	2.6975002638	1.3354271446
H	3.6110279452	1.9422002682	2.8268781446
B	1.6322387583	2.6974537782	2.6395469379
H	1.3293361366	2.6975007126	3.7527159279
H	1.1348423764	1.6996937799	2.251705376
H	3.6110279209	3.4528002682	2.8268781446
H	1.1348936757	3.6955802284	2.2517411931
N	5.7002019764	0.0000003018	-0.1814618554
H	5.8312889764	0.0000003039	0.8843391446
H	6.1154529642	0.7553003084	-0.6052538554
B	4.1354229764	0.0000002766	-0.4310268554
H	3.8399689764	0.0000002719	-1.5462448554
H	3.6355419603	0.9980702686	-0.0466068554
H	6.1154529885	-0.7552996916	-0.6052538554
H	3.6355419924	-0.9980797314	-0.0466068554
N	8.1845759331	2.6975003417	2.4169121446
H	8.3227469331	2.6975003439	1.3520061446
H	8.5969999452	1.9422003483	2.8434561446
B	6.6181719331	2.6975003165	2.6560551446
H	6.3153089331	2.6975003116	3.7692951446
H	6.1208589491	1.6994203085	2.2683301446
H	8.5969999209	3.4528003483	2.8434561446
H	6.120858917	3.6955803085	2.2683301446
N	-6.7570920669	2.6975001017	-2.5197958554
H	-6.6189210669	2.6975001039	-3.5847018554
H	-6.3446680548	1.9422001083	-2.0932518554
B	-8.3234960669	2.6975000765	-2.2806528554
H	-8.6263590669	2.6975000717	-1.1674138554
H	-8.8208100509	1.6994200686	-2.6683778554
H	-6.3446680791	3.4528001083	-2.0932518554
H	-8.820810083	3.6955800686	-2.6683788554
N	-1.7712383171	2.6974921113	-2.5031168102
H	-1.6329178032	2.6975189267	-3.5681199287
H	-1.3585380305	1.94231183	-2.0767858936
B	-3.3375298809	2.6974754759	-2.2641119371
H	-3.6403870669	2.6975001518	-1.1508348554
H	-3.8348370509	1.6994201486	-2.6517998554
H	-1.3587870105	3.4528001884	-2.0765859339
H	-3.834837083	3.6955801486	-2.6517998554
N	3.214852933	2.6975205143	-2.4866388554

H	3.3530239331	2.6975002641	-3.5515458554
H	3.6272769452	1.9422002685	-2.0600948554
B	1.648426336	2.6975038526	-2.247502003
H	1.3456148037	2.6976629532	-1.1342962579
H	1.1511617352	1.6994040511	-2.6352145681
H	3.6272769209	3.4528002685	-2.0600948554
H	1.1511015967	3.6955601047	-2.6352309204
N	8.2008249331	2.6975003419	-2.4700608554
H	8.3389969331	2.6975003441	-3.5349668554
H	8.6132489452	1.9422003485	-2.0435168554
B	6.6344209331	2.6975003168	-2.2309178554
H	6.3315579331	2.6975003119	-1.1176778554
H	6.1371079491	1.6994203088	-2.6186428554
H	8.6132489209	3.4528003485	-2.0435168554
H	6.137107917	3.6955803088	-2.6186428554
N	-6.7733409803	-2.6974988986	2.3671771446
H	-6.6351699803	-2.6974998963	1.3022711446
H	-6.3609169682	-3.4527988919	2.7937211446
B	-8.3397449803	-2.6974989237	2.6063201446
H	-8.6426079803	-2.6974989286	3.7195601446
H	-8.8370589643	-3.6955789317	2.2185951446
H	-6.3609169924	-1.9421988919	2.7937211446
H	-8.8370589963	-1.6994289317	2.2185951446
N	-1.7873795332	-2.6974899099	2.3837547754
H	-1.649158379	-2.6975269614	1.3188112106
H	-1.3749486404	-3.4528020861	2.8102996681
B	-3.3537729803	-2.6974962162	2.6228991446
H	-3.6566359803	-2.6974988485	3.7361381446
H	-3.8510859643	-3.6955798516	2.2351731446
H	-1.3749495027	-1.9421970186	2.8102985594
H	-3.8510859963	-1.6994298516	2.2351731446
N	3.1986079127	-2.6974848498	2.4003661944
H	3.3367750197	-2.6974997362	1.3354281446
H	3.6110270318	-3.4527997318	2.8268781446
B	1.6322388494	-2.6974533011	2.6395469421
H	1.3293352262	-2.6975002477	3.7527159287
H	1.1348937938	-3.6955797716	2.2517421937
H	3.6110270076	-1.9421997318	2.8268781446
H	1.1348424106	-1.699703337	2.2517063744
N	8.1845760197	-2.6974996583	2.4169131446
H	8.3227470197	-2.6974996561	1.3520061446
H	8.5970000318	-3.4527996517	2.8434561446
B	6.6181720197	-2.6974996835	2.6560561446
H	6.3153090197	-2.6974996884	3.7692951446
H	6.1208580357	-3.6955796915	2.2683301446

H	8.5970000076	-1.9421996517	2.8434561446
H	6.1208580037	-1.6994296915	2.2683301446
N	-6.7570919803	-2.6974998983	-2.5197958554
H	-6.6189209803	-2.6974998961	-3.5847018554
H	-6.3446679682	-3.4527998917	-2.0932518554
B	-8.3234959803	-2.6974999235	-2.2806528554
H	-8.6263589803	-2.6974999283	-1.1674128554
H	-8.8208099643	-3.6955799314	-2.6683778554
H	-6.3446679924	-1.9421998917	-2.0932518554
H	-8.8208099963	-1.6994299314	-2.6683778554
N	-1.7712382301	-2.6974917473	-2.5031168113
H	-1.6329177166	-2.6975185588	-3.5681199287
H	-1.3587868991	-3.4527998115	-2.0765849345
B	-3.3375297942	-2.6974751627	-2.2641119371
H	-3.6403869803	-2.6974998482	-1.1508348554
H	-3.8348369643	-3.6955798514	-2.6517998554
H	-1.3585379684	-1.9423114464	-2.0767858898
H	-3.8348369963	-1.6994298514	-2.6517998554
N	3.2148530197	-2.6975199894	-2.4866388554
H	3.3530240197	-2.6974997359	-3.5515448554
H	3.6272770318	-3.4527997315	-2.0600948554
B	1.648426428	-2.6975033791	-2.2475020016
H	1.345614887	-2.6976624863	-1.1342962462
H	1.1511017175	-3.6955596485	-2.6352299198
H	3.6272770076	-1.9421997315	-2.0600948554
H	1.1511617891	-1.6994135939	-2.6352135682
N	8.2008250197	-2.6974996581	-2.4700598554
H	8.3389970197	-2.6974996559	-3.5349668554
H	8.6132490318	-3.4527996515	-2.0435168554
B	6.6344210197	-2.6974996832	-2.2309168554
H	6.3315580197	-2.6974996881	-1.1176778554
H	6.1371080357	-3.6955796912	-2.6186428554
H	8.6132490076	-1.9421996515	-2.0435168554
H	6.1371080037	-1.6994296912	-2.6186428554

Table S46: Harmonic vibrational frequencies of the 19-C_1 crystal model at the M06-2X/6-311++G($2df, 2pd$) level of theory.

Frequency (cm^{-1})	IR Intensity (km mol^{-1})	Raman Activites ($Å^4$ amu^{-1})
3544	110	159
3509	200	0
3432	77	0
2494	268	182
2482	194	0
2455	103	0

1652	10	1
1634	31	0
1400	127	0
1256	14	2
1195	24	0
1173	111	0
1094	47	6
1091	24	0
794	10	0
734	4	0
722	2	0
352	4	0
193	58	0
170	10	0
158	37	0
117	0	0
116	0	0
104	0	0

Table S47: Cartesian coordinates of the 16-C_1 crystal model at the M06-2X/6-311++G($2df, 2pd$) level of theory.

B	-1.7661701156	0.5535728729	-1.0561806053
N	-2.5775724058	-0.5133374812	-0.1304744689
H	-2.2405883115	0.4345680116	-2.165346202
H	-0.6067751221	0.2261303522	-1.0065200242
H	-1.9748332891	1.6393830211	-0.5756186334
H	-2.4026287425	-1.452057762	-0.4803991182
H	-2.261227105	-0.4409824654	0.8328002769
H	-3.5748131063	-0.3076659979	-0.170753787
H	3.3698937302	0.9042692341	1.5759713917
H	3.7210157608	0.4257932772	-0.3499368396
B	2.9070036765	0.8061421897	0.4567309329
H	2.3236749142	1.7960904409	0.0994682831
N	1.7957632565	-0.3752088448	0.5675796305
H	2.2417020812	-1.2426828289	0.8582828353
H	1.087638491	-0.1130454408	1.2499213001
H	1.3472108563	-0.5225191656	-0.3331033327
N	6.0812922929	-0.1017556418	1.2260099763
H	6.3058526493	-0.1338521606	2.2174323278
H	6.2396486145	-1.0298883354	0.840395459
H	5.0802543015	0.102619298	1.141404709
B	6.8930786958	1.0196177096	0.4549223075
H	8.0708948101	0.7197413174	0.5831897851
H	6.6210270184	2.0650847715	0.998654489

H	-0.5240523719	4.7716678222	2.6878684297
N	2.2934354576	3.5209835427	2.5044560892
H	2.572329069	3.4264991629	3.4771083884
H	2.4361791202	2.6218366909	2.0393576666
H	1.2949225303	3.7404551834	2.4694639044
B	3.1053441588	4.6421090838	1.7335366651
H	4.2762219135	4.3259587441	1.8074547586
H	2.8739173657	5.6850905834	2.3247883712
N	4.0799815193	-0.6317999275	-3.2008408379
H	4.1979750376	-0.5209183869	-2.1928461247
H	4.3539538763	-1.5749542023	-3.4606577354
H	3.0826777333	-0.5131713957	-3.3972997732
B	4.8920632866	0.4895038643	-3.971927073
H	6.5260356602	0.9676618157	-0.6958814723
H	4.6500879088	0.3126814497	-5.1552973895
H	6.0666540391	0.2936244236	-3.7195151763
H	1.5475367355	-0.139137632	-4.9588166993
H	4.4896449916	1.5499412819	-3.5643803221
H	1.3938879365	0.4710802652	-3.0415036992
H	-2.5016920938	4.2139654132	-1.7449949807
H	0.1469728216	1.2305836093	-4.4351959723
H	-1.6108539204	5.3055196587	1.0691287583
H	-3.6423673481	4.7915122243	-3.3057416859
N	0.292167158	2.9909323791	-1.9222986748
H	0.5188589356	3.011262478	-0.9282523997
H	0.5278205328	2.0718675915	-2.297143566
H	-0.7089662624	3.1555383249	-2.0320402424
B	1.1041534901	4.1121049014	-2.6933378549
H	2.6863651985	4.6457814265	0.6003200088
H	0.7674561212	4.0251557362	-3.8617787169
H	2.2783220117	3.870174262	-2.5304709456
H	-0.1375740508	3.93698088	0.8904665388
H	-2.1730086912	3.4320915025	-3.5855387325
H	0.7679437394	5.1729546092	-2.2021836462
N	3.1766344267	-3.7566059624	2.9765871194
H	3.3785568962	-3.7200897959	3.9747220592
H	3.4278574444	-4.6857667216	2.644389855
H	2.1754725357	-3.6110816988	2.8484889301
B	3.9886108816	-2.6354248104	2.2055391964
H	5.1600204339	-2.8622153856	2.3958653403
H	3.6275901494	-1.5788853496	2.6792899304
H	0.49096314	-2.6243673329	3.1218627113
H	-3.4095631475	1.1229090254	4.4200021211
N	-0.6112374251	-0.1340429781	4.2551839038
H	-0.320474821	-0.1816690017	5.230079126

H	-0.4486604881	-1.0408624016	3.819244928
H	-1.6088398049	0.0873336061	4.2225199315
B	0.200704992	0.9870834064	3.4841522296
H	1.3688467482	0.6736970178	3.5275575965
H	-0.0421299702	2.0383050151	4.0305622273
N	1.1755123641	-4.2865593859	-1.4503910441
H	1.3752178666	-4.2245988755	-0.4532160698
H	1.43389596	-5.2140795484	-1.7816902534
H	-0.6329121693	-4.86807192	2.7224443284
H	0.3023955533	-1.7265155513	-3.4563742951
H	-2.6406531466	-5.411426959	-1.7356740771
H	0.1752613327	-4.1419801936	-1.5938254775
B	1.9874632526	-3.1654745748	-2.2213156242
H	3.678111147	-2.754251712	1.0330406963
H	1.6950090308	-3.285859411	-3.3943473582
H	3.1568301489	-3.365259567	-2.0020244934
H	0.6436843478	-3.2585608634	1.2191233283
H	-1.351762087	-3.7849889325	-3.1988764655
H	1.5975002507	-2.1101650076	-1.7552871269
N	-0.2067668681	-0.8970119531	-3.7669390275
N	-3.1112948089	-4.5519548816	-2.0163026788
N	-1.9933272618	3.2557555932	1.9385235733
N	-4.8980316943	-0.3993378107	3.6891434753
N	-3.9946289608	2.7256101297	-2.4883257514
N	-6.8991653481	-0.929379721	-0.7377081157
H	-1.6518750986	-4.2695582146	1.5835310781
H	-0.7647833923	-1.1494886937	-4.5794849061
H	-3.6504383726	-4.7818424739	-2.8532724682
H	-2.4110047042	2.8987248426	1.0787604745
H	-5.344789507	-0.7366782867	2.8386324916
H	-4.4587825392	2.3828804353	-3.3271004197
H	-7.3656123798	-1.2394884615	-1.5909560693
H	-1.7683071576	-3.7679382924	3.1460137475
H	-0.8431946715	-0.6100795993	-3.0215108826
H	-3.7835940216	-4.3093910805	-1.2918918433
H	-2.7446086386	3.5558953538	2.5556821786
H	-5.6401323181	-0.0598339767	4.3027574252
H	-4.7186848493	3.015165249	-1.8340126096
H	-7.6329725386	-0.6130930254	-0.1037433731
B	-0.0981999241	-2.8477899223	2.0825469889
B	0.8053644299	0.2772134534	-4.095279878
B	-2.0992026404	-3.3777294098	-2.3446667804
B	-0.981370321	4.4298472295	1.610177761
B	-3.8859391995	0.7746912695	3.3608683843
B	-2.9825080875	3.899792049	-2.816682298

B	-5.8870609685	0.2447433643	-1.0660482959
H	-1.511106221	-3.171991359	-1.2843240478
H	-5.3852535959	0.5544727687	0.0034333933
H	-0.7583067597	-1.902670875	1.7165291954
H	-2.7579084068	-2.4237534124	-2.6792025026
H	-4.5171913112	1.6375702016	2.8101681625
H	-6.535502454	1.1381414291	-1.5452049487
H	-1.5014020469	2.4790899093	2.3839630874
H	-4.4606913774	-1.1882033321	4.1605775252
H	-3.4914277848	1.9383035155	-2.073885744
H	-6.4564839497	-1.7451004057	-0.32223997
H	-0.2344886125	0.956869807	2.3398703458
H	-3.0448150147	0.2743148903	2.6258104137
H	-5.0726146306	-0.221852919	-1.8372676565
N	-1.1101305089	-4.0219406729	2.4105443079

Table S48: Harmonic vibrational frequencies of the 16-C_1 crystal model at the M06-2X/6-311++G($2df, 2pd$) level of theory.

Frequency (cm^{-1})	IR Intensity (km mol^{-1})	Raman Activites ($Å^4$ amu^{-1})
3568	151	59
3561	94	0
3549	121	0
3542	182	199
3446	17	0
3439	54	0
2562	330	84
2559	92	0
2532	143	0
2517	157	143
2473	80	0
2452	132	0
1649	24	14
1647	6	0
1636	0	0
1633	57	2
1325	84	0
1323	89	0
1263	7	4
1261	19	0
1209	36	0
1193	35	4
1172	63	0
1163	64	0
1100	40	2

1087	43	0
1085	16	0
1084	46	2
743	16	0
736	1	0
735	24	0
709	2	0
705	2	0
700	2	0
397	3	0
390	6	0
236	43	0
219	6	0
170	37	0
156	27	0
147	51	0
138	5	0
136	19	0
131	14	0
115	7	0
113	2	0
90	2	0
75	5	0

The full citations for `CFOUR`[6] and `Gaussian09`[7] are included in the Reference section of the SI.

References

(1) Sams, R. L.; Xantheas, S. S.; Blake, T. A. Vapor Phase Infrared Spectroscopy and Ab Initio Fundamental Anharmonic Frequencies of Ammonia Borane. *J. Phys. Chem. A* **2012**, *116*, 3124–3136.

(2) Vijay, A.; Sathyanarayana, D. N. SCF and electron correlation studies on structure, force constants and vibrational spectra of borane monoammoniate complex. *Chem. Phys.* **1995**, *198*, 345–52.

(3) Dillen, J.; Verhoeven, P. The End of a 30-Year-Old Controversy?: A Computational Study of the B-N Stretching Frequency of BH_3-NH_3 in the Solid State. *J. Phys. Chem. A* **2003**, *107*, 2570–2577.

(4) Suenram, R. D.; Thorne, L. R. Microwave spectrum and dipole moment of borane monoammoniate. *Chem. Phys. Lett.* **1981**, *78*, 157–60.

(5) Thorne, L. R.; Suenram, R. D.; Lovas, F. J. Microwave spectrum, torsional barrier, and structure of borane monoammoniate. *J. Chem. Phys.* **1983**, *78*, 167–71.

(6) Stanton, J. F.; Gauss, J.; Harding, M. E.; Szalay, P. G. CFOUR, Coupled-Cluster Techniques for Computational Chemistry. with contributions from A.A. Auer and R.J. Bartlett and U. Benedikt and C. Berger and D.E. Bernholdt and Y.J. Bomble and L. Cheng and O. Christiansen and M. Heckert and O. Heun and C. Huber and T.-C. Jagau and D. Jonsson and J. Jusélius and K. Klein and W.J. Lauderdale and D.A. Matthews and T. Metzroth and L.A. Mück and D.P. O'Neill and D.R. Price and E. Prochnow and K. Ruud and F. Schiffmann and W. Schwalbach and S. Stopkowicz and A. Tajti and J. Vázquez and F. Wang and J.D. Watts and the integral packages MOLECULE (J. Almlöf and P.R. Taylor) and PROPS (P.R. Taylor) and ABACUS (T. Helgaker and H.J. Aa. Jensen and P. Jørgensen and J. Olsen) and ECP routines by A. V. Mitin and C. van Wüllen. For the current version see http://www.cfour.de.

(7) Frisch, M. J.; Trucks, G. W.; Schlegel, H. B.; Scuseria, G. E.; Robb, M. A.; Cheeseman, J. R.; Scalmani, G.; Barone, V.; Mennucci, B.; Petersson, G. A.; Nakatsuji, H.; Caricato, M.; Li, X.; Hratchian, H. P.; Izmaylov, A. F.; Bloino, J.; Zheng, G.; Sonnenberg, J. L.; Hada, M.; Ehara, M.; Toyota, K.; Fukuda, R.; Hasegawa, J.; Ishida, M.; Nakajima, T.; Honda, Y.; Kitao, O.; Nakai, H.; Vreven, T.; Montgomery Jr.,; A., J.; Peralta, J. E.; Ogliaro, F.; Bearpark, M.; Heyd, J. J.; Brothers, E.; Kudin, K. N.; Staroverov, V. N.; Kobayashi, R.; Normand, J.; Raghavachari, K.; Rendell, A.; Burant, J. C.; Iyengar, S. S.; Tomasi, J.; Cossi, M.; Rega, N.; Millam, J. M.; Klene, M.; Knox, J. E.; Cross, J. B.; Bakken, V.; Adamo, C.; Jaramillo, J.; Gomperts, R.; Stratmann, R. E.; Yazyev, O.; Austin, A. J.; Cammi, R.; Pomelli, C.; Ochterski, J. W.; Martin, R. L.; Morokuma, K.; Zakrzewski, V. G.; Voth, G. A.; Salvador, P.; Dannenberg, J. J.; Dapprich, S.; Daniels, A. D.; Farkas, O.; Foresman, J. B.; Ortiz, J. V.; Cioslowski, J.; Fox, D. J. Gaussian09 Revision D.01. Gaussian Inc. Wallingford CT 2009.

Appendix C: Chapter 4 Supplementary Information

Supplementary Information for 'Examination of the structures, energetics, and vibrational frequencies of small sulfur-containing prototypical dimers, $(H_2S)_2$ and H_2O/H_2S'

Katelyn M. Dreux and Gregory S. Tschumper*

Department of Chemistry and Biochemistry, University of Mississippi, University, Mississippi 38677–1848 USA

† Corresponding author. Tel.:+1 662 915 7301; fax: +1 662 915 7300; tschumpr@olemiss.edu.

I. H_2S MONOMER

TABLE S1. Harmonic vibrational frequencies (ω in cm^{-1}) of H_2S at various levels of theory.

ha(D+d)Z	ha(T+d)Z	ha(Q+d)Z	ha(5+d)Z
	MP2		
2800	2796	2801	2801
2777	2778	2782	2782
1212	1213	1214	1216
	CCSD(T)		
2737	2731	2739	2739
2718	2716	2723	2724
1207	1207	1210	1212

TABLE S2. Select MP2/ha(Q+d)Z and CCSD(T)/ha(Q+d)Z fundamental modes, overtones and combination bands (ν in cm^{-1}) and their IR Intensities (I in km mol^{-1}) of H_2S.

	MP2		CCSD(T)	
Mode	ν	I	ν	I
2 ν_3	5357	0.06	5197	0.00
2 ν_1	5324	0.00	5188	0.06
ν_1 + ν_3	5298	0.04	5148	0.12
ν_2 + ν_3	3869	0.78	3787	0.68
ν_1 + ν_2	3856	0.52	3784	0.47
ν_3	2701	1.10	2626	0.00
ν_1	2685	0.35	2618	0.06
2 ν_2	2365	0.06	2355	0.07
ν_2	1187	0.37	1182	0.39

TABLE S3. MP2/ha(Q+d)Z VPT2 anharmonic frequencies of H_2S (ν in cm^{-1}) and their IR intensities (I in km mol^{-1}).

Mode	ν	I
ν_2	1187	0.37
ν_3	2701	1.10
ν_1	2685	0.35
2 ν_2	2365	0.06
ν_2 + ν_1	3856	0.52
ν_2 + ν_3	3869	0.78
2 ν_1	5324	0.03
2 ν_3	5357	0.00
ν_1 + ν_3	5298	0.04

TABLE S4. CCSD(T)/ha(Q+d)Z VPT2 anharmonic frequencies of H_2S, fundamental modes, overtones and combination bands (ν in cm^{-1}) and their IR intensities (I in km mol^{-1}).

Mode	ν	I
ν_2	1182	0.39
ν_1	2618	0.06
ν_3	2626	0.00
2 ν_2	2355	0.07
ν_1 + ν_2	3784	0.47
ν_3 + ν_2	3787	0.68
ν_3 + ν_1	5148	0.12
2 ν_1	5188	0.06
2 ν_3	5197	0.00

II. DIMER GEOMETRIES

TABLE S5. Select MP2 and CCSD(T) optimized intra- and inter- molecular bond lengths (R in Å) and angles (Θ in degrees) of $(H_2S)_2$ including CP and non-CP corrected optimized geometries with the ha(D+d)Z, ha(T+d)Z, ha(Q+d)Z and ha(5+d)Z basis sets.

	MP2/ha($\mathcal{X}+d$)Z				MP2/ha($\mathcal{X}+d$)Z CP			
	D	T	Q	5	D	T	Q	5
R(XH_d)	1.347	1.337	1.337	1.337	1.347	1.337	1.337	1.336
R(XH_f)	1.344	1.334	1.333	1.333	1.344	1.334	1.333	1.333
Θ(HXH)	92.8	92.5	92.5	92.5	92.9	92.5	92.5	92.5
R(YH)	1.344	1.334	1.333	1.333	1.344	1.334	1.333	1.333
Θ(HYH)	92.7	92.4	92.4	92.4	92.7	92.4	92.4	92.4
R(X···Y)	4.18	4.11	4.10	4.10	4.26	4.15	4.12	4.11
R(Y···H)	2.84	2.78	2.77	2.77	2.93	2.83	2.79	2.78
Θ(XH_d···Y)	174.5	172.5	171.7	171.3	169.9	171.4	171.3	171.2
Θ(X···Y$\vec{r}_{bi}$)	93.7	91.2	90.7	90.6	92.3	91.3	91.0	90.8
	CCSD(T)/ha($\mathcal{X}+d$)Z							
	D	T	Q					
R(XH_d)	1.351	1.341	1.341					
R(XH_f)	1.349	1.339	1.338					
Θ(HXH)	92.8	92.6	92.6					
R(YH)	1.350	1.339	1.339					
Θ(HYH)	92.7	92.5	92.5					
R(X···Y)	4.25	4.18	4.16					
R(Y···H)	2.90	2.85	2.83					
Θ(XH_d···Y)	174.9	172.2	171.1					
Θ(X···Y$\vec{r}_{bi}$)	94.3	91.2	90.4					

TABLE S6. Select MP2 and CCSD(T) optimized intra- and inter- molecular bond lengths (R in Å) and angles (Θ in degrees) of $HOH\cdots SH_2$ including CP and non-CP corrected optimized geometries with the ha(D+d)Z, ha(T+d)Z, ha(Q+d)Z and ha(5+d)Z basis sets.

	MP2/ha($\mathcal{X}+d$)Z				MP2/ha($\mathcal{X}+d$)Z CP			
	D	T	Q	5	D	T	Q	5
R(XH_d)	0.970	0.966	0.964	0.963	0.969	0.966	0.963	0.963
R(XH_f)	0.965	0.961	0.959	0.958	0.965	0.961	0.959	0.958
Θ(HXH)	104.4	104.3	104.5	104.6	104.4	104.3	104.5	104.6
R(YH)	1.345	1.334	1.334	1.333	1.345	1.334	1.334	1.333
Θ(HYH)	92.7	92.3	92.3	92.3	92.7	92.3	92.3	92.3
R(X$\cdots$Y)	3.53	3.46	3.46	3.46	3.59	3.50	3.48	3.47
R(Y$\cdots$H)	2.58	2.52	2.53	2.52	2.64	2.56	2.55	2.54
Θ($XH_d\cdots$Y)	165.0	164.4	163.2	163.1	164.2	163.2	163.1	163.0
Θ(X$\cdots$Y$\vec{r}_{bi}$)	83.2	81.5	80.8	80.7	82.8	80.6	80.8	80.8
	CCSD(T)/ha($\mathcal{X}+d$)Z							
	D	T	Q					
R(XH_d)	0.969	0.966	0.963					
R(XH_f)	0.966	0.961	0.959					
Θ(HXH)	104.4	104.4	104.6					
R(YH)	1.350	1.340	1.339					
Θ(HYH)	92.7	92.4	92.4					
R(X$\cdots$Y)	3.56	3.49	3.49					
R(Y$\cdots$H)	2.61	2.55	2.55					
Θ($XH_d\cdots$Y)	165.9	165.0	163.5					
Θ(X$\cdots$Y$\vec{r}_{bi}$)	84.1	82.0	81.1					

TABLE S7. Select MP2 and CCSD(T) optimized intra- and inter- molecular bond lengths (R in Å) and angles (Θ in degrees) of $HSH\cdots OH_2$ including CP and non-CP corrected optimized geometries with the ha(D+d)Z, ha(T+d)Z, ha(Q+d)Z and ha(5+d)Z basis sets.

	MP2/ha($\mathcal{X}+d$)Z				MP2/ha($\mathcal{X}+d$)Z CP			
	D	T	Q	5	D	T	Q	5
R(XH_d)	1.348	1.338	1.338	1.337	1.347	1.338	1.337	1.337
R(XH_f)	1.344	1.333	1.333	1.332	1.344	1.333	1.333	1.332
Θ(HXH)	93.0	92.6	92.6	92.6	93.0	92.6	92.6	92.6
R(YH)	0.966	0.962	0.959	0.959	0.966	0.962	0.959	0.959
Θ(HYH)	104.5	104.5	104.7	104.7	104.5	104.5	104.7	104.7
R(X$\cdots$Y)	3.58	3.54	3.52	3.52	3.62	3.56	3.54	3.53
R(Y$\cdots$H)	2.23	2.20	2.19	2.19	2.28	2.23	2.20	2.19
Θ($XH_d\cdots$Y)	178.1	176.7	176.7	176.6	175.9	176.4	176.5	176.5
Θ(X$\cdots$Y$\vec{r}_{bi}$)	149.9	154.1	156.3	156.1	151.7	156.8	156.6	156.1
	CCSD(T)/ha($\mathcal{X}+d$)Z							
	D	T	Q					
R(XH_d)	1.352	1.342	1.342					
R(XH_f)	1.349	1.339	1.338					
Θ(HXH)	93.0	92.7	92.7					
R(YH)	0.966	0.962	0.959					
Θ(HYH)	104.5	104.5	104.7					
R(X$\cdots$Y)	3.62	3.57	3.56					
R(Y$\cdots$H)	2.27	2.23	2.22					
Θ($XH_d\cdots$Y)	178.0	176.2	176.4					
Θ(X$\cdots$Y$\vec{r}_{bi}$)	148.9	147.9	150.9					

III. DIMER ENERGETICS

TABLE S8. All MP2 and CCSD(T) dissociation energies (D_e in kcal mol^{-1}), including the harmonic and VPT2 zero-point vibrational corrected dissociation energies (D_0^{harm} and D_0^{VPT2} in kcal mol^{-1}) of $(H_2S)_2$, HOH$\cdots$SH$_2$, HSH$\cdots$OH$_2$.

	MP2								
	$(H_2S)_2$			HOH$\cdots$SH$_2$			HSH$\cdots$OH$_2$		
	D_e	D_0^{harm}	D_0^{VPT2}	D_e	D_0^{harm}	D_0^{VPT2}	D_e	D_0^{harm}	D_0^{VPT2}
ha(D+*d*)Z	+1.90	+0.86	+1.06	+3.02	+1.52	+1.69	+2.96	+1.71	+2.04
ha(T+*d*)Z	+1.85	+0.94	+1.09	+3.03	+1.58	+1.73	+2.80	+1.64	+1.87
ha(Q+*d*)Z	+1.88	+0.99	+1.14	+3.02	+1.60	+1.73	+2.81	+1.66	+1.86
ha(5+*d*)Z	+1.89	+1.01		+3.02	+1.62		+2.81	+1.65	
ha(6+*d*)Z[a]	+1.90			+3.02			+2.81		
	CCSD(T)								
	$(H_2S)_2$			HOH$\cdots$SH$_2$			HSH$\cdots$OH$_2$		
	D_e	D_0^{harm}	D_0^{VPT2}	D_e	D_0^{harm}	D_0^{VPT2}	D_e	D_0^{harm}	D_0^{VPT2}
ha(D+*d*)Z	+1.68	+0.67	+0.83	+2.88	+1.39	+1.58	+2.77	+1.53	+1.85
ha(T+*d*)Z	+1.63	+0.76	+0.84	+2.91	+1.47	+1.54	+2.66	+1.49	+1.60
ha(Q+*d*)Z	+1.66	+0.80	+0.95	+2.91	+1.50	+1.66	+2.68	+1.51	+1.71
ha(5+*d*)Z[b]	+1.67			+2.91			+2.68		
ha(6+*d*)Z[b]	+1.67			+2.91			+2.68		

[a] Single point energies computed using the MP2/ha(5+*d*)Z optimized geometries

[b] Single point energies computed using the CCSD(T)/ha(Q+*d*)Z optimized geometries

TABLE S9. All MP2 and CCSD(T) harmonic and anharmonic ZPVE corrections (HARM and VPT2 in Hartees) of $(H_2S)_2$, $HOH\cdots SH_2$, $HSH\cdots OH_2$.

	MP2					
	$(H_2S)_2$		$HOH\cdots SH_2$		$HSH\cdots OH_2$	
	HARM	VPT2	HARM	VPT2	HARM	VPT2
ha(D+*d*)Z	0.0326	0.0319	0.0393	0.0385	0.0389	0.0378
ha(T+*d*)Z	0.0324	0.0318	0.0392	0.0385	0.0387	0.0379
ha(Q+*d*)Z	0.0324	0.0318	0.0392	0.0385	0.0388	0.0380
ha(5+*d*)Z	0.0324		0.0392		0.0388	
	CCSD(T)					
	$(H_2S)_2$		$HOH\cdots SH_2$		$HSH\cdots OH_2$	
	HARM	VPT2	HARM	VPT2	HARM	VPT2
ha(D+*d*)Z	0.0320	0.0313	0.0389	0.0380	0.0385	0.0374
ha(T+*d*)Z	0.0317	0.0311	0.0388	0.0381	0.0384	0.0377
ha(Q+*d*)Z	0.0318	0.0311	0.0389	0.0381	0.0385	0.0377

IV. DIMER HARMONIC VIBRATIONAL FREQUENCIES

TABLE S10. Harmonic vibrational frequencies (ω in cm^{-1}) of $(H_2S)_2$ at various levels of theory.

MP2/ha($\mathcal{X}+d$)Z				MP2/ha($\mathcal{X}+d$)Z CP				CCSD(T)/ha($\mathcal{X}+d$)Z		
D	T	Q	5	D	T	Q	5	D	T	Q
2796	2793	2797	2797	2797	2793	2798	2797	2735	2729	2736
2791	2788	2792	2792	2791	2788	2792	2792	2731	2725	2732
2773	2774	2778	2778	2774	2774	2778	2778	2716	2713	2720
2747	2739	2740	2738	2753	2743	2742	2740	2704	2695	2699
1218	1217	1218	1220	1216	1217	1218	1219	1214	1212	1214
1210	1211	1212	1214	1210	1211	1212	1214	1206	1205	1208
298	279	276	276	259	264	270	273	277	258	256
179	158	157	156	150	149	152	154	167	147	147
93	79	78	77	71	73	75	76	90	74	74
92	73	70	69	66	65	66	67	88	69	67
66	62	61	60	53	57	59	59	62	57	56
42	37	36	35	38	36	35	35	40	35	33

TABLE S11. Harmonic vibrational frequencies (ω in cm^{-1}) of $HOH\cdots SH_2$ at various levels of theory.

MP2/ha($\mathcal{X}+d$)Z				MP2/ha($\mathcal{X}+d$)Z CP				CCSD(T)/ha($\mathcal{X}+d$)Z		
D	T	Q	5	D	T	Q	5	D	T	Q
3921	3918	3933	3936	3925	3920	3934	3936	3897	3896	3914
3761	3757	3773	3774	3772	3764	3776	3776	3763	3763	3781
2794	2791	2796	2795	2795	2792	2796	2795	2733	2728	2735
2771	2773	2777	2777	2772	2773	2777	2777	2714	2713	2719
1639	1638	1639	1638	1641	1637	1639	1638	1656	1656	1657
1210	1211	1212	1214	1210	1211	1212	1214	1206	1205	1208
445	438	432	433	417	421	425	428	429	423	417
291	283	279	279	272	273	275	277	281	274	271
127	128	126	126	117	121	123	125	124	124	123
124	118	115	114	114	112	112	112	120	112	108
90	91	87	85	82	84	84	84	88	88	83
69	63	59	59	60	57	57	58	67	64	61

TABLE S12. Harmonic vibrational frequencies (ω in cm^{-1}) of $HSH\cdots OH_2$ at various levels of theory.

MP2/ha($\mathcal{X}+d$)Z				MP2/ha($\mathcal{X}+d$)Z CP				CCSD(T)/ha($\mathcal{X}+d$)Z		
D	T	Q	5	D	T	Q	5	D	T	Q
3945	3944	3959	3962	3959	3945	3959	3963	3918	3920	3938
3812	3818	3834	3836	3834	3819	3834	3836	3801	3810	3828
2792	2790	2794	2794	2795	2790	2795	2794	2732	2726	2733
2743	2740	2740	2738	2741	2743	2741	2739	2704	2697	2700
1632	1628	1631	1630	1632	1629	1632	1631	1649	1646	1649
1221	1220	1221	1222	1220	1219	1220	1222	1217	1215	1218
369	359	361	361	354	346	354	358	349	345	347
158	146	145	145	141	137	141	143	151	145	143
109	106	107	107	105	102	105	106	105	103	105
107	101	100	100	99	98	99	100	104	99	97
97	86	85	87	86	84	86	87	94	88	86
80	69	67	67	66	65	66	66	77	68	66

V. DIMER THERMOCHEMISTRY

TABLE S13. MP2 electronic binding energies and thermochemical quantities (E_{bind}, ΔH, $T\Delta S$, and ΔG in kcal mol^{-1}) of $(H_2S)_2$, HOH$\cdots$SH$_2$, and HSH$\cdots$OH$_2$.

			H_2S Dimer		
	ha(D+d)Z	ha(T+d)Z	ha(Q+d)Z	ha(5+d)Z	ha(6+d)Z[a]
E_{bind}	−1.90	−1.85	−1.88	−1.89	−1.90
ΔH	−0.61	−0.61	−0.64	−0.66	−0.67
$T\Delta S$	−4.37	−3.92	−3.85	−3.82	−3.82
$\Delta H - T\Delta S$	+3.76	+3.32	+3.21	+3.16	+3.16
ΔG	+3.76	+3.31	+3.21	+3.16	+3.16
			HOH$\cdots$SH$_2$		
	ha(D+d)Z	ha(T+d)Z	ha(Q+d)Z	ha(5+d)Z	ha(6+d)Z[a]
E_{bind}	−3.02	−3.03	−3.02	−3.02	−3.02
ΔH	−1.62	−1.65	−1.65	−1.66	−1.66
$T\Delta S$	−5.17	−5.08	−4.98	−4.96	−4.96
$\Delta H - T\Delta S$	+3.55	+3.42	+3.33	+3.30	+3.30
ΔG	+3.55	+3.42	+3.33	+3.30	+3.30
			HSH$\cdots$OH$_2$		
	ha(D+d)Z	ha(T+d)Z	ha(Q+d)Z	ha(5+d)Z	ha(6+d)Z[a]
E_{bind}	−2.96	−2.80	−2.81	−2.81	−2.81
ΔH	−1.62	−1.49	−1.50	−1.50	−1.51
$T\Delta S$	−4.79	−4.50	−4.49	−4.50	−4.50
$\Delta H - T\Delta S$	+3.17	+3.01	+2.98	+3.00	+3.00
ΔG	+3.16	+3.01	+2.98	+3.00	+3.00

[a] Computed using the thermochemical corrections from MP2/ha(5+d)Z harmonic frequency computation

VI. DIMER VPT2 FREQUENCIES

TABLE S14: MP2/ha(Q+d)Z and CCSD(T)/ha(Q+d)Z VPT2 vibrational frequencies (ν in cm^{-1}) and CCSD(T)/ha(Q+d)Z IR intensities (I in km mol^{-1}) of $(H_2S)_2$.

	MP2/ha(Q+d)Z	CCSD(T)/ha(Q+d)Z	
Mode	ν	ν	I
ν_{12}	24.79	29.25	15.42
ν_8	38.05	39.29	8.26
ν_{11}	39.77	47.50	5.04
ν_7	48.81	54.34	21.09
$2\nu_{12}$	42.65	57.76	0.57
$\nu_{12}+\nu_8$	60.95	65.81	0.02
$\nu_{12}+\nu_{11}$	50.45	66.89	0.93
$2\nu_8$	68.56	70.51	0.17
$2\nu_{11}$	63.86	71.23	1.48
$\nu_{11}+\nu_8$	75.95	86.45	0.24
$\nu_8+\nu_7$	78.11	90.27	0.60
$\nu_{12}+\nu_7$	71.41	90.81	0.01
$\nu_{11}+\nu_7$	77.07	91.40	0.41
$2\nu_7$	88.22	100.07	0.35
ν_6	123.42	135.40	2.82
$\nu_8+\nu_6$	147.78	169.97	0.83
$\nu_{12}+\nu_6$	136.41	172.71	0.45
$\nu_7+\nu_6$	156.11	181.51	1.09
ν_{10}	215.29	190.88	5.00
$\nu_{12}+\nu_{10}$	191.26	211.47	0.26
$\nu_{11}+\nu_6$	146.04	217.42	0.87
$\nu_{10}+\nu_8$	217.10	220.17	0.01

$\nu_{11}+\nu_{10}$	218.35	227.73	1.47
$\nu_{10}+\nu_{7}$	227.93	233.62	0.13
$2\nu_{6}$	207.30	247.01	1.26
$\nu_{10}+\nu_{6}$	275.65	311.09	0.00
$2\nu_{10}$	333.07	334.85	3.36
ν_{5}	1186.91	1179.53	0.42
ν_{4}	1186.56	1179.82	1.29
$\nu_{12}+\nu_{5}$	1212.80	1209.60	0.02
$\nu_{12}+\nu_{4}$	1213.38	1209.90	0.37
$\nu_{8}+\nu_{4}$	1222.08	1216.37	0.53
$\nu_{8}+\nu_{5}$	1225.05	1219.15	0.29
$\nu_{11}+\nu_{4}$	1224.11	1226.66	0.07
$\nu_{11}+\nu_{5}$	1227.47	1226.90	0.01
$\nu_{7}+\nu_{4}$	1234.11	1233.10	0.39
$\nu_{7}+\nu_{5}$	1235.57	1233.88	0.28
$\nu_{6}+\nu_{4}$	1296.58	1308.92	1.59
$\nu_{6}+\nu_{5}$	1305.20	1316.57	0.03
$\nu_{10}+\nu_{5}$	1378.77	1371.01	0.01
$\nu_{10}+\nu_{4}$	1379.51	1371.45	0.02
$2\nu_{4}$	2364.58	2350.70	0.23
$2\nu_{5}$	2365.95	2350.72	0.03
$\nu_{5}+\nu_{4}$	2370.38	2357.38	0.06
ν_{3}	2662.73	2605.87	33.06
ν_{2}	2682.37	2609.86	1.31
ν_{1}	2695.73	2620.64	3.91
ν_{9}	2697.32	2622.76	1.95
$\nu_{12}+\nu_{3}$	2690.45	2636.05	0.01
$\nu_{12}+\nu_{2}$	2715.38	2638.67	0.01

$\nu_{12}+\nu_1$	2723.10	2648.57	0.19
$\nu_8+\nu_2$	2720.22	2648.84	0.01
$\nu_8+\nu_3$	2707.94	2649.98	0.09
$\nu_{12}+\nu_9$	2721.52	2651.15	0.11
$\nu_{11}+\nu_2$	2717.51	2657.21	0.00
$\nu_{11}+\nu_3$	2710.17	2659.07	0.00
$\nu_8+\nu_1$	2734.05	2660.38	0.02
$\nu_9+\nu_8$	2735.35	2661.70	0.00
$\nu_7+\nu_2$	2731.25	2664.35	0.01
$\nu_7+\nu_3$	2718.03	2664.80	1.15
$\nu_{11}+\nu_1$	2737.04	2668.49	0.00
$\nu_{11}+\nu_9$	2737.11	2670.32	0.07
$\nu_7+\nu_1$	2744.47	2674.96	0.04
$\nu_9+\nu_7$	2746.39	2677.23	0.01
$\nu_6+\nu_2$	2799.01	2745.18	0.00
$\nu_6+\nu_3$	2797.67	2754.56	0.07
$\nu_6+\nu_1$	2812.62	2756.38	0.01
$\nu_9+\nu_6$	2814.09	2758.00	0.00
$\nu_{10}+\nu_2$	2873.71	2800.40	0.01
$\nu_{10}+\nu_3$	2875.10	2811.21	0.07
$\nu_{10}+\nu_1$	2887.91	2812.64	0.00
$\nu_{10}+\nu_9$	2888.42	2813.34	0.01
$\nu_4+\nu_3$	3835.24	3771.14	0.69
$\nu_5+\nu_2$	3855.06	3774.19	0.44
$\nu_4+\nu_1$	3866.03	3782.37	1.15
$\nu_9+\nu_5$	3866.29	3782.78	0.86
$\nu_5+\nu_3$	3847.96	3784.42	0.09
$\nu_4+\nu_2$	3867.47	3788.66	0.06

$\nu_5+\nu_1$	3881.04	3799.06	0.11
$\nu_9+\nu_4$	3882.10	3801.36	0.08
$2\nu_3$	5231.89	5123.62	0.84
$\nu_9+\nu_2$	5291.43	5138.30	0.05
$2\nu_1$	5308.51	5156.89	0.03
$2\nu_2$	5319.70	5171.94	0.04
$2\nu_9$	5349.06	5196.68	0.01
$\nu_3+\nu_1$	5344.06	5202.89	0.15
$\nu_3+\nu_2$	5344.18	5214.62	0.01
$\nu_9+\nu_3$	5359.44	5228.03	0.01
$\nu_2+\nu_1$	5377.90	5230.17	0.00
$\nu_9+\nu_1$	5393.00	5243.34	0.00

TABLE S15: MP2/ha(Q+d)Z and CCSD(T)/ha(Q+d)Z VPT2 vibrational frequencies (ν in cm^{-1}) and CCSD(T)/ha(Q+d)Z IR intensities (I in km mol^{-1}) of HOH$\cdots$SH$_2$.

	MP2/ha(Q+d)Z	CCSD(T)/ha(Q+d)Z	
Mode	ν	ν	I
ν_{12}	33.14	47.47	86.60
ν_8	71.90	65.48	54.18
ν_{11}	100.17	85.90	5.94
$2\nu_{12}$	50.29	86.56	8.97
ν_7	100.96	97.75	53.54
$\nu_{12}+\nu_8$	109.87	115.83	2.56
$\nu_{12}+\nu_{11}$	107.64	116.59	9.60
$2\nu_8$	136.48	123.31	0.42

$\nu_{12}+\nu_7$	131.08	143.53	0.08
$\nu_{11}+\nu_8$	165.19	146.30	0.12
$\nu_8+\nu_7$	165.77	157.74	0.68
$2\nu_{11}$	194.43	167.61	0.93
$\nu_{11}+\nu_7$	193.16	176.21	0.11
$2\nu_7$	192.79	186.51	0.09
ν_6	248.59	244.01	21.90
$\nu_8+\nu_6$	299.76	309.11	5.34
$\nu_{11}+\nu_6$	314.22	312.15	1.26
$\nu_{12}+\nu_6$	237.45	312.59	2.06
$\nu_7+\nu_6$	319.15	330.13	1.26
ν_{10}	363.35	349.10	55.26
$\nu_{12}+\nu_{10}$	317.51	378.41	11.04
$\nu_{10}+\nu_8$	380.64	398.25	0.03
$\nu_{10}+\nu_7$	410.97	432.19	1.42
$\nu_{11}+\nu_{10}$	410.34	438.24	6.54
$2\nu_6$	429.21	457.90	1.70
$\nu_{10}+\nu_6$	518.83	595.68	0.09
ν_{10}	363.35	636.71	55.26
ν_5	1188.56	1179.96	0.17
$\nu_{12}+\nu_5$	1224.24	1226.99	0.01
$\nu_8+\nu_5$	1260.55	1246.26	0.09
$\nu_{11}+\nu_5$	1293.26	1266.77	0.00
$\nu_7+\nu_5$	1289.95	1278.27	0.09
$\nu_6+\nu_5$	1420.50	1425.94	0.09
$\nu_{10}+\nu_5$	1514.97	1529.85	0.00
ν_4	1577.54	1602.13	38.46
$\nu_{12}+\nu_4$	1595.46	1649.79	5.75

$\nu_8+\nu_4$	1646.09	1664.19	6.42
$\nu_{11}+\nu_4$	1680.75	1688.51	0.00
$\nu_7+\nu_4$	1678.17	1699.68	2.58
$\nu_6+\nu_4$	1800.49	1839.58	10.21
$\nu_{10}+\nu_4$	1909.25	1957.13	0.47
$2\nu_5$	2367.68	2350.56	0.05
ν_3	2675.66	2608.25	2.40
ν_9	2699.90	2621.25	2.96
$\nu_{12}+\nu_3$	2688.67	2655.15	0.04
$\nu_{12}+\nu_9$	2732.69	2668.09	0.20
$\nu_8+\nu_3$	2747.08	2673.25	0.07
$\nu_9+\nu_8$	2778.27	2685.96	0.00
$\nu_{11}+\nu_3$	2788.93	2693.50	0.02
$\nu_7+\nu_3$	2776.43	2705.92	0.05
$\nu_{11}+\nu_9$	2799.55	2706.64	0.11
$\nu_9+\nu_7$	2805.54	2718.83	0.01
$\nu_5+\nu_4$	2766.11	2782.09	0.00
$\nu_6+\nu_3$	2905.59	2852.03	0.00
$\nu_9+\nu_6$	2932.08	2865.06	0.00
$\nu_{10}+\nu_3$	3001.37	2956.31	0.03
$\nu_{10}+\nu_9$	3024.65	2969.34	0.02
$2\nu_4$	3120.25	3168.59	2.50
ν_2	3619.07	3621.25	106.39
$\nu_{12}+\nu_2$	3647.99	3671.40	0.07
$\nu_8+\nu_2$	3699.64	3693.20	0.18
$\nu_{11}+\nu_2$	3737.80	3713.11	0.05
$\nu_7+\nu_2$	3726.41	3722.74	9.32
ν_1	3777.68	3730.90	111.81

$\nu_5+\nu_3$	3848.55	3772.02	0.56
$\nu_{12}+\nu_1$	3858.48	3779.49	2.39
$\nu_9+\nu_5$	3865.37	3780.48	1.12
$\nu_8+\nu_1$	3851.44	3798.21	0.69
$\nu_{11}+\nu_1$	3878.90	3817.39	1.93
$\nu_7+\nu_1$	3881.14	3831.55	0.20
$\nu_6+\nu_2$	3868.48	3880.60	0.03
$\nu_6+\nu_1$	4009.57	3976.49	0.60
$\nu_{10}+\nu_2$	3971.65	3989.88	0.05
$\nu_{10}+\nu_1$	4108.34	4085.11	0.17
$\nu_4+\nu_3$	4253.17	4210.36	0.00
$\nu_9+\nu_4$	4277.40	4223.33	0.00
$\nu_5+\nu_2$	4807.52	4801.07	0.00
$\nu_5+\nu_1$	4966.22	4910.86	0.00
$\nu_9+\nu_3$	5287.02	5134.94	0.05
$2\nu_3$	5306.10	5168.45	0.04
$2\nu_9$	5354.23	5193.81	0.01
$\nu_4+\nu_2$	5179.78	5208.07	3.28
$\nu_4+\nu_1$	5336.11	5314.18	7.99
$\nu_3+\nu_2$	6294.38	6229.27	0.02
$\nu_9+\nu_2$	6318.60	6242.41	0.02
$\nu_3+\nu_1$	6453.26	6339.09	0.00
$\nu_9+\nu_1$	6477.49	6352.84	0.01
$2\nu_2$	7106.73	7119.54	0.10
$\nu_2+\nu_1$	7294.31	7239.96	0.99
$2\nu_1$	7430.98	7337.39	0.76

TABLE S16: MP2/ha(Q+d)Z and CCSD(T)/ha(Q+d)Z VPT2 vibrational frequencies (ν in cm^{-1}) and CCSD(T)/ha(Q+d)Z IR intensities (I in km mol^{-1}) of HSH$\cdots$OH$_2$.

	MP2/ha(Q+d)Z	CCSD(T)/ha(Q+d)Z	
Mode	ν	ν	I
ν_6	74.33	4.32	45.61
$\nu_{11}+\nu_8$	31.53	49.33	2.75
ν_{11}	60.12	57.79	22.65
ν_{12}	49.60	58.43	11.41
$\nu_{11}+\nu_6$	146.02	65.51	0.21
$\nu_{12}+\nu_8$	44.82	75.51	2.27
ν_7	83.01	77.44	76.14
$\nu_8+\nu_7$	73.21	80.14	1.47
$\nu_{12}+\nu_6$	110.29	88.54	0.96
$\nu_7+\nu_6$	155.23	97.80	0.31
ν_{11}	60.12	107.41	22.65
ν_{12}	49.60	108.05	11.41
$\nu_{12}+\nu_{11}$	128.18	119.57	3.75
$\nu_{12}+\nu_7$	119.58	129.47	0.25
$\nu_{11}+\nu_7$	138.53	130.09	0.00
ν_7	83.01	148.05	76.14
$\nu_{10}+\nu_8$	241.02	226.71	0.11
$\nu_{10}+\nu_6$	316.77	237.71	0.03
ν_{10}	266.88	241.33	32.08
$\nu_{11}+\nu_{10}$	297.73	268.85	0.20
$\nu_{12}+\nu_{10}$	311.67	294.88	0.02

$\nu_{10}+\nu_7$	338.55	305.48	0.67
ν_{10}	266.88	418.07	32.08
ν_5	1190.19	1178.50	1.30
$\nu_8+\nu_5$	1179.34	1183.13	0.30
$\nu_6+\nu_5$	1258.19	1199.54	1.74
$\nu_{12}+\nu_5$	1238.80	1236.64	0.00
$\nu_{11}+\nu_5$	1253.82	1238.57	0.08
$\nu_7+\nu_5$	1272.53	1254.99	0.01
$\nu_{10}+\nu_5$	1458.65	1420.19	0.08
ν_4	1581.81	1597.74	72.99
$\nu_8+\nu_4$	1575.02	1608.63	15.51
$\nu_6+\nu_4$	1659.89	1629.66	0.51
$\nu_{12}+\nu_4$	1630.75	1656.23	11.61
$\nu_{11}+\nu_4$	1641.74	1656.49	0.05
$\nu_7+\nu_4$	1665.05	1675.41	0.22
$\nu_{10}+\nu_4$	1850.53	1840.65	0.49
ν_5	1190.19	2347.47	1.30
ν_3	2663.62	2608.41	54.52
ν_2	2695.94	2615.16	3.84
$\nu_8+\nu_2$	2686.58	2623.94	0.01
$\nu_8+\nu_3$	2662.48	2625.44	0.42
$\nu_6+\nu_2$	2773.41	2646.43	0.06
$\nu_6+\nu_3$	2762.37	2657.37	0.02
$\nu_{11}+\nu_3$	2724.33	2668.80	0.00
$\nu_{12}+\nu_3$	2721.88	2669.62	0.13
$\nu_{11}+\nu_2$	2757.05	2672.99	0.00
$\nu_{12}+\nu_2$	2744.91	2673.30	0.00
$\nu_7+\nu_3$	2748.35	2687.33	4.16

$\nu_7+\nu_2$	2778.92	2692.66	0.10
$\nu_5+\nu_4$	2772.00	2776.25	0.00
$\nu_{10}+\nu_2$	2963.64	2857.99	0.00
$\nu_{10}+\nu_3$	2957.93	2868.57	0.00
$\nu_4+\nu_0$	1581.81	3162.63	72.99
ν_1	3665.70	3637.18	8.45
$\nu_8+\nu_1$	3657.51	3646.86	2.22
$\nu_6+\nu_1$	3744.61	3670.76	0.05
$\nu_{12}+\nu_1$	3725.90	3693.72	1.08
$\nu_{11}+\nu_1$	3721.73	3695.13	0.00
$\nu_7+\nu_1$	3748.94	3714.98	0.02
ν_9	3769.46	3734.10	72.40
$\nu_9+\nu_8$	3748.88	3744.00	0.20
$\nu_9+\nu_6$	3848.16	3768.30	0.03
$\nu_5+\nu_3$	3838.89	3772.94	0.77
$\nu_5+\nu_2$	3868.52	3774.96	1.06
$\nu_{12}+\nu_9$	3817.80	3790.83	8.55
$\nu_{11}+\nu_9$	3829.75	3792.31	6.49
$\nu_9+\nu_7$	3852.50	3812.02	0.00
$\nu_{10}+\nu_1$	3933.16	3879.05	0.01
$\nu_{10}+\nu_9$	4036.47	3975.83	0.38
$\nu_4+\nu_3$	4244.57	4205.55	0.06
$\nu_4+\nu_2$	4277.69	4212.82	0.00
$\nu_5+\nu_1$	4855.82	4815.72	0.00
$\nu_9+\nu_5$	4959.63	4912.69	0.00
ν_3	2663.62	5130.46	54.52
ν_2	2695.94	5147.21	3.84
$\nu_3+\nu_2$	5347.02	5193.47	0.13

$\nu_4+\nu_1$	5230.10	5218.90	0.12
$\nu_9+\nu_4$	5331.69	5311.04	5.12
$\nu_3+\nu_1$	6327.77	6244.45	0.03
$\nu_2+\nu_1$	6361.57	6252.25	0.00
$\nu_9+\nu_3$	6431.71	6341.47	0.01
$\nu_9+\nu_2$	6465.36	6349.20	0.00
ν_1	3665.70	7190.06	8.45
$\nu_9+\nu_1$	7276.09	7208.80	2.27
ν_9	3769.46	7372.44	72.40

VII. CARTESIAN COORDINATES

TABLE S17. Cartesian coordinates of H_2S at the MP2/ha(Q+d)Z level of theory.

S	0.000000	0.000000	0.000000
H	0.000000	0.000000	1.332818
H	1.331792	0.000000	−0.052285

TABLE S18. Cartesian coordinates of H_2S at the CCSD(T)/ha(Q+d)Z level of theory.

S	0.00000000	0.00000000	0.10383165
H	0.00000000	−1.82490967	−1.64696887
H	0.00000000	1.82490967	−1.64696887

TABLE S19. Cartesian coordinates of $(H_2S)_2$ at the MP2/ha(Q+d)Z level of theory.

H	0.000000	0.000000	1.332878
S	0.000000	0.000000	0.000000
H	1.335560	0.000000	−0.057267
S	4.061428	0.000000	−0.576830
H	3.943299	0.962073	−1.492395
H	3.943299	−0.962073	−1.492395

TABLE S20. Cartesian coordinates of $(H_2S)_2$ at the CCSD(T)/ha(Q+d)Z level of theory.

H	−2.3313770936	−1.2724654482	0.0000000000
S	−2.0987784147	0.0454790770	0.0000000000
H	−0.7689443571	−0.1276226205	0.0000000000
S	2.0644877421	−0.0561484908	0.0000000000
H	2.0940765059	0.8692812988	0.9668894589
H	2.0940765059	0.8692812988	−0.9668894589

TABLE S21. Cartesian coordinates of HOH$\cdots$SH$_2$ at the MP2/ha(Q+d)Z level of theory.

O	−0.027282	2.233466	0.000000
H	−0.883896	2.663746	0.000000
H	−0.230580	1.291503	0.000000
S	−0.027282	−1.228804	0.000000
H	0.884628	−1.081054	0.961844
H	0.884628	−1.081054	−0.961844

TABLE S22. Cartesian coordinates of HOH$\cdots$SH$_2$ at the CCSD(T)/ha(Q+d)Z level of theory.

O	−4.31361550	0.11361342	0.00000000
H	−5.17596557	−1.47965831	0.00000000
H	−2.54705029	−0.32225839	0.00000000
S	2.27170814	−0.10308512	0.00000000
H	2.05796983	1.63452209	1.82690920
H	2.05796983	1.63452209	−1.82690920

TABLE S23. Cartesian coordinates of HSH$\cdots$OH$_2$ at the MP2/ha(Q+d)Z level of theory.

S	−0.032338	−1.340886	0.000000
H	1.295786	−1.449256	0.000000
H	0.015504	−0.004224	0.000000
O	−0.032338	2.183377	0.000000
H	−0.267588	2.720325	0.759384
H	−0.267588	2.720325	−0.759384

TABLE S24. Cartesian coordinates of HSH$\cdots$OH$_2$ at the CCSD(T)/ha(Q+d)Z level of theory.

S	−2.41046287	0.08519391	0.00000000
H	−2.68733861	−2.42822416	0.00000000
H	0.12016182	−0.07126950	0.00000000
O	4.31305636	−0.06903895	0.00000000
H	5.29247923	0.44625728	1.43568283
H	5.29247923	0.44625728	−1.43568283

Appendix D: Chapter 5 Supplementary Information

Supplementary Information for 'Exploring the $(H_2S)_2$ potential energy surface'

Katelyn M. Dreux and Gregory S. Tschumper[†]

Department of Chemistry and Biochemistry, University of Mississippi, University, Mississippi 38677–1848 USA

[†] Corresponding author. Tel.:+1 662 915 7301; fax: +1 662 915 7300; tschumpr@olemiss.edu.

I. GEOMETRICAL PARAMETERS

TABLE S1: Select CCSD(T)/ha(Q+*d*)Z intramolecular bond lengths (R in Å) and angles (Θ in degrees) of the $(H_2S)_2$ structures.

	$R(S_2H_1)$	$R(S_2H_3)$	$\Theta(H_1S_2H_3)$	$R(S_4H_5)$	$R(S_4H_6)$	$\Theta(H_5S_2H_6)$
I	1.338	1.341	92.6	1.339	1.339	92.5
II	1.338	1.341	92.5	1.339	1.339	92.5
III	1.338	1.341	92.6	1.339	1.339	92.4
IV	1.338	1.339	92.6	1.339	1.338	92.6
V	1.339	1.339	92.5	1.339	1.339	92.5
VI	1.339	1.339	92.1	1.338	1.338	92.6
VII	1.338	1.338	92.7	1.338	1.338	92.7
VIII	1.338	1.339	92.4	1.338	1.338	92.8
IX	1.338	1.338	92.1	1.338	1.338	92.6

II. HARMONIC VIBRATIONAL FREQUENCIES

TABLE S2: Number of imaginary frequencies (n_i) of the $(H_2S)_2$ structures.

	I	II	III	IV	V	VI	VII	VIII	IX
MP2/ha(D+*d*)Z	0	0	1	1	1	2	2	2	3
MP2/ha(T+*d*)Z	0	0	1	1	1	2	2	2	3
MP2/ha(Q+*d*)Z	0	0	1	1	1	2	2	2	3
MP2/ha(5+*d*)Z	0	0	1	1	1	2	2	2	3
CCSD(T)/ha(D+*d*)Z	0	0	1	1	1	2	2	2	3
CCSD(T)/ha(T+*d*)Z	0	0	1	1	1	2	2	2	3
CCSD(T)/ha(Q+*d*)Z	0	0	1	1	1	2	2	2	3

TABLE S3: Harmonic vibrational frequencies of H_2S at the MP2/ha(Q+d)Z level of theory.

Irrep.	Frequency (cm^{-1})	IR Intensity (km mol^{-1})
a_1	2782	0
a_1	1214	1
b_1	2801	1

TABLE S4: Harmonic vibrational frequencies of I at the MP2/ha(Q+d)Z level of theory.

Irrep.	Frequency (cm^{-1})	IR Intensity (km mol^{-1})
a'	2792.3	4.4
a'	2778.2	1.3
a'	2740.4	77.6
a'	1217.9	3.8
a'	1212.1	1.3
a'	156.6	4.0
a'	78.0	28.5
a'	61.2	13.1
a''	2797.4	2.6
a''	275.9	3.4
a''	70.0	10.8
a''	35.7	16.2

TABLE S5: Harmonic vibrational frequencies of II at the MP2/ha(Q+d)Z level of theory.

Irrep.	Frequency (cm^{-1})	IR Intensity (km mol^{-1})
a′	2792.1	4.2
a′	2778.6	1.1
a′	2740.8	79.3
a′	1219.4	2.2
a′	1212.0	1.4
a′	155.8	32.9
a′	79.3	6.3
a′	66.0	0.2
a″	2797.9	2.4
a″	275.1	3.6
a″	75.8	0.9
a″	17.8	2.1

TABLE S6: Harmonic vibrational frequencies of III at the MP2/ha(Q+*d*)Z level of theory.

Irrep.	Frequency (cm^{-1})	IR Intensity (km mol^{-1})
a	2796.8	2.3
a	2792.2	4.1
a	2777.8	1.2
a	2741.4	70.9
a	1219.3	3.9
a	1212.3	0.5
a	257.6	3.7
a	170.5	10.3
a	85.3	26.1
a	75.6	6.7
a	60.4	7.0
a	−31.5	10.3

TABLE S7: Harmonic vibrational frequencies of IV at the MP2/ha(Q+d)Z level of theory.

Irrep.	Frequency (cm^{-1})	IR Intensity (km mol^{-1})
a_g	2795.0	0.0
a_g	2771.8	0.0
a_g	1214.0	0.0
a_g	259.4	0.0
a_g	74.8	0.0
a_g	47.7	0.0
a_u	2794.3	6.8
a_u	2772.4	7.5
a_u	1213.6	4.2
a_u	123.9	41.0
a_u	21.2	23.2
a_u	−67.3	39.6

TABLE S8: Harmonic vibrational frequencies of V at the MP2/ha(Q+d)Z level of theory.

Irrep.	Frequency (cm^{-1})	IR Intensity (km mol^{-1})
b	2793.9	4.9
b	2771.7	8.0
b	1213.6	1.7
b	64.7	22.2
b	−68.9	53.6
a	2794.8	1.5
a	2771.0	0.2
a	1215.6	2.4
a	258.1	0.3
a	115.4	4.0
a	66.9	0.5
a	40.2	3.5

TABLE S9: Harmonic vibrational frequencies of VI at the MP2/ha(Q+d)Z level of theory.

Irrep.	Frequency (cm^{-1})	IR Intensity (km mol^{-1})
a′	2796.2	0.8
a′	2780.9	0.5
a′	2777.8	2.8
a′	1216.7	0.7
a′	1203.8	3.6
a′	119.2	38.4
a′	60.7	0.1
a′	−48.9	5.3
a″	2799.5	2.6
a″	150.7	24.3
a″	135.7	0.0
a″	−51.1	1.7

TABLE S10: Harmonic vibrational frequencies of VII at the MP2/ha(Q+d)Z level of theory.

Irrep.	Frequency (cm^{-1})	IR Intensity (km mol^{-1})
a_g	2800.2	0.0
a_g	2779.3	0.0
a_g	1204.5	0.0
a_g	79.6	0.0
a_g	56.5	0.0
a_u	147.3	9.3
a_u	−99.5	48.4
b_g	−157.9	0.0
b_u	2799.9	2.1
b_u	2780.5	1.6
b_u	1217.2	0.2
b_u	72.9	30.3

TABLE S11: Harmonic vibrational frequencies of VIII at the MP2/ha(Q+d)Z level of theory.

Irrep.	Frequency (cm^{-1})	IR Intensity (km mol^{-1})
a′	2802.5	2.7
a′	2797.1	7.3
a′	2782.4	0.2
a′	2776.1	11.7
a′	1216.5	1.5
a′	1210.4	5.8
a′	90.4	15.0
a′	52.3	1.5
a′	21.3	7.0
a″	108.5	0.2
a″	−75.5	10.6
a″	−148.3	34.4

TABLE S12: Harmonic vibrational frequencies of IX at the MP2/ha(Q+d)Z level of theory.

Irrep.	Frequency (cm^{-1})	IR Intensity (km mol^{-1})
a_1	2783.8	0.4
a_1	2780.3	0.7
a_1	1215.1	1.4
a_1	1203.4	1.6
a_1	43.6	0.0
a_2	−116.9	0.0
b_1	92.7	1.1
b_1	−104.8	46.3
b_2	2801.1	0.2
b_2	2800.1	2.6
b_2	47.5	0.4
b_2	−64.9	22.3

TABLE S13: Harmonic vibrational frequencies of H_2S at the CCSD(T)/ha(Q+d)Z level of theory.

Irrep.	Frequency (cm^{-1})	IR Intensity (km mol^{-1})
a_1	2722	0
a_1	1210	1
b_1	2739	0

TABLE S14: Harmonic vibrational frequencies of I at the CCSD(T)/ha(Q+d)Z level of theory.

Irrep.	Frequency (cm^{-1})	IR Intensity (km mol^{-1})
a'	2731.9	3.0
a'	2720.3	0.1
a'	2698.8	46.7
a'	1214.4	3.6
a'	1208.3	1.1
a'	146.7	4.3
a'	73.7	26.0
a'	56.3	13.3
a''	2735.9	0.4
a''	256.5	3.7
a''	66.6	11.0
a''	32.7	15.0

TABLE S15: Harmonic vibrational frequencies of II at the CCSD(T)/ha(Q+*d*)Z level of theory.

Irrep.	Frequency (cm^{-1})	IR Intensity (km mol^{-1})
a′	2731.3	3.8
a′	2720.5	0.1
a′	2699.4	47.1
a′	1215.7	2.1
a′	1208.3	1.2
a′	144.2	31.9
a′	74.0	5.5
a′	61.5	0.3
a″	2736.2	0.3
a″	255.4	3.9
a″	71.9	0.9
a″	15.0	0.4

TABLE S16: Harmonic vibrational frequencies of III at the CCSD(T)/ha(Q+*d*)Z level of theory.

Irrep.	Frequency (cm^{-1})	IR Intensity (km mol^{-1})

TABLE S17: Harmonic vibrational frequencies of IV at the CCSD(T)/ha(Q+*d*)Z level of theory.

Irrep.	Frequency (cm^{-1})	IR Intensity (km mol^{-1})
a_g	2734.5	0.0
a_g	2716.7	0.0
a_g	1210.5	0.0
a_g	247.1	0.0
a_g	70.9	0.0
a_g	51.0	0.0
a_u	2733.9	1.8
a_u	2717.1	2.7
a_u	1210.4	3.8
a_u	117.2	38.4
a_u	28.5	24.9
a_u	−59.6	35.7

TABLE S18: Harmonic vibrational frequencies of V at the CCSD(T)/ha(Q+*d*)Z level of theory.

Irrep.	Frequency (cm^{-1})	IR Intensity (km mol^{-1})

TABLE S19: Harmonic vibrational frequencies of VI at the CCSD(T)/ha(Q+*d*)Z level of theory.

Irrep.	Frequency (cm^{-1})	IR Intensity (km mol^{-1})
a′	2736.9	0.0
a′	2723.9	0.4
a′	2721.4	0.2
a′	1213.2	0.6
a′	1201.7	3.2
a′	112.1	35.4
a′	56.6	0.1
a′	−47.8	6.3
a″	2739.2	0.4
a″	141.7	24.4
a″	127.6	0.0
a″	−43.8	1.5

TABLE S20: Harmonic vibrational frequencies of VII at the CCSD(T)/ha(Q+d)Z level of theory.

Irrep.	Frequency (cm^{-1})	IR Intensity (km mol^{-1})
a_g	2739.8	0.0
a_g	2722.7	0.0
a_g	1201.7	0.0
a_g	67.9	0.0
a_g	49.0	0.0
a_u	131.6	6.4
a_u	−94.3	48.2
B_g	−152.0	0.0
B_u	2739.1	0.5
B_u	2723.6	0.2
B_u	1212.9	0.2
B_u	59.0	29.2

TABLE S21: Harmonic vibrational frequencies of VIII at the CCSD(T)/ha(Q+*d*)Z level of theory.

Irrep.	Frequency (cm^{-1})	IR Intensity (km mol^{-1})
a′	2741.7	0.4
a′	2737.2	4.0
a′	2725.3	0.0
a′	2721.4	4.5
a′	1212.4	1.5
a′	1207.1	4.9
a′	86.0	15.1
a′	47.3	1.0
a′	25.4	5.7
a″	100.2	0.1
a″	−70.2	9.4
a″	−140.0	33.7

TABLE S22: Harmonic vibrational frequencies of IX at the CCSD(T)/ha(Q+*d*)Z level of theory.

Irrep.	Frequency (cm^{-1})	IR Intensity (km mol^{-1})
A_1	2725.6	0.0
A_1	2723.1	0.0
A_1	1211.4	1.4
A_1	1201.1	1.4
A_1	40.2	0.0
A_2	−109.8	0.0
B_1	2740.1	0.2
B_1	2739.3	0.3
B_1	48.3	0.6
B_1	−58.8	21.2
B_2	86.8	1.3
B_2	−101.5	44.6

III. CARTESIAN COORDINATES

TABLE S23: Cartesian coordinates of H_2S at the MP2/ha(Q+d)Z level of theory.

S	0.000000	0.000000	0.000000
H	0.000000	0.000000	1.332818
H	1.331792	0.000000	−0.052285

TABLE S24: Cartesian coordinates of I at the MP2/ha(Q+d)Z level of theory.

H	0.000000	0.000000	1.332878
S	0.000000	0.000000	0.000000
H	1.335560	0.000000	−0.057267
S	4.061428	0.000000	−0.576830
H	3.943299	0.962073	−1.492395
H	3.943299	−0.962073	−1.492395

TABLE S25: Cartesian coordinates of II at the MP2/ha(Q+d)Z level of theory.

S	−2.124635	−0.071304	0.000000
H	−2.209644	1.258873	0.000000
H	−0.788183	−0.042118	0.000000
S	1.986718	−0.038040	0.000000
H	2.119796	0.875333	−0.962132
H	2.119796	0.875333	0.962132

TABLE S26: Cartesian coordinates of III at the MP2/ha(Q+d)Z level of theory.

S	−2.086269	−0.079267	0.002559
S	2.024038	−0.024778	−0.095325
H	−2.247900	1.242460	0.061688
H	−0.767122	0.032862	−0.182260
H	2.109673	1.123165	0.577492
H	1.901048	−0.733760	1.027339

TABLE S27: Cartesian coordinates of IV at the MP2/ha(Q+d)Z level of theory.

S	2.011866	0.000000	0.000000
S	−2.011866	0.000000	0.000000
H	1.005124	−0.875522	0.000000
H	−1.005124	0.875522	0.000000
H	2.302233	−0.246454	1.277539
H	−2.302233	0.246454	−1.277539

TABLE S28: Cartesian coordinates of V at the MP2/ha(Q+d)Z level of theory.

S	0.000000	2.029413	−0.073958
S	0.000000	−2.029413	−0.073958
H	0.000000	2.100183	1.257286
H	0.000000	−2.100183	1.257286
H	0.850496	1.001217	−0.073958
H	−0.850496	−1.001217	−0.073958

TABLE S29: Cartesian coordinates of VI at the MP2/ha(Q+d)Z level of theory.

H	0.958180	−1.137200	0.000000
S	0.000000	−2.064288	0.000000
H	−0.958180	−1.137200	0.000000
S	0.000000	1.858865	0.000000
H	0.000000	2.780590	−0.963040
H	0.000000	2.780590	0.963040

TABLE S30: Cartesian coordinates of VII at the MP2/ha(Q+d)Z level of theory.

S	0.000000	1.779604	0.000000
S	0.000000	−1.779604	0.000000
H	1.287279	1.434406	0.000000
H	−1.287279	−1.434406	0.000000
H	0.285550	3.081830	0.000000
H	−0.285550	−3.081830	0.000000

TABLE S31: Cartesian coordinates of VIII at the MP2/ha(Q+d)Z level of theory.

S	0.033178	−2.197969	0.000000
H	−1.278160	−2.436421	0.000000
H	−0.152183	−0.877066	0.000000
S	0.033178	2.037024	0.000000
H	−0.766903	3.102788	0.000000
H	1.135555	2.785808	0.000000

TABLE S32: Cartesian coordinates of IX at the MP2/ha(Q+d)Z level of theory.

H	0.000000	0.957847	1.249925
S	0.000000	0.000000	2.176676
H	0.000000	−0.957847	1.249925
S	0.000000	0.000000	−1.971223
H	0.000000	0.962289	−2.893553
H	0.000000	−0.962289	−2.893553

TABLE S33: Cartesian coordinates of H_2S at the CCSD(T)/ha(Q+d)Z level of theory.

S	0.00000000	0.00000000	0.10383165
H	0.00000000	−1.82490967	−1.64696887
H	0.00000000	1.82490967	−1.64696887

TABLE S34: Cartesian coordinates of I at the CCSD(T)/ha(Q+d)Z level of theory.

H	−2.3313770936	−1.2724654482	0.0000000000
S	−2.0987784147	0.0454790770	0.0000000000
H	−0.7689443571	−0.1276226205	0.0000000000
S	2.0644877421	−0.0561484908	0.0000000000
H	2.0940765059	0.8692812988	0.9668894589
H	2.0940765059	0.8692812988	−0.9668894589

TABLE S35: Cartesian coordinates of II at the CCSD(T)/ha(Q+d)Z level of theory.

H	−2.1768806265	1.2978253717	0.0000000000
S	−2.1116792630	−0.0389607304	0.0000000000
H	−0.7706725864	−0.0332248622	0.0000000000
S	2.0652660929	−0.0550766318	0.0000000000
H	2.2099783803	0.8593123622	−0.9669517483
H	2.2099783803	0.8593123622	0.9669517483

258

TABLE S36: Cartesian coordinates of III at the CCSD(T)/ha(Q+d)Z level of theory.

S	−4.000600542299	−0.148575994469	0.003054100322
S	3.881253792107	−0.068488759440	−0.172925190582
H	−4.285362937134	2.359786799385	0.156228533139
H	−1.503042347497	0.043840973645	−0.380602978297
H	4.085679793338	2.235516014474	0.851604459417
H	3.612273494365	−1.166107724966	2.090707429906

TABLE S37: Cartesian coordinates of IV at the CCSD(T)/ha(Q+d)Z level of theory.

H	2.3299306036	−1.2498642472	0.1513285213
S	2.0374587619	0.0484122693	0.0080871349
H	1.0369204852	−0.2093487172	−0.8441388089
S	−2.0374587460	−0.0484122693	−0.0080871507
H	−1.0369204693	0.2093487172	0.8441387931
H	−2.3299310216	1.2498642101	−0.1513280185

TABLE S38: Cartesian coordinates of V at the CCSD(T)/ha(Q+d)Z level of theory.

TABLE S39: Cartesian coordinates of VI at the CCSD(T)/ha(Q+d)Z level of theory.

H	−0.9636344158	−1.1148677910	0.0000000000
S	0.0000002170	−2.0439129035	0.0000000000
H	0.9636277852	−1.1148604724	0.0000000000
S	−0.0000000053	1.9340043684	0.0000000000
H	−0.0000000529	2.8582240674	0.9678961656
H	−0.0000000529	2.8582240674	−0.9678961656

TABLE S40: Cartesian coordinates of VII at the CCSD(T)/ha(Q+d)Z level of theory.

H	3.1326505799	−0.2355338396	0.0000000000
S	1.8240172294	0.0447301643	0.0000000000
H	1.4816877502	−1.2488849095	0.0000000000
S	−1.8240172294	−0.0447301643	0.0000000000
H	−1.4816877502	1.2488849095	0.0000000000
H	−3.1326505799	0.2355338396	0.0000000000

TABLE S41: Cartesian coordinates of VIII at the CCSD(T)/ha(Q+d)Z level of theory.

H	2.4049117070	1.2782977960	0.0000000000
S	2.2001905334	−0.0442432683	0.0000000000
H	0.8695470093	0.1040735520	0.0000000000
S	−2.1124280964	0.0067417283	0.0000000000
H	−3.1375671336	0.8665005625	0.0000000000
H	−2.9210522775	−1.0591794250	0.0000000000

TABLE S42: Cartesian coordinates of IX at the CCSD(T)/ha(Q+d)Z level of theory.

H	0.9632513550	0.0000000000	−1.2297896504
S	0.0000000000	0.0000000000	−2.1586835081
H	−0.9632513550	0.0000000000	−1.2297896504
S	0.0000000000	0.0000000000	2.0487468738
H	−0.9671908412	0.0000000000	2.9735951718
H	0.9671908412	0.0000000000	2.9735951718

VITA

1. Education Doctor of Philosphy (Chemistry) University of Mississippi 2018*
   Advisor: Dr. Gregory S. Tschumper
   Bachelor of Science (Chemistry) Southeastern Louisiana University 2012
   Advisor: Dr. Thomas Sommerfeld

2. Professional Experience and Training Graduate Research Assistant 2013-2018
   Graduate Teaching Assistant 2012-2016
   Linux Clusters Institute High Performance Computing Workshop 2015

3. Publications

   (a) Fotie, Jean; Kemami Wangun, Hilaire V.; Dreux, Katelyn; Sommerfeld, Thomas; Pittman, Jacob. Magn. Reson. Chem. 50, 1, 68 (2012). Unusual open chain quinolinyl peroxol and its alcohol counterpart obtained through a modified Skraup-Doebner-Von Miller quinoline synthesis: theoretical studies and complete 1H- and 13C-NMR assignments.

   (b) Sommerfeld, Thomas; Dreux, Katelyn M. J. Chem. Phys., 137, 24, 224302/1 (2012). Characterizing the excess electron of $Li(NH_3)_4$.

(c) Sommerfeld, Thomas; Dreux, Katelyn M.; Joshi, Robin. JPCA, 118, 35, 7320 (2014). Excess Electrons Bound to Molecular Systems with a Vanishing Dipole but Large Molecular Quadrupole.

(d) A.J. Huckaba, F. Giordano, L.E. McNamara, K.M. Dreux, N.I. Hammer, G.S. Tschumper, S.M. Zakeeruddin, M. Grtzel, M.K. Nazeeruddin and J.H. Delcamp Adv. Energy Mater. 5, 1401629 (2014). Indolizine-Based Donors as Organic Sensitizer Components for Dye-Sensitized Solar Cells.

(e) K.M. Dreux and G.S. Tschumper, Comp. Theor. Chem., 1072, 21-27 (2015). Anchoring the potential energy surface of an important atmospheric van der Waals dimer, the $H_2O\cdots O_2$ complex.

(f) K.M. Dreux, L.E. McNamara, J.T. Kelly, A.M. Wright, N.I. Hammer and G.S. Tschumper, J. Phys. Chem. A, 131, 5884-5893 (2017). Probing Dative and Dihydrogen Bonding in Ammonia Borane with Electronic Structure Computations and Raman under Nitrogen Spectroscopy.

(g) K.M. Dreux and G.S. Tschumper, J. Comput. Chem., $SUBMITTED$. Examination of the structures, energetics, and vibrational frequencies of small sulfur-containing prototypical dimers, $(H_2S)_2$ and H_2O/H_2S.

4. Presentations

(a) Dreux, Katelyn M. and Tschumper, Gregory S. (November 2017) Host/Guest Interactions in Methylene-Bridged Resorcinarenes. 25th Conference on Current Trends in Computation Chemistry. Jackson, Mississippi.

(b) Dreux, Katelyn M. and Tschumper, Gregory S. (May 2017) The structures, energetics, and vibrational signatures of small hydrogen-bonded dimers involving H_2S. Southeastern Theoretical Chemistry Association Conference 2017. University, Mississippi.

(c) Dreux, Katelyn M. and Tschumper, Gregory S. (May 2016) Balancing the inter- and intra- molecular forces in ammonia borane clusters: Dihydrogen bonding and Coordinate Covalent bonds. Southeastern Theoretical Chemistry Association Conference 2016. Tallahassee, Florida.

(d) Dreux, Katelyn M. and Tschumper, Gregory S. (November 2015) Balancing inter- and intra-molecular forces: The challenging case of dihydrogen bonding and coordinate covalent bonding in ammonia borane clusters. Joint SE/SW Regional ACS Meeting (SERMACS/SWRM) 2015. Memphis, Tennessee.

(e) Dreux, Katelyn M. and Tschumper, Gregory S. (May 2014). The H_2O/O_2 Dimer. Southeastern Theoretical Chemistry Association Conference 2014. Atlanta, Georgia.

(f) Dreux, Katelyn M. and Tschumper, Gregory S. (April 2013). The Atmospherically Important van der Waals Complex: the $H_2O\cdots O_2$ Dimer. 2014 Mississippi EPSCoR Annual State Meeting. Starkville, Mississippi.

(g) Dreux, Katelyn M. and Tschumper, Gregory S. (September 2012). π-stacking in Aromatic Systems. 2012 Mississippi EPSCoR Annual State Meeting. Starkville, Mississippi.

5.	Awards ACS Graduate Student Research Award	June 2018
	Graduate Student Achievement Award	Spring 2017
	GAANN Fellow	Spring 2013
	Mississippi EPSCoR Poster Competition Award, 1st Place	Spring 2014
	Mississippi EPSCoR Poster Competition Award, 1st Place	Spring 2013